VARIABILITY OF CIRCULATION IN THE COOS ESTUARY

by

MARÍA JOSÉ MARÍN JARRÍN

A DISSERTATION

Presented to the Department Earth Sciences
and the Division of Graduate Studies of the University of Oregon
in partial fulfillment of the requirements
for the degree of
Doctor of Philosophy

December 2021

DISSERTATION APPROVAL PAGE

Student: María José Marín Jarrín

Title: Variability of Circulation in the Coos Estuary

This dissertation has been accepted and approved in partial fulfillment of the requirements for the Doctor of Philosophy degree in the Department of Earth Sciences by:

David Sutherland   Chairperson
Rebecca Dorsey   Core Member
Melanie Fewings   Core Member
Diego Melgar   Core Member
Alan Shanks   Institutional Representative

and

Krista Chronister   Vice Provost for Graduate Studies

Original approval signatures are on file with the University of Oregon Division of Graduate Studies.

Degree awarded December 2021

DISSERTATION ABSTRACT

María José Marín Jarrín

Doctor of Philosophy

Department of Earth Sciences

December 2021

Title: Variability of Circulation in the Coos Estuary

The Coos Estuary, is the second largest estuary in Oregon in terms of area and
volume, after the Columbia River Estuary, with extensive tidal flats and subsidiary
sloughs. Estuaries, like the Coos, are utilized for habitat and refuge by many organisms,
such as oysters, crabs, fish, and phytoplankton. Despite its importance, it had been highly
understudied, and its characteristics had been defined based on general definitions of
estuaries. The estuary is shaped like an inverted-U, due to a 4-km long bend centered
around 15 km from the mouth. This torturous geometry is common among estuaries in
the Pacific Northwest, and complicates circulation.

In Chapter 2 I describe the influence of winds on the subtidal flow in the main
estuarine channel. Velocity time series show that during high and moderate discharge, the
exchange flow deepens and strengthens in the classical sense: seaward flow at the surface
and landward flow at depth. However, we find reversals where landward flow occurs for
periods of more than a day during neap tides and downwelling-favorable northward
winds. I further explored in situ data in combination with idealized numerical simulations

to quantify the effect of winds, tides, river discharge and coastal currents on the observed flow.

In Chapter 3 I describe the impact of the combination of drought, El Niño and marine heatwaves in 2014- 2016, in the water temperature of the estuary. This warming was observed in stations inside the estuary, with higher anomalies at the shallower stations, where an extensive decline of eelgrass (*Zostera marina*) has been observed. Water temperature increased landward, suggesting that river input and atmospheric heat flux may be important contributors to the anomalous conditions observed.

In Chapter 4 I used a numerical model to explore the variability of timescales within the Coos Estuary. Timescales in the estuary vary in space and time, hence whole-volume approaches may be over/underrepresenting these scales. I also explored the influence of connectivity between different areas due to its impact on the transport and availability of Olympia oyster (*Ostrea lurida*) larvae in the Coos Estuary.

This dissertation includes previously both previously published/unpublished and co-authored material.

CURRICULUM VITAE

NAME OF AUTHOR: María José Marín Jarrín

GRADUATE AND UNDERGRADUATE SCHOOLS ATTENDED:

    University of Oregon, Eugene.
University of New Hampshire, NH, USA.
Escuela Superior Politécnica del Litoral, Ecuador.

DEGREES AWARDED:

    Doctor of Philosophy, Earth Sciences, 2021, University of Oregon
Masters in Science, Earth Sciences, 2016, University of New Hampshire
Oceanógrafa, 2009, Escuela Superior Politécnica del Litoral

AREAS OF SPECIAL INTEREST:

    Equatorial Oceanography
Estuarine physics
Numerical ocean modeling

PROFESSIONAL EXPERIENCE:

    Graduate Teaching and Research Fellow, University of Oregon, Department of
Earth Sciences, 2016-2021

Oceanographic Investigator. National Institute of Oceanography (INOCAR),
Department of Ocean Sciences. Guayaquil, Ecuador. 2013 – 2014

Fisheries Investigator. National Institute of Fisheries (INP) of Ecuador, Guayaquil,
Ecuador. 2012 -2013

Technical Hydrographer. National Institute of Oceanography (INOCAR),
Department of Ocean Sciences. Guayaquil, Ecuador. 2011

GRANTS, AWARDS, AND HONORS:

    "CONVOCATORIA ABIERTA 2013, primera fase" National Secretary of Superior
Education, Science, Technology and Innovation. Ministry of Education of
Ecuador (August/2014 – September/2016).

Spring award for EPOC Conference participation. Department of Earth Science,
University of Oregon, Summer/2017.

Spring award for EPOC Conference participation. Department of Earth Science,
University of Oregon, Summer/2018.

PUBLICATIONS:

Marin Jarrin, Maria J., and Thomas C. Lippmann. "Interannual variability of mixed layer dynamics in the Ecuadorian Ocean." Journal of Geophysical Research: Oceans 124.12 (2019): 8777-8797.

ACKNOWLEDGMENTS

This work is a culmination of the faith and support of my family, friends, colleagues, and mentors. My deepest gratitude goes to you all, even if not listed here.

Firstly, thank you to the *Ocean and Ice Lab* and Dave Sutherland, my PI and advisor. Dave, the greatest thanks for your support and wisdom, especially in helping me see the bigger picture and not taking on many side projects. Fellow graduate students, undergraduate students and postdocs, past and present. Alex Hager, Nicole Abib, Ted Conroy, Bass Dye, Kristin Schild, Kiya Riverman, Emily Eidam, have been an amazing support, from data analysis to bonding over food.

I am very thankful to my committee, Dr. Rebecca Dorsey, Dr. Diego Melgar Montezuma, Dr. Melanie Fewings, Dr. Alan Shanks, who have provided incredible wisdom and thoughtful feedback over my degree process. Thank you for your suggestions, helping me stay on track and encouragement.

Dr. Kelly Sutherland (Oregon Institute of Marine Biology, OIMB) and her *Form, Function and Flow in the Plankton* Lab. Particular gratitude for friendship, support and bonding over many shared interests to Marco Corrales-Ugalde, Aliza Karim, Reyn Yoshioka and Hilarie Sorensen. Their emotional and technical support have allowed me to overcome the many challenges faced through this dissertation. Also, thanks to OIMB research community, and CMLC. The amazing scientific group in SSNERR who helped

me in understanding the data, acquiring it and analyzing it: Ali Helms, Bree Yednock and Jenni Schmitt.

The Earth Sciences Department at UO, especially the graduate students and staff. Monserratte Cascante and Marla Trox I owe you so much of my sanity, resilience and happiness. As well as the volunteers and staff at Catholic Community Services and St. Jude's Catholic church, from whom I learnt a lot about life outside of the University bubble, enjoyed non-scientific talks and got help to appreciate my place in this world.

Finalmente, debo agradecer a mis papas, Rolando y Alexandra, por su apoyo en directo y a la distancia, soporte, y amor incondicional. A mi hermano y su familia, Jose, Michelle, Lucy y Danny, mis biólogos. Y a toda mi familia que me apoya desde donde estén. No hay palabras.

To Ecuador

TABLE OF CONTENTS

LIST OF FIGURES

LIST OF TABLES

CHAPTER I

INTRODUCTION

Estuaries act as productive mixing zones between oceanic and riverine waters, providing many ecosystem and cultural services (Milcu et al., 2013; Sherman and DeBruyckere, 2018; Zapata et al., 2018), and motivating numerous studies to examine the links between environmental conditions and ecosystem health (Costanza et al., 1997; Seppelt et al., 2011). Many species have adapted to the strong temporal and spatial gradients in circulation, salinity and temperature that exist within estuaries, which also influence a species' transport and survival within an estuary.

Traditionally, subtidal (i.e., low-pass filtered to remove tidal variability) estuarine circulation is viewed as a balance between the along-channel baroclinic pressure gradient and vertical mixing. The resulting flow is termed the estuarine exchange flow, or gravitational circulation, and using some assumptions, can be predicted for partially-mixed estuaries as a function of river discharge, tidal currents, and bathymetry (e.g., Hansen and Rattray, 1965; MacCready and Geyer, 2010). However, the characteristics of real estuaries, including channel curvature (Geyer, 1993; Lacy and Monismith, 2001; Chant, 2002a; Kranenburg et al., 2019) or strong temporal forcing, can complicate the simplified theory's assumptions. Hence, time dependence is an important factor in small, strongly-forced estuaries (Banas et al., 2004; Bolaños et al., 2013; Conroy et al., 2020). Understanding how variations in the estuarine circulation interact over a range of time scales is still needed, especially as applied to how estuarine flow influences biological patterns.

In the Pacific Northwest (PNW), estuaries are influenced on the ocean side by the primarily wind-driven California Current System (CCS; Hickey and Banas 2003). These winds driving the CCS along the west coast of North America are forced by atmospheric circulation related to the North Pacific High and the Aleutian Low, which vary seasonally. In the summer the North Pacific High migrates northward producing southward-directed upwelling-favorable winds (Huyer 1983; Hickey and Banas 2003; Davis et al. 2014, and others). Upwelled waters on the PNW continental shelf are typically colder, with higher salinity, higher nutrients and lower oxygen levels. During winter, storms produce episodic river discharge events that result in lower salinity, lower temperature and higher turbidity along the coast (Hickey and Banas, 2003; Huyer et al., 2007).

The Coos Estuary is the second largest estuary in Oregon in terms of area and volume, and is located inshore of a narrow continental shelf south of Stonewall Bank (Hickey and Banas, 2003). Water properties inside the Coos Estuary are significantly correlated with continental shelf values as measured by the Stonewall buoy, especially during the dry upwelling season (Strub et al., 1987; Miller and Shanks, 2004; Huyer et al., 2007). During the winter, higher discharge originating from numerous small creeks and rivers, produce a highly stratified estuary which can affect the temperature, salt content of the estuary, transport of particles, etc. Using a year-long realistic numerical hindcast model, Conroy et al., (2020) found that the Coos Estuary has a tidally-driven exchange flow and salt flux that persists year-round, despite the seasonal changes in river discharge. The model also showed that the Coos Estuary is time-dependent, with geometry driving important dispersive processes.

On top of the seasonal variability in forcing, several warm-water events have been registered in the PNW, including El Niño events (Huyer et al., 2002; Peterson et al., 2017), and marine heat waves (Gentemann et al., 2017; Shanks et al., 2020). These modified ocean properties are then further transported towards the mouth of the estuaries in the PNW and can travel up-estuary affecting the ecosystem at different timescales and magnitudes (Hickey et al., 2003).

The question driving this dissertation is *how does the circulation in the Coos Estuary vary spatially and temporally, and how does it affect the ecosystem*? Hence, Chapter 2 explores the spatial and temporal variability of wind effects on circulation and salinity of the Coos Estuary by looking at specific combinations of tides, river discharge and winds. Due to the U-shape of the Coos Estuary, observations and numerical model experiments show different impacts of winds on each side of the bend. These anomalies in salinity and velocity can affect exchange flow and salt content in the estuary which can modify transport of particles in the estuary. This Chapter has been submitted to the *Journal of Estuarine, Coastal and Shelf Science - Elsevier*. I am the lead author on the paper, developing the methodology, analyzing the data and writing the manuscript. David Sutherland (University of Oregon), served as advisor, aiding in data interpretation and manuscript editing.

Though most of the density gradient in the Coos Estuary is driven by salinity, in the summer temperature gradients may enhance the advection of waters through the estuary. In Chapter 3 I use long-term observations, to evaluate the impact of the ambient ocean conditions, river discharge and atmospheric heat flux on the water temperature in the

estuary. This Chapter focuses on 2014-2017, which were characterized by strong interannual variability, and can be linked to an observed decrease in eelgrass (*Zostera marina*) abundance. This Chapter will be submitted to the *Journal Frontier of Marine Sciences*. I am the lead author on the paper, developing the methodology, analyzing the data and writing the manuscript. David Sutherland (University of Oregon), served as advisor, aiding in data interpretation and manuscript editing. Alicia Helms (South Slough National Estuarine Research Reserve) provided eelgrass data, feedback on manuscript drafts and aided in manuscript editing.

The effect that water properties can have on an ecosystem also depends on the length of time it remains in the area. Hence, in Chapter 4 I use a numerical model to show the strong spatial variability of timescales in the estuary, related to the forcing as well as the geometry and bathymetry of the study area. These timescales can contribute to stress in areas of ecological importance and should be considered when developing restoration plans, for example, for the Olympia oyster (*Ostrea lurida*) larvae in the Coos Estuary.

CHAPTER II

INFLUENCE OF WINDS ON THE CIRCULATION OF A SMALL ESTUARY

WITH COMPLEX GEOMETRY

This Chapter has been submitted to the J*ournal of Estuarine, Coastal and Shelf Science* - Elsevier. I am the lead author on the paper, developing the methodology, analyzing the data and writing the manuscript. David Sutherland (University of Oregon), served as advisor, aiding in data interpretation and manuscript editing.

    1. Introduction

Estuaries are the mixing zones between rivers and the coastal ocean, and are utilized for habitat and refuge by many organisms, such as oysters, crabs, fish, and phytoplankton (Garvine, 1991; Epifanio and Garvine, 2001; Janzen and Wong, 2002; Cloern et al., 2017; Sharples et al., 2017). Many species have adapted to the strong temporal and spatial gradients in salinity and temperature that exist within estuaries. The same drivers that set these hydrographic gradients can also directly affect a species' transport and survival within an estuary. For example, during 1997-1998, the Willapa Bay, WA, estuary received an increased amount of green crab larvae that was correlated to high river discharge (Yamada et al., 2005). Once introduced, this green crab population could then self-sustain due to relatively long retention in parts of the estuary (>1 month timescales) caused by a combination of tidal and channel curvature effects (Banas et al., 2009).

Subtidal (i.e., low-pass filtered to remove tidal variability) estuarine circulation is traditionally viewed as a balance between the along-channel baroclinic pressure gradient and vertical mixing. The resulting steady flow is termed the gravitational circulation, or estuarine exchange flow, and sets the along-estuary gradients that dictate conditions felt by organisms on longer time-scales. Using certain assumptions, this exchange flow can be predicted for partially-mixed estuaries as a function of river discharge, tidal currents that act to mix the water column, and bathymetry (e.g., Hansen and Rattray, 1965; MacCready and Geyer, 2010). Many characteristics of real estuaries, however, complicate the simplified theory's assumptions. These include channel curvature (Geyer, 1993; Lacy and Monismith, 2001; Chant, 2002b; Kranenburg et al., 2019) and strong temporal forcing (i.e., unsteadiness) due to tides, winds, discharge, or other factors. Indeed, in small, strongly-forced estuaries, time dependence is an important factor, especially in estuaries where the discharge regime is on the same order as the estuarine response time (Banas et al., 2004; Bolaños et al., 2013; Conroy et al., 2020). Thus, understanding how variations in the estuarine circulation interact over a range of time scales is still needed, especially as applied to how estuarine flow influences biological patterns.

Wind forcing occurs over a large range of distinct time and space scales, including local diurnal winds, passing storms, seasonally-varying offshore winds that drive upwelling/downwelling, and remote winds that create coastally-trapped waves that affect sea level (e.g., Geyer, 1997; Giddings and MacCready, 2017; Janzen and Wong, 2002; Lai et al., 2018; Purkiani et al., 2016; Scully et al., 2005; Uncles and Stephens,

2011; Valle-Levinson et al., 2001). During storm events, wind stress mixes the water column and reduces stratification (Blumberg and Goodrich, 1990; Li and Li, 2011); however, the same wind stress can modulate the estuarine exchange flow through vertical shear wind straining (Scully et al., 2005; Chen and Sanford, 2009). Additionally, the response of exchange flow to wind depends on the lateral bathymetry, where downwind flow on the shoals is produced by wind-driven flow, while in the channel upwind flow is produced (Csanady, 1973; Lerczak and Geyer, 2004; Sanay and Valle-Levinson, 2005; Chen and Sanford, 2009). This lateral variability can feed into the barotropic flow by changing sea level gradients locally (Nidzieko and Monismith, 2013). Hence, wind complicates the estuarine exchange flow conceptual model by adding unsteadiness, influencing stratification, and inducing horizontal gradients (Xie and Eggleston, 1999; Xia et al., 2011; Pfeiffer-Herbert et al., 2015). Although research examining the interaction of wind and estuarine circulation is not new, previous numerical studies have primarily used idealized geometries that ignore the realistic shape of many estuaries that alters their response to wind (e.g., Chen and Sanford, 2009; Coogan and Dzwonkowski, 2018; Purkiani et al., 2016). Here, we explore wind forcing on the observed circulation in the strongly-forced, geometrically-complex Coos Estuary, located in southern Oregon on the US West Coast, and expand our understanding across the entire estuary using a set of numerical model experiments.

2. Background

2.1 The Coos Estuary

Estuaries are found all over the coastal Pacific Northwest (PNW - Figure 1) and the Coos Estuary is the second largest in terms of surface area and volume. The Coos Estuary is located south of Heceta Bank (Figure 1a), inshore of a relatively narrow continental shelf (Hickey and Banas, 2003), and is home to ecologically important native species such as Olympia oysters (*Ostrea lurida*) and eelgrass (*Zostera marina*) (O'Higgins and Rumrill, 2007). The estuary shape is an inverted-U, due to a 4-km long bend centered around 15 km from the mouth. This torturous geometry is common among estuaries in the PNW. The main navigational channel is dredged annually from the mouth up to 24 km near the Coos River entrance to maintain 11 m of depth and 91 m of width (U.S. Army Corps of Engineers, 2015). Areas outside the channel consist primarily of tidal flats and subsidiary sloughs (Emmett et al., 2000; Groth and Rumrill, 2009). Tidal flats, with water depth ≤ 1.5 m, cover an area of approximately 15 km^2 or 30% of the estuarine area (Eidam et al. 2020).

Freshwater discharge into the estuary comes from numerous small creeks and rivers, with the largest flow from the South Fork Coos River that ranges from 2 to 800 m$^3 \cdot$s^{-1}. Discharge peaks are associated with storms that bring strong and shifting winds (Figure 2). The lunar semidiurnal M$_2$ tidal height amplitude is about 0.8 m, with mean tidal currents of 1.1 m$\cdot$s^{-1} resulting in an average tidal excursion of 14 km (Baptista, 1989).

Previous observations show that the Coos Estuary salinity structure resembles a salt-wedge during high river discharge, a well-mixed estuary during low discharge, and a partially-mixed estuary during moderate discharge (Sutherland and O'Neill, 2016). Based

on a year-long realistic numerical hindcast model, Conroy et al., (2020) found the Coos Estuary to be time-dependent, with local geometry driving important dispersive processes such as tidal trapping and jet-sink flow. Additionally, the model showed that the Coos Estuary has a tidally-driven exchange flow and salt flux that persists year-round, despite the seasonal changes in river discharge (Conroy et al., 2020). Large winter discharge events drive a mean flow that pushes salt out estuary, while in the dry summer, adjustment times are longer than summer itself, resulting in oceanic salinities up to 20 km landward. However, the model neglected wind.
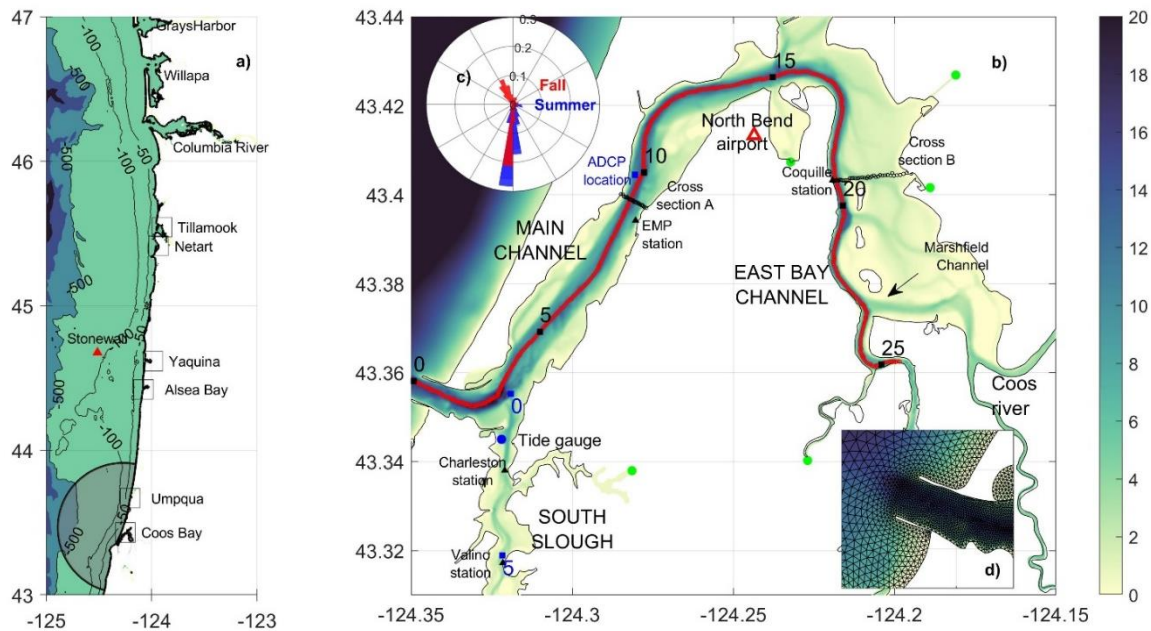
Figure 1. a) Map of example PNW estuaries, indicating the Coos (model domain in black outline) and the location of the Stonewall buoy (red triangle). b) Zoom-in on the Coos Estuary, showing bathymetry (color) and the location of water quality monitoring stations (black triangles), meteorological station at the North Bend airport (red triangle), velocity stations (blue square), and tide gauge (blue circle). Black numbers refer to distance (in km) from the mouth along the thalweg. Blue numbers show distance (in km) from the intersection of South Slough with the main estuary. c) Wind stress direction and magnitude (N·m^{-2}) during the summer (blue) and fall (red) at the North Bend airport station. d) The unstructured FVCOM model grid at the mouth of the estuary where average horizontal resolution is 30 m.

Winds in the PNW blow primarily southward in the summer months of May

through September (Figure 1). These winds drive persistent summer upwelling along the

coast, where surface waters move offshore and cold, salty, nutrient-rich waters move

upwards and onshore towards the coast (Hickey and Banas, 2003). During the wet season

(November to April) winds shift to northward on average, with the strongest winds

associated with passing storms (Hickey and Banas, 2003). Additionally, during the

summer a strong diurnal sea breeze blows eastward with wind stresses up to 0.3 N·m^{-2}.

2.2 Theoretical background

We start with the momentum balance for a linear, quasi-steady, non-rotational and

laterally invariant subtidal circulation (Hansen and Rattray, 1965; Geyer, 1997; Valle-

Levinson et al., 2019), which is given by

$$A_z \frac{\partial^2 u}{\partial z^2} = g \frac{\partial \eta}{\partial x} + \frac{g}{\rho_0} \frac{\partial \rho}{\partial x} H, \qquad (1)$$

where, A_z is the vertical eddy viscosity, u is the along-estuary velocity at depth z,

g is the gravitational acceleration, η is the water elevation, ρ is the density and H is the

water depth. Despite the questionable validity of these assumptions for the complex Coos

Estuary, Eq 1 can be used to examine the combined influence of horizontal density

gradient and wind forcing in a qualitative sense. Eq 1 has a solution of the form (Hansen

and Rattray, 1965)

$$u(z) = \frac{3}{2}u_a\left[1 - \frac{z^2}{H^2}\right] - \frac{gH^3}{48\rho}\frac{\partial\rho/\partial x}{A_z}\left[9\left(1 - \frac{z^2}{H^2}\right) - 8\left(1 + \frac{z^3}{H^3}\right)\right] + \frac{H}{4\rho}\frac{\tau_{wx}}{A_z}\left[4\left(1 + \frac{z}{H}\right) - \right.$$

$$\left. 3\left(1 + \frac{z^2}{H^2}\right)\right] \tag{2}$$

where τ is the wind stress, and u_a is the depth-averaged velocity. The first term describes the barotropic component that is driven by river discharge and sea level. The second term, the baroclinic pressure, describes the flow driven by density gradients, is sensitive to the water depth, and depends inversely on A_z (which depends on tidal forcing and stratification). The third term denotes the subtidal flow driven by wind stress and depends on depth and A_z. Using this solution, we can define the wind stress needed to balance the baroclinic pressure gradient force as the Wedderburn number (W), (Monismith, 1986; Geyer, 1997; Chen and Sanford, 2009):

$$W = \frac{\tau_{wx}L}{\Delta\rho gH^2}, \tag{3}$$

where L is the length of an estuary and $\Delta\rho$ is the horizontal density difference along the estuary.

3. Methods

3.1 Observations

Water velocity time series were collected from late 2013 until early 2015 using a bottom-mounted, upward-looking SonTek 150 kHz Acoustic Doppler Current Profiler (ADCP) by South Slough National Estuarine Research Reserve (SSNERR). The ADCP was located in the main channel seaward of the North Bend, close to the northern shoals, at about 10 m depth, hence these data potentially miss the deepest landward flow in the

channel (Figure 1, Table 1). The top and bottom bins were excluded to eliminate surface and bottom effects. All velocity data were rotated to be oriented in the along-channel direction, corresponding to the principal component direction at each location.

Hourly tidal height time series were obtained from a NOAA tide gauge at Charleston, OR (Figure 1). Subtidal variability was obtained using a low-pass Godin filter (consecutive 24-24-25 hour filters), and sea level anomalies were calculated as deviations from the subtidal signal. Tidal constituents from sea level were computed using the T-TIDE harmonic analysis software (Pawlowicz et al., 2002).

Water property data were obtained from several monitoring stations located throughout the estuary (Figure 1b, Table 1). Salinity, along with other water quality parameters, is measured every 15 minutes at all stations. We only discuss salinity and water level records here. The Charleston Bridge and Valino stations are telemetered to provide near real-time data access by SSNERR, at 3.0 and 5.6 km from the mouth inside South Slough, respectively (Figure 1, Table 1). The Confederated Tribes of the Coos, Lower Umpqua and Siuslaw (CTCLUSI) monitor water quality at two additional stations: Bureau of Land Management (BLM) and Empire Docks (EMP), with data available from 2011 to present at distances of 8.1 and 6.9 km from the mouth, respectively (Figure 1, Table 1). Beyond North Bend, the Coquille Indian Tribe monitor a station 18 km from the mouth (Coquille WQ). Finally, along-estuary hydrography in the estuary was described by Sutherland and O'Neill (2016), from conductivity-temperature-depth (CTD) profiles collected during 2012-2014.

Table 1. Oceanographic and meteorological stations analyzed in this study with locations shown in Fig. 1. Instrument height above bottom (HAB) is shown, along with mean water depth (m) and distance from the estuary mouth (km).

Station	Institution	Time range	Depth (m) / HAB (m)	Distance (km)
Water quality stations				
Valino Island	SSNERR	1999–	2.4 / 0.5	5.6
Charleston	SSNERR	2002–	4.0 / 0.5	3.0
EMP	CTCLUSI	2011–2014	6.0 / 0.5	6.9
BLM	CTCLUSI	2011–2014	5.0 / 0.5	8.1
Coquille	Coquille Tribe	2013–2017	11.9 / 0.5	18
Water velocity data				
ADCP location	SSNERR	2013–2015	10.5 / 9.5	10.0
Sea level from tide gauge				
Charleston 9432780	NOAA	1991–	3.0 / --	3.0
River discharge				
South Fork at Coos river 14323600	CoosWa	2003–	44 (elev.)	49
Meteorological stations (wind magnitude and direction)				
North Bend airport	NOAA 24284	1949–	5.1 (elev.)	12.5
Stonewall buoy	NOAA 46050	1991–	3.8 (elev.)	147.5

River discharge data from the South Fork Coos River gauge (Figure 1, Table 1) from 2003 to present was used as a proxy for the total freshwater input to the estuary (Baptista, 1989). Although there are more than 13 sources of freshwater input, the Coos River is the main source of freshwater to this system (~66% of total discharge), of which the South Fork is the main component (Conroy et al., 2020).

Wind velocity data were extracted from a meteorological station at the North Bend Southwest Oregon Regional Airport (Figure 1, Table 1). We use oceanographic

wind convention. Importantly, northward winds correspond to up-estuary winds in Main

Channel before the bend (Figure 1), yet, they are down-estuary in the East Bay Channel

(beyond the bend). For comparison with the shelf, winds at the Stonewall Buoy (Figure 1,

Table 1) are also obtained for the time span of the study.

3.2 Numerical Simulations

3.3 Model setup and validation

We use the Finite Volume Coastal Ocean Model (FVCOM) to simulate the impact

of winds on the circulation in the Coos Estuary. FVCOM is a prognostic, finite-volume,

free-surface, three-dimensional primitive equation model with an unstructured grid (Chen

et al., 2003, 2018; Huang et al., 2008; Qi et al., 2009). FVCOM was chosen because it

resolves tidal elevations, water properties, and currents in areas with complex

topographical features and has a robust wetting/drying scheme. The model domain covers

the entire estuary with an open boundary well outside the mouth of the estuary (Figure

1a). The horizontal grid has a spatial resolution that varies from ~30 m within the bay to

~3 km at the outer boundary (other model parameters are specified in Sup. Table 1) The

vertical coordinate has 20 levels in a uniform hybrid terrain-following grid. The model

bathymetry within the estuary was interpolated from 2014 USGC Coastal LiDAR data

and in-situ single-beam echosounder surveys (Conroy et al., 2020). Model boundary

conditions include idealized tidal forcing at 52 open boundary nodes (Figure 1), using

only the M_2 semidiurnal tidal constituent extracted from the Charleston tide gauge. The

simulations were initiated with a 1-month spin-up period for each forcing scenario, which

were then subsequently used as initial conditions for each wind-event case. For all runs, the initial salinity equaled 34, while a salinity of 0 was imposed at the river input locations. This set up is similar to previously validated realistic hindcast simulations Conroy et al., (2020); Eidam et al., 2020). However, to save computational time, we use a slightly coarser horizontal resolution (up to a factor of 2 inside the estuary), and conduct a qualitative validation (see results) to ensure the model reproduces the main estuarine characteristics.

3.4 Model experiments

To investigate the dependence of estuarine circulation on wind strength and direction, we designed a set of six baseline simulations in which tidal forcing and river discharge (Q_r) are held steady for 30 days at representative magnitudes. Two fixed tidal amplitudes represent the fortnightly variability: an amplitude of 0.79 m for neap tides and 1.17 m for spring tides. We vary Q_r to mimic the seasonality: 1) High (rain event during the wet season), 2) Moderate (mean wet season), and 3) Low (mean dry season). The high discharge case uses a South Fork Coos River discharge of 187 $m^3 \cdot s^{-1}$, which is exceeded ~25% of the time during a typical year. We use 19 $m^3 \cdot s^{-1}$ for the moderate case, which occurs 45% of the time in an average year, and $Q_r = 1.5$ $m^3 \cdot s^{-1}$ for the low discharge case, representing the remaining roughly 30% of time in a given year.

Using Eq. 3, we calculate the wind stress needed to balance the baroclinic pressure gradient force, with a mean water depth $H = 10$ m. Based on hydrographic sections (Sutherland and O'Neill (2016), the estuary length $L = 14$ km, while the salinity

gradient varies from 5 psu·km^{-1} (rainy season) to 1 psu·km^{-1} (dry season). Using this relationship, we estimate that a τ_{wx} of 0.2 N·m^{-2}, a typical storm-related magnitude, is comparable to the baroclinic pressure gradient. Hence, we develop experiments using two wind stress magnitudes, 0.2 N·m^{-2} and 0.1 N·m^{-2}, and two spatially-uniform wind directions, northward and southward. Hence, we have 24 total wind simulations to test the effect of four distinct wind types (weak and strong northward winds, and weak and strong southward winds) across the typical seasonal span of tidal and river forcing represented by the base cases (Sup. Table 2).

3.5 Data analysis

We employ an along/across estuary coordinate system for both observations and model output based on the local orientation of the channel thalweg. In this coordinate system, the along-estuary component is positive landwards. In the first 15 km, the estuary is parallel to the coast (in what we will call Main Channel, km 4 to 15) at which point it reverses direction around a U-shaped bend (North Bend). We define two cross-sectional transects (Figure 1) to explore the circulation before the bend (Cross section A), and after the bend (Cross section B). The channel portion landward of the bend will be referred to as East Bay Channel (km 15 to 22).

To explore the subtidal variability, we apply a 24-24-25 hour Godin filter to all the time series used. Hourly model outputs were further processed by averaging 2 days before the wind events, to obtain the "pre-event" values, and the 2 days during the wind forcing for the "event" analysis. Anomalies are calculated as event minus pre-event

16

values. We define the salinity gradient as the difference between the salinity at the mouth (S_{mouth}) and any distance along the thalweg at distinct depths. Stratification (ΔS) is calculated by differencing the surface and bottom values of modeled salinity fields, which along with along-estuary gradients can be affected by the lateral structure of salinity (Geyer et al., 2020).

4. Results

4.1 Observed estuarine conditions

We examine observed estuarine water properties, circulation, and forcing over two winter seasons and one summer season (Figure 2). The subtidal along-estuary velocity exhibits a clear two-layer pattern (Figure 2b), with down-estuary velocities at the surface and up-estuary velocities deeper than 7 m (Figure 3a). The upper several meters have velocities of -0.19 m·s^{-1}, with faster speeds (-0.21 m·s^{-1}) related to rain events in spring, summer and winter, at a lag of 31 hours from the peak discharge (Figure 2d, Figure 3a). The calculated barotropic component using Eq. 2 (Figure 2, 3), shows a unidirectional out-estuary flow, with stronger negative velocities at the surface during high discharge ($R^2=0.5$).

By subtracting the barotropic component from the ADCP measurements, the remaining field represents density-driven and wind-driven flow (Eq. 2; Figure 2b). Though the magnitude of the velocity of this residual depends on the choices made for the barotropic component (Eq. 2), the vertical distribution depends on the magnitude of horizontal pressure gradient and wind stress (Geyer, 1997). This residual field highlights

the bidirectional flow, with out-estuary velocities at the surface averaging -0.07 m·s^{-1} (±0.04 m·s^{-1} standard deviation), and up-estuary flow at depth of 0.06 m·s^{-1} (±0.04 m·s^{-1} standard deviation). During discharge events (Figure 3a), the whole water column moves in the out-estuary direction at the ADCP location. During the dry season (Figure 3a), surface layer along-estuary velocities decrease to their minimum values (-0.10 m·s^{-1}, Figure 3a). A clear spring-neap modulation is also present in the subtidal flow (Figure 2b).
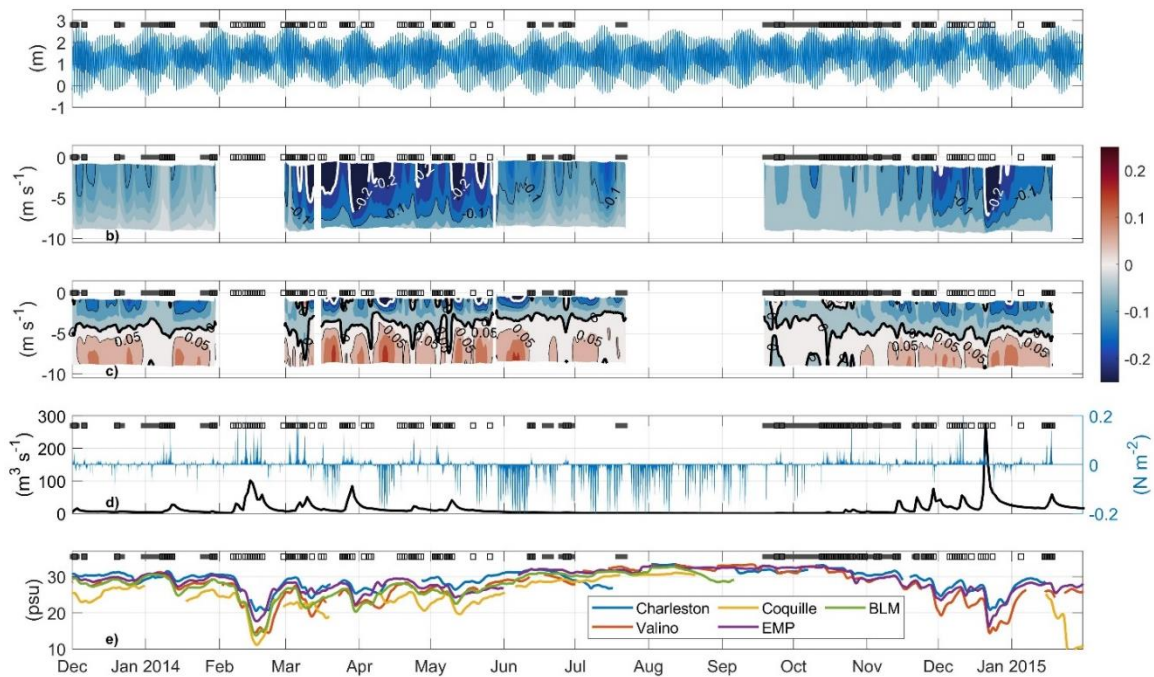
Figure 2. a) Sea level (m) at the Charleston tide station (Figure 1), (b) combined density plus wind-driven components of velocity calculated using Eq. 2, c) advective component of velocity calculated using Eq. 2, (d) river discharge at South Fork (left axis) and meridional wind stress at the North Bend airport (right axis), (e) salinity at water quality stations located throughout the estuary. Gray squares at the top of each panel represent times when subtidal near-surface velocities (<1.3 m of depth) are weaker than -0.1 m·s^{-1}, while black squares are shown at times when northward wind stress exceeds 0.1 N·m^{-2}.

18
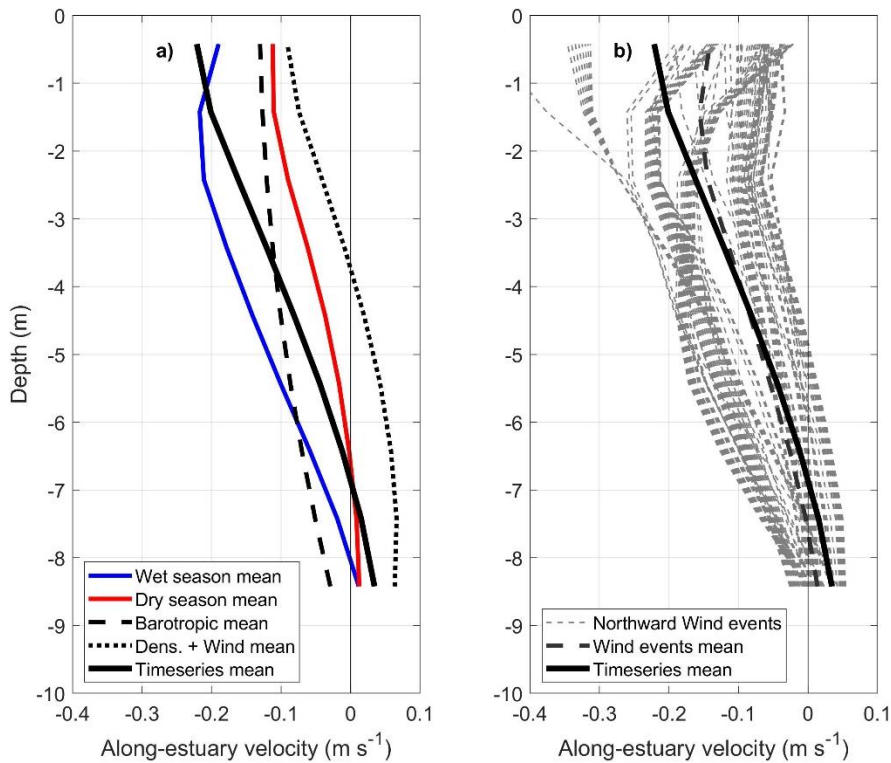
Figure 3. a) Subtidal velocity profiles from the ADCP location during high discharge (blue), during the dry season (red), and time series mean (black). Time series' barotropic component mean (broken line) and density + wind-driven component mean (dotted line) are also shown. b) Velocity profiles during northward wind events (thin gray lines), the wind-events mean profile (thick gray), and the overall time series mean (black).

Salinity varies seasonally in the estuary (Figure 2e), with relatively large magnitude freshening events detected in Main Channel (Coquille, BLM, Charleston) that coincide with discharge events between November and May (Figure 2d). The highest salinity values (>30) occur from July to October as the estuary accumulates salt due to reduced freshwater input. Higher salinities are also related to coastal upwelling events, e.g., in June 2014. CTD profiles show the water column to be strongly stratified in salinity close to the ADCP location during the rainy months (Sutherland and O'Neill, 2016), while during the drier months, stratification is reduced (Figure 4c). Based on the

19

CTD surveys, the observed along-estuary salinity gradient is positive in the rainy months (i.e., salt decreasing up estuary), while during the dry months these gradients are reduced and sometimes reversed, related to freshwater input from side channels (Figure 4a, Conroy et al., 2020).

4.2 Simulated estuarine conditions

We find a general agreement between observed and simulated estuarine dynamics, as evidenced by the behavior of the salt intrusion as a function of river flow (Figure 4b). Salinity gradients are relatively small across the low discharge cases, similar to the observed salt structure (Figure 4b). Observed and modeled stratification fall in a similar magnitude range, with increases in stratification related to increases in river discharge (Figure 4c). Under high discharge, stratification in Main Channel reaches maximum levels (1.5 psu·m^{-1}), where salty water enters the estuary due to the density gradient. Both the stratification and salinity gradient as a function of river discharge agree with the observed power law variability found previously by Sutherland and O'Neill (2016) (Figure 4).

The model matches observations of velocity and salinity at the ADCP location (Figure 5), and agrees with the previously validated, realistic simulations (Conroy et al. 2020). The subtidal along-channel velocity has a two-layer structure throughout the simulated time periods (Figure 5b, d), showing stronger magnitudes during spring tides and high discharge forcing, similar to the high-resolution model (not shown). Though the model shows slightly higher velocity magnitude at depth, the general structure of a two-

layer flow is observed throughout the time-series (Figure 5b, d). Similar to Conroy et al.,

(2020), the coarser resolution model also has a mean fresh bias during the dry season,

though this does not significantly affect the along-estuary salinity gradient. Due to this

fresh bias, the simulated salinity magnitudes do not match the observations (Figure 5),

most likely due to the idealized nature of the model forcing. Despite these small

differences, the model results give us confidence in using it to understand wind effects on

the estuarine salinity fields and circulation.
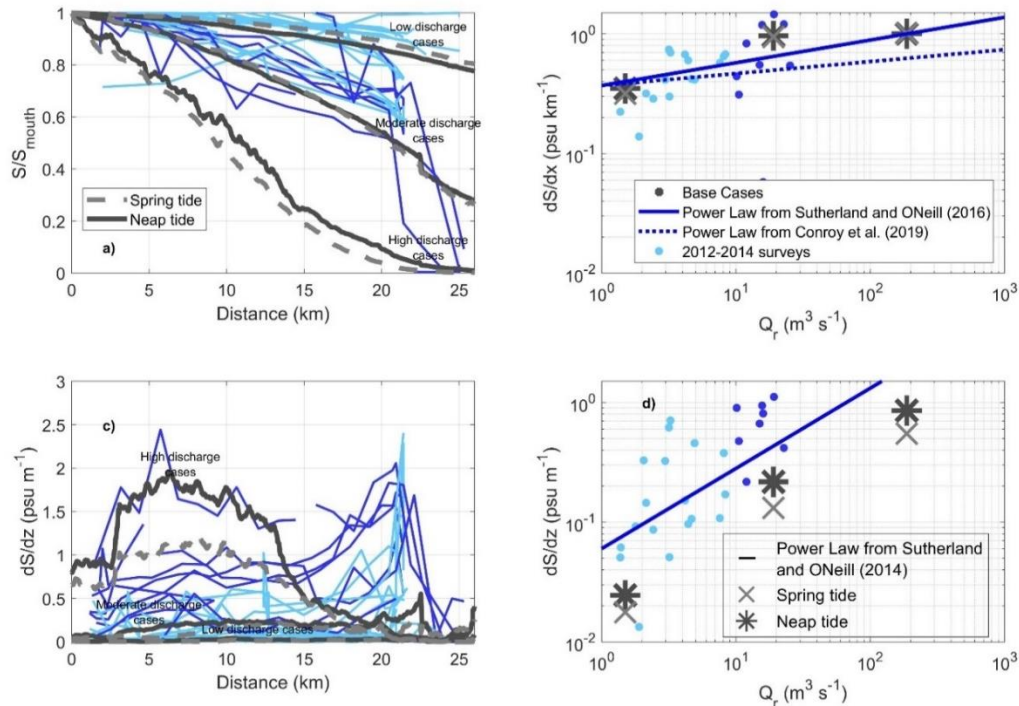
Figure 4. Base case, no-wind experiments (gray lines and symbols) vs. 2012-2014 surveys (colored by discharge – see Figure 4b). a) Depth-averaged salinity (S) normalized by the observed salinity at the mouth (S_{mouth}) as a function of along-estuary distance for the base cases and survey transects. b) Along-estuary salinity gradient for each base case (in gray crosses and asterisks) and observations as a function of river discharge, Q_r. c) Vertical stratification as a function of along-estuary distance for Base Cases and surveys. (d) Vertical stratification as a function Q_r. Black lines in b and d show a power law fit based on previous studies.

21

4.3 Observed wind events and estuary response

We find that the seasonally changing N-S wind component at the offshore
Stonewall buoy is significantly correlated to the sea level anomaly at the Charleston tide
gauge (R^2=0.45, at 18 hours of lag, with wind leading sea level), with positive anomalies
during storms, and negative anomalies in the upwelling season during southward wind
peaks (Sup. Fig. 1). Winds at the airport are also strongly correlated (R^2=0.62 with a 7-
hour lead) to the offshore wind at Stonewall.

Using the ADCP time series we find a total of 129 days when the subtidal out-
estuary upper layer flow in Main Channel was reduced to at least -0.15 m·s^{-1} (gray
squares in Figure 2). About 1/3 of these events (44 out of 129) were preceded by a
change in wind direction from southward to northward (highlighted with black squares in
Figure 2). Correspondingly, subtidal salinities (Figure 2e) show a slight increase with the
change in wind direction, followed by a strong decrease as Q_r increases, since the storms
also bring heavy precipitation. Velocity profiles during northward wind events (Figure
3b) show a reduction in out-estuary speed in the upper 5 m of the water column. This
depth-varying effect suggests the importance of the opposing wind stress, possibly
modified by additional barotropic effects (sea level set-up). The duration of the
northward wind events is approximately 1 to 2 days.

We use an example northward wind event to show the effects of τ_{wx} on the
circulation of the Coos Estuary (Figure 5). From 3 to 5-May-2014, τ_{wx} is mainly
northwards and peaks near 0.15 N·m^{-2}, while tides transition from spring to neap (Figure
5). Q_r is relatively constant at 10 m^3·s^{-1}, until 8-May when it increases to about 40 m^3·s^{-1}

at the same time a second wind event is observed. Surface subtidal velocity in Main Channel over this time period (Figure 5) varies between -0.3 and -0.1 m·s^{-1}, with the weakest out-estuary velocities during the wind event. Subtidal salinity fluctuations also respond to the decrease in out-estuary velocities with a salinity increase of 0.3 in Charleston, 0.15 in EMP and 0.5 in Coquille Figure 5). During the second wind event, a 0.1 salinity increase is registered in Charleston, 0.6 in EMP, and 1.9 in Coquille, until the discharge increases.

The wind record shows 51 events in which wind direction is southward during at least one day (Figure 2d). Southward winds within the estuary act in the same direction as exchange flow in Main Channel and opposite to the exchange flow in East Bay Channel. Velocity profiles at the ADCP location during southward wind events (Figure 2b) show a stronger out-estuary speed in the upper 5 m and stronger up-estuary speed at depth.

For the southward wind cases, we show an example from 18-May to 27-May (Figure 5). In this case, Q_r does not drastically change during the selected period, while τ_{wx} transitions to upwelling-favorable (southward) starting on 20-May, albeit with a strong diurnal variability. Velocities in this period show an increase at depth in the up-estuary direction with a peak of 0.05 m·s^{-1} on 21-May. At the surface, out-estuary velocities strengthen from -0.2 to -0.4 m·s^{-1}. Salinity in the estuary (Figure 5k) initially decrease when winds change direction, but then increases steadily during the upwelling-favorable conditions.
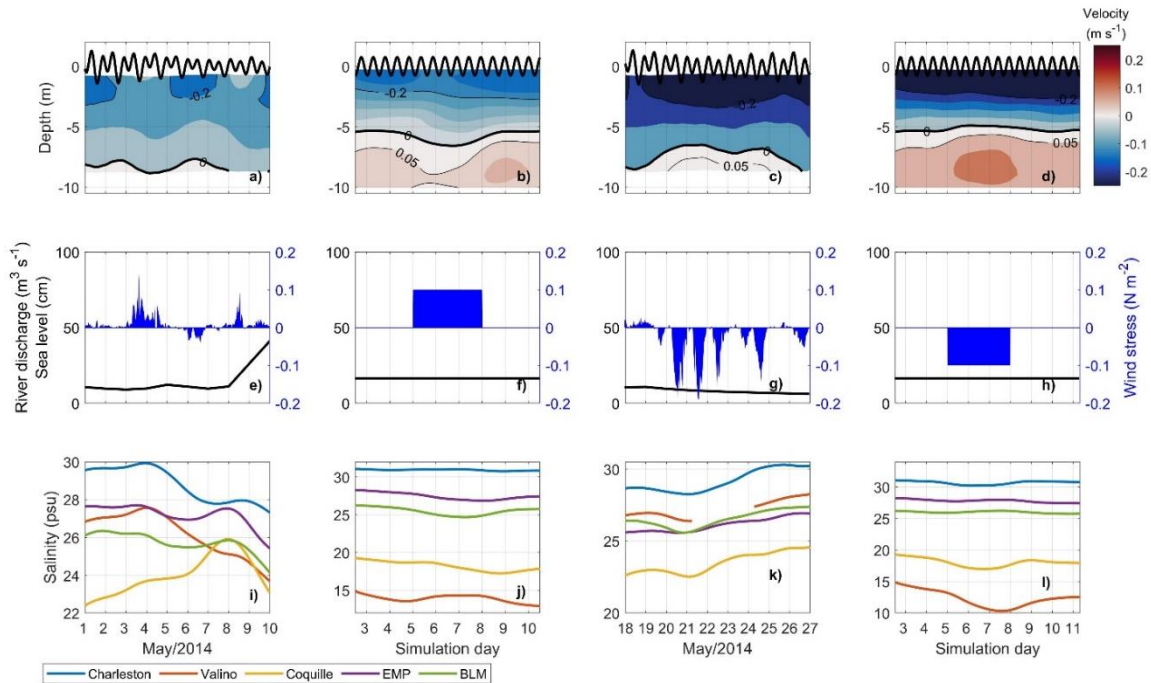
Figure 5. Comparison of observed and modeled conditions in the Coos Estuary during northward (1 to 10-May-2014) and southward (18 to 27-May-2014) wind events. (a) Observed subtidal along-estuary water velocity (m·s-1) at the ADCP location, from observations. (b) Same as in a, but from model output. (c) Same as in a, but observed during southward winds. (d) Same as in c, but from model output. (e) Observed South Fork discharge (black) and wind stress. (f) Same as in e, but from model input. (g) Same as in a, but observed during southward winds. (h) Same as in g, but from model input. (i) Observed salinity at three sites in Main Channel and South Slough. (j) Same as in i, but from model output. (k) Same as in i, but observed during southward winds. (l) Same as in k, but from model output. Notice the y-axis is different for all salinity plots. See Figure 1 for location of stations.

The magnitude of the wind's effect on estuarine circulation is modulated by tidal cycle as reductions in surface velocity occur more frequently during neap tides and transitions (87% of all events, Figure 2). However, despite this qualitative indication that reversal events occur more often during neap tides, it is difficult to disentangle the separate effects of wind, tidal influence, and river discharge on the observed subtidal flow from one location. Thus, we turn to the numerical simulations to examine the spatio-temporal influence of wind stress on the entire estuary.

24

4.4 Numerical simulations

4.5 Base cases

We use the no-wind base cases to characterize the circulation, salinity field, and stratification across the estuary over a range of tidal and discharge forcing. We find the strongest out-estuary velocities along the thalweg during high discharge conditions with an up-estuary flow only below 8 m depth (Figure 6a). During moderate and low discharge cases, velocities are in general smaller, with a shallower location at which velocities change direction (5 m, Figure 6d and g, Sup. Fig. 2). This response is similar to that observed at the ADCP location (Figure 3). In response to this velocity pattern, salinity varies significantly with river forcing, affecting both stratification and along-estuary gradient (Figure 6). During high discharge, stratification is increased along the estuary (Figure 4c), with nearly fresh water reaching Marshfield Channel ($S < 3$, 23 km from the mouth). Higher stratification is observed in Main Channel (1.59 psu·m^{-1} during neap, 0.98 psu·m^{-1} during spring tide) while in East Bay Channel, stratification is reduced (0.31 psu·m^{-1} during neap, 0.24 psu·m^{-1} during spring tide). During moderate and low discharge, stratification decreases (0.22 and 0.25 psu·m^{-1} on average over the estuary, respectively, Figure 6).

At the surface, subtidal flow under moderate discharge is directed along the thalweg, with stronger velocities under the neap tide conditions (Figure 7a) than during spring tides for the moderate discharge case (spring case not shown). The out-estuary flow curves around both North Bend and estuary mouth, converging towards the deeper

parts of the channel. During the moderate and low discharge cases, out-estuary velocity is

weaker than the high discharge experiments, allowing for salinities of 30 to be registered

at the surface further up the estuary (4 km in the moderate discharge case and 16 km in

the low discharge case - Figure 6), and decreasing stratification.
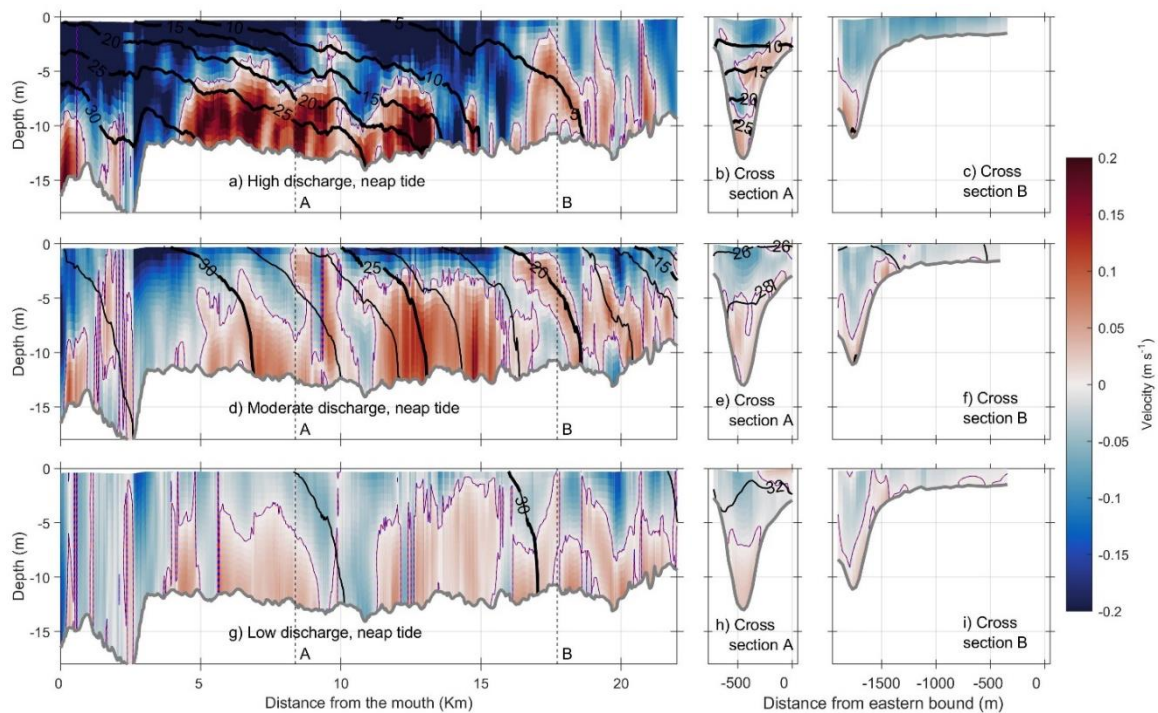
Figure 6. Salinity and along-estuary velocity distribution along the thalweg for the no-wind base cases under neap amplitude forcing and the three river discharges. (a) Subtidal along-estuary water velocity (color) and salinity (contours) along the thalweg, under high discharge. (b, c) Subtidal along-estuary water velocity (color) and salinity (contours) at Cross sections A and B, under high discharge. (d) Same as a, but for moderate discharge. (e, f) Subtidal along-estuary water velocity (color) and salinity (contours) at Cross sections A and B, under moderate discharge. (g) Same as a, but for low discharge. (h, i) Subtidal along-estuary water velocity (color) and salinity (contours) at Cross sections A and B, under low discharge. Location of Cross sections are shown in Figure 1.
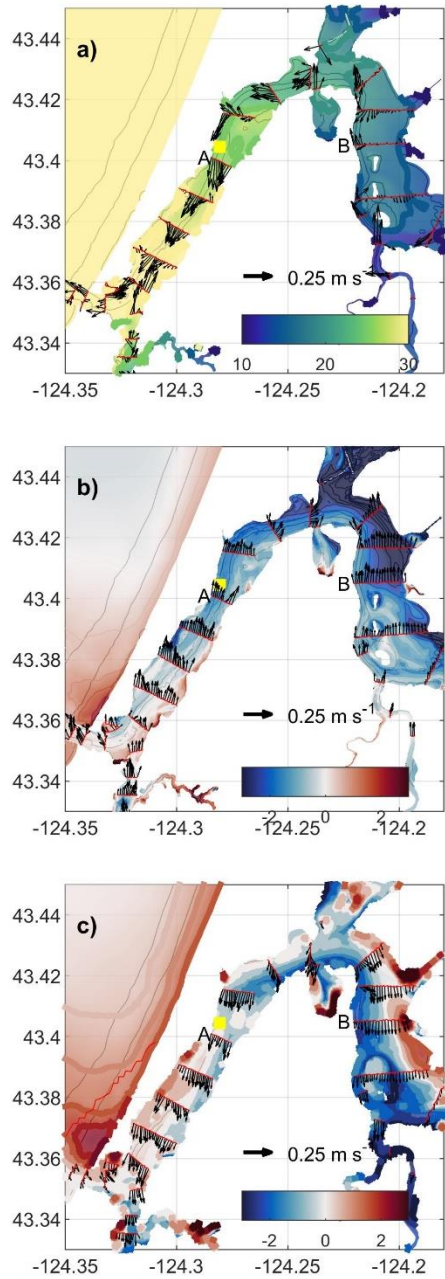
Figure 7. (a) Subtidal surface velocity (arrows) and surface salinity (contours) during neap tides and moderate discharge, averaged over 2 days for no winds (base case). (b) Subtidal surface salinity anomalies (event minus pre-event values in contours) and surface velocity anomalies (arrows) during weak northward wind event. (c) Same as b, but for the weak southward wind event. Location of the ADCP is marked with a yellow square.

27

The cross sections indicate that circulation in the estuary is more 3-D and complex than the typical 2-layer flow. For example, under high discharge, flow in Main Channel is laterally sheared (Figure 6b), while under lower discharge flow has a stronger vertical variability (Figure 6e, h). This produces salinity slightly enhanced on the eastern side, while the flow on the thalweg has lower salinities (Figure 7a). These differences are observed in East Bay Channel as well, where up-estuary velocity is observed in the thalweg and out estuary velocity is observed over the flats (Figure 6c, f, i). Lateral salinity gradients, induced by differential advection, can affect the along-estuary gradient and stratification, and in turn the effect that winds can have on estuarine circulation.

4.6 Simulated wind events and estuarine response

a) Northward wind events

Wind stress towards the north produces increased surface flow in the same direction, which in Main Channel is up-estuary and in East Bay Channel and South Slough is out-estuary (Figure 7b). This anomalous flow pattern leads to accumulation of fresher waters in North Bend. Our observations at the ADCP location, just south of the bend, agree with the results of our idealized experiments: an average decrease in salinity and velocity is observed at a time related to the change from no-wind to increased wind (Figure 5).

The full extent of our model allows us to explore the spatially-variable response to wind forcing of salinity and velocity, mainly due to the inverted U-shape of the Coos Estuary. We illustrate the overall estuarine response by focusing on the moderate

discharge case with neap tides, as many of the features are shared across all forcing ranges, and discuss the other cases where important differences emerge.

In the first few kilometers of Main Channel, salinity at the surface increases along the southern edge up to 7.5 km from the mouth (Figure 7b) due to wind straining (1-6 m of depth). In this area, fresher water is observed along the northern side, where out-estuary velocities are reduced (anomalies shown in black arrows in Figure 7b). In response to reduced velocities at the surface, exchange flow at depth is reduced as well (0.05 m·s^{-1} slower), producing fresher deep waters at the entrance of the estuary. In East Bay Channel, wind is in the same direction as exchange flow at the surface, and small positive anomalies are observed in the surface velocity field (northward arrows in Figure 7b). The freshest waters at the surface (4.5 fresher than base case) are accumulated on the northern side of North Bend, due to the enhanced surface flow from both sides of the bend pushing the less-dense waters in this direction (average 0.8 cm under high discharge, 0.2 cm higher water levels under moderate discharge, and 0.1 cm under low discharge). The general distribution of surface salinity anomalies is similar between spring (not shown) and neap tides; however, salinity anomalies are greater during neap tides due to enhanced stratification (Figure 8a).
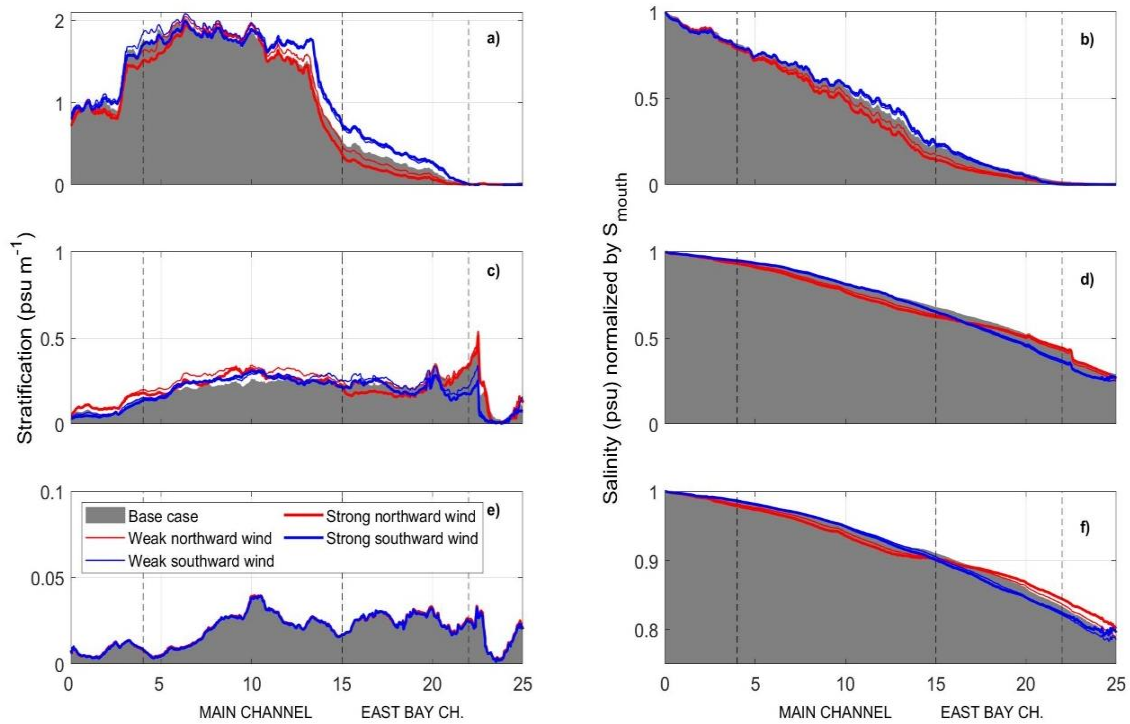
Figure 8. Stratification along the thalweg under neap tide for base cases (gray), northward winds (red) and southward winds (blue) for a) high, c) moderate and e) low discharge. Depth-averaged salinity (normalized by salinity at the mouth) under neap tide for base cases (gray), northward winds (red) and southward winds (blue) for b) high, d) moderate and f) low discharge. Width of lines dependent on strength of wind forcing. Note the range of stratification and salinity gradient is constrained to see variability landward of the mouth. Broken lines show Main Channel and East Bay Channel area.

Cumulatively, the impact of winds on salinity and velocity in the Coos Estuary is fundamentally influenced by the estuarine geometry and bathymetry (Figure 8). Strong northward winds increase the along-estuary depth-averaged salinity gradient under all river discharge cases and neap tide conditions. In the high river discharge case, the salinity gradient decreases 0.25 and 0.14 psu·km^{-1} in Main Channel and East Bay Channel, respectively. This difference in $\partial S/\partial x$ under high discharge is mostly driven by changes in the surface salinity (Figure 7b). In the moderate discharge case, salinity

gradient increases 0.18 psu·km^{-1} in Main Channel, while in East Bay Channel it increases

0.07 psu·km^{-1} (Figure 8b). Finally, in the low discharge cases, a difference of 0.05

psu·km^{-1} and 0.0009 psu·km^{-1} is observed in Main Channel and East Bay Channel,

respectively.

Stratification can be affected by winds via two methods: mixing and straining.

Due to wind straining, northward winds accumulate fresher waters in North Bend, while

at depth saltier waters are found close to the mouth and fresher waters in East Bay

Channel (Figure 9a). This produces a slight increase in stratification in Main Channel of

0.003 psu·m^{-1} (Figure 8c-d), while in East Bay Channel stratification decreases by 0.04

psu·m^{-1}, under moderate discharge. The strong stratification observed in the high

discharge base case in Main Channel increases under wind forcing (0.03 psu·m^{-1}), while

in East Bay Channel winds produce a decrease of stratification of 0.13 psu·m^{-1} (Figure

8a-b). The low discharge base cases have the highest salinities throughout the water

column. When northward winds are applied to that same low discharge case, stratification

increases a small amount (0.01 psu·m^{-1}) in Main Channel and a negligible amount in East

Bay Channel (Figure 8e-f).

Cross sections in the estuary show that the impact of winds on the Coos Estuary is

not symmetrical: at Cross section A (Figure 9b), slower out-estuary velocities are

observed in the upper layer, while at depth up-estuary velocities are strengthened.

Salinity is reduced at all levels, with greatest negative anomalies at the surface (-1.5). On

the East Bay Channel Cross section (B - Figure 9c), out-estuary flow above the thalweg is

enhanced at the surface due to winds forcing in the same direction as exchange flow. On

the flats, the out-estuary flow is slightly reduced producing the fresher water mass

observed in Figure 7b.
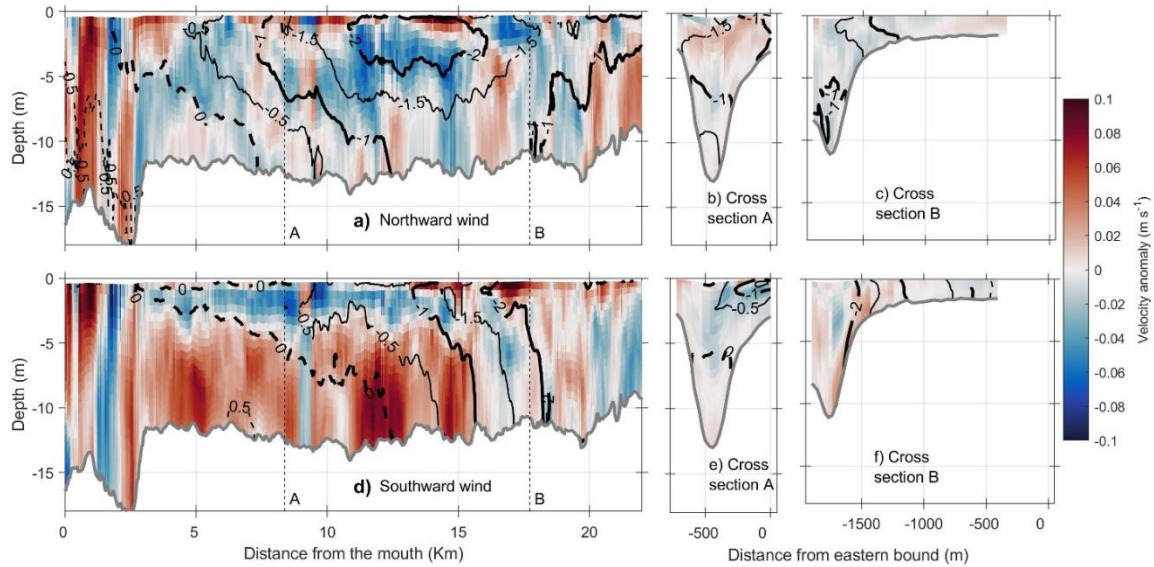
Figure 9. Velocity (color) and salinity (lines) anomalies under moderate discharge, neap tides, and weak northward winds (top panels) and for weak southward winds (lower panels). (a, d) show velocity and salinity in the thalweg and locations of Cross sections, (b, e) show velocity and salinity anomalies at Cross section A, and (c, f) at Cross section B. Location of Cross sections are shown in Fig. 1b.

Temporal changes to salinity averaged over the whole estuary volume are shown

in Figure 10. Before winds are applied, the estuary is losing salt under high and moderate

discharge. As northward winds are applied, fresher water is accumulated around North

Bend, which slightly increases salinity due to a reduced advective salt loss as winds are in

opposite direction. This slight increase of salinity continues after the winds are turned off

due to the remaining increase in salt at depth (Figure 9a). Increased salinity beyond North

Bend (Figure 8d) allows the estuary to increase salinity after the winds are turned off in

the low discharge cases (Figure 10c).

32

b) Southward wind events

Our numerical model results show that southward winds produce an enhanced outflow of fresher water at the surface, creating significant lateral and temporal variability, similar to the observations. At the ADCP location (Main Channel), winds act in the same direction as surface flow, strengthening exchange flow at the surface, while at depth, velocities become more landward due to upwelling at the coast, again similar to observations (Figure 5).

Southward winds move fresher waters away from North Bend and towards the southeastern side of Main Channel and western side of East Bay, where the thalweg is located (Figure 7c). The lateral gradient in velocity due to flow following the thalweg produces reduced salinity on the western side of Main Channel, observed at Cross Section A (Figure 9b). Increased out-estuary flow at the surface in Main Channel is accompanied by enhanced up-estuary velocity at depth, which produces higher salinities at depth in Main Channel. In East Bay thalweg, fresher waters are observed (1.5 fresher) due to reduced exchange flow which decreases the inflow of salty waters in the thalweg, while on the shallow flats the output of freshwater is moved towards Marshfield channel, producing slightly higher salinities (1.38, Figure 9f). This transport of waters south from both sides of the Bend produce in the moderate discharge case, a set down of 1.4 cm in the area (1.2 cm under high discharge and 1.5 cm under low discharge forcing).
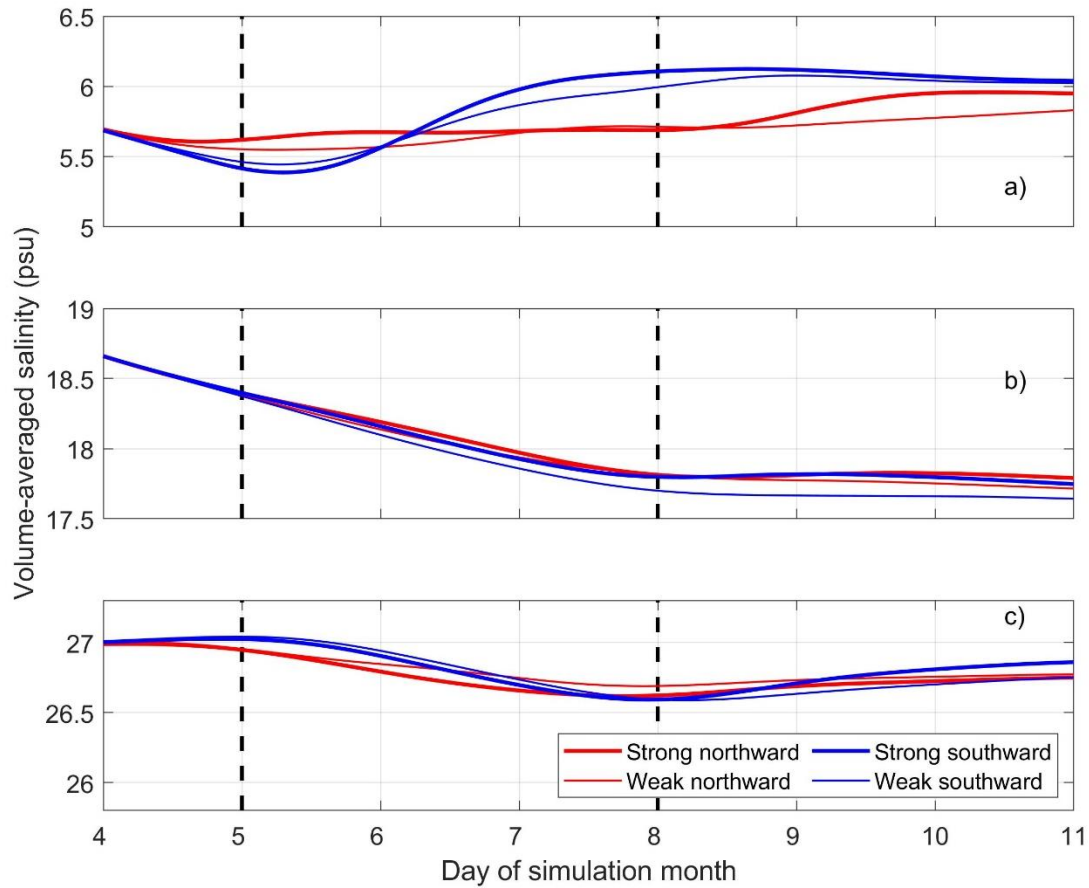
Figure 10. (a) Temporal variability of volume-averaged salinity over the whole estuary for the high discharge case. Different colors represent the direction of the wind forcing, while the line width depends on strength of wind forcing. Broken vertical black lines show when the winds are turned on and off. (b) Same as in a, but for moderate discharge. (c) Same as in a, but for low discharge.

As the length of the estuary changes with river discharge (Figure 4), the effects of southward winds on stratification and salinity gradient along the thalweg also changes spatially, especially due to the presence of North Bend (Figure 8). When southward winds are applied, stratification near North Bend increases, similar to what is observed under northward winds (Figure 8a, c, e). The change in stratification is tied to an increase in salinity due to increased up-estuary flow at depth, which in turn also increases $\partial S/\partial x$

(Figure 8b, d, f). Estuary-averaged salt shows that salinity initially decreases under high discharge, as winds are in the same direction as advection in Main Channel (Figure 10a). After a day of wind influence, salinity begins to increase due to a strengthened exchange flow which brings saltier water at depth in most of the water column (not shown). Under moderate discharge, the accumulated fresher water in East Bay Channel (Figure 9) is slowly exported from the estuary until salinity reaches a stable value of 17.7.

Interestingly, both wind directions increase the overall salinity of the estuary. However, the increase across the estuary is due to different processes: in the northward wind case, winds accumulate fresher waters in North Bend, due to reduced exchange flow in Main Channel and enhanced exchange flow in East Bay Channel, not allowing the fresher water out of the estuary. In the southward case, exchange flow is enhanced at the mouth due to wind straining at the surface and upwelling at depth, and secondary flow transports salt towards the shallow flats.

5. **Discussion**

Observations shown here indicate that despite the tidal dominance on setting the exchange flow magnitude in the Coos Estuary, strong winds can force reversals in surface velocities and influence the along-estuary salinity field (Figure 2, 5). Northward winds drive these reversal events in the Main Channel and occur more often under neap tide conditions (Figure 2). The numerical simulations support the observations, showing that northward wind stress weakens the out-estuary flow at the surface along the thalweg in Main Channel, while on the shallower portions flow is reduced or even reversed (Figure

9). Beyond the bend, the U-shaped geometry effectively reverses the direction of the wind's effect. That is, in East Bay Channel, northward winds act in the same direction as exchange flow at the surface, enhancing the exit of fresher water, leading to a pile-up of fresher water between 12 and 16 km. In contrast, southward winds shove surface waters towards the south, increasing the inflow of saltier waters along the northern boundaries of the estuary.

Our observations and modeling experiments show that despite the strong dependence of salinity gradient on river discharge and tidal forcing, winds can also affect the salinity gradient in the Coos Estuary (Figure 8). When wind forcing is turned on, the overall salinity increases under both northward and southward wind forcing, albeit with spatial and temporal variability (Figure 10): northward winds increase the salinity gradient in Main Channel due to a piling of fresher waters in North Bend, while southward winds increase it in East Bay Channel due to a transport of fresher waters south and upwelling at the mouth. Although high discharge events occur only 25% of the time, the estuary response to winds is amplified during those conditions due to an increased stratification and salinity gradient (Figure 8). Observations during northward winds (Figure 5) show that these changes to salinity and velocity seem to be transient, due to the onset of increasing river discharge that coincides with the storm event. Longer-lasting winds occur as observed under upwelling-favorable southward winds.

In Main Channel at depth, the exchange flow resembles the dynamics of a relatively simpler estuarine geometry (Monismith, 1986; Chen and Sanford, 2009; Li and Li, 2011). However, due to both the presence of a complicated channel curvature and the

abundant tidal flats, significant across-estuary variability develops in East Bay. These results emphasize the spatial variability that wind induces on estuaries with complex geometries (e.g., Coogan et al., 2020; Guo and Valle-Levinson, 2008; Purkiani et al., 2016; Valle-Levinson et al., 2001), or ones with channel-flats geometries (Ralston and Stacey, 2005; Geyer et al., 2020), both of which are common in estuaries across the PNW and the globe.

5.1 Wind-induced temporal variability of salinity

The Coos Estuary was found to be unsteady due to both strong tidal forcing and short timescales of river discharge events (Conroy et al. 2020). By accounting for wind forcing, which was neglected previously but varies on even shorter time scales then the river discharge, the salinity and velocity that characterize the Coos Estuary are changed (Figure 5). This combination of strong tides, episodic river forcing, and winds makes the Coos Estuary comparable to numerous other small, strongly forced systems (Simpson et al., 2001; Banas et al., 2004; Lerczak et al., 2006; Ralston et al., 2010a).

To explore the impacts of this unsteadiness, Chen and Sanford (2009) and Li and Li (2011) explored the impact of winds on the salt flux of an idealized, partially-mixed estuary, and illustrated an important temporal variability attributed to the adjustment of sea level due to a barotropic seiche (advective flux). Our results also show a barotropic sea level adjustment due to water piled in North Bend under northward winds (Figure 7b), and may explain the temporal variability of salinity in our observations (Figure 5, Sup. Fig. 3). Additionally, Conroy et al., (2020) shows enhanced eulerian flux of salt in

Main Channel due to higher levels of discharge, which affects the eulerian flux of salt. Our results show that under wind influence the exchange flow is affected due to winds being in opposite or the same direction at the surface. This additional eulerian flux would also increase the salinity gradient and shift salt flux towards the tidal and eulerian fluxes (Sup. Fig. 3).

5.2 Biological implications

Linkages between the physical and biological components of an estuary can be direct (e.g., currents advecting larvae through certain parts of a system), or indirect (e.g., changes to estuarine circulation lead to changes in temperature or salinity levels that affect organisms differently). Changes in the overall salt content of an estuary, whether due to river discharge, tides and/or winds, can thereby reduce or expand areas where larvae or other organisms can survive (Childers et al., 1990; Peterson, 2003; Teodósio et al., 2016). At the same time, changes in water level, including wind-driven changes, can decrease access of organisms to specific areas of an estuary where they can find shelter (Minello et al., 2012). Our study shows that wind forcing influences salinity in the Coos Estuary, with long-lasting changes (i.e., persistent days beyond the wind event, Figure 5). Though in some cases the velocity returns to its original values after the winds have been turned off, the estuary-averaged salinity does not return to its pre-event values (Figure 10). These significant changes occur especially when the river discharge falls within high (26% of the time) or moderate (45% of the time), accounting for >70% of each year. Additionally, there is enhanced salinity and velocity variability on tidal flats due to wind

forcing, related to processes such as lateral trapping (Okubo, 1973; MacVean and Stacey, 2011; Conroy et al., 2020). Tidal flats in an estuary lead to ebb-tide dominance (Fortunato and Oliveira, 2005), and may be of much importance to the lateral salt flux in shallow, strongly stratified estuaries, such as the Coos or the San Francisco Bay (Ralston and Stacey, 2007; Ralston et al., 2010b), due to the abundant amount of shallow areas.

The transport of less-mobile organisms, such as larvae, can be enhanced by winds. For example, in Chesapeake Bay, Hare et al. (2005) showed that the up-estuary flux of young fish larvae was dominated by a combination of tidal, wind, and residual bottom inflow. Our results also show wind-enhanced transport when winds are blowing northwards (Figure 10), with a stronger impact on the shallower parts of the estuary, e.g., stronger up-estuary flow on the eastern side of Main Channel (Figure 7). In the southward wind cases, the exchange flow is strengthened at the surface in the out-estuary direction, enhancing up-estuary velocities at depth. This deep pathway may be a channel for larvae, phytoplankton, contaminants and other buoyant particles, to access the estuary. Recently, during 2014, an increased population of green crab larvae was found in areas up to North Bend (Yamada et al., 2020), and latitudinally as far north as Puget Sound (Grason et al., 2018). This anomalous transport of green crab populations has been related to changes in basin scale patterns, such as marine heatwaves (Peterson et al., 2017) and El Niños (Brasseale et al., 2019). Within an estuary, the effect of changes in climatological wind patterns could lead to up-estuary transport of organisms to outside their observed range. Indeed, many climate change scenarios predict intensified winds in the PNW (Bakun et al., 2015).

Roegner et al. (2007) also found a significant correlation between larval recruitment and tidal processes, showing that larvae entered South Slough during neap tides and not with spring tides, with slightly enhanced recruitment under upwelling (northward) winds. Our results show that during neap tides both stratification and salinity gradients increase during the majority of forcing conditions allowing for larvae that are transported at depth to move further up-estuary (Figure 4). Additionally, this increase in stratification and salinity gradient allows for a stronger susceptibility of the water column to winds (Chen and Sanford, 2009), in which the residence times of organisms may increase (Geyer, 1997).

6. Conclusions

Observations from a year-long velocity time-series in the Coos Estuary, OR, show that under northward wind stress, the normal out-estuary exchange-flow pattern is reversed at the surface. Salinity at nearby water quality stations in the estuary show a slight increase during the initial onset of these winds, before quickly freshening due to the increased river discharge brought by the storm. Winds play two additional roles in the estuary, acting as an extra source of mixing that affect stratification and by piling up water that creates barotropic pressure gradient forces. These wind-driven processes affect the mainly tidally-driven estuarine circulation. Importantly, they affect the estuarine circulation disparately based on the geometry of the estuary that is an inverted-U shape, producing contrasting effects of the wind on each side of the bend.

We conducted numerical experiments to investigate the spatial and temporal variability of wind effects on circulation and salinity of the Coos Estuary, by looking at specific combinations of tides, river discharge and winds, and their effects on salinity and velocity distributions throughout the estuary. Despite the idealized characteristic of our forcing, salinity gradients and stratification show good agreement with observational data in Main Channel. Stratification is inversely proportional to river discharge, and during high discharge we find the highest stratification levels under neap tide conditions. When winds blow northward, anomalies in salinity and velocity are created due to fresher water piling up on the north side of the estuary. Additionally, changes are related to the reduction of velocity in Main Channel, due to winds opposing the direction of exchange flow, while beyond North Bend, winds act to strengthen the out-estuary circulation at the surface. In the case of southward winds, salt is pushed out-estuary at the surface in Main Channel, increasing stratification in the thalweg, and accumulating fresher waters along the southern side. Beyond North Bend, southward winds act in the opposite direction as exchange flow, keeping the fresher waters accumulated in East Bay Channel close to the thalweg, while shallower waters grow slightly more saline.

Changes to stratification and salinity gradient due to winds impact the flux of salt into and out of the estuary, which is not a transient effect and shows a strong dependence on the river discharge. Under high discharge, most of the impact of winds occurs in Main Channel, where winds exert opposite effects on the surface velocity: northward winds are in the opposite direction as exchange flow and the barotropic pressure gradient force for, while southward winds are in the same direction as both. After the winds have been

41

turned off, the accumulated fresh water exits the estuary at the surface while strengthened exchange flow at depth increases salinity slightly. Southward winds affect the lower part of the water column increasing salinity even after the winds have been turned off, due to upwelling at the mouth. Moderate and low discharge cases have a similar response to winds, however, due to reduced stratification and along-estuary salinity gradient, the effect on salt is smaller, producing the estuary to lose less salt and reaching a stable salinity after the winds have been turned off. Interestingly, in these lower discharge cases, due to reduced stratification, the effect of winds on circulation and salinity content is stronger on both sides of the estuary.

CHAPTER III

WATER TEMPERATURE VARIABILITY IN THE COOS ESTUARY AND ITS POTENTIAL LINK TO EELGRASS LOSS

This Chapter will be submitted to the J*ournal Frontier of Marine Sciences*. I am the lead author on the paper, developing the methodology, analyzing the data and writing the manuscript. David Sutherland (University of Oregon), served as advisor, aiding in data interpretation and manuscript editing. Alicia Helms (South Slough National Estuarine Research Reserve) provided eelgrass data, feedback on manuscript drafts and aided in manuscript editing.

1. Introduction

Estuaries act as mixing zones between oceanic and riverine waters, providing many ecosystem and cultural services (Milcu et al., 2013; Sherman and DeBruyckere, 2018; Zapata et al., 2018), and motivating numerous studies to examine the links between environmental conditions and ecosystem health (Costanza et al., 1997; Seppelt et al., 2011). In the Pacific Northwest (PNW; Figure 1), estuaries are influenced on the ocean side by the primarily wind-driven California Current System (CCS; Hickey and Banas 2003). These winds driving the CCS along the west coast of North America are forced by atmospheric circulation related to the North Pacific High and the Aleutian Low, which vary seasonally. In the winter the Aleutian Low migrates southward, producing downwelling-favorable winds along the PNW, while in summer the North Pacific High

migrates northward producing southward-directed upwelling-favorable winds (Huyer 1983; Hickey and Banas 2003; Davis et al. 2014, and others). Upwelled waters on the PNW continental shelf are typically colder (Figure 1b), with higher salinity, higher nutrients and lower oxygen levels. During winter, storms produce episodic river discharge events that result in lower salinity, lower temperature and higher turbidity along the coast (Hickey and Banas, 2003; Huyer et al., 2007).

The CCS has significant hydrographic interannual variability on top of its seasonality (Figure 1c). These interannual variations are dominated by the El Niño Southern Oscillation (ENSO), where positive values of the Ocean Niño Index (ONI) are related to higher temperatures and sea level at the mouth of PNW estuaries (Wyrtki, 1984; Huyer et al., 2002). On decadal time scales, variations can be related to the Pacific Decadal Oscillation (PDO) and the North Pacific Gyre Oscillation (NPGO), which emerge as the first and second principal components of sea surface temperature and sea surface height, respectively (Di Lorenzo et al., 2008; Capotondi et al., 2019). The NPGO correlates with wind stress in the North Pacific, with weakened wind-driven upwelling occurring when the index is negative (Di Lorenzo et al., 2008). A positive PDO pattern, which is associated with a strengthened Alaskan gyre, is correlated to increased coastal upwelling between 38°N and 48°N (Chhak and Di Lorenzo, 2007; Di Lorenzo et al., 2008). Marine heatwaves in the PNW are a result of decreased surface cooling in the Gulf of Alaska and decreased equatorward Ekman transport due to the atmospheric ridge (Di Lorenzo and Mantua, 2016; Capotondi et al., 2019). In addition, the anomalous high-amplitude ridge system in the North Pacific that brought drought conditions to the PNW

exacerbated the increased water temperature caused by a marine heatwave. During the winter of 2013, a marine heatwave termed the "Blob" (Bond et al., 2015) was observed in the North Pacific and moved onto the shelf from Sep-2014 until Mar-2015, increasing SST more than 1.5ºC at the Stonewall buoy. Positive anomalies (>1.5ºC) were observed at Stonewall again from Jul-2015 to May-2016 related to another marine heatwave (Di Lorenzo and Mantua, 2016; Gentemann et al., 2017). During 2014–2016, when the Coos Estuary showed anomalously warm waters, the Equatorial Pacific was anomalously warm due to an El Niño event (Jacox et al., 2016). The triad of Sep-Oct-Nov 2014 ONI index registered SST anomalies greater than 0.5 ºC in the Niño 3.4 region (5ºN-5ºS, 120º-170ºW), which led to an officially declared El Niño in the Equatorial Pacific (https://origin.cpc.ncep.noaa.gov/). Though this first El Niño warm pulse was weak (0.5 ºC in May-2014), another El Niño event produced SST anomalies of 4 ºC in 2015, with maximum anomalies between Nov-2015 and Jan-2016. Positive anomalies were observed in this ENSO area until March-April-May 2016, with a peak of anomalies of 2.6 ºC at the end of 2015.

Notably, anthropogenic global warming is resulting in increased temperatures as well, which are predicted to increase stratification and reduce availability of nutrients higher in the water column, akin to the variations observed during El Niño years (Schneider, 1993; Di Lorenzo et al., 2009; Barnard et al., 2017).

The seasonal patterns in the continental shelf hydrodynamics influence the ecology of the PNW ocean and estuaries. For example, many local fish and invertebrates spawn in the winter to ensure the retention of pelagic eggs and larvae nearshore

(Logerwell et al., 2003; Bi et al., 2011; Shanks et al., 2020). Plants are also influenced by the seasonal patterns in temperature. For example, eelgrass (*Zostera marina*) carries fewer leaves in the winter, while in the summer, they present a greater number of longer and thicker shoots (Phillips et al., 1983). This marine flowering plant forms broad meadows in intertidal and shallow subtidal flats, as well as fringe meadows on steeper shorelines, hence specific genotypes are selectively adapted to different habitats and environmental stressors (Phillips, 1984; Hessing-Lewis et al., 2011). Thom et al. (2003) showed the greatest densities of eelgrass in the Coos Estuary, OR, were found in the most marine-influenced sites. These sites had a smaller seasonal temperature range, while the stations further away from the mouth of the estuary were subjected to broader temperature ranges, higher turbidity, and lower salinity.

Many environmental parameters, outside a specific species-dependent range, can cause stress on the fauna and flora of estuaries, including salinity, water temperature, turbidity, light availability, air temperature, water velocity, and nutrient levels (Thom et al., 2003; Echavarria-Heras et al., 2006; Lee et al., 2007; Nejrup and Pedersen, 2008; Kaldy, 2012, 2014; Salo and Pedersen, 2014; Basilio et al., 2017; Daly et al., 2017). For example, declines in eelgrass populations have been observed in the PNW and were related to increased water temperatures after the 1997-1998 El Niño event (Thom et al., 2003). Water temperatures above 25°C can significantly reduce photosynthetic and respiration rates (Nejrup and Pedersen, 2008; Gao et al., 2017; Beca-Carretero et al., 2018), inhibit leaf growth (Zimmerman et al., 1989), as well as increase susceptibility to eelgrass wasting disease (Kaldy, 2014; Groner et al., 2021). As a response to warm

seasons, *Z. marina* may respond by reproducing sexually through the production of

flowers and seeds (Lee et al., 2007). These seeds can also be affected by temperature by

changing the size and chemical composition (Jarvis et al., 2012; Delefosse et al., 2016),

and if the temperature stress is perennial, the eelgrass beds may not be able to survive

(Jarvis et al., 2012).
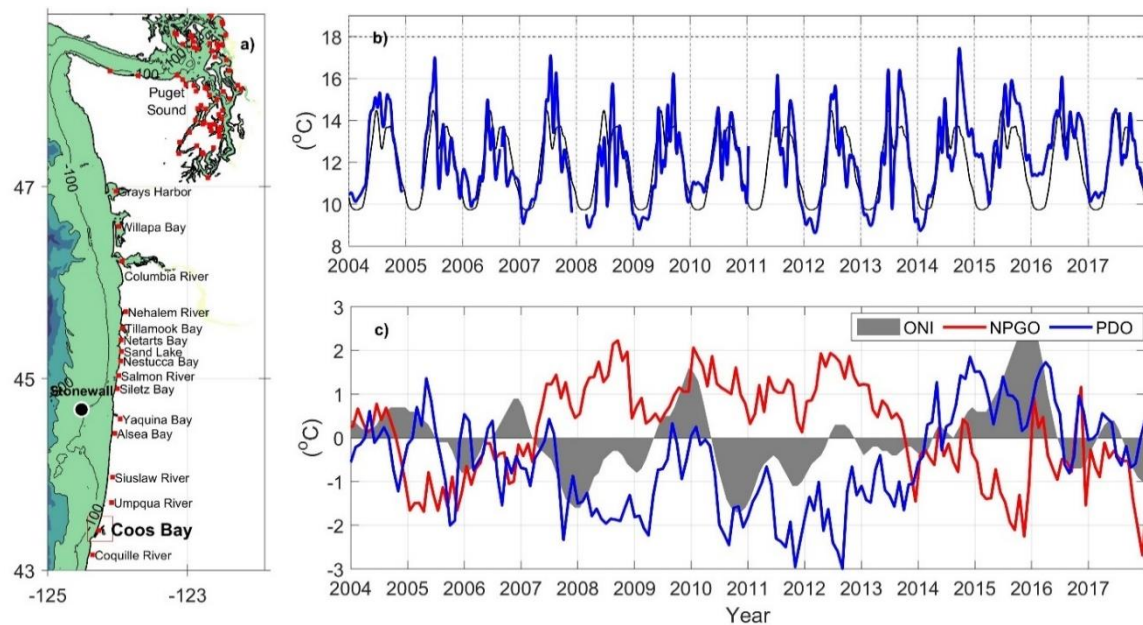
Figure 1. a) Estuaries in the PNW where eelgrass (Zostera marina) is present, including our study area (Coos Bay), and the Stonewall buoy (black circle). b) Water temperature at the Stonewall buoy with the climatological mean calculated for 2004-2014 (black) and the daily averaged values with a 30-day low pass filter (blue). c) Basin scale indices (water temperature anomaly): Oceanic Niño Index (ONI; gray area), North Pacific Gyre Oscillation (NPGO; red line), Pacific Decadal Oscillation (PDO; blue line).

Here, we study the seasonal and interannual variability of water temperature

within the Coos Estuary to explore its links with a recently observed decrease in eelgrass

abundance. Using long-term observations, we evaluate the impact of the ambient ocean

conditions, river discharge and atmospheric heat flux on the water temperature in the

estuary. Our observations show that temperature varies locally and seasonally across specific regions of the estuary, much like the observed eelgrass declines, and is driven by a combination of basin scale variability and local forcing modulated by bathymetry.

2. Study area

The Coos Estuary is located inshore of a narrow continental shelf south of Stonewall Bank (Hickey and Banas, 2003) and is the second largest estuary in Oregon in terms of area and volume (Figure 1). Water temperatures inside the Coos Estuary are significantly correlated with continental shelf values as measured by the Stonewall buoy (Strub et al., 1987; Miller and Shanks, 2004; Huyer et al., 2007). At the Stonewall buoy, temperature shows seasonal variability related to the CCS circulation patterns: equatorward winds drive cold upwelled waters towards the coast during the summer, while during the winter southward winds produce downwelling accompanied with warmer waters. On top of the seasonal variability, several warm-water events have been registered at the Stonewall buoy, including El Niño events which produced 1-2°C anomalies (Huyer et al., 2002; Peterson et al., 2017). Other events include the marine heat waves related to atmospheric high-pressure ridges, which in 2014 produced an anomaly of 7°C in 1 hour at the Stonewall buoy (Gentemann et al., 2017; Shanks et al., 2020). These ocean properties are then further transported towards the mouth of the estuaries in the PNW and can travel up-estuary at a rate on the order of 10km d^{-1}, at least in the case of Willapa Bay (Hickey and Banas 2003).
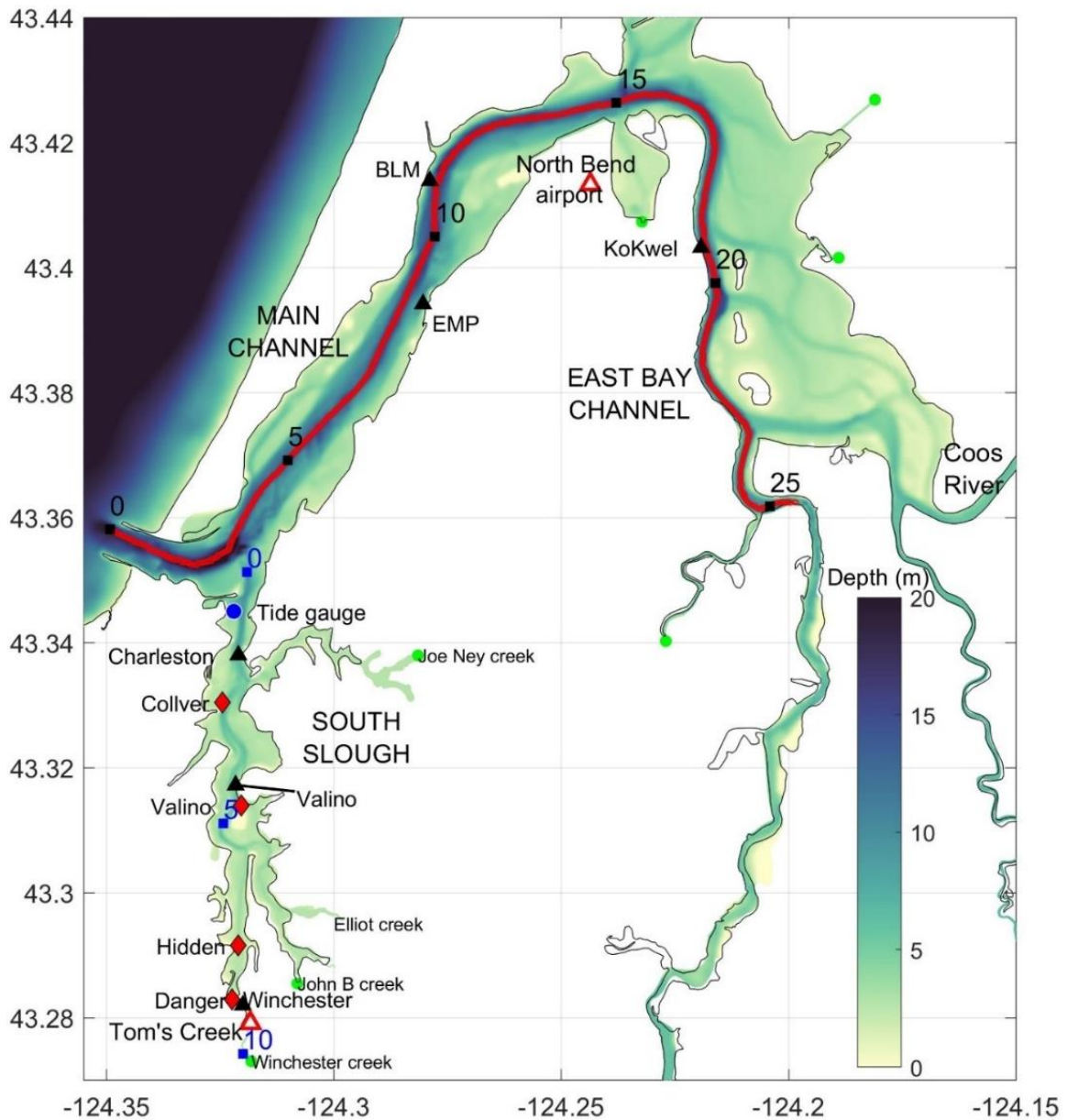
Figure 2. The Coos Estuary, showing bathymetry in meters below mean sea level (colored contours) and the location of water quality monitoring stations (black triangles), meteorological stations (red triangle), tide gauge (blue circle), freshwater sources (green circles), and eelgrass stations (red diamonds). Black numbers refer to distance (in km) from the mouth along the thalweg; blue numbers show distance (in km) from the intersection of South Slough with the main estuary.
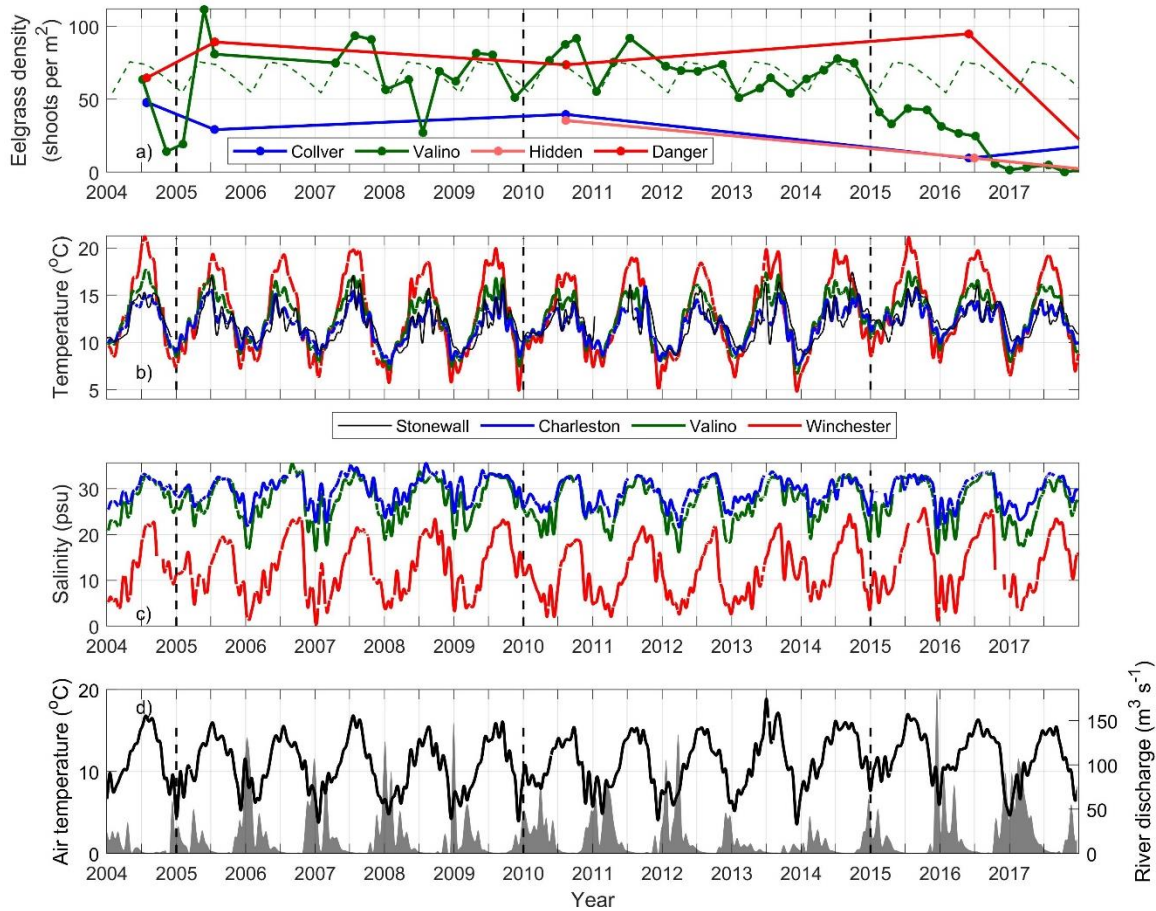
Figure 3. a) Eelgrass density at 4 stations in South Slough. The 2004-2014 climatology for Valino is shown in broken green line. (b) Long-term hydrographic characteristics at 4 SSNERR stations, Charleston WQ (blue), Valino WQ (thick green), Winchester WQ (red) and the Stonewall buoy (black), showing low-pass filtered water temperature over 2014–2018. (c) same as in (b) but for salinity. (d) Air temperature at the North Bend Airport meteorological station (black) and South Fork of the Coos River discharge (gray). For locations, see Figure 2.

The propagation of oceanic signals into the estuary is produced by a combination of baroclinic, barotropic and diffusive processes, which are dependent on the geometry, depth, and forcing characteristics of each estuary. The main channel of the Coos Estuary (Figure 2) is annually dredged from the mouth to 24 km up-estuary near the Coos River entrance, to maintain 11 m of depth and 91 m of width (Eidam et al., 2020). Adjacent

tidal flats, inlets and sloughs branch out of the main channel; these shallow areas range between 0.5 m above MLLW to 1.0 bellow MLLW of depth, extend approximately 15 km^2 and provide the primary habitat for *Zostera marina* (Emmett et al., 2000; Groth and Rumrill, 2009; Eidam et al., 2020). The main source of freshwater is the South Fork Coos River in the eastern portion of the estuary (Figure 2), which has a total discharge that ranges from 2 to 800 m^3 s^{-1}, with maximum peaks related to wintertime storm events. Additionally, there are numerous other sources of freshwater, including the Winchester, Elliot and Joe Ney Creeks that feed into South Slough. South Slough is a shallow sub-estuary that trends southward about 3 km from the mouth of the main estuary. South Slough has a natural depth of 5 m in its un-dredged sinuous channel. South Slough is home to the South Slough National Estuarine Research Reserve (SSNERR), which maintains the water quality stations and conducts eelgrass surveys throughout the main estuary and in South Slough.

The subtidal estuarine exchange flow in the Coos Estuary is relatively constant throughout the year as it is dominated by tides, with a small secondary increase in winter as river discharge ramps up (Conroy et al., 2020). The main semidiurnal tidal constituent, M$_2$, height amplitude is 0.8 m, with mean tidal currents of 1 m s^{-1} resulting in a tidal excursion of 14 km (Baptista, 1989). Sutherland and O'Neill (2016) showed that the Coos Estuary has characteristics of a salt-wedge during high river discharges, a well-mixed estuary during low discharges, and a partially-mixed estuary during moderate discharge times. They also found that, as in other estuaries in the PNW, Ekman-driven upwelling moves high-salinity, low-temperature, high-nutrients, low-oxygen waters into

the estuary (Sutherland and O'Neill, 2016). Though estuaries are expected to be exporters of nutrients (e.g., Roegner et al., 2002, 2011), Roegner and Shanks (2001) found that the Coos Estuary, specifically the seaward portion of South Slough, is an importer of nutrients in the summer, due to the close proximity of the coastal ocean.

3. Methods

3.1 Environmental conditions

Water properties, sea level, river discharge and meteorological conditions were assessed using data from several monitoring stations located throughout the estuary, with most data inside South Slough (Figure 2 and Table 1). Charleston Bridge, Valino Island and Winchester Arm stations are telemetered to provide near real-time data access by SSNERR (http://nvs.nanoos.org). Temperature, salinity and various other parameters, are measured automatically every 15 minutes at all stations (Figure 3). The instruments are maintained monthly to limit biofouling by SSNERR (NOAA National Estuarine Research Reserve System (NERRS), 2020).

River discharge data from the South Fork Coos River gauge (Figure 2, Table 1) from 2003 to present were used as a proxy for the variation in freshwater input to the estuary. Additionally, there are river discharge and water temperature data at Winchester Creek, the main source of freshwater entering the landward end in South Slough, available from 2011 and 2013-2016 (Figure 2 and Table 1). Hourly tidal height time series were obtained from a NOAA tide gauge in Charleston (Figure 2 and Table 1).

Table 1. Information on oceanographic and meteorological stations analyzed in this study. Locations shown in Figure 1. Instrument height above bottom is shown, as depths change tidally.

Station	Institution	Date range	Water depth / Sensor height (m)	Distance from mouth (km)
Eelgrass sampling stations				
Collver Point	SSNERR	2004–present	Intertidal	4.5
Valino Island	SSNERR	2004–present	Intertidal	6.3
Hidden Creek	SSNERR	2010–present	Intertidal	8.8
Danger Point	SSNERR	2004–present	Intertidal	9.9
Water quality stations (water temperature, salinity)				
Charleston Bridge (CH)	SSNERR	2002–present	4.0 / 0.5	3.0
Valino Island (VA)	SSNERR	1999–present	2.4 / 0.5	5.6
Winchester Creek (WI)	SSNERR	1995–present	1.1 / 0.5	7.1
Empire Docks (EMP)	CTCLUSI	2011–2014	6.0 / 0.5	6.9
North Spit BLM	CTCLUSI	2008–2016	10.5/0.5	8.2
KoKwel Wharf (Coquille)	Coquille Indian Tribe	2013–2017	19	18.6
Sea level from tide gauge				
Charleston #9432780	NOAA	1991–present	3.0 / –	3.0
Meteorological stations (wind, air temperature)				
North Bend airport WBAN #24284	NOAA	1949–present	5.1 (elev.)	12.5
Stonewall buoy NDBC #46050	NOAA-NDBC	1991–present	3.8 (elev.)	147.5
Charleston Met. Station	SSNERR	2001–2015	9–11.4 m above ground	5.2
Tom's Creek Met. Station	SSNERR	2016–present	1.5–4.0 m above ground	10.1
River gauge station				
South Fork of Coos River. St.#14323600	Coos Watershed Association	2003–present	44 (elev.)	49
Winchester Creek	Coos Watershed Association	2010–2011; 2015–present	3.5 m (depth of channel)	10.8

Meteorological data were obtained from stations both offshore and on land. Offshore wind data, taken to be representative of upwelling or downwelling conditions at the coast, were obtained from the NOAA Stonewall Bank buoy (Figure 1), approximately 120 km north of the estuary. We use the hourly wind data to calculate the along-shore north-south component of wind stress (Large and Pond 1981). Surface water temperatures were also obtained from the Stonewall buoy at hourly intervals. On land, wind velocity data were extracted from a meteorological station at the North Bend Southwest Oregon Regional Airport (Table 1, location shown in Figure 2). Additionally, SSNERR maintained a time series of wind and other meteorological variables at Charleston from 2001-May 2015. This station was later moved to Tom's Creek in 2016. Due to the lack of data during 2015, we use data from the airport location to characterize the wind forcing. The North Bend airport also provides air temperature, relative humidity, barometric pressure, total solar radiation and precipitation.

3.2 Eelgrass (*Zostera marina*) in the Coos Estuary

Changes in the environmental conditions of an estuary have been observed to modify the seasonal trends of *Zostera marina* (Table 2). Due to the observed response of *Z. marina* to temperature, salinity and turbidity (Table 2), we use eelgrass as a proxy of response to environmental stressors in the Coos Estuary. The availability of observations and the importance of eelgrass to the ecosystem here and worldwide (e.g., Short and Coles, 2001) makes it a relevant system to explore. Table 2 synthesizes the current

literature on temperature, salinity and turbidity on eelgrass density in estuaries in the

PNW. Importantly, there is spatial and temporal variability amongst different areas.

Table 2 Temperature, salinity and turbidity optimal physiological values and thresholds for the survival of *Zostera marina* in the Pacific Northwest.

Parameter	*Optimal values*	*Threshold*	*Location*	*Season/Month*	*Source*
Temperature	10–20 °C	>18 °C	Coos Bay, OR	July-August (1998-2001)	(Thom et al., 2003)
	16–19.1 °C	>18 °C	Willapa Bay, WA	July-August (1998-2001)	(Thom et al., 2003)
	15–23 °C	>25 °C (stressful) >30 °C (lethal)	Yaquina Bay, OR (collected)	In lab	(Kaldy, 2014)
	15.4–24.2 °C	>32 °C	Puget Sound, WA		(Phillips, 1984; Thom et al., 2018; Thom & Albright, 1990)
		1.5 – 2.5 °C above normal	San Diego, CA		(Johnson et al., 2003)
Salinity	24.5–32.1 psu		Coos Bay, OR	July-August (1998-2001)	(Thom et al., 2003)
	13.3–29.2 psu		Willapa Bay, WA	July-August (1998-2001)	(Thom et al., 2003)
Turbidity or Irradiance		limited to substrates where at least 1% of the incident light remains	South Oyster Bay, Long Island Sound, New York		(Phillips, 1984)

SSNERR surveys eelgrass in the Coos Estuary, including quarterly to annual

monitoring of percent cover, shoot density, canopy height and flowering shoot counts at 4

locations in South Slough (Table 1). Collver Point, Valino Island, Hidden Creek, and

Danger Point, are sampled using SeagrassNet and NERRS biomonitoring protocols

(Short et al., 2006). Eelgrass characteristics are sampled at 0.25 m^2 quadrats along

permanent transects during low tides (Sup. Fig. 1). From 2004 to 2015, Valino Island

transects contained 12 plots, and from 2016 to present 6 plots were added to the low and

mid transects for a total of 18 plots. The location of these transects allow to sample the

variability of eelgrass in the intertidal zone.

There are different ways of assessing eelgrass in an estuary using remotely-sensed

techniques, such as airborne lidar or vessel-mounted sonar systems. In the Coos, estuary-

wide eelgrass presence was obtained through aerial photography and high density lidar

intensity images in 2005 and 2016 with the aid of the US Environmental Protection

Agency (EPA) and the Pacific Marine and Estuarine Fish Habitat Partnership (PMEP),

respectively (Clinton et al., 2007; Sherman and DeBruyckere, 2018). In May 2005, false

color, near-infrared aerial photography was used, with validation surveys done in situ to

classify the number of pixels belonging to a given habitat (e.g., density of eelgrass) that is

covered by the specific habitat (Sup. Fig. 2a). In July 2016, airborne, multispectral

imagery was collected for Coos Bay which was used to develop a scheme that only

determined the presence/absence of eelgrass beds (Sup. Fig. 2b).

3.3 Climatology and statistics

In order to compare the oceanographic and meteorological conditions of the Coos

Estuary between 2014-2016 with the years before the observed eelgrass decline, we used

the available data from 2004-2014 to calculate daily averages and standard deviations. Once the daily climatology was calculated, event-driven variability was filtered out by using a low-pass 30-day filter. Correlations between time series were calculated at different time lags, with significance level of 95%, using the large N (number of observations) approximation $\hat{\rho}_{crit}(\alpha, N) = \frac{q_t\left(\frac{\alpha}{2}, N-2\right)}{\sqrt{N}}$, where q_t refers to the Student's-t distribution with N-2 degrees of freedom, and α is the lower-tail confidence region, in our case 0.05. The water-year climatological cumulative river discharge was calculated from October 1st to September 30th, from 2004 to 2014 We define dry conditions in the estuary to be values below 95% of the climatological cumulative discharge value.

4. Results

4.1 Climatological environmental conditions in the Coos Estuary

Water temperature and salinity levels in the Coos Estuary are influenced by the atmosphere (wind and heat fluxes), ambient ocean conditions, and river discharge (Figure 3). During the winter, storms produce enhanced northward winds locally over the estuary (Figure 4). These same storms bring rain, increasing river discharge into the estuary episodically (Figure 4). Over the climatological period examined here (2004-2014), river discharge between November and May reached an average of 32 m³ s⁻¹ (although peaks in distinct years show much higher individual event magnitudes), after which is a dry period between June and October, where the average discharge decreased by an order of magnitude to 3.2 m³ s⁻¹ (Figure 4d). The average water-year cumulative discharge

calculated for the South Fork Coos River is 6330 m^3 s^{-1}. In a typical year, 90% of this

cumulative discharge is accumulated between November and April.
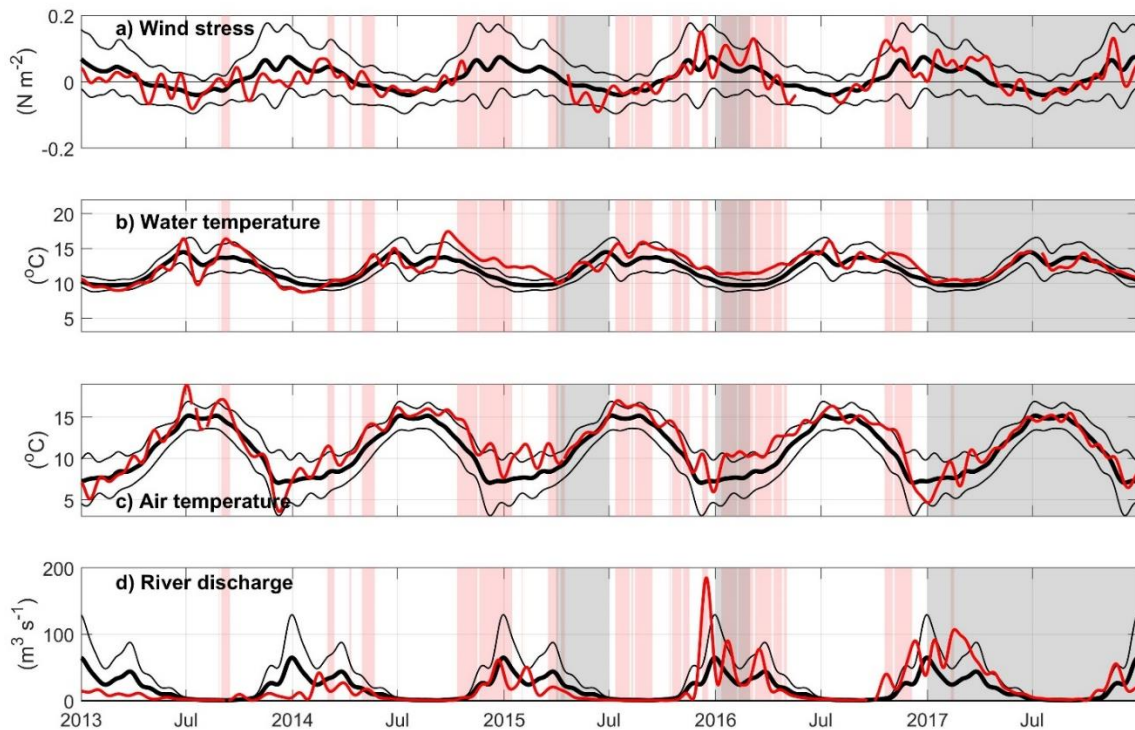
Figure 4. Environmental conditions outside the estuary during 2013-2017. a) Daily averages with a 30-day low pass filter of North-South wind stress (N m^{-2}) from the North Bend Airport meteorological station (red lines) showing 2004-2014 climatological mean calculated for 2004-2014 (thick black lines), thin black lines show ±1 standard deviation. Vertical red bands show periods in which water temperature at Charleston WQ is 1 standard deviation above the 2004-2014 climatology (Figure 6d). Vertical gray bands show periods in which eelgrass density at Valino is at least 1 standard deviation below the 2004-2014 climatology. b) same as (a) but for surface water temperature (°C) at the Stonewall buoy, c) same as (a) but for air temperature (°C) at the North Bend Airport meteorological station, d) same as (a) but for South Fork Coos River discharge (m^3 s^{-1}).

During the dry summer, air temperature reached maximum values of 13.5°C at

the North Bend airport station, while in winter, values below 8 °C were recorded (Figure

4c). Outside the estuary, water temperatures at the Stonewall buoy location (Figure 4b)

showed a similar pattern of seasonal variability: during the summer, temperatures

increased (average 13 °C), albeit with event-driven decreases in temperature between July and September when upwelling brings colder waters to the coast. During the winter, colder water temperatures were observed at Stonewall (average 10 °C), related to wintertime atmospheric heat loss.

Inside the estuary, the 2004-2014 climatology of water temperatures show maximum values between July and October (Figure 5), which coincides with the highest air temperature values (Figure 4c) and reduced freshwater input (Figure 4d). The highest water temperatures were observed in stations further away from the mouth (KoKwel and Winchester) during this season (Figure 5). Salinity was also high during the dry summer period with maximum values at the station closest to the mouth (Charleston, 29.2 psu). Winchester Creek data (Figure 6f) showed that river temperature increases yet remains ~2 °C cooler than both the Valino and Winchester locations in the estuary. At the end of the dry period, before freshwater increases, Charleston WQ (station closest to the mouth of the estuary) registered temperatures up to 3.5 °C colder and 9.6 psu saltier than Winchester WQ (station furthest up-estuary in South Slough), due to the influence of upwelling on the coastal ocean (positive wind values in Figure 4a). Valino WQ (station located mid-estuary in South Slough) also registered the influence of cold salty upwelled waters, while Winchester WQ and Winchester Creek temperature continued to increase (Figure 5).
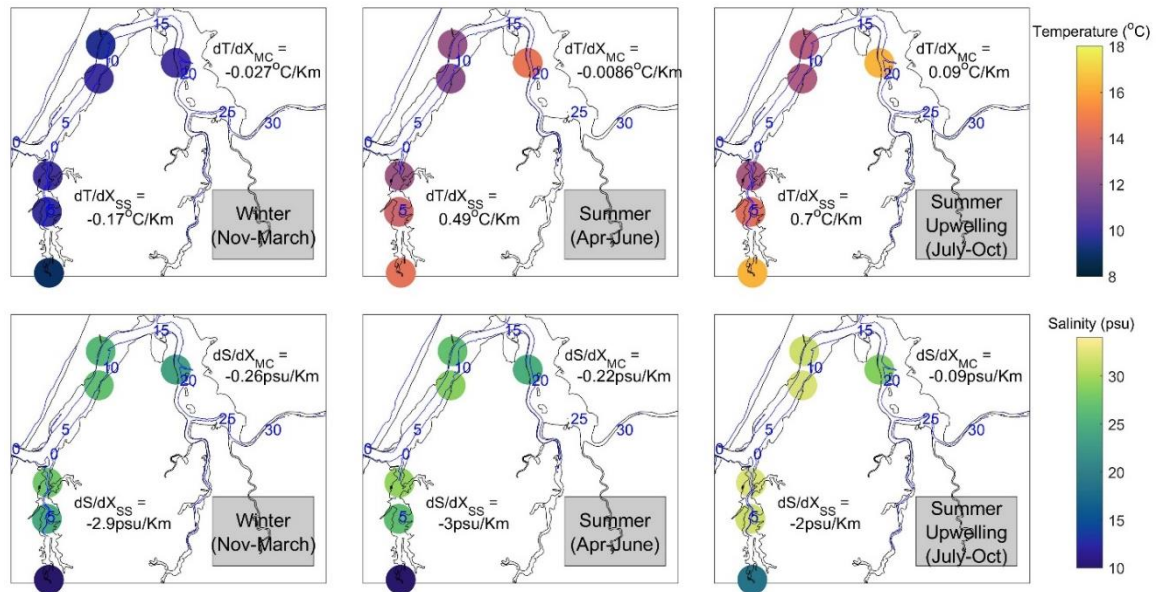
Figure 5. Spatial distribution of temperature (top plots) and salinity (bottom plots) 2004-2014 climatology derived at stations inside the Coos Estuary during Winter (left), Summer (middle) and Upwelling (right) time periods. Blue numbers refer to distance (km) from the mouth along the thalweg in the main channel and along the channel in South Slough.

The rainy period, from November to March, was characterized by colder waters in Winchester Creek (Figure 6f). During this season all stations had similar temperatures (Figure 5), with even lower peaks during increases in discharge related to storms (Figure 4b). Due to the increase in freshwater input, salinity decreases, with lowest values in the stations closest to the river mouths (Winchester and KoKwel Wharf). Despite KoKwel Wharf being closer to the input of freshwater from Coos River, temperature is slightly higher (10.2 °C, Figure 5). Long time series for the EMP, BLM, and KoKwel Wharf WQ stations were not available, however, existing data from 2013-2016 (Figure 6a-c) shows the strong seasonal pattern of temperature and salinity in these stations within the main channel. Salinity is highest at EMP, the station closest to the mouth, while KoKwel

Wharf (closer to the main freshwater source) responds with greater amplitude variations

to storm events (i.e., much fresher during February).
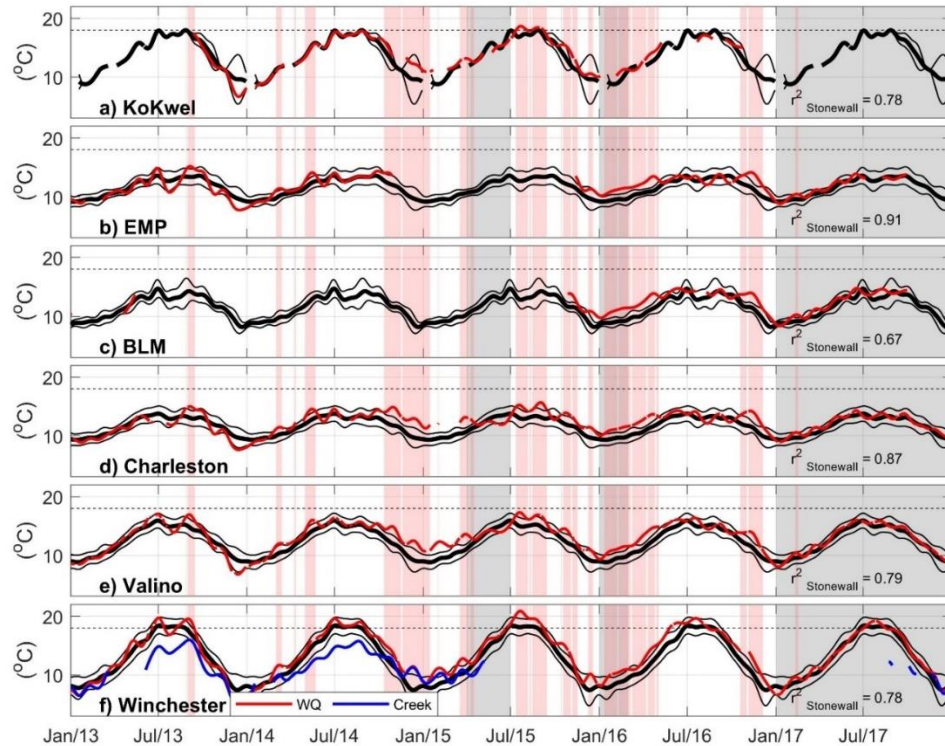
Figure 6. Coos Estuary water temperature during 2013-2017, thick black lines show 2004-2014 climatological mean, thin black lines show +/- 1 standard deviation, thin red line shows daily averages with a 30-day low pass filter. Red bands show periods in which water temperature at Charleston WQ is 1 standard deviation above the 2004-2014 climatology (Figure 6d). Gray bands show periods in which eelgrass density at Valino is below the 2004-2014 climatology by one standard deviation. Correlation between Charleston WQ and the Stonewall buoy shown in text (significance level = 0.04). a) KoKwel Wharf, b) EMP, c) BLM, d) Charleston, e) Valino and f) Winchester WQ and Winchester Creek (blue). 18 °C eelgrass temperature threshold in broken black line for reference.

4.2 A few stressful years

A combination of anomalous atmospheric and oceanic processes occurred in the

PNW from late 2013 until 2017: during the winter of 2013, "The Blob" was observed in

the North Pacific due to a high-pressure system, moving into the shelf from Sep-2014

until Mar-2015, increasing sea surface temperature more than 1.5 ºC (the eelgrass

threshold, Figure 1b). At the end of 2014, a strong El Niño event was registered in the

Equatorial Pacific (up to 2.6 ºC anomalies by the end of 2015, Figure 1c), influencing the

PNW with warm anomalies of more than 1.5ºC from Jul-2015 to May-2016, with

additional input of heat due to another marine heatwave (Figure 1b). These anomalies

would exceed the temperature threshold for eelgrass in the PNW (Table 2).
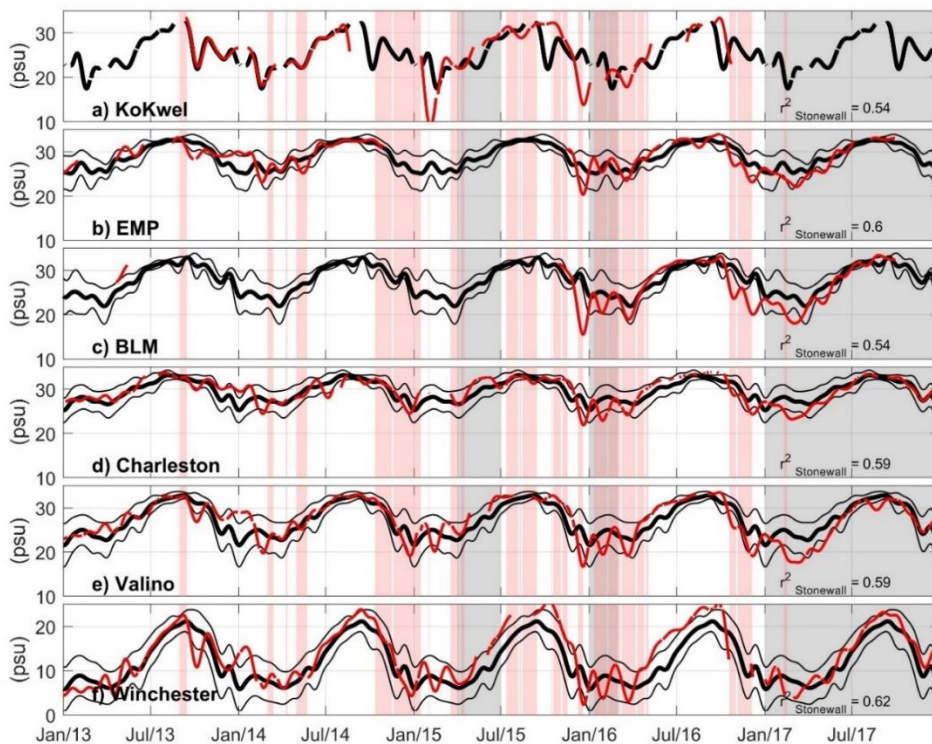
Figure 7. Coos Estuary salinity during 2013-2017, thick black lines show 2004-2014 climatological mean, thin black lines show ±1 standard deviation, thin red line shows daily averages with a 30-day low pass filter. Red bands show periods in which water temperature at Charleston WQ is 1 standard deviation above the 2004-2014 climatology (Figure 6d). Gray bands show periods in which eelgrass density at Valino is below the 2004-2014 climatology by one standard deviation. Correlation between Charleston WQ and the Stonewall buoy shown in text. a) KoKwel Wharf, b) EMP, c) BLM, d) Charleston, e) Valino and f) Winchester WQ.

The persistent high-pressure also impeded the arrival of winter storms in 2013-2014, reducing river discharge and increasing air temperature at the estuaries in the PNW (Wang et al., 2014). During the winter of 2013-2014, the PNW experienced drought conditions reflected in the below-average water-year cumulative discharge at the South Fork Coos River location: 3240 m^3 s^{-1} during 2013, and 4750 m^3 s^{-1} during 2014, only 50% and 71% of the 2004-2014 climatological cumulative of 6330 m^3 s^{-1}, respectively (Figure 4d). Lower river discharge is also related to the higher-than-average salinity during 2013 and 2014 (Figure 7). During this warm period, the Coos Estuary experienced extended time periods with water temperature ≥1.5ºC than the mean: Charleston WQ registered 107 of the anomalously warm days during 2014, 116 days in 2015 and 146 days in 2016 (Sup. Fig. 3, calculated using the low-pass filtered data). The intrusion of anomalously warmer water in the Coos Estuary is especially noticeable during the Fall and Winter of 2014–2016 (Figure 6). In fact, of the days ≥1.5 ºC the mean, 80% occurred during the winter months of October to December. In Oct-2014, water temperature registered 1 standard deviation above the mean at KoKwel Wharf, Charleston, Valino and Winchester, until the following Apr-2015. From Jul-2015 until May-2016, anomalously warm waters were again observed, with short periods within 1 standard deviation of the mean. Despite the proximity of Valino WQ and Winchester WQ to the ocean boundary (5.6 and 7.1 km respectively, Figure 2), these stations showed a greater number of days with temperature anomalies above 1.5 °C in 2013-2016 compared to other water quality stations at similar or greater distance (Sup. Fig. 3). Winchester Creek also showed waters 2°C warmer than its 2004-2014 climatology in 2015, when discharge values were close

to normal (Figure 6f). These temperatures were close to the estuarine water quality station at Winchester, during the rainy winter season of 2015 (Figure 6f).

5. **Discussion**

Water quality, river discharge, air temperature, and wind stress data all demonstrate the strong seasonality in the Coos Estuary that mimics the larger scale CCS patterns (Figure 3). Warmer, saltier estuarine characteristics are observed between April and June, after which upwelling-favorable conditions produce cold, saltier waters at the ocean boundary, which finally transition to rainy, fresher and colder conditions in the estuary due to increased precipitation and reduced solar input. This seasonality is affected by interannual variations of the surrounding atmosphere and ocean, which modulate the estuary on all its boundaries, i.e., from the ambient ocean waters at its mouth, the river discharge input, and the atmospheric heat fluxes on its surface. However, the results do indicate that there is significant spatial variability in how the estuary responds to these larger-scale interannual variations due to local bathymetry and geometry constraints. For example, during the warmer years of 2014-2016, Valino WQ and Winchester WQ are relatively warmer for extended periods of time than stations that are further away from the mouth (e.g., BLM, KoKwel). This disparate response to environmental forcing may stress species, such as eelgrass, which occupy distinct regions of the estuary. By disentangling the impact of the temporal variations in estuarine water forcing with spatial factors (e.g., depth and distance from the mouth), we provide a framework to discuss how

64

changing estuarine conditions might stress organisms differentially. We start by 1) examining changes outside the estuary at the basin scale, then move into 2) along-estuary gradients and spatial variability in hydrographic conditions before considering 3) long-term temporal variability due to the expected future warming under anthropogenic climate change. Finally, we examine the dramatic eelgrass decrease observed within the Coos Estuary in the context of the temperature variability described above.

5.1 Basin scale variability

Though many organisms grow in wide temperature ranges, a persistent anomaly may stress organisms such as eelgrass beyond recovery (e.g., >1.5 ℃ above normal, Table 2). During the winter of 2013–2014, the PNW experienced drought conditions, related to a persistent atmospheric high-pressure ridge linked to variability in the North Pacific Oscillation (Figure 1), a known precursor of El Niño conditions (Wang et al., 2014; Di Lorenzo and Mantua, 2016). The high-pressure also affected the arrival of winter storms in the PNW, resulting in the below-average water-year cumulative discharge in the Coos River (Figure 4d) and increased air temperature in the Coos Estuary (Figure 4c). This combination produced anomalously warm water temperatures during 2014 in the Coos Estuary. During the winter of 2013, the "Blob" was observed in the North Pacific and moved onto the shelf from Sep-2014 until Mar-2015, increasing SST more than 1.5℃ at the Stonewall buoy. Positive anomalies (>1.5℃, Figure 1b) were observed at Stonewall again from Jul-2015 to May-2016 related to another marine heatwave (Di Lorenzo and Mantua, 2016). During the El Niño event in 2015 SST

anomalies of 4 ºC where registered at the Stonewall buoy, with maximum anomalies between Nov-2015 and Jan-2016. This El Niño event increased the likelihood of storms and precipitation in the PNW, increasing river discharge at the Coos River, as registered during 2015-2016 (Alexander et al., 2002; Goodman et al., 2018). This atmospheric connection also reduces upwelling-favorable winds which would normally bring colder waters during the late summer to the Coos Estuary (Capotondi et al., 2019).

Though the El Niño conditions can have a strong impact on the PNW, observational and modelling efforts (Jacox et al., 2016) indicate that the temperature anomalies observed on the continental shelf (Figure 1b) were mostly related to the marine heatwave. At the Stonewall buoy, the combination of these basin-scale processes produced enhanced water temperature (>1.5ºC warmer than the 2004-2014 climatology) during the fall and winter of 2014, 2015 and slightly during 2016 (Figure 4b). The warm anomalies were slightly reduced during the upwelling seasons of each year but picked up again after the winds started to relax (Figure 4a). These anomalies were observed in estuaries from San Francisco Bay (up to 3ºC, Cloern et al. 2017), to Puget Sound (up to 1 ºC, Jackson et al. 2018). In the Coos Estuary, anomalies up to 2ºC, where observed in Charleston, 3 km from the mouth in March-2015. Increased water temperature at the ocean boundary will increase the heat that can be advected into the estuary and alter the along-estuary temperature gradient.

5.2 Along-estuary differences in temperature

Water temperature and salinity levels in estuaries are controlled by the interaction of advective fluxes, atmospheric fluxes and exchanges with the ocean boundary at the estuary mouth and the river boundaries at each freshwater input (Smith, 1983; Stevenson and Niiler, 1983). Our subtidal data show that estuarine temperature is strongly correlated to the temperature variability on the nearby continental shelf, but the correlation weakens with distance from the mouth (Sup. Fig. 4). Additional spatial variability is induced by the heterogenous input of freshwater: the main estuary receives the input of the largest magnitude sources of river water (>10 freshwater sources) while South Slough has fewer sources with relatively smaller magnitudes (374 m^3 s^{-1} for the entire estuary, 8.8 m^3 s^{-1} for South Slough). The differential discharge will affect the advection of heat throughout the sub-estuaries, as well as the retention time of heat, salinity or any particulates within an area. Though tidal advection is a major factor in the estuary (Conroy et al., 2020), South Slough shows greater temporal temperature variability than the main channel, most likely due to a combination of shallower channels and increased areas of tidal flats (Sutherland and O'Neill, 2016).

A qualitative approach to the heat budget in the Coos Estuary allows one to spatially and temporally fingerprint the anomalously warm water in the estuary during 2014–2016. The heat budget for an estuarine volume is determined by advective fluxes, atmospheric fluxes and exchanges with the boundaries (Smith, 1983; Stevenson and Niiler, 1983). Here, we define a simplified heat budget for a shallow and vertically well mixed estuary as

$$\frac{\partial T_{av}}{\partial t} + u_{av} \frac{\partial T_{av}}{\partial x} + Residual = \frac{Q_0}{\rho C_p h} \tag{1}$$

where T_{av}, v_{av} and u_{av} are depth-averaged temperature and horizontal current

(along-estuary and across-estuary), respectively. We neglect several terms in the full heat

budget, which are contained in the "Residual" term in Eq. 1 and are described next. Since

surface to bottom differences in temperature in the Coos Estuary are out of phase with

sea level differences, as well as with velocity (Roegner and Shanks, 2001; Conroy et al.,

2020), we assume heat divergence and entrainment are small. We also neglect the vertical

heat flux through the sediment at the bottom, given the turbidity in the estuary as well as

the amount of vegetation that both reduce the exchange of heat between the sediment and

the water (Evans et al., 1998; McKay and Iorio, 2008). The first term in Eq. 1 represents

the storage of heat in the water column, and is a partially measurable variable, since the

measurements are only obtained at a single depth (0.5 m). Sutherland and O'Neill (2016)

show that in most of the profiles along the estuary, temperature isolines are nearly

vertical, indicating well-mixed conditions. Hence, we assume that the point

measurements represent the water column, though this assumption is most uncertain

during high discharge (Sutherland and O'Neill, 2016). In the Coos Estuary, heat storage

at Valino WQ and EMP WQ (Figure 8a) is very small and does not show a clear seasonal

pattern. The second term in Eq. 1 represents the horizontal advective flux divergence of

heat past a point in the along-estuary direction. The across-estuary advective heat flux

divergence is also ignored as we can assume that the across-channel velocity is 2

magnitudes smaller than the along-estuary component. The term on the RHS expresses

the atmospheric heat flux, where Q_0 is the net surface heat flux, ρ is density averaged

over the water column and C_p is the specific heat of sea water, both calculated as a function of temperature and salinity, and h is the time-varying (t) water depth. Given that the atmospheric heat flux is inversely proportional to depth, enhanced heat flux is expected in shallower areas, on average, such as South Slough.

The surface heat flux, Q_0, may be decomposed into the incoming solar short-wave radiation, outgoing longwave radiation, latent heat exchange due to evaporation or condensation, sensible heat exchange at the surface and heat exchange due to precipitation (assumed here to be negligible). Shortwave and longwave radiation, obtained from the NCEP-NCAR Reanalysis (Kalnay et al., 1996) at the land location closest to the Coos Estuary (123.75ºW, 44.7611ºN) have the greatest magnitudes, with values that fluctuate seasonally between 250 and 50 W m^{-2} (shortwave) and -90 and -50 W m^{-2} (longwave) similar to other studies in the PNW (OSU, 1971; Yang et al., 2011; Rinehimer and Thomson, 2014). Sensible and latent heat fluxes are estimated using bulk formulae from the MATLAB Air-Sea toolbox (https://github.com/sea-mat/air-sea), using the water quality parameters at Valino WQ and the meteorological observations at the North Bend airport. Sensible and latent heat, though smaller, also show a seasonal pattern with positive values in July and August, related to wind and the air-sea temperature difference. Sensible heat flux releases heat from the sea surface to the atmosphere when the water is warmer (most of the year except between July and September), while latent heat releases heat due to evaporation, though it can be suppressed during upwelling-favorable wind conditions (May to September). Figure 8b shows that Q_0 is highest in the summer and lowest in the winter. Compared to the 2004-2014 climatology, Q_0 during

2014–2016 was anomalously positive (when data are available), mainly due to the shortwave radiation from March to July in those years, and parallels the anomalously high air temperature (Figure 4c). In the Coos Estuary, as in other estuaries in the PNW, depth is modified heavily by humans: dredging in the main channel occurs once a year along the main channel, while in South Slough no dredging occurs and the channel sits at a more natural depth (~5m). Hence, more temperature variability due to atmospheric heat flux is expected in South Slough than in the main channel.
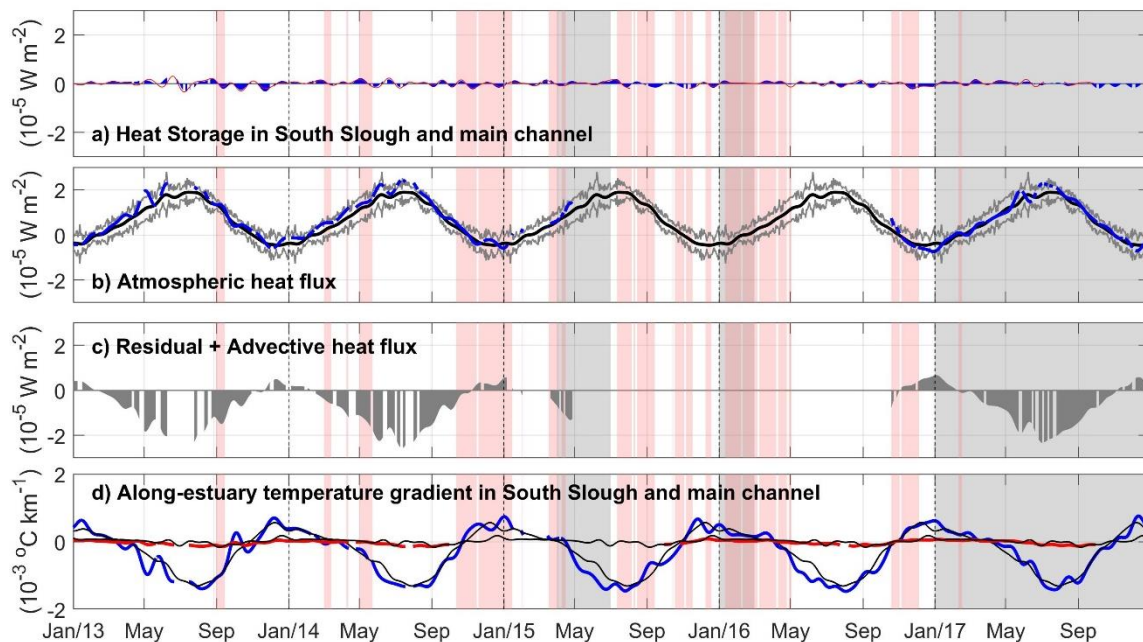
Figure 8. Heat budget components in the Coos Estuary during 2013-2017. (a) Heat storage in South Slough (blue) and the main channel (red). (b) Atmospheric heat flux using data from the Valino water quality station. (c) Residual + Advective heat flux (Heat storage minus Atmospheric heat flux), and (d) Along-estuary temperature gradient in South Slough (Charleston to Winchester) in blue and in the main channel (Charleston to KoKwel Wharf) in red. Positive $\partial T_{av}/\partial x$ indicates that the station closest to the ocean is warmer than the station furthest up-estuary. Red bands show periods in which water temperature at Charleston WQ is above the 2004-2014 climatology +1 standard deviation (Figure 6d). Gray bands show periods in which eelgrass density at Valino is below the 2004-2014 climatology by one standard deviation.

The last component of the heat budget is the advective heat flux, which contains the along channel advective heat transport (second term in Eq. 1). Though we do not have velocity measurements in the estuary, we calculate the advective component by assuming that the heat storage minus atmospheric heat flux (Figure 8), is dominated by the horizontal (along and across) advective heat fluxes. These horizontal heat flux divergences depend on the temperature gradient and velocity. The temperature gradient is dependent on the ocean end-member and river end-member (Figure 8d). The 2004-2014 climatology of temperature gradient in South Slough (between Charleston and Winchester WQ stations, 4.1 km apart) shows a strong seasonal pattern, while the main channel (between Charleston and BLM WQ stations, 7.3 km apart) shows a smaller seasonal gradient. Stronger differences between Charleston and Winchester are observed during the dry season (up to -7 ℃ in late July), due to minimal river discharge and cooler upwelled waters of the oceanic site. In the winter, positive values of $\frac{\partial T_{av}}{\partial x}$, are observed in South Slough, when cooler river discharge closer to Winchester WQ reduces temperature (Figure 6d) there while the oceanic values do not vary much relatively. Water temperature at Valino WQ is significantly correlated ($r^2 = 0.62$) to the along-estuary temperature gradient calculated here, with a change in sign of $\frac{\partial T_{av}}{\partial x}$ at 11.6 °C. A simple back-of-the-envelope calculation of the second term in Eq. 1 using $\frac{\partial T_{av}}{\partial x}$ requires velocities of 0.01 m s^{-1} in South Slough, which can be roughly estimated from observations by dividing the river discharge by the estuarine cross-sectional area of interest. We used available data from water-penetrating airborne lidar survey (Conroy et al., 2020), to calculate the area for a cross section near Valino, and a scaled river for the

watershed area in Winchester, Joe Ney Creek, Elliot Creek and John B. Creek (Figure 2),

This produces maximum velocities of 0.014 m s^{-1} in the winter, confirming our

Advective flux calculations.

On top of the anomalous atmospheric heat flux during 2014–2016 shown above,

the advective heat flux shows changes due to variability of the along-estuary temperature

gradient as well as changes to river discharge. Our data show that during the dry seasons

of 2014–2016 (Figure 8d), the temperature gradient was stronger (more negative,

especially in 2015–2016), due to warmer waters in the oceanic end member. This is

observed in the shallow South Slough (r^2=0.6, Stonewall warmer 43 days before South

Slough $\frac{\partial T_{av}}{\partial x}$), as well as in the main channel. During the rainy season, the temperature

gradient is usually driven by increased discharge due to storm events (Menniti et al.,

2020). In the Coos Estuary, discharge from the Coos River increases 18 days before the

along-estuary temperature gradient changes sign to positive values at South Slough ($\frac{\partial T_{av}}{\partial x}$

r^2=0.6; Figure 4d). In 2013-2014, drought-induced reduced river discharge (Figure 4)

would have decreased the advective export of water, while in 2014–2016 closer-to-

normal river discharge would have exported anomalously warm waters (from

atmospheric heat flux) from upriver toward the mouth of the estuary (see winter of 2015

in Figure 6).

5.3 Long term variability

The combination of anomalously warm water in the PNW with anomalously

warm air temperature and advection of riverine waters, produced anomalously warm

estuarine waters, with a greater impact in the shallow South Slough during 2014–2016.

These potentially stressful years motivate the question if we can expect this combination

to occur more or less often in a warming climate. Observations along the PNW coast

(including the ones presented here) show responses related to the large-scale climatic

patterns (e.g., ENSO, PDO and NPGO), where positive basin-scale temperature

anomalies led to increased temperature and salinity inside estuarine systems (Johnson et

al., 2003; Cloern et al., 2017; Jackson et al., 2018). Climate model simulations suggest

that in the future, an increased variance of the North Pacific Oscillation (NPO) can be

expected (Wang et al., 2014; Black et al., 2018; Capotondi et al., 2019), which was the

leading cause of the marine heatwave (the Blob) and also connected to the drought

conditions in the PNW. El Niño events, correlated to higher temperature and sea level in

the PNW are expected to occur more often in the future (Wang et al., 2014; Di Lorenzo

and Mantua, 2016). El Niño events have also been correlated to a more intense

downwelling and later onset of summer upwelling in the PNW both of which would

produce warmer temperatures in the ocean end-member (Frischknecht et al., 2015).

Additionally, though it is still unclear whether river discharge will increase or decrease

with climate change in the PNW, most models agree that in South Slough, Yaquina,

Willapa and Coquille estuary, higher discharge is expected in October and November,

while lower discharge is expected in July and August (Steele et al., 2012), moving the

warm dry period in these estuaries earlier in the year, similar to that observed in 2014–

2016.

In a warming climate, when large-scale oscillations are predicted to occur more frequently (Di Lorenzo and Mantua, 2016), we expect an increase in the temperature of PNW estuaries, as well as an extended dry, warm season. This extended dry season can affect the ecosystem by changing the range of temperature, salinity, and stratification (which affects mixing). Changes in stratification can lead to hypoxia (Officer et al., 1984) and affect organisms such as eelgrass or oysters (Borde et al., 2003; Thom et al., 2003; Black et al., 2014). Finally, these changes to temperature may affect the baroclinic circulation in estuaries, by intensifying or weakening the along-channel density differences (Hickey et al., 2003; Raimonet and Cloern, 2017).

5.4 Effects on eelgrass (*Zostera marina*)

In response to thermal change, different species may migrate, decline or die, with a differential response due to local species adaptations (Walther et al., 2002; Parmesan and Yohe, 2003; Kaldy, 2012, 2014; Poloczanska et al., 2013; Sawall et al., 2021). Eelgrass, which plays a key role in the coastal zone worldwide (Phillips, 1984; Hosack et al., 2006; Lee II and Brown, 2009), has decreased in abundance in the Coos Estuary with significant spatial and temporal variability associated to the water characteristics in the area (Figure 3a). In 2005, aerial photography data revealed high eelgrass density in the Coos Estuary covering 24×10^6 m^2 of total area (Sup. Fig. 2a). Higher density is observed in locations closer to the mouth of the estuary, where colder more saline oceanic waters flood the tidal flats. In 2016, Lidar survey reveals a decrease of eelgrass-covered area in the Coos Estuary, with higher presence in the main channel than in South Slough (Sup.

Fig. 2b), despite the proximity of the sub-estuary to the mouth of the estuary and influence of coastal waters (Raimonet and Cloern, 2017). Previously, Thom et al. (2003) showed that stations in the Coos Estuary closer to the mouth had higher values of eelgrass density (100–200 shoots per m^2) related to the influence of oceanic, low-turbidity waters, while stations farther away from the mouth of the estuary had smaller density, related to increased turbidity due to the input of freshwater. Thom et al. (2003) also showed that eelgrass decline was associated to anomalously warm waters during the 1997–1998 El Niño, which were again observed in the estuary between 2014 and 2016 (Figure 1). Though the whole estuary showed the impact of higher temperature (Figure 6), a stronger decline of eelgrass was registered in stations within the southern section of South Slough (Figure 3). In these stations, water temperature was above 1.5 ℃ of the 2004-2014 climatology during more days than at stations in the main channel (Sup. Fig. 3a) and greater than 18 ℃ during more days than normal (Sup. Fig. 3b).

The quarterly eelgrass surveys of Valino Island since 2004 give an unprecedented long-term view of eelgrass health in South Slough (Figure 2, Sup. Fig. 2c). Valino Island showed mean (μ) densities of 50 shoots per m^2 (with standard deviations, σ = 31). Data from the Danger Point site, south of Valino Island and surveyed much less frequently, showed similar values (μ = 54, σ = 43). Two other sites at Collver Point and Hidden Creek, showed lower eelgrass densities (μ= 32, σ= 14; μ= 11, σ= 17) throughout the available years. Due to the timing of sampling only once per quarter, assessing the seasonal trend is statistically challenging, as we cannot resolve frequencies greater than 6 months. Nonetheless, eelgrass in South Slough, as represented by the Valino Island site,

showed a robust seasonal pattern in mean shoot density that typically increases in summer, and declines in the fall/winter (Figure 3). Canopy height, number of flowering shoots and percent cover displayed a similar seasonality (not shown). Other eelgrass data collected by the Oregon Department of Fish and Wildlife (ODFW SEACOR) and Oregon State University, provide assessment of eelgrass in the Coos Estuary in scattered locations throughout other parts of the estuary during 2015–2018. These stations show higher values of eelgrass density (60-326 eelgrass shoots per m^2) compared to the South Slough stations (Sup. Fig. 2c), through most of the surveys. These ocean-dominated stations do not show a strong decline in eelgrass density during the anomalous years, as that observed in the more estuarine-dominated South Slough.

During 2013–2014, *Z. marina* phenology at Valino followed the expected seasonal pattern (Figure 3a): low percent cover and density in the winter months, with density of 54 shoots per m^2 during the Nov-2013 survey. In summer 2014, high productivity was registered at Valino, with a value of 78 shoots per m^2. By Apr-2015, however, eelgrass density decreased to significantly lower than the long-term mean (33 shoots per m^2), after the warming of estuaries waters during the previous fall and winter. Beyond the seasonal high of Jul-2015 (44 shoots per m^2), density remained very low with values around 5 shoots per m^2 through to present day. This decay was not only observed in the density, but in the height of the canopy and the total percent cover. The other eelgrass survey sites at Collver Point, Danger Point, and Hidden Creek, also show low density, canopy height, number of flowering shoots and percent cover in the annual survey during this period (June-July 2016). Of these stations, only Collver, the most

marine station, seems to recover with densities of 20 shoots per m^2 (Jun-2021). Surveys

from stations outside of South Slough, show a small decrease yet not as large in

magnitude or as long-lasting as at Valino Island, where a decay from 170 to 90 eelgrass

shoots per m^2 was observed from Feb-2015 to Jul-2016 (Sup. Fig. 2c).

Since eelgrass is sensitive to temperature stress, as it can increase the

photosynthetic and respiration rates (Beca-Carretero et al., 2018), and lead to higher

susceptibility to wasting disease (Kaldy, 2014), our results suggest that the marine

heatwaves and increased air temperatures contributed to the eelgrass density decline in

2015 (Figure 4). Despite the short seasonal increase in eelgrass cover, the density of

eelgrass at Valino Island declined again in 2016 when anomalously warm waters related

to the El Niño event were again observed. Eelgrass at Valine has not fully recovered

since (Figure 3). Stronger declines in eelgrass density were registered in the stations in

South Slough compared to stations in the main channel (Sup. Fig. 2c) which are warmer

for extended periods of time, especially during 2014-2016 (Sup. Fig. 3). This temperature

anomaly can be attributed not only to the distance from the oceanic end-member and the

river end-member, but also to storage of heat in shallower areas, such as those where

eelgrass is found (0.5–1.0 m MLLW).

6. Conclusions

In the Pacific Northwest, long-term and large spatial-scale processes, such as El

Niño and marine heatwaves, imprint interannual variability on top of typical seasonal

trends. Here we used 14 years of data from the Coos Estuary, in southwestern Oregon, to

quantify the effects of anomalous oceanic and atmospheric conditions on the estuary, which includes a dramatic die-off in eelgrass.

Superimposed on the interannual and long-term trends, PNW estuaries have a strong seasonal variability in temperature, in which lower water temperatures occur between November and March due to increased river discharge and wintertime atmospheric heat loss, producing a negative along-estuary temperature gradient. During the dry season, warmer air temperature and reduced river discharge increase water temperature, increasing the along-estuary temperature gradient. Between July and October, equatorward winds at the coast produce the upwelling of cold, saline, nutrient rich waters, increasing the temperature gradient further, which impacts the presence of organisms throughout the estuary.

The combination of drought in 2013–2014, El Niño in 2014, Blob in 2014–2015, and El Niño in 2016, produced anomalously warm waters in the coastal ocean outside of the estuary, along with hotter air temperatures and increased river discharge during the El Niño events. Inside the estuary, the warming was recorded in all the available water quality observations, with higher anomalies found in the shallower locations and those located further away from the estuary mouth. Water temperature increased landward, suggesting that river input and atmospheric heat flux may be important contributors to the anomalous conditions observed. These relatively higher temperatures found landward changed the overall along-estuary temperature gradient in the estuary with higher values in the beginning of the dry season before upwelling at the coast begins. These enhanced temperature gradients, along with relatively higher absolute temperatures in the upper

estuary can cause stress on organisms, such as eelgrass, potentially explaining at least part of the die-off observed.

Though time series available in the PNW are relatively short to assess long-term trends, the observations analyzed here show a) a shift to a later, shorter rainy season; and 2) an increased synchrony of decadal and interannual processes. As global temperatures warm due to climate change, we can expect an increased number of marine heatwaves and El Niño events, which will increase the temperature in Pacific Northwest estuaries, leading to changes in seasonal timing and potentially shifting the habitat areas in estuary ecosystems.

CHAPTER IV

SPATIAL VARIABILITY OF RESIDENCE TIME IN THE COOS ESTUARY AND ITS IMPACT ON THE ECOLOGY OF THE REGION

Maria Jose Marin Jarrin, David A. Sutherland

1. Introduction

In aquatic systems, the transport of biological species depends on the hydrodynamic processes that transport water and its contents, as well as species-specific behaviors of organisms. A first-order approach to describe this transport is to quantify the characteristic timescales of a particular water parcel within an estuary, such as residence or flushing time. Residence or flushing time can be broadly defined as the amount of time a water parcel or a particle within the water parcel, takes to leave a specified volume, such as an estuary (Wang et al., 2004; Meyers and Luther, 2008; Ascione Kenov et al., 2012; Geyer and Ralston, 2018). These water parcels or particles, are subject to transport and mixing processes that are spatially heterogeneous (Lemagie and Lerczak, 2015). In an estuary setting, depending on the research focus, a relatively long or short residence time can be harmful or beneficial for the environment. For example, microplastics in areas with short residence times will quickly leave an estuary, with very few numbers of particles settling at depth (van Sebille et al., 2019). Residence time is not only used for particles, but also for neutrally buoyant or passive organisms and dissolved materials, enhancing the usefulness of this timescale for understanding the import and export of

nutrients (Ralston et al., 2015), chlorophyll (Lucas et al., 2009; Qin and Shen, 2019), and contaminants (Pecly and Roldão, 2013; Geyer and Ralston, 2018). Residence time for some larval organisms can be modified by additional vertical or horizontal swimming behaviors, such as a constant sinking or migration at several speeds (for example, Peteiro and Shanks, 2015).

Residence time is modulated by the timescale of physical transport processes that determine the circulation in an estuary, which can change in time and space (Lemagie and Lerczak, 2015). Estuarine circulation is a function of river discharge, tidal currents that act to mix the water column, and bathymetry (e.g., Hansen & Rattray, 1965; MacCready & Geyer, 2010). Storm events can increase river discharge on the time scale of several days, flushing an estuary and fully replacing the volume of water (Gong et al, 2007). Bathymetry also affects residence time, e.g., when water parcels in shallow areas are flushed out quickly during a tidal cycle, but can be pushed back into the estuary on the next flood tide (Banas and Hickey, 2005; Wheat et al., 2019). In some numerical simulations, particles can be trapped or grounded in areas of strong current shear (REF: maybe a Banas paper?); observationally, floats and drifters have also been seen to ground on broad intertidal areas and later refloat, though this is likely due to their physical size (Brink et al., 2000; Kimbro et al., 2009; Pawlowicz et al., 2019).

Another important timescale for characterizing estuarine transport processes is exposure time. While residence time stops once the particle exits the area of interest, exposure time includes particles re-entering the area over the length of the modeling runs (de Brauwere et al., 2011). Exposure time may result in different values when applied to

tidal systems, where water leaves and returns several times through tidal pumping at the estuary mouth (Stommel and Farmer, 1952; Chen et al., 2011b). By comparing the residence and exposure time scale one can calculate the return coefficient, which is related to the fraction of water leaving during ebb that returns during flood. The return coefficient can also be used to assess the impact on an organism when they are exposed to the open ocean (Arega et al., 2008).

The concept of connectivity is defined by quantifying the amount of particles found in an area from different regions, and the flux or transport between those regions (Monsen et al., 2002; Cowen and Sponaugle, 2009). Connectivity, therefore, can be used to explore where particles released in specific areas ultimately end up or if they stay within their source region. Connectivity matrices can be developed to highlight areas where high retention of particles or self-seeding occurs (Haase et al., 2012; Defne and Ganju, 2015; Wheat et al., 2019). Connectivity can also help visualize how different subregions act as sources or sinks of important biological species, such as sources of low-oxygen waters (e.g., Wild-Allen and Andrewartha 2016) or the fate of phytoplanktonic organisms (e.g., George et al. 2011). Hence, by examining the temporal and spatial variability of connectivity (such as larvae, phytoplankton, upwelled oceanic waters), we may estimate the magnitude of potential ecological stress of residence times within certain regions for particles of interest.

Here we study the Coos Estuary, which is a strongly forced, geometrically complex estuary where many organisms and their habitats exist in both spatially and hydrodynamically distinct areas. The main channel of the Coos Estuary, which is dredged

once a year, has a stronger estuarine circulation flow that drives exchange, while shallower areas, like South Slough, see exchange occur through stronger tidal dispersion effects (Sutherland and O'Neill, 2016; Conroy et al., 2020). Lateral circulation with midchannel convergence creates lateral salinity gradients, especially in areas further away from the mouth (Conroy et al., 2020). We use a numerical model to show that residence times and exposure times vary along- and across-estuary, influencing the distribution of species. Our results also show that limited connectivity between regions inside the estuary and a relatively high amount of returning particles both lead to increased residence times in the estuary overall. Estuarine time scales, like residence and exposure time, can serve as proxies for certain ecological stressors and should be considered when developing restoration plans for spawning organisms that need to self-recruit. Specifically, we ask three questions: 1) What determines residence time in the Coos Estuary? 2) How does residence time vary in space? 3) How does the return coefficient and connectivity contribute to residence time? We end by illustrating the impact of residence time and connectivity on the transport of Olympia oyster (*Ostrea lurida*) larvae in the Coos Estuary.

2. The Coos Estuary

The Coos Estuary, south of Heceta Bank (Figure 1b), is located inshore of a relatively narrow continental shelf (Hickey and Banas, 2003). It is the second largest estuary in Oregon, in terms of area and volume, after the Columbia River estuary (Figure 1a), and is shaped like an inverted U. The main channel is annually dredged from the

mouth of the estuary to 24 km near the Coos River entrance to maintain 11 m of depth

and 91 m of width (Engineers, 2015). Shallow areas outside the channel cover an area of

approximately 15 km^2 and consist primarily of tidal flats, subsidiary inlets and sloughs

(Emmett et al., 2000; Groth and Rumrill, 2009; Eidam et al., 2020). The main source of

freshwater is the South Fork of the Coos river in the eastern portion of the estuary, with a

total mean discharge that ranges from 2 to 800 m^3 s^{-1}, with storm-related peaks (Figure

1b).

Notably, the South Slough National Estuarine Research Reserve (SSNERR) is a

shallow section (~5 m deep) within the southern part of the Coos Estuary, that branches

out 2.5 km from the estuary mouth (Figure 1b). Contrary to the typical nutrient export

common for estuarine systems (Largier, 2020), South Slough routinely imports nutrient-

rich ocean water (Roegner and Shanks, 2001), due to its proximity to the estuary mouth

and relatively short dynamical length that means ocean influence reaches much of the

SSNERR (Rumrill, 2007).

Using a 3D numerical model of the Coos Estuary, Conroy et al., (2020) showed

that tides drive most of the exchange flow, and tidal amplitude increases from the mouth

until its maximum value at Ishtmus Slough. By examination of surface velocity and

divergence in Conroy (2018), the circulation in the Coos Estuary is not a simple function

of distance to channel or mouth of the estuary. Velocity gradients developed on wide

tidal flats (see figure 7d in Conroy, 2018), while heterogeneity appeared in model results

at smaller scales (like the sloughs). They also used the model to estimate an adjustment

time based on the Total Exchange Flow method (MacCready, 2011), defined as the

amount of time for the depth-averaged flow to erode the length of the salinity intrusion.

Using this approach, estuary-averaged adjustment time was found to be around 15 days in

the winter, which is longer than the duration of individual storm events (~1-5 days), and

was found to vary with tidal forcing. In the summer, adjustment times were found to be

up to 900 days, much longer than the entire season, and thus not allowing the system to

approach steady state. The model also shows enhanced dispersion in the subestuaries

related to tidal trapping due to the tides being slightly out of phase. Tidal trapping occurs

when maximum salinity is not reached at the end of flood tide, when maximum velocity

is reached (MacVean and Stacey, 2011). This creates zones that trap flooding waters

which are released on the ebb out of phase, and can produce landward salt flux (Garcia et

al., 2021).

Hyde (2007) used a 3-D model of the estuary to calculate flushing times. Flushing

time is a volume-averaged approach that assumes complete mixing of the estuarine

volume, and omits any knowledge of the dominant circulation processes (Lemagie and

Lerczak, 2015). Nevertheless, their flushing time results show a strong dependency on

river discharge, with longer flushing times (80-150 days) during the summer due to lower

river discharge, and the opposite during winter (10-60 days; Hyde, 2007). Their results

also show that water parcels remain in South Slough for longer periods than in the main

estuary, which they attribute to shallower depths and lower tidal exchange.

In estuaries with large intertidal areas, particles in a water parcel (e.g., planktonic

larvae) can remain in an area for extended amounts of time, which can aid in the survival

of a species. In the Coos Estuary, *Ostrea lurida* (Olympia oysters) spawn in the summer

in synchrony with high temperature (13–16 ℃), low stratification and extended residence time (Pritchard et al., 2015, 2016). For the species to survive, the larvae must remain in the estuary between 7 to 20 days, after which the larvae settle onto hard substrate (Pritchard et al., 2015). In the Coos Estuary, adult oysters are more abundant in East Bay (Cooston and Ishtmus Slough) and in Haynes Inlet on the northern side of the estuary (Figure 1b), in part due to the presence of hard substrate (i.e., sandstone, shell, bark, basalt, and gravel). No life stages of oysters are present at the airport or Empire in the main channel, which is thought to be related to areas with salinities above 20 psu, an indication of significant tidal influence and proximity to the estuary mouth (Baker, 1995; Peteiro and Shanks, 2015). In South Slough, Olympia oysters were reintroduced in 2008, yet their adult density is far below the density observed in the main estuary at present. It is hypothesized that increased sedimentation in South Slough may limit the retention ability of the area, and larvae cannot settle properly (Wasson et al., 2015). Volume-averaged approaches to flushing time were used to compare the larval stage success in the estuary, however spatial variability of success may be related to specific hydrodynamic conditions, which has not been fully addressed.
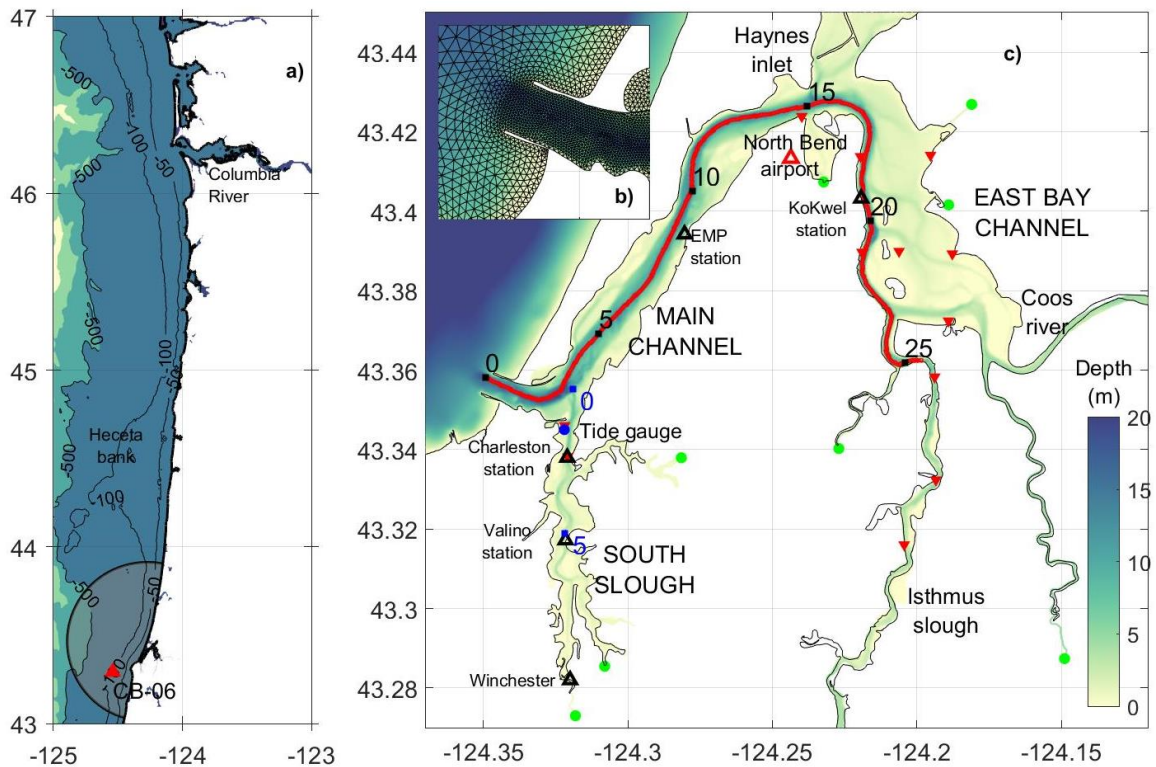
Figure 1. a) Regional Pacific Northwest map showing the model domain in black outline and the location of the CB-06 buoy (red triangle). b) The unstructured FVCOM model grid at the mouth of the estuary. c) Zoom-in on the Coos Estuary, showing bathymetry (colored contours) and the location of water quality monitoring stations (black triangles), meteorological station at the North Bend airport (red triangle), tide gauge (blue circle), and oyster habitats (red triangles). Black numbers refer to distance (in km) from the mouth along the thalweg. Blue numbers show distance (in km) from the intersection of South Slough with the main estuary.

3. Methods

3.1 Flushing time: the freshwater method

Numerical methods for determining residence time can have high computational requirements, so other methods may be preferable for a preliminary estimate. These methods may be based on observational data, such as the freshwater method to calculate flushing time. Flushing time refers to the exchange characteristics of a water body,

regardless of the actual physical processes at play (Monsen et al., 2002). The method

estuarine salinity and oceanic salinity is significant (Ferguson et al., 2004). This ratio can

be predicted by relating the fraction of volume of freshwater in the estuary to the

freshwater input (Q_r):

$$\tau_{FW} = \frac{V \, R_{FW}}{Q_r} \tag{3}$$

where

$$R_{FW} = \frac{S_0 - S_{average}}{S_0} \tag{4}$$

This method has been previously applied to the Coos Estuary by Arneson, (1976)

showing a range from 1 to 49 days due to variability in river discharge and the volume of

fraction that is flushed.

We use the freshwater method here to validate the modeling results (described

below) and compare the usefulness of the Lagrangian method. We assess hydrographic

conditions using data from several monitoring stations located throughout the estuary,

with most data focused inside South Slough, where most data are obtained from (Figure 1

and Table 1). Salinity is measured automatically every 15 minutes at all stations.

Charleston Bridge (2002-present), Valino Island (1999- present) and Winchester Arm

(1995-present) stations are telemetered to provide near real-time data access by SSNERR

(NOAA National Estuarine Research Reserve System (NERRS), 2020). Two additional

stations are monitored by the Confederated Tribes of the Coos, Lower Umpqua and

Siuslaw (CTCLUSI): Bureau of Land Management (BLM) and Empire Docks (EMP),

with data available from 2011 to present (Figure 1, Table 1). The KoKwel Indian Tribe

monitor a station 18 km from the mouth (KoKwel WQ), beyond the bend.

Table 1 Information on oceanographic and meteorological stations analyzed in this study (locations in Figure 1c). Instrument height above bottom is shown, as depths change tidally.

Station	Institution	Date range	Water depth / Sensor height (m)	Distance from mouth (km)
Water quality stations (water temperature, salinity)				
Charleston Bridge (CH)	SSNERR	2002–present	4.0 / 0.5	3.0
Valino Island (VA)	SSNERR	1999–present	2.4 / 0.5	5.6
Winchester Creek (WI)	SSNERR	1995–present	1.1 / 0.5	7.1
Empire Docks (EMP)	CTCLUSI	2011–2014	6.0 / 0.5	6.9
North Spit BLM	CTCLUSI	2008–2016	10.5/0.5	8.2
KoKwel Wharf (Coquille)	KoKwel Indian Tribe	2013–2017	19	18.6
Sea level from tide gauge				
Charleston #9432780	NOAA	1991–present	3.0 / –	3.0
River gauge station				
South Fork of Coos River. St.#14323600	Coos Watershed Association	2003–present	44 (elev.)	49

We calculate the tidally averaged salinity ratio as the difference in salinity

between the Charleston water quality station and the average salinity between all the

stations available (Table 1), using Eq. 3. Model outputs are compared to the salinity ratio

for validation, as well as to calculate the total volume used in Eq. 3. River discharge for

the observations and modeled flushing time calculation uses the modeled discharge, since

our observations only include the South Fork River discharge, which is ~50% of the total freshwater modeled volume.

3.2 Numerical modeling

We use hydrodynamic numerical simulations to explore the impact of circulation, geometry, bathymetry and connectivity on residence times in the Coos Estuary (Figure 1). The Finite Volume Coastal Ocean Model (FVCOM) is a prognostic, finite-volume, free-surface, three-dimensional primitive equation model with unstructured grids (Chen et al., 2003, 2018; Huang et al., 2008; Qi et al., 2009). FVCOM can resolve tidal elevations, water properties, and currents in areas with complex topographical features, such as intertidal regions in estuaries. Unstructured triangular cells, as well as the wetting and drying capability of FVCOM are important features for modeling the inverted-U shape of the Coos Estuary. The model domain covers the entire Coos Estuary with a western open boundary located in the ambient Northern Pacific Ocean. The horizontal grid has spatial resolution that varies from 15 m within the bay to 3 km at the outer boundary. The vertical coordinate has 20 levels in uniform hybrid terrain-following grids. The model bathymetry within the estuary was developed by Conroy et al., (2020), interpolated from 2014 Lidar data and in-situ surveys (echo-sounders and GPS).

Boundary conditions for the model include offshore tidal forcing (at 52 open boundary nodes) and freshwater discharge input at 15 nodes using the values from a river gauge at South Fork (Figure 1c). The model was initiated with a salinity of 34 psu, applied to the entire domain, which estimates the mean salinity offshore from the Coos

Estuary buoy (CB-06 -Figure 1a), while a salinity of 0 psu was imposed at freshwater

inputs. We ran the model for a one-month spin-up period, and these results were used as

initial conditions for subsequent seasonal simulations. One-month long circulation

outputs were created for the two distinct seasons observed in the Coos Estuary, as well as

other estuaries in the Pacific Northwest: the low-discharge summer and the storm-driven

winter (Figure 2a). Both runs include the subtidal forcing (spring-neap cycle) which is the

main component of variability in the estuary, as well as an increase in river discharge

during the winter.
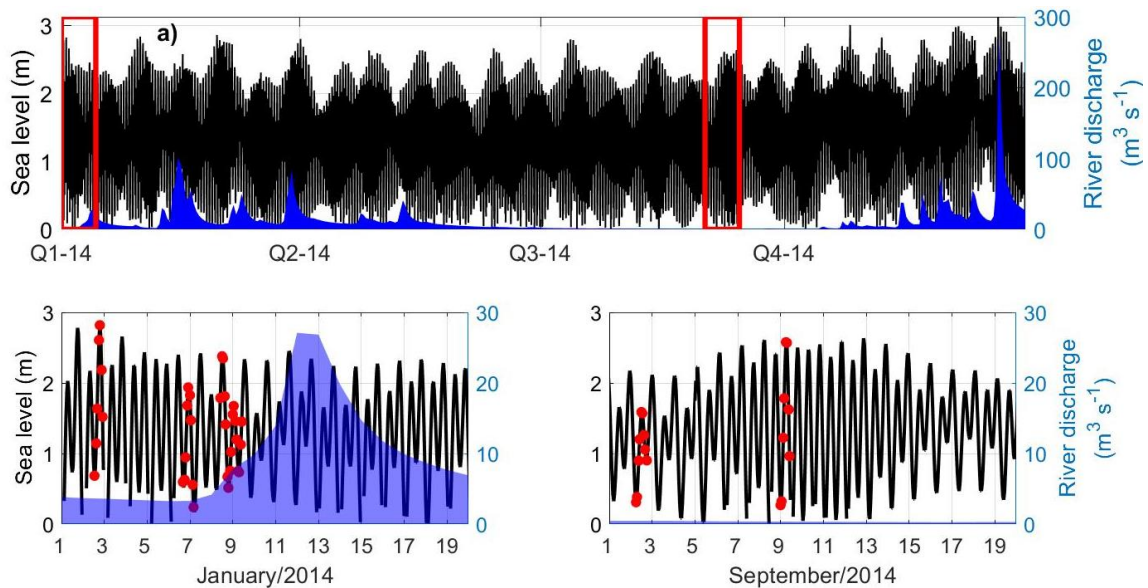
Figure 2. a) Time series of sea level at the Charleston tide gauge (left axis in black line) and river discharge at the South Fork of Coos River gauge (right axis in blue) during 2014. Red boxes show the numerical modeling periods for winter and summer. b) Zoom-in of winter showing drop dates for experiments (red circles) on sea level (left axis in black). River discharge at the South Fork of Coos River is shown in blue on the right axis, notice the different ranges in the subplots. c) Same as (b) but for summer.

3.3 Residence time: Particle tracking experiments

Several methods for calculating estuarine timescales have been developed that incorporate the hydrodynamics and geometry of an area (Monsen et al., 2002). Residence time calculations may be based on observational data or numerical modeling, and usually come with tradeoffs between ease of use with sparse observations. While numerical models can resolve spatial variability for example when using particle tracking methods (Lemagie and Lerczak, 2015), the temporal scales are constrained by computational resources. On the other hand, observational studies can inform on longer temporal scales, although high spatial resolution is not achievable (Largier, 2003). Here we focus on particle tracking results from the hydrodynamic model described above, in a varied combination of tidal stage and river discharge conditions. The MATLAB Lagrangian Tracker (MALT) particle tracking module of FVCOM was used to obtain trajectories from the model velocity fields (Figure 1). MALT is a Lagrangian particle tracking module that solves a nonlinear system of ordinary differential equations (Chen et al., 2011a). In order to solve these equations, we chose to use the explicit Runge-Kutta (ERK) in time with a 4-Stage RK4 scheme, which allows one to solve the ordinary differential equation in the 3 dimensions. The velocity fields were interpolated using an FVCOM-based linear interpolation of fields, with a time step of 60 seconds. We defined an additional turbulent variability by adding a vertical and random-walk value of horizontal diffusion (Liu et al., 2011). The particles were initialized in a grid of 100 m x 100 m horizontal squares across the whole estuary (Figure 3-5). At each location particles were dropped at the surface, bottom and mid-column on the original sigma layer FVCOM

vertical grid, to determine if there is significant vertical variability in residence time. At the open boundary, particles were allowed to exit the domain.

Residence time and connectivity were calculated based on the results of 26 numerical experiments in the summer and 51 in the winter. Both seasons included a spring and a neap tide, and the winter season includes a neap tide in which river discharge increased due to a storm event (called winter event). Particles were dropped at hourly intervals from high to low tide and tracked for 20 days. Here, residence time was calculated as rate of change of the amount of tracer in the estuary defined as

$$\frac{dC}{dt} = -\frac{Q_{out}}{V}C = -\frac{Q_r}{V}\frac{S_0}{S_0 - S_{avg}}C = -\frac{C}{\tau_f} \qquad [1]$$

Thomann & Mueller (1987), defined an exponential decay (e-folding timescale, or about 37% of the initial quantity of particles) as the solution to this equation. For each model step, the percentage of particles that remain in the estuary is determined. Residence time for the whole estuary was calculated as the time it takes to reach 37% of the initial particles remaining. Spatially-varying residence time was determined in the same way, but using the starting position locations in 300 m x 300 m squares, i.e., 9 particles are dropped within each square. These 9 particles were followed until only 37% of them remained in the estuary, similar to the method used in the Yaquina estuary, OR, USA Lemagie & Lerczak (2015).

Exposure time is calculated similarly to residence time, yet explicitly includes particles that exit and re-enter the estuary (de Brauwere et al., 2011). Exposure time is

then used to calculate the return coefficient (r), as the difference between exposure time (E) and residence time (τ_f):

$$r = \frac{E - \tau_f}{\tau_f} \qquad [2]$$

If no water returns into the estuary then $E = \tau_f$ and $r = 0$, i.e., all the water is flushed out and none of the particles are returned. When $r = 1$, water quickly leaves the domain but reenters many times or stays within the estuary for a long time. The return coefficient has also been related to the "return flow factor", used in other methods of residence time calculations, such as the Tidal Prism method (Arega et al., 2008) yet it cannot be estimated simply from basin geometry. Thus, the r-value can be used to place simpler methods in context, and in comparing observations with model outputs.

Connectivity matrices were determined as the proportion of the initial particles in one region that ended up in a different region after a set amount of time. Here we use a timescale of 20 days, due to that timescale's relevant for Olympia oyster spawning (Pritchard et al., 2015). These regions were initially considered in a grid of 300 m x 300 m squares, as I used for residence time. However, preliminary connectivity results in these 300 m grids showed most variability within broad regions of ecological importance: South Slough, Main Channel, Cooston and Isthmus Slough (Figure 1c), and the adjacent continental shelf. We only show results in these summarized areas here.
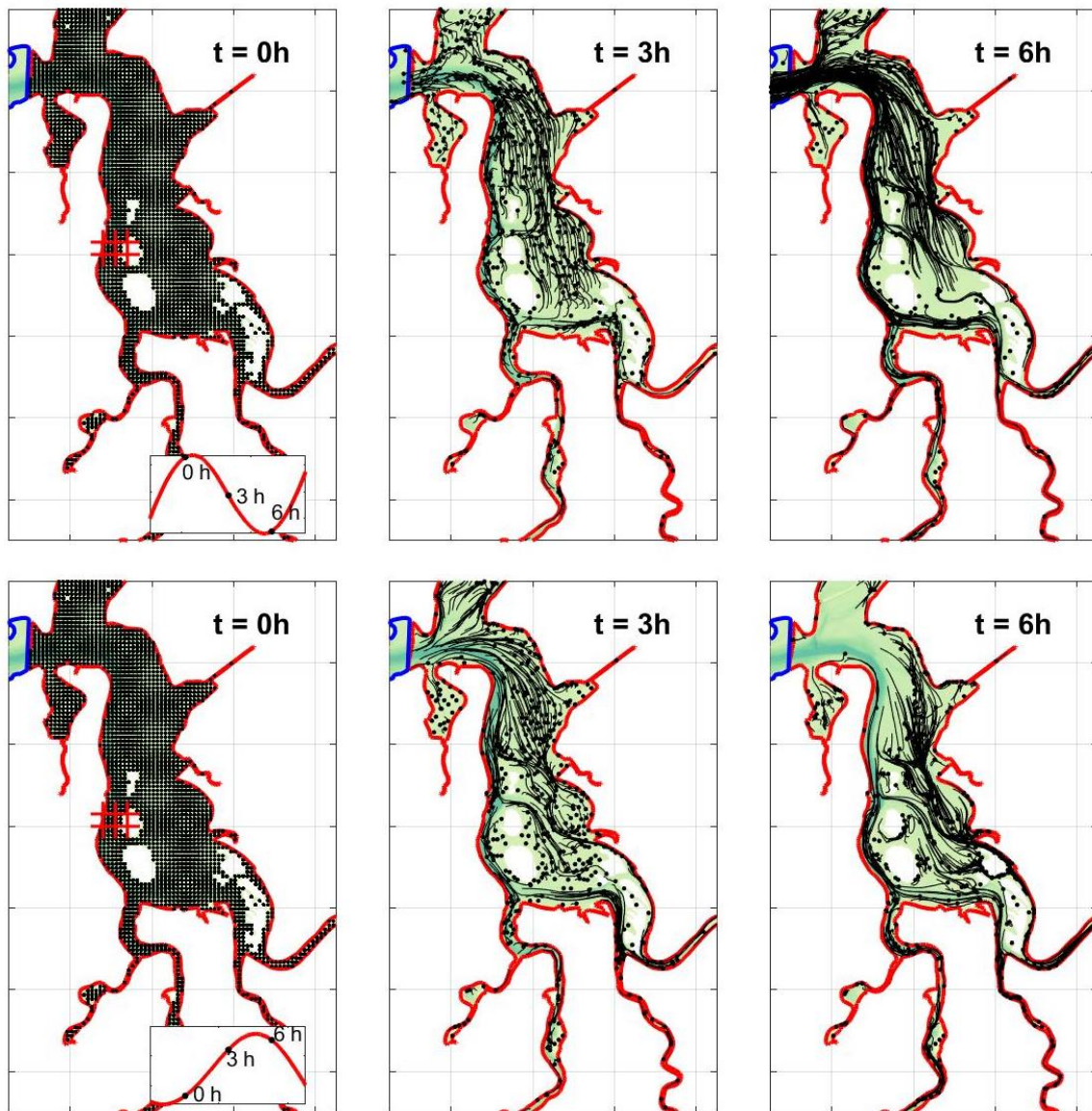
Figure 3. a) Particle releases during neap ebbing tide at t = 0 hours in East Bay. The 300m x 300m grid for residence time calculation is shown in red, as well as the sea level at which each subplot is shown. b) same as (a) but for location where particles end up at t = 3 hours. c) same as (a) but for location where particles end up at t = 6 hours. d) same as (a) but for location where particles start at t = 0 hours during a neap flooding tide. e) same as (d) but for location where particles end up at t = 3 hours. f) same as (d) but for location where particles end up at t = 6 hours.
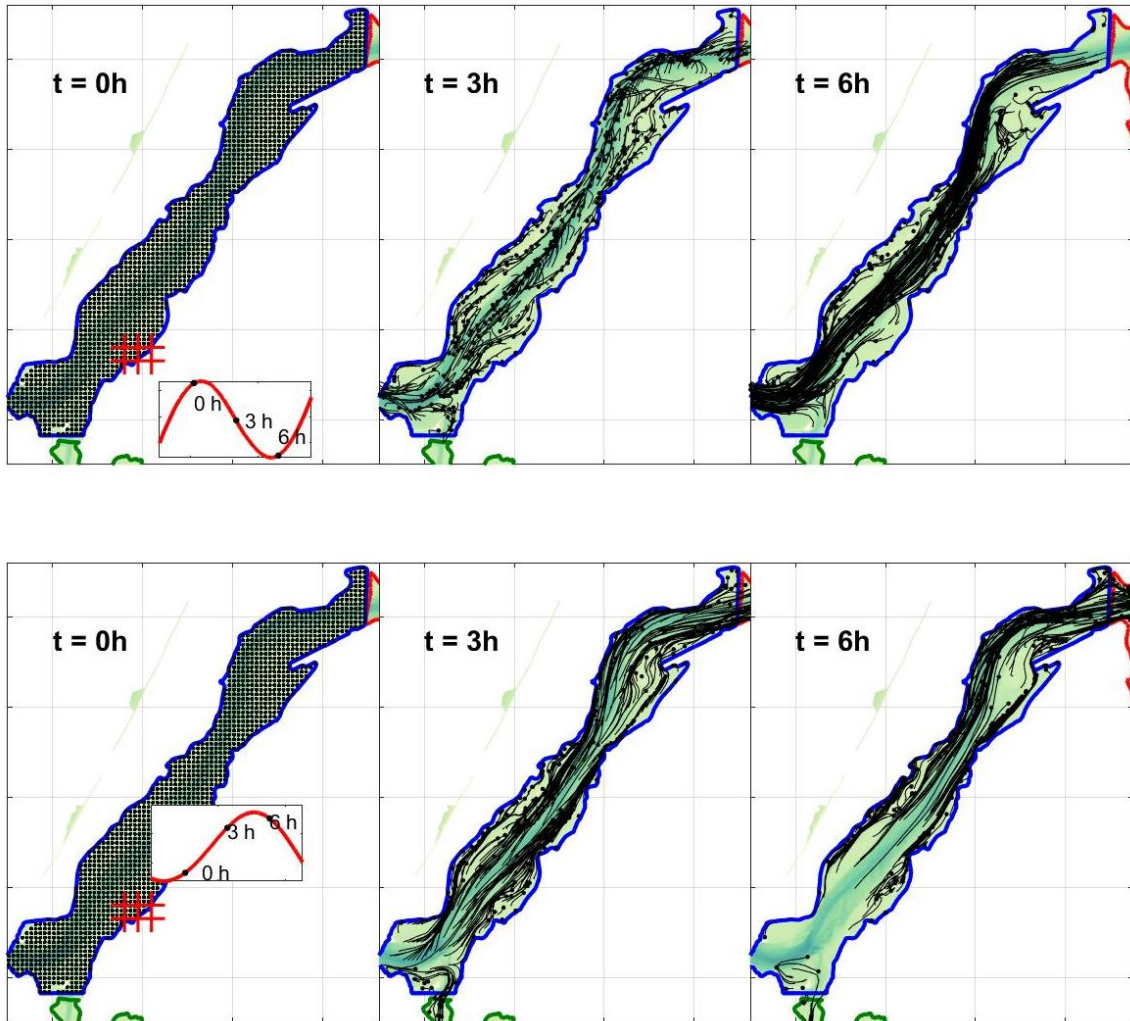
Figure 4. a) Particle releases during neap ebbing tide at t = 0 hours in the main channel. The 300m x 300m grid for residence time calculation is shown in red, as well as the sea level at which each subplot is shown. b) same as (a) but for location where particles end up at t = 3 hours. c) same as (a) but for location where particles end up at t = 6 hours. d) same as (a) but for location where particles start at t = 0 hours during a neap flooding tide. e) same as (d) but for location where particles end up at t = 3 hours. f) same as (d) but for location where particles end up at t = 6 hours.
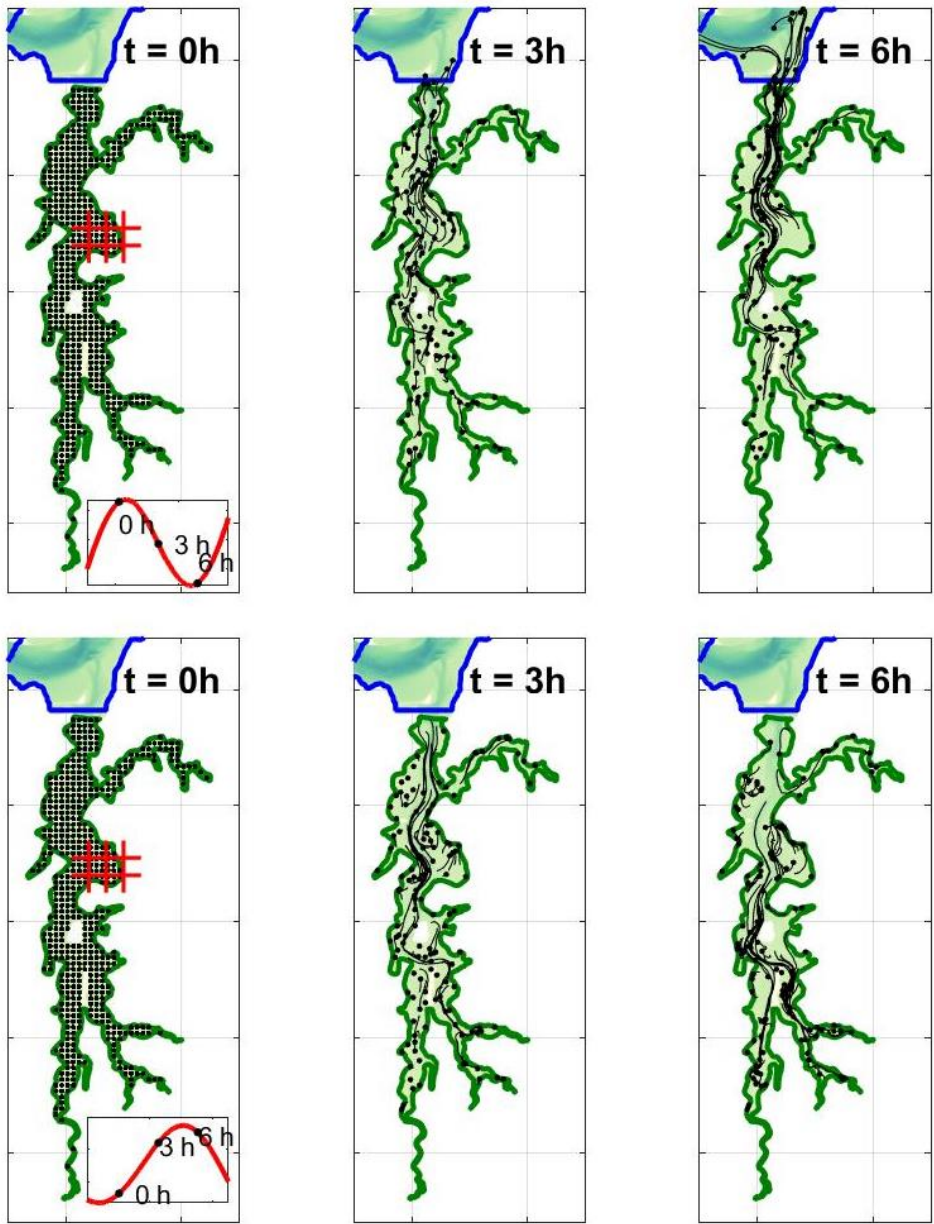
Figure 5. a) Particle releases during neap ebbing tide at t = 0 hours in South Slough. The 300m x 300m grid for residence time calculation is shown in red, as well as the sea level at which each subplot is shown. b) same as (a) but for location where particles end up at t = 3 hours. c) same as (a) but for location where particles end up at t = 6 hours. d) same as (a) but for location where particles start at t = 0 hours during a neap flooding tide. e) same as (d) but for location where particles end up at t = 3 hours. f) same as (d) but for location where particles end up at t = 6 hours.

Due to the potential effect of residence time on the successful spawning of Olympia oysters (Groth and Rumrill, 2009; Pritchard et al., 2015; Wasson et al., 2015), we also ran summertime experiments by dropping particles at locations where Olympia oysters are currently found (locations in Figure 1). Though Olympia oysters are capable of controlling their depth through vertical swimming, horizontal currents are usually 10-100 times stronger than their average swimming speeds (Peteiro and Shanks, 2015; McIntyre et al., 2020). Hence, we assume oyster particles act as passive particles. Environmental parameters such as temperature, salinity and velocity may affect the survival of larvae, as well as the retention in settlement-appropriate locations. In species like *Ostrea lurida*, survival to adult stage is linked to retention within the estuary. For Olympia oysters, this ecological survival rate from recruitment to 6 months is about 1% (Baker, 1995; Peteiro and Shanks, 2015). Thus, for these oyster experiments, we determine the time at which only 1% of the particles initially dropped are observed remaining inside the estuary (Peteiro and Shanks, 2015).

4. Results

Our observations and numerical simulations show that the characteristic estuarine timescales (freshwater flushing time, residence time and exposure time) have a strong tidal dependance, a secondary river discharge dependance and an influence of both distance from the mouth and depth.

4.1 Total volume residence time

4.1.1 Freshwater method

River discharge in the Coos Estuary has a strong seasonal signal, which is the main driver of variation in the freshwater method calculation of flushing time (Figure 6b). The observational salinity ratio (R_{FW}, Eq. 4) is 0.1 units lower than the model outputs in both seasons, partially due to the spatial locations (Figure 1, depths shown in Table 1) at which each time series was obtained (Figure 6c-d). Despite the difference between observations and model outputs, a similar trend is observed: as river discharge increases, the salinity ratio doubles in magnitude. τ_{FW} using observational time series 12 days on average during winter and even shorter during storm events (e.g., $\tau_{FW} = 4$ days, between Jan-7 to 14th, Figure 6e). During the drier summer, τ_{FW} increases to an average of 80 days in the observations, when freshwater discharge is close to its minimum (Figure 6f). The model output shows an order of magnitude difference between winter and summer flushing times (20 and 207 days, respectively), and reproduces the decreases in τ_{FW} due to increases in river discharge.
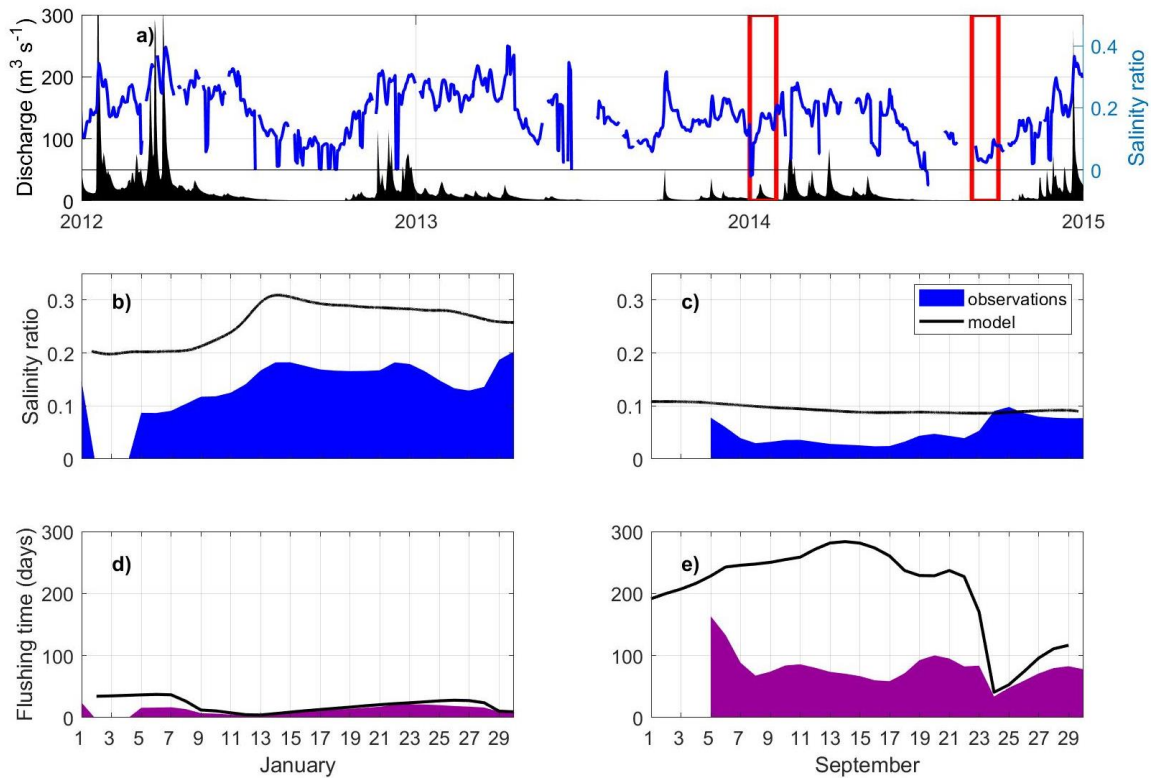
Figure 6. Tidally filtered freshwater flushing time and associated features in the Coos Estuary during the 2012-2014 calculated using Eq. 3. a) River discharge model input total river discharge (sum of 15 freshwater sources in black line) on the left axis. Salinity ratio from Eq. 3 on the right axis calculated using observations shown in Table 1. b) Salinity ratio calculated using observations (blue) and model outputs (black line) during the winter, using data shown in (a) in red box. c) same as (b) but for summer. d) Freshwater flushing time calculated using observations (purple) during the winter and model outputs (black line). e) same as (d) but for summer.

4.1.2 Whole-estuary residence time

The particle tracking analyses using MALT showed that over all the experiments, more than 65% of the particles on average were flushed out of the Coos Estuary by the 20-day mark. Around 13% of particles exit the estuary during the first ebbing tide of each experiment, while during a flood tide experiments the particles are moved up-estuary 2 km on average over all the experiments (see for example Figure 3-5). On the ebb tide,

particles are moved towards deeper channels in each region, while during the flood tide

particles move through channels but also re-enter areas outside of the channels (Figure 5).

Of the particles that do not exit the estuary, about 86% of them are grounded inside the

estuary by the end of the 20-day simulations.
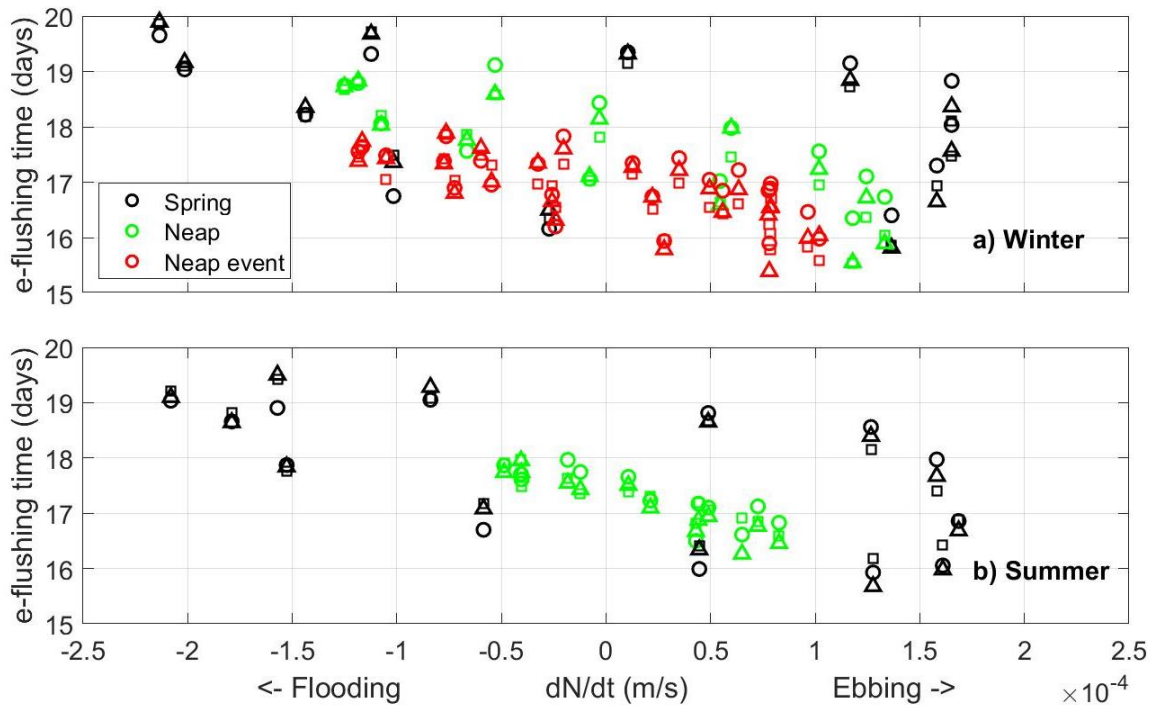
Figure 7. a) Flushing time in relation to tidal cycle (change in sea level in time), from particle tracking experiments in the winter, colored by subtidal cycle. Symbols correspond to initial depth location (circle at the surface, triangle in the middle of the water column, square at the bottom). b) same as (a) but for summer.

Residence time calculated over the whole estuary shows a strong temporal pattern

related to the tidal forcing. Figure 7 shows the e-folding time as a function of tidal stage.

The residence time varies between 17 (average spring tide) and 18 days (average neap

tide) in the summer to 18 (average spring tide) and 17 (average neap tide) days in the

winter. The winter-event experiment residence time was lower than the neap winter, with an e-folding flushing time of 17 days, and a strong tidal influence (Figure 7). A sharp initial decrease in concentration is observed in the spring tide cases in both seasons, related to increased water velocities. No significant difference is observed between surface, bottom and mid-column experiments ($R^2 = 0.7$), however bottom particles are in general more correlated to tidal stage ($R^2 = 0.8$) than surface particles ($R^2 = 0.6$) in both seasons (Figure 7). During ebbing tides, surface particles (circles in Figure 7) remain in the estuary for slightly extended residence time than during flood (slope = -0.5). Bottom particles tides (squares in Figure 7) show a stronger influence of tides between ebbing and flooding (slope = -0.7).

4.2 Spatial variability of residence time

The spatially-variable residence times show the importance of distance from the mouth, with longer residence times in areas further away from the mouth (East Bay) and in South Slough (Figure 8). On top of the along-estuary differences in residence time, there are across-channel gradients, with shorter residence times in the thalweg than on the estuary sides, where particles remain in dry cells for extended periods of time.

The three main areas of ecological importance (Figure 1c) have distinct residence times. In winter, residence time averaged over the main channel was 8 days, while beyond the bend in the estuary (at $x = 15$ km) residence time increased to >19 days. Residence time averaged over South Slough was 15 days, despite being closer to the mouth (x = 3-10 km). These differences are related to velocity, with velocities 2 times

stronger in the main channel than in the East Bay channel, and 1.5 times stronger than in

South Slough. During the summer, residence time also increased with distance (Figure 8),

with shorter residence times in the main channel (9 days) than those further away, such as

the East Bay channel (>19 days), or South Slough (>15 days, at x = 3-10km). Within

each area, there is also important variability (Figure 9c-d), for example within the East

Bay region there is a similar probability of residence time to be 1 - 5,7, or 10 days long,

in both the winter and the summer. A similar probability distribution is observed for

South Slough, while in the main channel, the highest probability is of residence time to

be between 0 and 0.5 days. This probability distribution is related to the inclusion of flats

and sloughs in the area-averaged calculations.
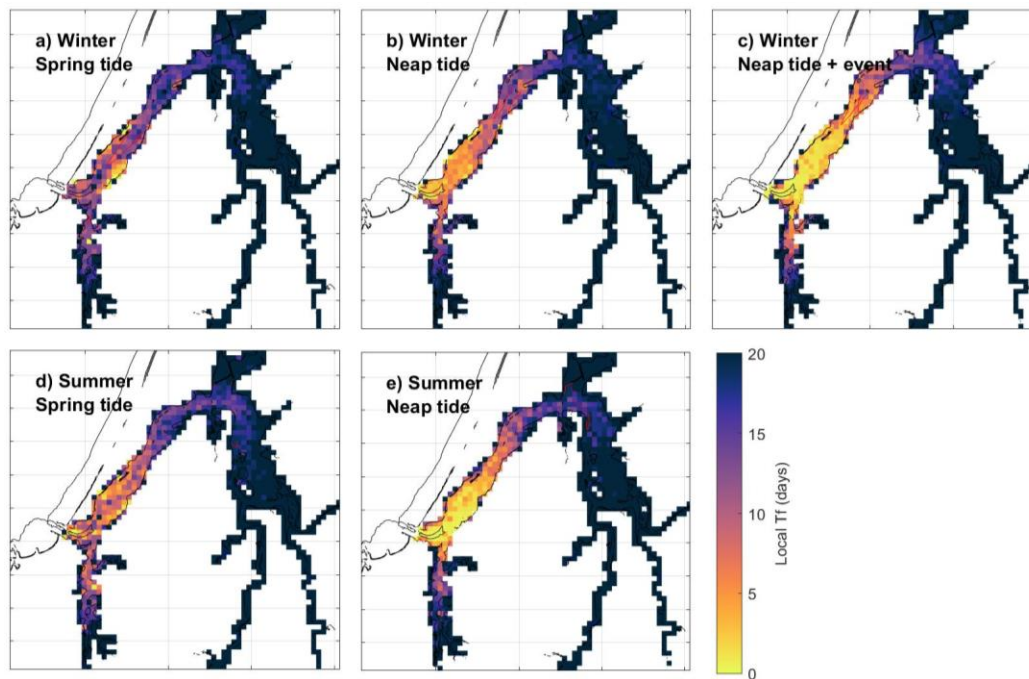
Figure 8. a) Spatial variability of residence time during the winter averaged over the 13 experiments during the spring tide. Location of 30 psu isoline in red. b) same as (a) but for neap tide. c) same as (a) but for the storm event during neap tide. d) Spatial variability of residence time during the summer averaged over the 13 experiments during the spring tide. e) same as (d) but for neap tide.
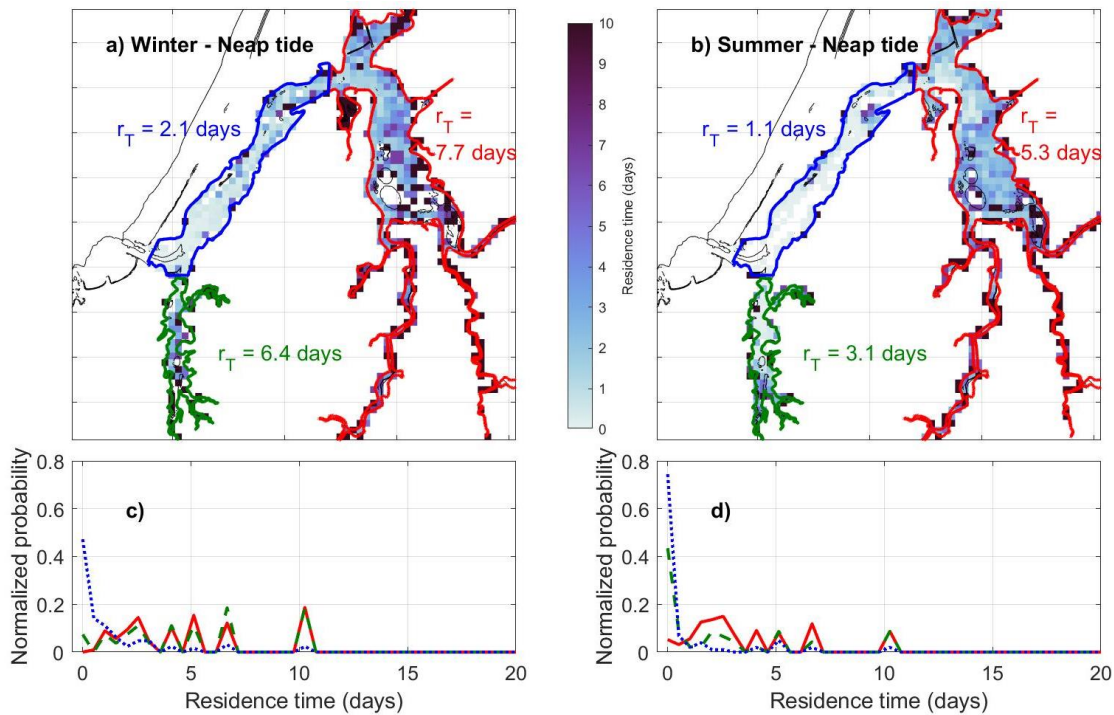
Figure 9. a) Example spatial variability of residence time during the spring high tide experiment over the winter (Figure 2). Averaged residence time in Main Channel, South Slough and East Bay shown in text. b) Same as (a) but for summer. c) Spatially-varying normalized probability of residence time (colored according to a) during the winter. d) same as (c) but for the summer.

In South Slough, the longest residence times are observed during neap tides (Figure 8), especially under the smaller high tides in the summer, that are due to the semi-diurnal M2 tidal constituent. In addition, there is some dependence on bathymetry as the flats get flushed out fastest, particularly evident after 6 hours of run time (Figure 5). Similar variability is observed in the winter, with residence time increasing with distance from the mouth. A sharp decline in particle concentration is observed during the largest spring falling tides in both seasons and particularly within the main channel (Figure 4). This strong tidal dependence is also observed in the winter event case, related to extended residence times in South Slough and East Bay (Figure 3).

104

Across-channel gradients of residence time vary between areas, with a common low residence time portion in the deepest part of the section (Figure 8). East Bay in general has high residence time throughout the width of the channel (17-20 days). In South Slough the thalweg has very short residence time of 4-6 days, while on of the sides of the cross section, residence times of 20 days are found. In the main channel, the average residence time in the spring and neap tide is between 7 and 20 days, with the strongest across-channel differences during the neap tide. These sections are found in a similar distribution to salinity isolines, hence, related to across-channel distribution of velocity (see red lines in Figure 8).

4.3 Return coefficient

The return coefficient (Eq. 3) allows us to compare how much water exits the estuary with how much of it returns in a later time. This coefficient is of interest due to the possibility of water parcels (or particles) reentering the estuary with characteristics mixed between estuarine and oceanic waters. The average return coefficient in the winter is 0.1 after the 20 day runs (Figure 10). This means that about 10% of the estuarine water that has been ejected during the 20-day time period to Coos Bay at some point. The average return coefficient in the summer is twice as big, as expected from a smaller river plume, hence more particles have an opportunity to return. Additionally, return coefficient under neap tide forcing is higher than during spring tide conditions, unlike residence time. During spring tides, increased velocities export particles further away from the estuary than during neap tide due to jet-sink dynamics (Conroy et al., 2020).

The across-channel averaged, along-estuary return coefficient is highest in areas closest to the mouth during both seasons (Figure 9). Most of these particles are sourced along the channel thalweg. Compared to the residence times, there is an increased return coefficient in areas where the residence time is relatively short. By definition, residence time does not include returning particles. Hence, despite particles in the main channel leaving quickly once dropped, between 10 and 20% of them return to the estuary.

Our results of return coefficient can be compared to the salinity ratio calculated by the freshwater method (described above). Salinity ratio compares oceanic salinity (here calculated at Charleston) with the average salinity inside the estuary, although the freshwater method does not consider any estuarine mixing processes. Salinity ratio calculations showed higher values for higher discharge, which produced lower flushing times, while the opposite was observed for the lower discharge ranges. Our return coefficient calculations show that during the winter a smaller volume of water returns to the estuary, which would increase the difference between Charleston and the estuary-averaged salinity. In the summer, our return coefficient shows slightly higher percentages of particles returning into the estuary, which would reflect in a higher estuarine salinity, reducing the salinity ratio.
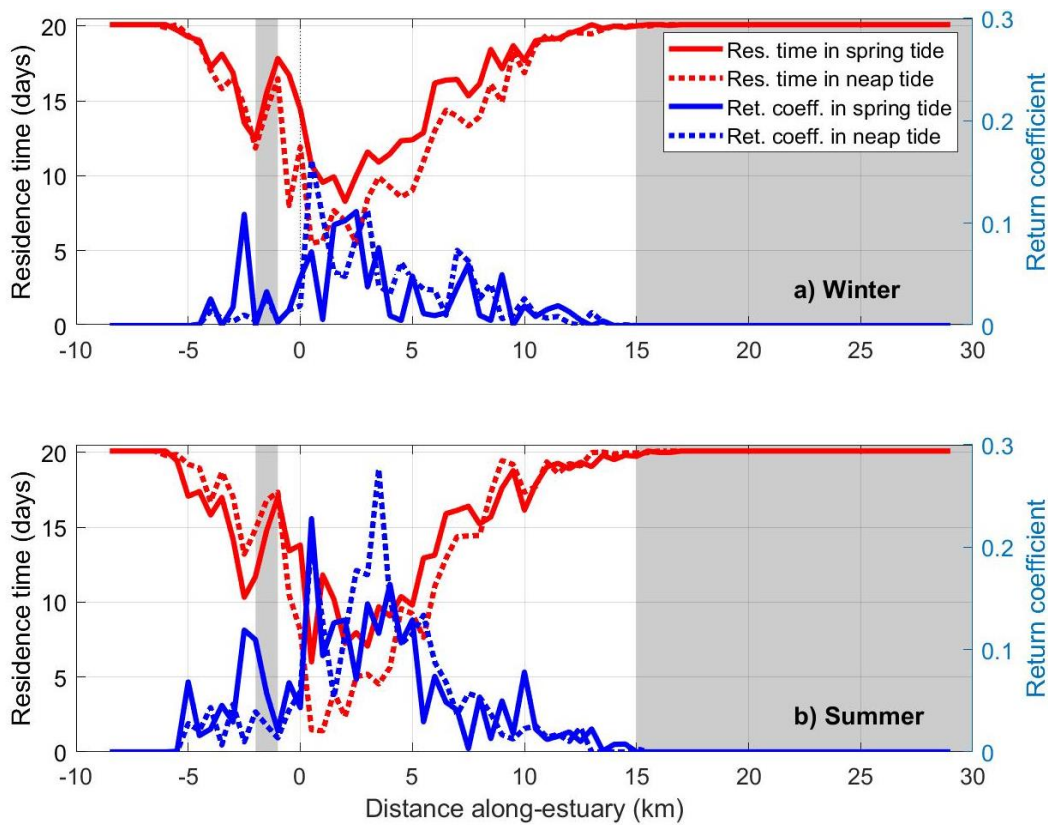
Figure 10. a) Along-estuary variability of Residence time (left axis) and return coefficient (right axis, Eq. 3) during the winter for the spring tide (line) and neap tide (broken line), averaged across the width of the channel at 1000m grids. Areas where Olympia oysters have been found (Figure 1) shown in gray. b) same as (a) but for summer.

4.4 Connectivity

Our summarized connectivity matrix (Figure 11) shows the proportion of particles that are transported amongst the Shelf, South Slough, main channel, and two portions of the East Bay Channel: Cooston and Isthmus Slough (Figure 1b). Our results show that the bend separates the estuary in two portions: particles dropped seaward of the bend exit the estuary, or stay in main channel or South Slough, while particles that are dropped

landward of the bend stay in their source region or move further up-estuary (Figure 11).

In the summer there is a slight increased connectivity of the two areas (Figure 11d-e).
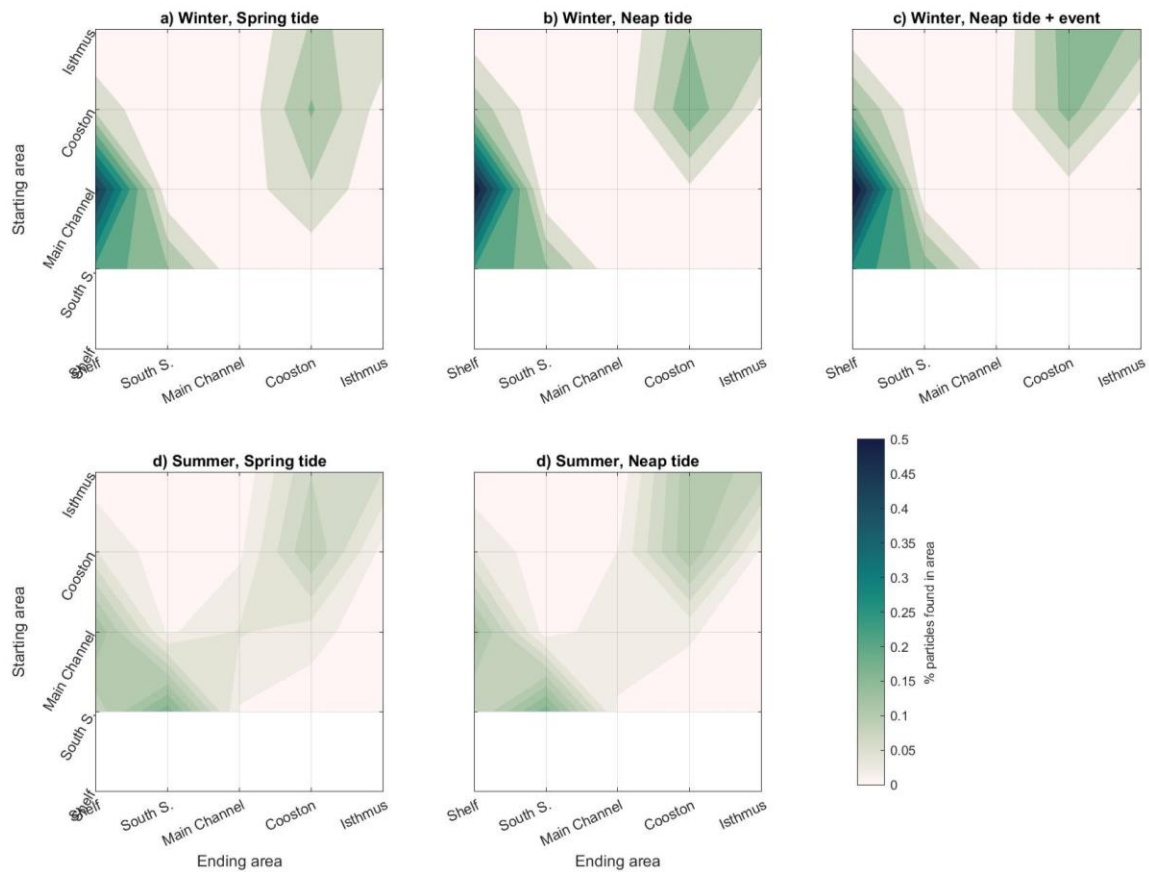
Figure 11. (a) Connectivity matrices for the winter spring tide case representing the relative time spent within the Shelf, South Slough, Main Channel, Cooston and Isthmus Slough regions. The x-axis indicates the ending region, while the y-axis indicates the source region. The color shows the % of particles averaged over the 13 experiments. b) same as (a) but for neap tide. c) same as (a) but for the storm event during neap tide. d) same as (a) but for the summer. e) same as (b) but for the summer.

For both seasons, about 25% of the initial particles exit South Slough and remain

in the main estuary after a tidal cycle (Figure 11). In the winter, when freshwater

discharge is increased, particles that are dropped in South Slough preferentially leave the

estuary, exiting onto the shelf (55%). In these experiments, only 15% return to the Slough or are retained within it. During the summer, the proportions of particles that remain in each area after a tidal cycle are almost evenly divided. Additionally, more particles are retained in South Slough during neap than during spring tides.

4.5 Oyster larvae experiments

Transport of Olympia oyster larvae between different areas in the Coos Estuary was estimated using the hydrodynamic characteristics of the summer season. The oyster larvae experiments are focused on areas of importance for oyster habitat (Figure 1), where particles are dropped in observed oyster locations and tracked for 20 days, the length of the larval period. The oyster experiments show that particles dropped in the Coos Estuary are flushed quickly out of the estuary, reaching 1% of availability after 6 days in areas where oyster habitats are observed (colored pixels in Figure 12a and b). Particles dropped during the spring tide get flushed out faster (Figure 12b), reaching 1% after 4.5 days, than the neap tide (1% of particles found after 6.6 days; Figure 12a). Particles dropped at the bottom of the water column take 2 more extra days to reach 1% of concentration in the estuary in the spring tide (not shown). Bottom particles dropped during the neap tide in the summer take half a day less to reach the 1% threshold for the oyster population to survive. Hence, the oyster population would have a greater chance of survival if they are dropped during the neap tide at the surface, or during the spring tide at depth from their habitats.

As observed in the Connectivity experiments, the oyster experiments also show that particles move within different areas, increasing the concentration of particles. In the neap tide experiments, the oyster larvae particles that are dropped in East Bay stay within the area (red area in Figure 12c), while a small percentage move towards main channel and are eventually exported out of the estuary (purple area in Figure 12c). Particles that are dropped initially in South Slough are quickly moved towards the main channel and exit the estuary (blue and purple areas in Figure 12g). About 1% of the particles stay in South Slough after 7 days in areas close to its main channel (Figure 12d), the minimum time threshold for oyster larvae to grow enough to settle at depth. During the spring tide, a similar, yet slightly faster behavior is observed, with particles exiting the estuary quickly once the tidal cycle has reached the maximum spring amplitude (on Sept-11, Figure 2c). Due to the larger tidal amplitude, most of the particles from South Slough exit the estuary within the first tidal cycle and 1% of larvae particles is reached earlier (4.6 days) than the other regions (7.7 days in East Bay, Figure 12d).

Connectivity between different areas, which is important for larvae to find hard substrate and the hydrographic characteristics needed for survival (see Coos Bay area section) is also shown in Figure 12. At least 50% of the particles that are released from the South Slough area exit the estuary through the mouth for each tidal forcing. The East Bay area, on the other hand, retains a greater proportion of its particles. A very small percentage of particles (2%; Figure 12c, d) move from East Bay to South Slough, and similarly from South Slough to East Bay (Figure 12g, h). There is a reduced percentage

of particles that start in the main channel that end in East Bay or South Slough (red and

blue areas in Figure 12e and Figure 12f, respectively).
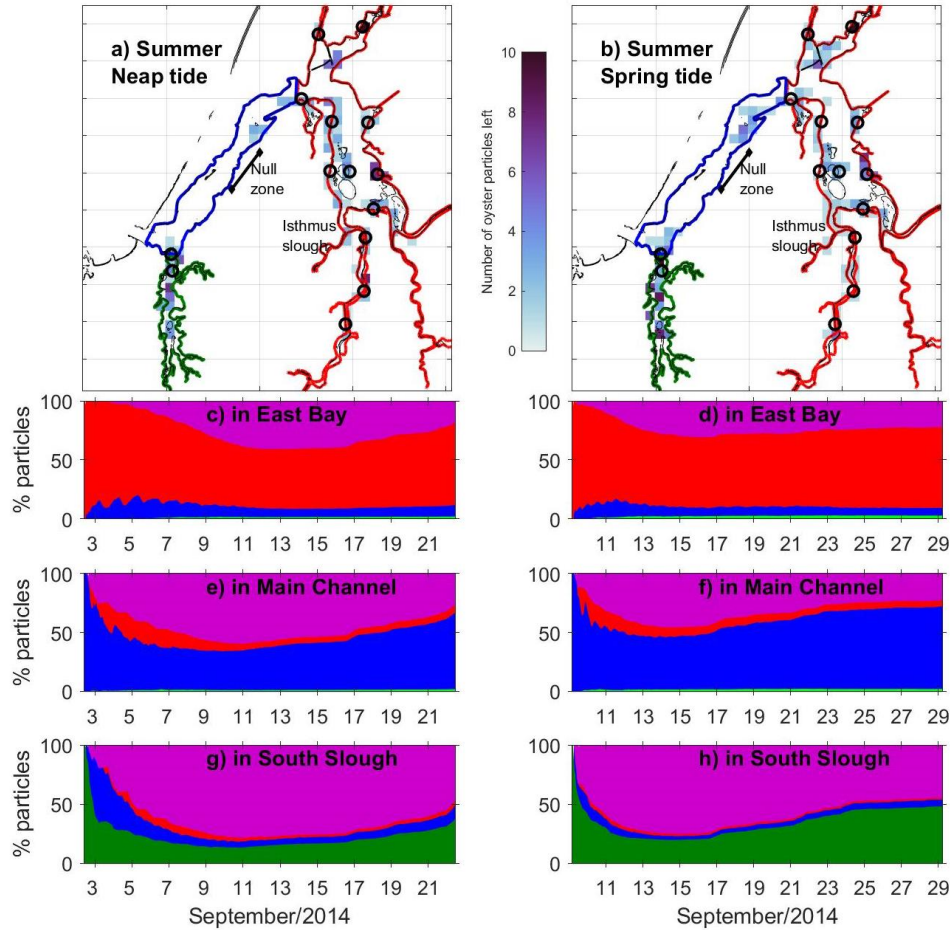
Figure 12. a) Number of oyster larvae particles in each grid (distance 500m) remaining after 20 day run during summer neap tide. Dropping location shown in black circles, where adult oysters are found. Areas of interest in outlined colors: East Bay in red, Main Channel in blue, South Slough in green. b) same as (a) but for spring tide in the summer. c) Temporal variability of percentage of particles that are found in East Bay during the summer neap tide. The colors identify the area where they are from: green from South Slough, blue from Main Channel red from East Bay, purple from the Shelf. d) same as (c) but for spring tide. e) same as (c) but particles found in Main Channel. f) same as (e) but for spring tide. g) same as (c) but particles found in South Slough. h) same as (g) but for spring tide.

5. Discussion

Estuarine timescales (i.e. residence, exposure times) in geometrically complex estuaries, like the Coos Bay Estuary, are further complicated if the strong tidal forcing and episodic discharge events influence the overall estuarine circulation. This complexity leads to physical processes that are not accounted for in the typical freshwater method approach, or even the estuary-averaged approach due to the vast number of shallow areas and a deep, dredged thalweg. Using the freshwater method in the Coos Estuary results in flushing times between 20 and 200 days (from winter and summer, respectively), while the particle tracking experiments show values between 15 and 20 days depending on the tidal stage (Figure 7). These order of magnitude differences between methods were also observed in Yaquina Bay, another tidally-forced estuary in Oregon (Lemagie and Lerczak, 2015).

The spatially variable residence time calculations (Figure 8) additionally show a dependence on distance from the mouth, across-channel bathymetry, velocity and geometry. One primary result we find is that residence time heterogeneity is determined by storage mechanisms in shallower areas, like the numerous sloughs, as well as the estuarine geometry (Figure 8). The shortest residence times are found closer to the mouth in the main channel during the summer neap tide experiments. Areas furthest away from the mouth, in East Bay channel, are found closest to our run-time (20 days) in most of the experiments. Within each region, particles closest to the thalweg exit the estuary fastest, while particles on the sides have longer residence times.

Connectivity analysis for East Bay channel also shows self-seeding, which suggests water parcels landward of the bend reside there for extended periods of time (Figure 11). South Slough, despite being less than 10 km away from the mouth, shows higher residence times than the main channel over its first 15 km. This difference is related to tidal trapping in the subestuary: tides in South Slough, which are 20º out of phase, produce flooding velocities in the area, when the main channel is ebbing (Conroy et al., 2020). These up-estuary velocities in South Slough would store particles for extended periods of time increasing residence time (Garcia et al., 2018).

Our choice of 20-day runs was based on the length of time oyster larvae spend in the water column before settling (Pritchard et al., 2015), as well as computational constraints. As seen above, some of our particles need more time to exit the estuary, especially during the dry summer (Figure 8). However, the tides in the Coos Estuary are mixed semi-diurnal with a spring-neap cycle that can rapidly flush out most of the particles that are available to do so, similar to Yaquina Bay (Lemagie and Lerczak, 2015). The extended length of residence time is mostly due to particles found in shallow areas, where they can temporarily become inactive (due to being in a dry node). We address the impact of grounded and "stuck" particles due to modeling artifacts in the next section.

5.1 Grounded particles

The MALT numerical code allows particles to exit the open boundary at the ocean side and not return. Within the estuary, however, particles can become inactive

113

when they are found in a dry node. We allow particles to become active again if these nodes become wet again. Hence, we can define two types of inactive particles: those that exit the open boundary and those that are grounded within the estuary. Particles that get stuck in the model boundary inside the estuary are a critical part of the natural behavior of particles floating in an estuary, for non-biological particles such as logs, plastic, etc. These particles can momentarily encounter a dry node during an ebb tide, but become active again during a flood tide. This active-inactive-active behavior may not be relevant for biological particles, as larvae will swim with the water parcels towards wet areas. Hence the residence time for particles found in dry nodes may be under estimated.

Despite the constraints of dry nodes and inactive particles, our experiments show that about 60% of the particles that get stuck in the model experiments are grounded within the edges of the estuary, while the rest are stuck next to the jetties (Figure 1b) or are found in the open ocean. The Oregon Department of Fish and Wildlife has sampled the edges of the estuary and found them populated by clams (Butter, Cockle, Gaper, Native Littleneck clams), crabs (Dungeness and red crab), and other organisms (https://www.dfw.state.or.us/mrp/shellfish/Seacor/findings_coos_bay.asp). Similar to our results of particles stuck near the jetties, Peteiro & Shanks (2015) found viable oyster larvae at the mouth. However, due to high velocity in the area, larvae found in this area may not be able to reenter the estuary and settle (Pritchard et al., 2015).

5.2 Impact of South Slough on residence time

The simulations show that under different tidal and river forcing, residence time in the estuary varies spatially with higher residence time in three important areas: the edges of the estuary, shallow areas where lower velocities are expected, and in areas up-estuary of the large channel bend roughly 15 km from the mouth (Figure 1). Conroy (2018) shows convergence in the fast-flowing thalweg, where Lagrangian particles accumulate and exit the estuary within the first tidal cycle. They also show divergence towards the edges of the estuary, where particles would accumulate in areas of lower velocity, increasing residence time.

The naturally shallow South Slough has longer residence times overall than the main channel (Figure 9), like the more distant East Bay channel (starting around $x = 15$ km). These differences arise due to lower along-estuary velocity (1.5x slower than the main channel), which in turn, affect the transport of particles through the subestuary. In South Slough, particles move in average 2 km over a tidal cycle (1.5 km in summer and 3 km in the winter, Figure 5), while in the main channel they move 3 km (2.5 km in summer and 3.5 km in the winter, Figure 4). Additionally, velocity in South Slough is slightly out of phase with velocity in the main channel, producing tidal trapping (lateral exchange with shoals and side channels; Okubo, 1973). As water from main channel exits the estuary in the ebbing tide, part of it enters South Slough, increasing the concentration of particles in the slough (see for example particle tracks in Figure 5). In a similar way, tidal trapping occurs in smaller sloughs within South Slough providing storage area for particles which are out of phase with the main branch (Garcia et al., 2018). This phenomenon was observed in South Slough where chlorophyll values were recorded

slightly out of phase with sea level (Roegner and Shanks, 2001). The authors related this to the entrance of additional waters from the Joe Ney Creek, a small slough on the northeastern side of South Slough.

Finally, channel curvature is common, yet its effect on estuarine circulation is much more complex than river bends due to the potential asymmetries between ebb and flood and within subtidal and seasonal variability (Kranenburg et al., 2019). The geometry of the Coos Estuary helps to reduce the along-estuary velocity, shown in areas of convergence, especially in East Bay channel (Conroy et al., 2020). Reduced velocity up-estuary of the North Bend (2x slower than in the main channel), increases the number of particles that remain in the area, hence increasing residence time. These differences in velocity along the thalweg produce areas that are tidally restricted, producing a "null zone" (Pritchard et al., 2016), where the barotropic forcing are in balance, and there is little out-estuary transport from the East Bay area. Due to the strong tidal forcing in the estuary, particles will eventually exit the estuary, however the presence of the "null zone" extends the temporary availability of particles in the area.

5.3 Ecological implications: the Olympia oyster

Residence time gradients across the full estuarine system have significant implications for the ecology of the region. Organisms on tidal flats depend on the tidal delivery of nutrients and prey: water parcels and particles are drained on every ebb and transported to the deeper thalweg, while new, mixed or old water returns to and interacts with the sediment and benthic organisms during the flood (Banas et al., 2007). If the

116

water parcels and particles remain on the flats longer than a tidal cycle, organisms may be able to encounter food (or not) for longer periods of time (Defne and Ganju, 2015). Also, larval stages of benthic organisms are subject to the physical characteristics of the water column (Pritchard et al., 2015). For example, in Tomales Bay, CA, recruitment of Olympia oyster larvae was correlated to residence time that varied from the intertidal to subtidal habitats (Kimbro et al., 2009). This spatial gradient was related to upwelled waters and residence times that increased phytoplankton abundance and changed the growth and size of juvenile oysters in the estuary.

Our oyster larvae experiments show that 1% of the particles that originate in East Bay, remain in this area after 20 days, where most of the Olympia oyster habitat at present is found (Pritchard et al., 2015, 2016). 60% of these remaining particles are found in the same area (Figure 12), especially along the sides of East Bay. Particles available for settling are found as far up-estuary as Isthmus Slough. The retention in this area is aided by the location of the "null zone" described above which helps to retain the particles (Pritchard et al., 2016). Longer residence times are observed during neap tides than during spring, where oysters preferentially spawn in Isthmus Slough (Oates, 2013). Similar preference for neap tide spawning is observed in Puget Sound (Hopkins, 1937)

These results are relevant to a wide range of applications requiring analysis of residence time and connectivity in the estuaries' perimeter, including the transport of oyster larvae in the context of habitat restoration. The success of restoration projects within the Coos Estuary depends on the knowledge of hydrodynamic transport, which will determine the effectiveness of processes such as larvae propagation in established

oyster habitats. Our results highlight that Olympia oyster restoration efforts in the East

Bay Channel (Figure 1) are successful, as release larvae that can travel through the

estuary and settle in the same locations after 20 days, during the dry summer season.

South Slough shows a similar amount of particle retention as East Bay (Figure 12).

Interestingly, however, South Slough has not had successful oyster restoration projects

(Wasson et al., 2015). Thus, the lack of viable oyster populations may be due to other

stressors, such as non-optimal hydrographic conditions (e.g., temperature, salinity,

turbidity) or high sedimentation rates that bury the oysters. Due to the small scale

bathymetric gradients and relative proximity to unconstrained boundary conditions, our

model validation in South Slough is not as good as in the main channel (see extended

validation in Conroy, Sutherland, and Ralston 2020). Future work should target a robust

sampling (in space and time) of South Slough to better model the spatial patterns of tidal

amplitude within this subestuary. We believe that clearer spatial and temporal patterns of

residence time may aid decision-making on future restoration projects.

6. **Conclusions**

Residence time, broadly defined as the amount of time a newly dropped particle

takes to leave an area, is related to the timescale of physical transport processes that

determine the circulation in the estuary and the geomorphology of the area, which can

change in time and space. Depending on the focus of the research, a long or short

residence time can be harmful or beneficial to the organisms in an estuary. The Coos

Estuary is a strongly tidally forced estuary, with additional seasonal forcing due to

freshwater input. Previous efforts to determine timescales in estuaries using volume-averaged methods do not include all the mixing processes that occur, especially in geometrically complex estuaries such as those found in the Pacific Northwest. These calculations find most of the dependency of timescales on river discharge, with residence times that range from 48 to 1 days. However, recent modeling efforts determined that most of the circulation in the estuary is driven by tidal forcing, instead of river forcing. Here we used a 3-D model to understand the variability of residence time in the estuary in the two main seasons, over a variety of tidal magnitudes.

Our spatially variable residence time calculations show the strong tidal dependence of residence time, with longer residence times during spring tides in areas further away from the estuary mouth, as expected. However, there is an additional contribution to particle transport due to across-channel bathymetry, velocity and geometry. Particles closest to the thalweg exit the estuary fastest, while particles on the sides have longer residence times. High heterogeneity in residence time is also observed in shallower areas due to tidal trapping mechanisms, as that produced by the numerous sloughs which export water parcels out of phase with the main channel. Areas beyond the bend, i.e. East Bay, also store particles for extended periods, which confirms the presence of the "null zone", beyond which Olympia oyster (*Ostrea lurida*) larvae are less likely to be transported out of the estuary and could successfully settle. South Slough, is located 2 km from the mouth and extends ~10km, which if compared to the main channel would have similar residence times. However, due to tidal trapping mechanisms in the main channel, residence times in the northern part of this slough are short, while the southern

part of the subestuary has residence times between 15-20 days. Despite extended residence times, Olympia oyster population in this part of the estuary are not observed, hence there may be an additional stressor (temperature, salinity, nutrients, substrate, etc.) which may explain the lack of a self-sustaining *O. lurida* population. Connectivity additionally shows exchange of particles between areas of ecological importance, which must be considered when preparing restoration projects. Our work here highlights the importance of spatially variable timescales in estuaries with complex geometries and extensive flats.

CHAPTER V

CONCLUSIONS

How does the circulation in the Coos Estuary vary spatially and temporally, and how does it affect the ecosystem?

This work highlights how local geometry and bathymetry set bounds on how estuarine circulation and salinity fields respond to river and tidal forcing at different spatial and temporal scales. I used observations and numerical simulations to look at the effect of winds and temperature on estuarine dynamics in the Coos Estuary, which like many small, strongly-forced estuaries in the Pacific Northwest, does not conform to the traditional funnel-shaped estuary. These changes to circulation can affect the timescales of particles in the estuary and in turn affect the organisms critical to the functioning of the Coos Estuary ecosystem.

Although often considered secondary, wind can drive significant variations in the salinity field, as well as inducing locally strong along and across-estuary gradients. The numerical simulations developed in Chapter 2 used idealized forcing to separate the contribution of tides, river discharge, and winds, on subtidal salinity and velocity fields. We find that wind can lead to reversals in the out-estuary surface flow despite the tidal dominance on subtidal circulation, in accordance with the limited available observations. Northward winds pile fresher waters in the north side of the estuary, and decrease exchange flow due to the winds opposing the main channel surface outflow, which may ultimately enhance the transport of particles along estuary. Southward winds pile fresher

waters on the southern sides of the estuary, where most of the flats are found, and act to enhance the loss of salt. These transient winds drive non-transient changes to salt content in the estuary: high discharge cases show a general increase of salt, while low and moderate discharge show a reduced loss of salt in the estuary after the winds are turned off. The wind-driven spatial and temporal variability quantified here in the salinity and velocity distribution underscores the importance of local geometry constraints on estuarine dynamics, especially as many estuaries continue to evolve either due to natural environmental changes or to anthropogenic impacts.

In Chapter 3, the spatial and temporal variability of subtidal water temperatures in the Coos Estuary is analyzed. Water temperature dictate where organisms can survive and is determined by oceanic, atmospheric and riverine heat fluxes, modulated by the distinct geometry and bathymetry of the system. Using observations, I explore the impact of anomalously warm oceanic and atmospheric conditions during 2014-2016 on the estuarine temperature. The arrival of a marine heatwave in September 2014 increased water temperature in the greater Pacific Northwest region by more than 1.5°C until March 2015, and again from July to August 2015. Additionally, in 2014-2016, the Equatorial Pacific showed increased temperatures due to El Niño events. Inside the Coos Estuary, the warming was recorded in all the available water quality observations, with higher anomalies found in the shallower locations and those located further away from the estuary mouth. Water temperature increased landward, suggesting that river input and atmospheric heat flux may be important contributors to the anomalous conditions observed. These relatively higher temperatures found landward changed the overall

along-estuary temperature gradient in the estuary with higher values in the beginning of the dry season before upwelling at the coast begins. These enhanced temperature gradients, along with relatively higher absolute temperatures in the upper estuary can cause stress on organisms, such as eelgrass, which declined sharply, but only in certain locations within the estuary. As global temperatures continue rising due to climate change, increased numbers of marine heatwaves and El Niño events are expected, leading to higher temperature stress on the marine ecosystem within estuaries.

Together Chapters 2 and 3 show the impact of secondary forcing on the circulation of the estuary. However, the effect of winds and temperature are in a shorter timescale than the tidal forcing in this estuary. Hence in Chapter 4 I used the validated numerical model for the Coos Estuary to understand the variability of timescales in the estuary. Volume-averaged values have been shown to not represent mixing processes in estuaries, which are of high importance to the Coos Estuary. The Lagrangian particle tracking method used here showed that particles exit the estuary preferentially if located closer to the mouth and in the deeper channel. Areas further away from the estuary, such as East Bay Channel, have a longer residence time additionally due to the geometry of the estuary (curvature at about 15km from the mouth). Because of this extended residence time, oyster larvae can settle in the hard substrate found in the area and repopulate.
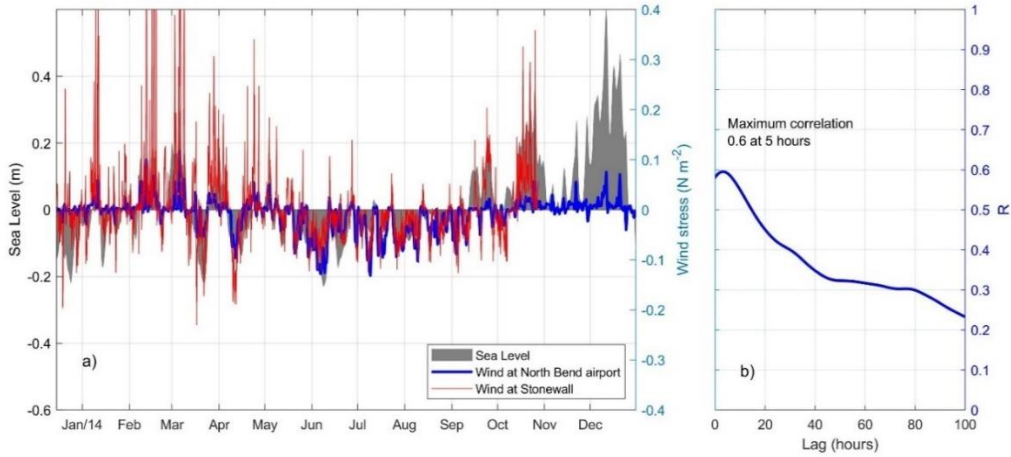
Sup. Fig. 1: a) Sea level at the Charleston tide gauge (gray on left axis), and wind stress (right axis) at the North Bend Airport (blue line) and Stonewall buoy (red line – for comparison). b) Correlation between subtidal sea level (Charleston tide gauge) and wind stress (at North Bend Airport).
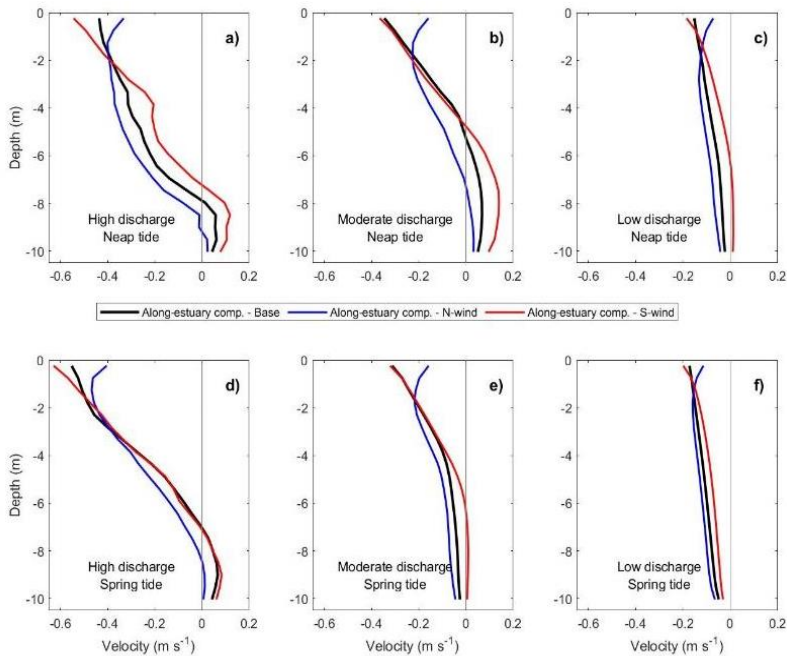
Sup. Fig. 2: Modeled along-estuary velocity (m·s^{-1}) in a location close to the ADCP, separated by discharge (columns) and tidal range (rows). In each panel, we show the pre-wind event along-estuary velocity profile (black), the velocity profile during strong northward winds (blue), and during strong southward winds (red).
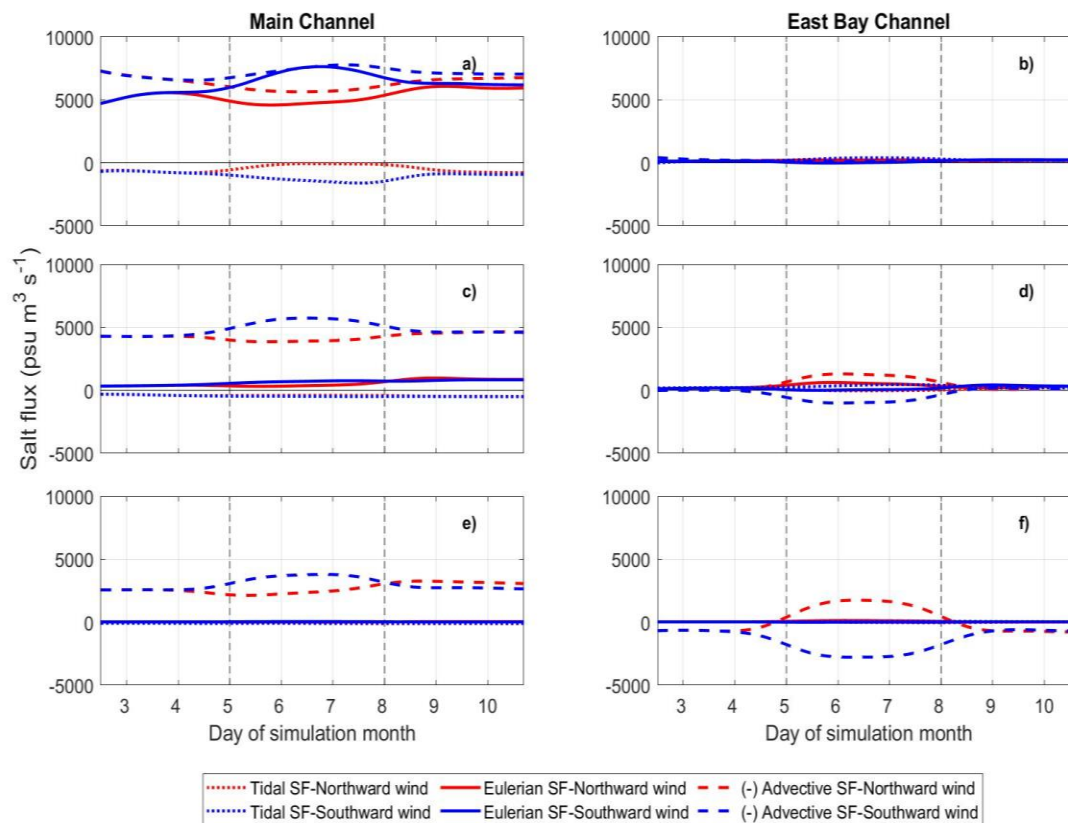
Sup. Fig. 3: Temporal variability of salt flux components (eulerian, tidal and advective) at Main Channel (Cross section A) and East Bay Channel (Cross section B) shown separately in each column for the neap tide cases, northward winds (red lines), and southward winds (blue lines). (a-b) High discharge conditions. (c-d) Same as a-b, for moderate discharge. (e-f) Same as a-b, but for low discharge. Broken lines show the time when winds are applied.
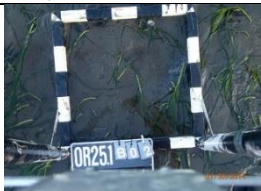
Sup. Table 1. Model setup parameters.

Parameter	*Values*
Number of cells/nodes	65799/35691
Time step for the external mode	0.1 s
Ratio of internal time step to external time step	10
Minimum water depth used for the wet/dry cells	0.5 m
Background eddy viscosity	$1. e^{-4} m^2 s^{-1}$
Background eddy diffusivity	$1. e^{-5} m^2 s^{-1}$
Minimum eddy diffusivity (constant)	$5. e^{-4}$

Sup. Table 2. Forcing values in each model experiment, including the no-wind Base cases (1-6) and the wind perturbation cases (7-30). River discharge (input at South Fork Coos River), tidal range applied at boundary, and wind speed for model experiments. Positive is northward wind.

Case	River forcing	Tidal forcing	Wind forcing (stress)
BASE CASES			
1	High – 187 m^3·s^{-1}	Neap – 0.79 m	-
2	High – 187 m^3·s^{-1}	Spring – 1.17 m	-
3	Moderate – 19 m^3·s^{-1}	Neap – 0.79 m	-
4	Moderate – 19 m^3·s^{-1}	Spring – 1.17 m	-
5	Low – 1.5 m^3·s^{-1}	Neap – 0.79 m	-
6	Low – 1.5 m^3·s^{-1}	Spring – 1.17 m	-
WIND PERTURBATION CASES			
7	High – 187 m^3·s^{-1}	Neap – 0.79 m	Strong northward (+0.2 N·m^{-2})
8	High – 187 m^3·s^{-1}	Neap – 0.79 m	Weak northward (+0.1 N·m^{-2})
9	High – 187 m^3·s^{-1}	Neap – 0.79 m	Weak southward (-0.1 N·m^{-2})
10	High – 187 m^3·s^{-1}	Neap – 0.79 m	Strong southward (-0.2 N·m^{-2})
11	Moderate – 19 m^3·s^{-1}	Neap – 0.79 m	Strong northward (+0.2 N·m^{-2})
12	Moderate – 19 m^3·s^{-1}	Neap – 0.79 m	Weak northward (+0.1 N·m^{-2})
13	Moderate – 19 m^3·s^{-1}	Neap – 0.79 m	Weak southward (-0.1 N·m^{-2})
14	Moderate – 19 m^3·s^{-1}	Neap – 0.79 m	Strong southward (-0.2 N·m^{-2})
15	Low – 1.5 m^3·s^{-1}	Neap – 0.79 m	Strong northward (+0.2 N·m^{-2})
16	Low – 1.5 m^3·s^{-1}	Neap – 0.79 m	Weak northward (+0.1 N·m^{-2})
17	Low – 1.5 m^3·s^{-1}	Neap – 0.79 m	Weak southward (-0.1 N·m^{-2})
18	Low – 1.5 m^3·s^{-1}	Neap – 0.79 m	Strong southward (-0.2 N·m^{-2})
19	High – 187 m^3·s^{-1}	Spring – 1.17 m	Strong northward (+0.2 N·m^{-2})
20	High – 187 m^3·s^{-1}	Spring – 1.17 m	Weak northward (+0.1 N·m^{-2})
21	High – 187 m^3·s^{-1}	Spring – 1.17 m	Weak southward (-0.1 N·m^{-2})
22	High – 187 m^3·s^{-1}	Spring – 1.17 m	Strong southward (-0.2 N·m^{-2})
23	Moderate – 19 m^3·s^{-1}	Spring – 1.17 m	Strong northward (+0.2 N·m^{-2})
24	Moderate – 19 m^3·s^{-1}	Spring – 1.17 m	Weak northward (+0.1 N·m^{-2})
25	Moderate – 19 m^3·s^{-1}	Spring – 1.17 m	Weak southward (-0.1 N·m^{-2})
26	Moderate – 19 m^3·s^{-1}	Spring – 1.17 m	Strong southward (-0.2 N·m^{-2})
27	Low – 1.5 m^3·s^{-1}	Spring – 1.17 m	Strong northward (+0.2 N·m^{-2})
28	Low – 1.5 m^3·s^{-1}	Spring – 1.17 m	Weak northward (+0.1 N·m^{-2})
29	Low – 1.5 m^3·s^{-1}	Spring – 1.17 m	Weak southward (-0.1 N·m^{-2})
30	Low – 1.5 m^3·s^{-1}	Spring – 1.17 m	Strong southward (-0.2 N·m^{-2})

APPENDIX B: SUPPLEMENTAL INFORMATION FOR CHAPTER IV

Jan, 2011	April, 2011	July, 2011	
Jan, 2014		July, 2014	Oct, 2014
Feb, 2015	Apr, 2015	July, 2015	Oct, 2015
Jan, 2016	Apr, 2016	July, 2016	Oct, 2016 (station B26)

Sup. Fig. 1. Eelgrass sampling in South Slough. Photographic record of eelgrass cover at the Valino Island mid elevation transect (quadrat B02 or B26 during Oct-2016) during 2011, and 2014-2016.
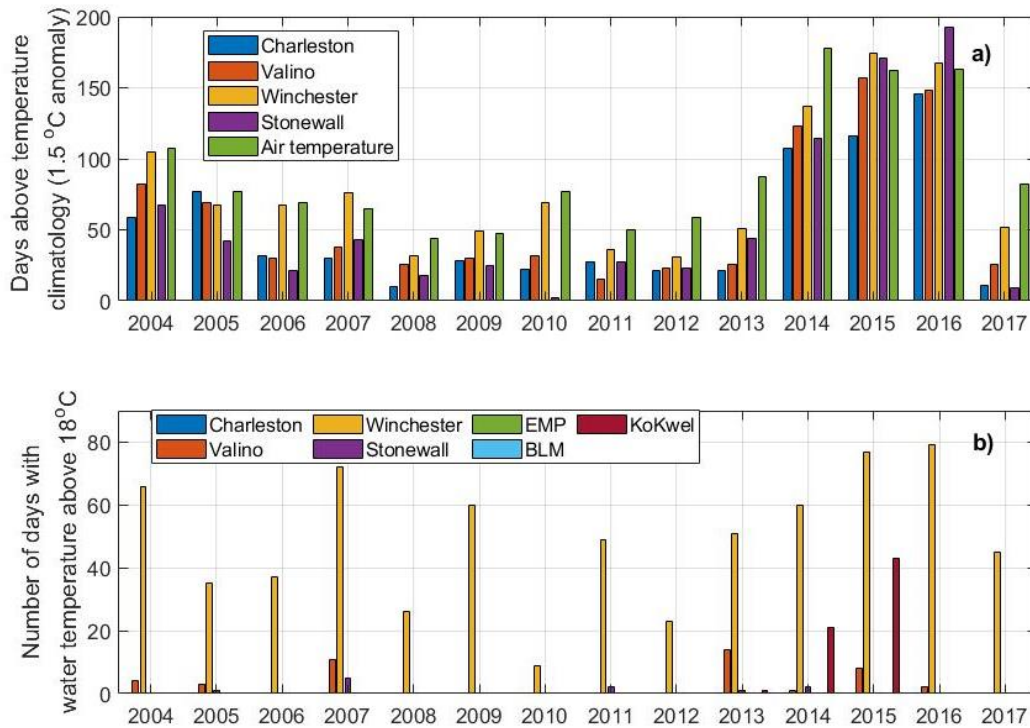
Sup. Fig. 2. Stressful number of days for eelgrass (Zostera marina) according to previous research (Table 2) using the low-pass filtered data (30-day filter). a) Number of days with temperatures 1.5 ℃ above climatology. b) Number of days with temperature above 18 ℃ at the water quality stations and Stonewall buoy (Table 1).
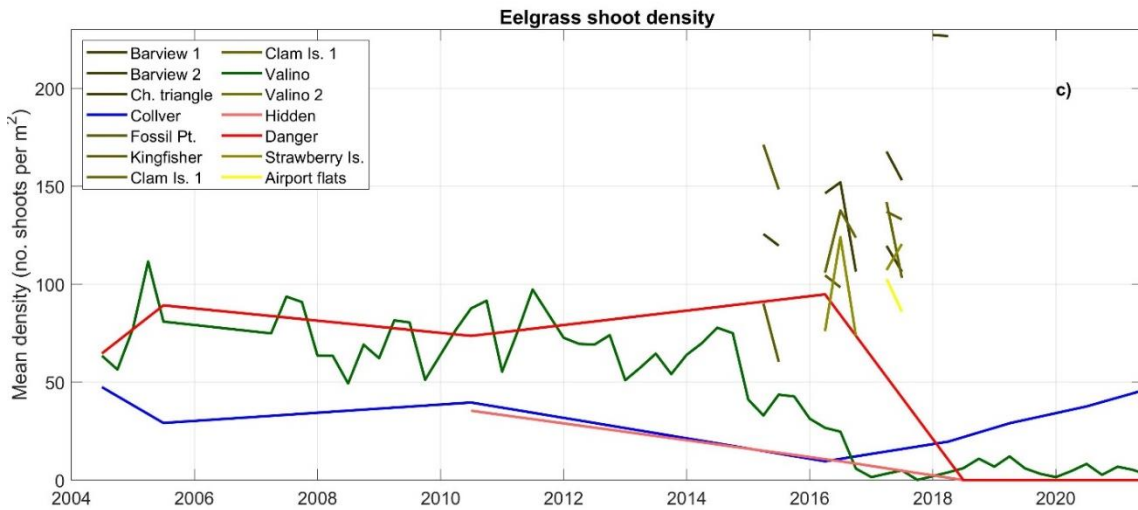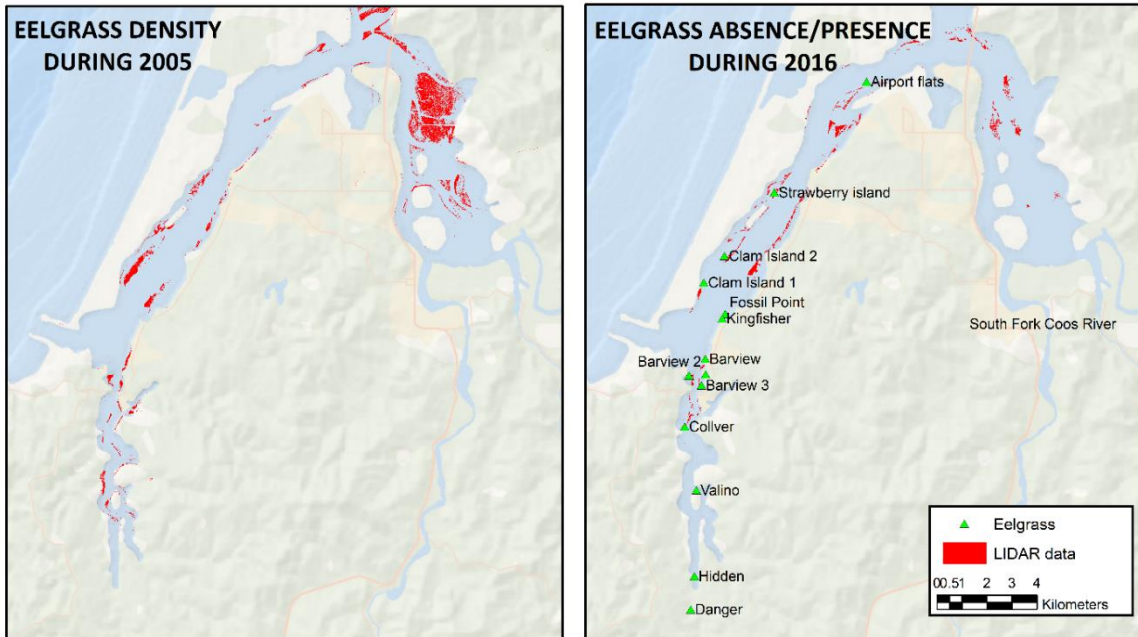
Sup. Fig. 3. a) Eelgrass absence/presence in the Coos Estuary from 2005 Lidar data. b) Eelgrass density in the Coos Estuary from 2016 Lidar data. Location of in-situ sampling performed by SSNERR, ODFW SEACOR and OSU is also shown. c) Density of eelgrass (number of shoots m-2) until present for all eelgrass measurements from stations shown in (b). Stations not sampled by SSNERR are colored by distance from the mouth. SSNERR stations in the same color as Figure 3).
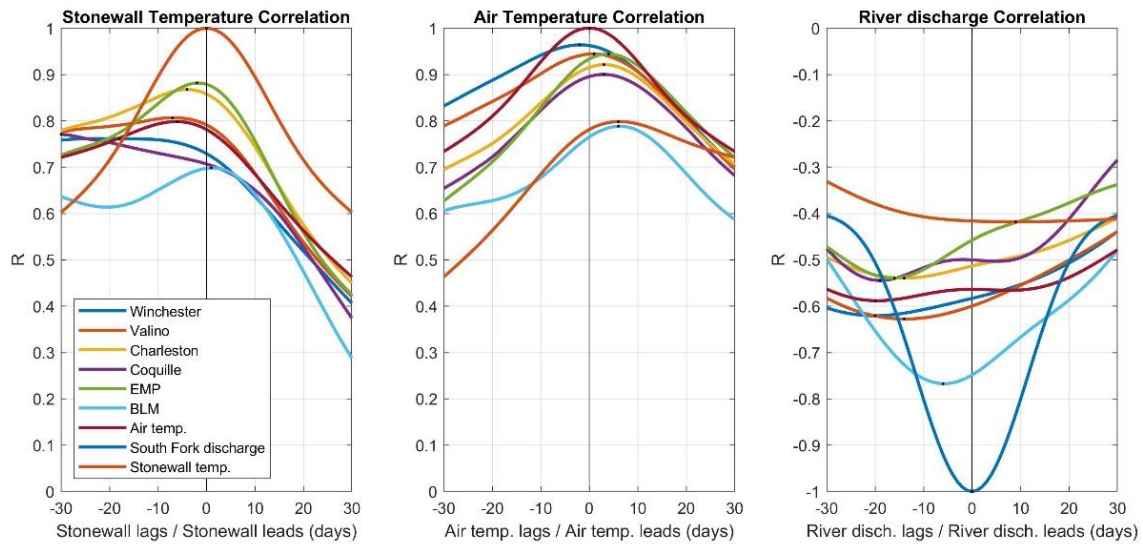
Sup. Fig. 4. Time series correlation between a) Stonewall water temperature (ocean end-member), b) North Bend airport air temperature (atmosphere end-member) and c) South Fork river discharge, and water quality station temperature. Maximum correlation is highlighted with black dots in each correlation line.

REFERENCES CITED

Chapter II

Alexander, M. A., Bladé, I., Newman, M., Lanzante, J. R., Lau, N.-C., and Scott, J. D. (2002). The Atmospheric Bridge: The Influence of ENSO Teleconnections on Air–Sea Interaction over the Global Oceans. *J. Clim.* 15, 2205–2231. doi:10.1175/1520-0442(2002)015<2205:TABTIO>2.0.CO;2.

Arega, F., Armstrong, S., and Badr, A. W. (2008). Modeling of residence time in the East Scott Creek Estuary, South Carolina, USA. *J. Hydro-Environment Res.* 2, 99–108. doi:10.1016/j.jher.2008.07.003.

Arneson, R. J. (1976). Seasonal Variations in Tidal Dynamics, Water Quality, and Sediments in the Coos Bay estuary.

Ascione Kenov, I., Garcia, A. C., and Neves, R. (2012). Residence time of water in the Mondego estuary (Portugal). *Estuar. Coast. Shelf Sci.* 106, 13–22. doi:10.1016/j.ecss.2012.04.008.

Baker, P. (1995). Review of ecology and fishery of the olympia oyster, Ostrea lurida with annotated bibliography. *J. Shellfish Res.* 14, 501–518.

Bakun, A., Black, B., Bograd, S. J., García-Reyes, M., Miller, a. J., Rykaczewski, R. R., et al. (2015). Anticipated Effects of Climate Change on Coastal Upwelling Ecosystems. *Curr. Clim. Chang. Reports*, 85–93. doi:10.1007/s40641-015-0008-4.

Banas, N., Hickey, B., Newton, J., and Ruesink, J. (2007). Tidal exchange, bivalve grazing, and patterns of primary production in Willapa Bay, Washington, USA. *Mar. Ecol. Prog. Ser.* 341, 123–139. doi:10.3354/meps341123.

Banas, N. S., and Hickey, B. M. (2005). Mapping exchange and residence time in a model of Willapa Bay, Washington, a branching, macrotidal estuary. *J. Geophys. Res. Ocean.* 110, 1–20. doi:10.1029/2005JC002950.

Banas, N. S., Hickey, B. M., MacCready, P., and Newton, J. A. (2004). Dynamics of Willapa Bay, Washington: A highly unsteady, partially mixed estuary. *J. Phys. Oceanogr.* 34, 2413–2427. doi:10.1175/JPO2637.1.

Banas, N. S., McDonald, P. S., and Armstrong, D. A. (2009). Green crab larval retention in Willapa Bay, Washington: An intensive Lagrangian modeling approach. *Estuaries and Coasts* 32, 893–905. doi:10.1007/s12237-009-9175-7.

Baptista, A. M. (1989). Salinity in Coos Bay, Oregon.

Barnard, P. L., Hoover, D., Hubbard, D. M., Snyder, A., Ludka, B. C., Allan, J., et al. (2017). Extreme oceanographic forcing and coastal response due to the 2015-2016 El Niño. *Nat. Commun.* 8, 6–13. doi:10.1038/ncomms14365.

Basilio, A., Searcy, S., and Thompson, A. R. (2017). Effects of the Blob on settlement of spotted sand bass, Paralabrax maculatofasciatus, to Mission Bay, San Diego, CA. *PLoS One* 12, 6–8. doi:10.1371/journal.pone.0188449.

Beca-Carretero, P., Olesen, B., Marbà, N., and Krause-Jensen, D. (2018). Response to experimental warming in northern eelgrass populations: Comparison across a range of temperature adaptations. *Mar. Ecol. Prog. Ser.* 589, 59–72. doi:10.3354/meps12439.

Bi, H., Peterson, W. T., and Strub, P. T. (2011). Transport and coastal zooplankton communities in the northern California Current system. *Geophys. Res. Lett.* 38, 1–5. doi:10.1029/2011GL047927.

Black, B. A., Sydeman, W. J., Frank, D. C., Griffin, D., Stahle, D. W., Garcia-Reyes, M., et al. (2014). Six centuries of variability and extremes in a coupled marine-terrestrial ecosystem. *Science (80-.).* 345, 1498–1502. doi:10.1126/science.1253209.

Black, B. A., van der Sleen, P., Di Lorenzo, E., Griffin, D., Sydeman, W. J., Dunham, J. B., et al. (2018). Rising synchrony controls western North American ecosystems. *Glob. Chang. Biol.* 24, 2305–2314. doi:10.1111/gcb.14128.

Blumberg, A. F., and Goodrich, D. M. (1990). Modeling of Wind-Induced Destratification in Chesapeake Bay. *Estuaries* 13, 236. doi:10.2307/1351914.

Bolaños, R., Brown, J. M., Amoudry, L. O., and Souza, A. J. (2013). Tidal, Riverine, and Wind Influences on the Circulation of a Macrotidal Estuary. *J. Phys. Oceanogr.* 43, 29–50. doi:10.1175/JPO-D-11-0156.1.

Bond, N. A., Cronin, M. F., Freeland, H., and Mantua, N. (2015). Causes and impacts of the 2014 warm anomaly in the NE Pacific. *Geophys. Res. Lett.* 42, 3414–3420. doi:10.1002/2015GL063306.

Borde, A. B., Thom, R. M., Rumrill, S., and Miller, L. M. (2003). Geospatial habitat change analysis in Pacific Northwest Coastal estuaries. *Estuaries* 26, 1104–1116. doi:10.1007/bf02803367.

Brasseale, E., Grason, E. W., McDonald, P. S., Adams, J., and MacCready, P. (2019). Larval Transport Modeling Support for Identifying Population Sources of European Green Crab in the Salish Sea. *Estuaries and Coasts* 42, 1586–1599. doi:10.1007/s12237-019-00586-2.

Brink, K. H., Beardsley, R. C., Paduan, J., Limeburner, R., Caruso, M., and Sires, J. G. (2000). A view of the 1993-1994 Califonia Current based on surface drifters, floats, and remotely sensed data. 105, 8575–8604.

Capotondi, A., Sardeshmukh, P. D., Di Lorenzo, E., Subramanian, A. C., and Miller, A. J. (2019). Predictability of US West Coast Ocean Temperatures is not solely due to ENSO. *Sci. Rep.* 9, 1–10. doi:10.1038/s41598-019-47400-4.

Chant, R. J. (2002a). Secondary circulation in a region of flow curvature : Relationship with tidal forcing and river discharge. 107, 1–11. doi:10.1029/2001JC001082.

Chant, R. J. (2002b). Secondary circulation in a region of flow curvature: Relationship with tidal forcing and river discharge. *J. Geophys. Res.* 107, 3131. doi:10.1029/2001JC001082.

Chen, C., Beardsley, R. C., Cowles, G., Qi, J., Lai, Z., Gao, G., et al. (2011a). An Unstructured-Grid, Finite-Volume Community Ocean Model. *FVCOM User Man.* 3rd editio, 1–409.

Chen, C., Liu, H., and Beardsley, R. C. (2003). An unstructured grid, finite-volume, three-dimensional, primitive equations ocean model: Application to coastal ocean and estuaries. *J. Atmos. Ocean. Technol.* 20, 159–186. doi:10.1175/1520-0426(2003)020<0159:AUGFVT>2.0.CO;2.

Chen, S.-N., Geyer, W. R., Ralston, D. K., and Lerczak, J. A. (2011b). Estuarine Exchange Flow Quantified with Isohaline Coordinates: Contrasting Long and Short Estuaries. *J. Phys. Oceanogr.* 42, 748–763. doi:10.1175/jpo-d-11-086.1.

Chen, S.-N., and Sanford, L. P. (2009). Axial Wind Effects on Stratification and Longitudinal Salt Transport in an Idealized, Partially Mixed Estuary*. *J. Phys. Oceanogr.* 39, 1905–1920. doi:10.1175/2009jpo4016.1.

Chen, T., Zhang, Q., Wu, Y., Ji, C., Yang, J., and Liu, G. (2018). Development of a wave-current model through coupling of FVCOM and SWAN. *Ocean Eng.* 164, 443–454. doi:10.1016/j.oceaneng.2018.06.062.

Chhak, K., and Di Lorenzo, E. (2007). Decadal variations in the California Current upwelling cells. *Geophys. Res. Lett.* 34, 1–6. doi:10.1029/2007GL030203.

Childers, D. L., Day, J. W., and Muller, R. A. (1990). Relating climatological forcing to coastal water levels in Louisiana estuaries and the potential importance of El Nino-Southern Oscillation events. *Clim. Res.* 1, 31–42. doi:10.3354/cr001031.

Clinton, P. J., Young, D. R., Specht, D. T., and Lee II, H. (2007). A Guide to Mapping Intertidal Eelgrass and Nonvegetated Habitats in Estuaries of the Pacific Northwest USA by Project Officer : Walter G . Nelson National Health and Environmental Effects Research Laboratory (NHEERL) Office of Research and D. Newport, OR.

Cloern, J. E., Jassby, A. D., Schraga, T. S., Nejad, E., and Martin, C. (2017). Ecosystem variability along the estuarine salinity gradient: Examples from long-term study of San Francisco Bay. *Limnol. Oceanogr.* doi:10.1002/lno.10537.

Conroy, T. B. (2018). The dynamics and exchange flow variability of the Coos estuary.

Conroy, T., Sutherland, D. A., and Ralston, D. K. (2020). Estuarine Exchange Flow Variability in a Seasonal, Segmented Estuary. *J. Phys. Oceanogr.* 50, 595–613. doi:10.1175/JPO-D-19-0108.1.

Coogan, J., and Dzwonkowski, B. (2018). Observations of wind forcing effects on estuary length and salinity flux in a river-dominated, microtidal Estuary, Mobile Bay, Alabama. *J. Phys. Oceanogr.* 48, 1787–1802. doi:10.1175/JPO-D-17-0249.1.

Coogan, J., Dzwonkowski, B., Park, K., and Webb, B. (2020). Observations of Restratification after a Wind Mixing Event in a Shallow Highly Stratified Estuary. *Estuaries and Coasts* 43, 272–285. doi:10.1007/s12237-019-00689-w.

Costanza, R., D'Arge, R., de Groot, R., Farber, S., Grasso, M., Hannon, B., et al. (1997). The value of the world's ecosystem services and natural capital. *Nature* 387, 253–260. doi:10.1038/387253a0.

Cowen, R. K., and Sponaugle, S. (2009). Larval Dispersal and Marine Population Connectivity. *Ann. Rev. Mar. Sci.* 1, 443–466. doi:10.1146/annurev.marine.010908.163757.

Csanady, G. T. (1973). Wind-Induced Barotropic Motions in Long Lakes. *J. Phys. Oceanogr.* 3, 429–438. doi:10.1175/1520-0485(1973)003<0429:WIBMIL>2.0.CO;2.

Daly, E. A., Brodeur, R. D., and Auth, T. D. (2017). Anomalous ocean conditions in 2015: Impacts on spring Chinook salmon and their prey field. *Mar. Ecol. Prog. Ser.* 566, 168–182. doi:10.3354/meps12021.

Davis, K. A., Banas, N. S., Giddings, S. N., Siedlecki, S. A., MacCready, P., Lessard, E. J., et al. (2014). Estuary-enhanced upwelling of marine nutrients fuels coastal productivity in the U.S. Pacific Northwest. *J. Geophys. Res. Ocean.*, 8778–8799. doi:10.1002/2014JC010248.Received.

de Brauwere, A., de Brye, B., Blaise, S., and Deleersnijder, E. (2011). Residence time, exposure time and connectivity in the Scheldt Estuary. *J. Mar. Syst.* 84, 85–95. doi:10.1016/j.jmarsys.2010.10.001.

Defne, Z., and Ganju, N. K. (2015). Quantifying the Residence Time and Flushing Characteristics of a Shallow, Back-Barrier Estuary: Application of Hydrodynamic and Particle Tracking Models. *Estuaries and Coasts* 38, 1719–1734. doi:10.1007/s12237-014-9885-3.

Delefosse, M., Povidisa, K., Poncet, D., Kristensen, E., and Olesen, B. (2016). Variation in size and chemical composition of seeds from the seagrass Zostera marina-Ecological implications. *Aquat. Bot.* 131, 7–14. doi:10.1016/j.aquabot.2016.02.003.

Di Lorenzo, E., Fiechter, J., Schneider, N., Braceo, A., Miller, A. J., Franks, P. J. S., et al. (2009). Nutrient and salinity decadal variations in the central and eastern North Pacific. *Geophys. Res. Lett.* 36, 2003–2008. doi:10.1029/2009GL038261.

Di Lorenzo, E., and Mantua, N. (2016). Multi-year persistence of the 2014/15 North Pacific marine heatwave. *Nat. Clim. Chang.* 6, 1042–1047. doi:10.1038/nclimate3082.

Di Lorenzo, E., Schneider, N., Cobb, K. M., Franks, P. J. S., Chhak, K., Miller, A. J., et al. (2008). North Pacific Gyre Oscillation links ocean climate and ecosystem change. *Geophys. Res. Lett.* 35, 2–7. doi:10.1029/2007GL032838.

Echavarria-Heras, H. A., Solana-Arellano, E., and Franco-Vizcaíno, E. (2006). The Role of Increased Sea Surface Temperature on Eelgrass Leaf Dynamics: Onset of El Niño as a Proxy for Global Climate Change in San Quintín Bay, Baja California. *Bull. South. Calif. Acad. Sci.* 105, 113–127. doi:https://doi.org/10.3160/0038-3872(2006)105[113:TROISS]2.0.CO;2.

Eidam, E. F., Sutherland, D. A. A., Ralston, D. K. K., Dye, B., Conroy, T., Schmitt, J., et al. (2020). Impacts of 150 Years of Shoreline and Bathymetric Change in the Coos Estuary, Oregon, USA. *Estuaries and Coasts*. doi:10.1007/s12237-020-00732-1.

Emmett, R., Llansó, R., Newton, J., Thom, R. M., Hornberger, M., Morgan, C., et al. (2000). Geographic Signatures of North American West Coast Estuaries. *Estuaries* 23, 765. doi:10.2307/1352998.

Engineers, U. S. A. C. of (2015). COOS BAY FEDERAL NAVIGATION CHANNEL AND CHARLESTON SIDE CHANNEL Dredging Project.

Epifanio, C. E., and Garvine, R. W. (2001). Larval transport on the Atlantic Continental Shelf of North America: A review. *Estuar. Coast. Shelf Sci.* 52, 51–77. doi:10.1006/ecss.2000.0727.

135

Evans, E. C., McGregor, G. R., and Petts, G. E. (1998). River energy budgets with special reference to river bed processes. *Hydrol. Process.* 12, 575–595. doi:10.1002/(SICI)1099-1085(19980330)12:4<575::AID-HYP595>3.0.CO;2-Y.

Ferguson, A., Eyre, B., and Gay, J. (2004). Nutrient cycling in the sub-tropical Brunswick estuary, Australia. *Estuaries* 27, 1–17. doi:10.1007/BF02803556.

Fortunato, A. B., and Oliveira, A. (2005). Influence of Intertidal Flats on Tidal Asymmetry. *J. Coast. Res.* 215, 1062–1067. doi:10.2112/03-0089.1.

Frischknecht, M., Münnich, M., and Gruber, N. (2015). Remote versus local influence of ENSO on the California Current System. *J. Geophys. Res. Ocean.* 120, 1353–1374. doi:10.1002/2014JC010531.

Gao, Y., Fang, J., Du, M., Fang, J., Jiang, W., and Jiang, Z. (2017). Response of the eelgrass (Zostera marina L.) to the combined effects of high temperatures and the herbicide, atrazine. *Aquat. Bot.* 142, 41–47. doi:10.1016/j.aquabot.2017.06.005.

Garcia, A. M. P., Geyer, W. R., and Randall, N. (2021). Exchange Flows in Tributary Creeks Enhance Dispersion by Tidal Trapping. *Estuaries and Coasts*. doi:10.1007/s12237-021-00969-4.

Garcia, A. M. P., Randall, N., Geyer, W. R., Kranenburg, W., and Ralston, D. K. (2018). Effect of Tributary Creeks on Estuarine Dispersion. *Am. Geophys. Union* 20, 1634490.

Garvine, R. W. (1991). Subtidal Frequency Estuary-Shelf Interaction: Observations Near Delaware Bay. *J. Geophys. Res.* 96, 7049–7064. doi:10.1029/91jc00079.

Gentemann, C. L., Fewings, M. R., and García-Reyes, M. (2017). Satellite sea surface temperatures along the West Coast of the United States during the 2014–2016 northeast Pacific marine heat wave. *Geophys. Res. Lett.* 44, 312–319. doi:10.1002/2016GL071039.

George, G., Vethamony, P., Sudheesh, K., and Babu, M. T. (2011). Fish larval transport in a macro-tidal regime: Gulf of Kachchh, west coast of India. *Fish. Res.* 110, 160–169. doi:10.1016/j.fishres.2011.04.002.

Geyer, W. R. (1993). Three-dimensional tidal flow around headlands. *J. Geophys. Res. Ocean.* 98, 955–966. doi:10.1029/92JC02270.

Geyer, W. R. (1997). Influence of wind on dynamics and flushing of shallow estuaries. *Estuar. Coast. Shelf Sci.* 44, 713–722. doi:10.1006/ecss.1996.0140.

Geyer, W. R., and Ralston, D. K. (2018). A mobile pool of contaminated sediment in the Penobscot Estuary, Maine, USA. *Sci. Total Environ.* 612, 694–707. doi:10.1016/j.scitotenv.2017.07.195.

Geyer, W. R., Ralston, D. K., and Chen, J. (2020). Mechanisms of exchange flow in an estuary with a narrow, deep channel and wide, shallow shoals. *J. Geophys. Res. Ocean.*, 1–25. doi:10.1029/2020jc016092.

Giddings, S. N., and MacCready, P. (2017). Reverse Estuarine Circulation Due to Local and Remote Wind Forcing, Enhanced by the Presence of Along-Coast Estuaries. *J. Geophys. Res. Ocean.* 122, 10184–10205. doi:10.1002/2016JC012479.

Goodman, A. C., Thorne, K. M., Buffington, K. J., Freeman, C. M., and Janousek, C. N. (2018). El Niño Increases High-Tide Flooding in Tidal Wetlands Along the U.S. Pacific Coast. *J. Geophys. Res. Biogeosciences* 123, 3162–3177. doi:10.1029/2018JG004677.

Grason, E., McDonald, S., Adams, J., Little, K., Apple, J., and Pleus, A. (2018). Citizen science program detects range expansion of the globally invasive European green crab in Washington State (USA). *Manag. Biol. Invasions* 9, 39–47. doi:10.3391/mbi.2018.9.1.04.

Groner, M., Eisenlord, M., Yoshioka, R., Fiorenza, E., Dawkins, P., Graham, O., et al. (2021). Warming sea surface temperatures fuel summer epidemics of eelgrass wasting disease. *Mar. Ecol. Prog. Ser.* 679, 47–58. doi:10.3354/meps13902.

Groth, S., and Rumrill, S. (2009). History of Olympia Oysters (Ostrea lurida Carpenter 1864) in Oregon Estuaries, and a Description of Recovering Populations in Coos Bay. *J. Shellfish Res.* 28, 51–58. doi:10.2983/035.028.0111.

Guo, X., and Valle-Levinson, A. (2008). Wind effects on the lateral structure of density-driven circulation in Chesapeake Bay. *Cont. Shelf Res.* 28, 2450–2471. doi:10.1016/j.csr.2008.06.008.

Haase, A. T., Eggleston, D. B., Luettich, R. A., Weaver, R. J., and Puckett, B. J. (2012). Estuarine circulation and predicted oyster larval dispersal among a network of reserves. *Estuar. Coast. Shelf Sci.* 101, 33–43. doi:10.1016/j.ecss.2012.02.011.

Hansen, D. V., and Rattray, M. (1965). Gravitational circulation in straits and estuaries. *J. Mar. Res.* 23, 104–122. doi:10.1098/rspb.2009.2214.

Hare, J. A., Thorrold, S., Walsh, H., Reiss, C., Valle-Levinson, A., and Jones, C. (2005). Biophysical mechanisms of larval fish ingress into Chesapeake Bay. *Mar. Ecol. Prog. Ser.* 303, 295–310. doi:10.3354/meps303295.

Hessing-Lewis, M. L., Hacker, S. D., Menge, B. A., and Rumrill, S. S. (2011). Context-Dependent Eelgrass-Macroalgae Interactions Along an Estuarine Gradient in the Pacific Northwest, USA. *Estuaries and Coasts* 34, 1169–1181. doi:10.1007/s12237-011-9412-8.

Hickey, B. M., and Banas, N. S. (2003). Oceanography of the U . S . Pacific Northwest Coastal Ocean and Estuaries with Application to Coastal Ecology. *Estuaries* 26, 1010–1031.

Hickey, B. M., Zhang, X., and Banas, N. S. (2003). Coupling between the California Current System and a coastal plain estuary in low riverflow conditions. *J. Geophys. Res.* 108, 1–20. doi:10.1029/2002JC001737.

Hopkins, A. E. (1937). "Experimental observations on spawning, larval development, and setting in the Olympia oyster Ostrea lurida," in *Bulletin of the United States Bureau of fisheries*, ed. F. T. Bell, 48:66.

Hosack, G. R., Dumbauld, B. R., Ruesink, J. L., and Armstrong, D. A. (2006). Habitat associations of estuarine species: Comparisons of intertidal mudflat, seagrass (Zostera marina), and oyster (Crassostrea gigas) habitats. *Estuaries and Coasts* 29, 1150–1160. doi:10.1007/BF02781816.

Huang, H., Chen, C., Cowles, G. W., Winant, C. D., Beardsley, R. C., Hedstrom, K. S., et al. (2008). FVCOM validation experiments: Comparisons with ROMS for three idealized barotropic test problems. *J. Geophys. Res. Ocean.* 113, 1–14. doi:10.1029/2007JC004557.

Huyer, A. (1983). Coastal upwelling in the California current system. *Prog. Oceanogr.* 12, 259–284. doi:10.1016/0079-6611(83)90010-1.

Huyer, A., Smith, R. L., and Fleischbein, J. (2002). The coastal ocean off Oregon and northern California during the 1997-8 El Niño. *Prog. Oceanogr.* 54, 311–341. doi:10.1016/S0079-6611(02)00056-3.

Huyer, A., Wheeler, P. A., Strub, P. T., Smith, R. L., Letelier, R., and Kosro, P. M. (2007). Progress in Oceanography The Newport line off Oregon – Studies in the North East Pacific. 75, 126–160. doi:10.1016/j.pocean.2007.08.003.

Hyde, N. (2007). Towards national estuarine modeling and characterization / classification systems : a pilot study for Coos Bay.

Jackson, J. M., Johnson, G. C., Dosser, H. V., and Ross, T. (2018). Warming From Recent Marine Heatwave Lingers in Deep British Columbia Fjord. *Geophys. Res. Lett.* 45, 9757–9764. doi:10.1029/2018GL078971.

Jacox, M. G., Hazen, E. L., Zaba, K. D., Rudnick, D. L., Edwards, C. A., Moore, A. M., et al. (2016). Impacts of the 2015–2016 El Niño on the California Current System: Early assessment and comparison to past events. *Geophys. Res. Lett.* 43, 7072–7080. doi:10.1002/2016GL069716.

Janzen, C. D., and Wong, K.-C. (2002). Wind-forced dynamics at the estuary-shelf interface of a large coastal plain estuary. *J. Geophys. Res. Ocean.* 107, 3138. doi:10.1029/2001JC000959.

Jarvis, J. C., Moore, K. A., and Kenworthy, W. J. (2012). Characterization and ecological implication of eelgrass life history strategies near the species' southern limit in the western North Atlantic. *Mar. Ecol. Prog. Ser.* 444, 43–56. doi:10.3354/meps09428.

Johnson, M. R., Williams, S. L., Lieberman, C. H., and Solbak, A. (2003). Changes in the abundance of the seagrasses Zostera marina L. (eelgrass) and Ruppia maritima L. (widgeongrass) in San Diego, California, following an El Niño event. *Estuaries* 26, 106–115. doi:10.1007/BF02691698.

Juarez, B., Valle-levinson, A., Chant, R., and Li, M. (2019). Estuarine , Coastal and Shelf Science Observations of the lateral structure of wind-driven flow in a coastal plain estuary. *Estuar. Coast. Shelf Sci.* 217, 262–270. doi:10.1016/j.ecss.2018.11.018.

Kaldy, J. (2012). Influence of light, temperature and salinity on dissolved organic carbon exudation rates in Zostera marina L. *Aquat. Biosyst.* 8, 1–12. doi:10.1186/2046-9063-8-19.

Kaldy, J. E. (2014). Effect of temperature and nutrient manipulations on eelgrass Zostera marina L. from the Pacific Northwest, USA. *J. Exp. Mar. Bio. Ecol.* 453, 108–115. doi:10.1016/j.jembe.2013.12.020.

Kalnay, E., Kanamitsu, M., Kistler, R., Collins, W., Deaven, D., Gandin, L., et al. (1996). The NCEP/NCAR 40-Year Reanalysis Project. *Bull. Am. Meteorol. Soc.* 77, 437–471. doi:10.1175/1520-0477(1996)077<0437:TNYRP>2.0.CO;2.

Kimbro, D. L., Largier, J., and Grosholz, E. D. (2009). Coastal oceanographic processes influence the growth and size of a key estuarine species, the Olympia oyster. *Limnol. Oceanogr.* 54, 1425–1437. doi:10.4319/lo.2009.54.5.1425.

Kranenburg, W. M., Geyer, W. R., Garcia, A. M. P., and Ralston, D. K. (2019). Reversed lateral circulation in a sharp estuarine bend with weak stratification. *J. Phys. Oceanogr.* 49, 1619–1637. doi:10.1175/JPO-D-18-0175.1.

Lacy, J. R., and Monismith, S. G. (2001). Secondary currents in a curved, stratified, estuarine channel. *J. Geophys. Res. Ocean.* 106, 31283–31302. doi:10.1029/2000JC000606.

Lai, W., Pan, J., and Devlin, A. T. (2018). Impact of tides and winds on estuarine circulation in the Pearl River Estuary. *Cont. Shelf Res.* 168, 68–82. doi:10.1016/j.csr.2018.09.004.

Largier, J. L. (2003). Consideration in estimating larval dispersal distances. *Ecol. Appl.* 13, 71–89.

Largier, J. L. (2020). Upwelling Bays: How Coastal Upwelling Controls Circulation, Habitat, and Productivity in Bays. *Ann. Rev. Mar. Sci.* 12, 415–447. doi:10.1146/annurev-marine-010419-011020.

Lee II, H., and Brown, C. A. (2009). Classification of Regional Patterns of Environmental Drivers And Benthic Habitats in Pacific Northwest Estuaries.

Lee, K. S., Park, S. R., and Kim, Y. K. (2007). Effects of irradiance, temperature, and nutrients on growth dynamics of seagrasses: A review. *J. Exp. Mar. Bio. Ecol.* 350, 144–175. doi:10.1016/j.jembe.2007.06.016.

Lemagie, E. P., and Lerczak, J. A. (2015). A Comparison of Bulk Estuarine Turnover Timescales to Particle Tracking Timescales Using a Model of the Yaquina Bay Estuary. *Estuaries and Coasts* 38, 1797–1814. doi:10.1007/s12237-014-9915-1.

Lerczak, J. A., and Geyer, W. R. (2004). Modeling the Lateral Circulation in Straight, Stratified Estuaries*. *J. Phys. Oceanogr.* 34, 1410–1428. doi:10.1175/1520-0485(2004)034<1410:MTLCIS>2.0.CO;2.

Lerczak, J. A., Geyer, W. R., and Chant, R. J. (2006). Mechanisms Driving the Time-Dependent Salt Flux in a Partially Stratified Estuary*. *J. Phys. Oceanogr.* 36, 2296–2311. doi:10.1175/jpo2959.1.

Li, Y., and Li, M. (2011). Effects of winds on stratification and circulation in a partially mixed estuary. *J. Geophys. Res. Ocean.* 116. doi:10.1029/2010JC006893.

Liu, W. C., Chen, W. B., and Hsu, M. H. (2011). Using a three-dimensional particle-tracking model to estimate the residence time and age of water in a tidal estuary. *Comput. Geosci.* 37, 1148–1161. doi:10.1016/j.cageo.2010.07.007.

Logerwell, E. A., Mantua, N., Lawson, P. W., Francis, R. C., and Agostini, V. N. (2003). Tracking environmental processes in the coastal zone for understanding and predicting Oregon coho (Oncorhynchus kisutch) marine survival. *Fish. Oceanogr.* 12, 554–568. doi:10.1046/j.1365-2419.2003.00238.x.

Lucas, L. V., Thompson, J. K., and Brown, L. R. (2009). Why are diverse relationships observed between phytoplankton biomass and transport time? *Limnol. Oceanogr.* 54, 381–390. doi:10.4319/lo.2009.54.1.0381.

MacCready, P. (2011). Calculating Estuarine Exchange Flow Using Isohaline Coordinates [*]. *J. Phys. Oceanogr.* 41, 1116–1124. doi:10.1175/2011JPO4517.1.

MacCready, P., and Geyer, W. R. (2010). Advances in Estuarine Physics. *Ann. Rev. Mar. Sci.* 2, 35–58. doi:10.1146/annurev-marine-120308-081015.

MacVean, L. J., and Stacey, M. T. (2011). Estuarine Dispersion from Tidal Trapping: A New Analytical Framework. *Estuaries and Coasts* 34, 45–59. doi:10.1007/s12237-010-9298-x.

McIntyre, B. A., McPhee-Shaw, E. E., Hatch, M. B. A., and Arellano, S. M. (2020). Location Matters: Passive and Active Factors Affect the Vertical Distribution of Olympia Oyster (Ostrea lurida) Larvae. *Estuaries and Coasts*. doi:10.1007/s12237-020-00771-8.

McKay, P., and Iorio, D. Di (2008). Heat budget for a shallow, sinuous salt marsh estuary. *Cont. Shelf Res.* 28, 1740–1753. doi:10.1016/j.csr.2008.04.008.

Menniti, C. M., Whitney, M. M., and Deignan-Schmidt, S. R. (2020). The Importance of Offshore Exchange for Water Temperatures in Norwalk Harbor. *Estuaries and Coasts*, 787–800. doi:10.1007/s12237-020-00710-7.

Meyers, S. D., and Luther, M. E. (2008). A Numerical Simulation of Residual Circulation in Tampa Bay. Part II: Lagrangian Residence Time. *Estuaries and Coasts* 31, 815–827. doi:10.1007/s12237-008-9085-0.

Milcu, A. I., Hanspach, J., Abson, D., and Fischer, J. (2013). Cultural ecosystem services: A literature review and prospects for future research. *Ecol. Soc.* 18. doi:10.5751/ES-05790-180344.

Miller, J. A., and Shanks, A. L. (2004). Ocean-estuary coupling in the Oregon upwelling region: Abundance and transport of juvenile fish and of crab megalopae. *Mar. Ecol. Prog. Ser.* 271, 267–279. doi:10.3354/meps271267.

Minello, T. J., Rozas, L. P., and Baker, R. (2012). Geographic Variability in Salt Marsh Flooding Patterns may Affect Nursery Value for Fishery Species. *Estuaries and Coasts* 35, 501–514. doi:10.1007/s12237-011-9463-x.

Monismith, S. (1986). An experimental study of the upwelling response of stratified reservoirs to surface shear stress. *J. Fluid Mech.* 171, 407. doi:10.1017/S0022112086001507.

Monsen, N. E., Cloern, J. E., Lucas, L. V., and Monismith, S. G. (2002). A comment on the use of flushing time, residence time, and age as transport time scales. *Limnol. Oceanogr.* 47, 1545–1553. doi:10.4319/lo.2002.47.5.1545.

Nejrup, L. B., and Pedersen, M. F. (2008). Effects of salinity and water temperature on the ecological performance of Zostera marina. *Aquat. Bot.* 88, 239–246. doi:10.1016/j.aquabot.2007.10.006.

Nidzieko, N. J., and Monismith, S. G. (2013). Contrasting Seasonal and Fortnightly Variations in the Circulation of a Seasonally Inverse Estuary, Elkhorn Slough, California. *Estuaries and Coasts* 36, 1–17. doi:10.1007/s12237-012-9548-1.

NOAA National Estuarine Research Reserve System (NERRS) (2020). System-wide Monitoring Program. *NOAA NERRS Cent. Data Manag. Off. website http//www.nerrsdata.org*. Available at: http://www.nerrsdata.org/ [Accessed June 11, 2020].

O'Higgins, T., and Rumrill, S. S. (2007). Tidal and Watershed Forcing of Nutrients and Dissolved Oxygen Stress within Four Pacific Coast Estuaries: Analysis of Time-Series Data collected by the National Estuarine Research Reserve System-Wide Monitoring Program (2000-2006) within Padilla Bay (WA),. *NOAA/UNH Coop. Inst. Coast. Estuar. Environ. Technol.*, 1689–1699. doi:10.1017/CBO9781107415324.004.

Oates, M. S. (2013). Obervations of Gonad Structure and Gametogenic Timing in a recovering population of Ostrea Lurida (Carpenter, 1864).

Officer, C. B., Biggs, R. B., Taft, J. L., Cronin, L. E., Tyler, M. A., and Boynton, W. R. (1984). Chesapeake Bay Anoxia: Origin, Development, and Significance. *Science (80-.).* 223, 22–27. doi:10.1126/science.223.4631.22.

Okubo, A. (1973). Effect of shoreline irregularities on streamwise dispersion in estuaries and other embayments. *Netherlands J. Sea Res.* 6, 213–224. doi:10.1016/0077-7579(73)90014-8.

OSU (1971). Oceanography of the nearshore coastal waters of the Pacific Northwest relating to possible pollution - Volume 1. Corvallis, Oregon 97331.

Parmesan, C., and Yohe, G. (2003). A globally coherent fingerprint of climate change. *Nature* 421, 37–42.

Pawlowicz, R., Beardsley, R. C., and Lentz, S. J. (2002). Classical tidal harmonic analysis including error estimates in MATLAB using T TIDE $. 28, 929–937.

Pawlowicz, R., Hannah, C., and Rosenberger, A. (2019). Lagrangian observations of estuarine residence times, dispersion, and trapping in the Salish Sea. *Estuar. Coast. Shelf Sci.* 225, 106246. doi:10.1016/j.ecss.2019.106246.

Pecly, J. O. G., and Roldão, J. S. F. (2013). Dye tracers as a tool for outfall studies: Dilution measurement approach. *Water Sci. Technol.* 67, 1564–1573. doi:10.2166/wst.2013.027.

Peteiro, L. G., and Shanks, A. L. (2015). Up and down or how to stay in the bay: Retentive strategies of Olympia oyster larvae in a shallow estuary. *Mar. Ecol. Prog. Ser.* 530, 103–117. doi:10.3354/meps11283.

Peterson, M. S. (2003). A Conceptual View of Environment-Habitat-Production Linkages in Tidal River Estuaries. *Rev. Fish. Sci.* 11, 291–313. doi:10.1080/10641260390255844.

Peterson, W. T., Fisher, J. L., Strub, P. T., Du, X., Risien, C., Peterson, J., et al. (2017). The pelagic ecosystem in the Northern California Current off Oregon during the 2014-2016 warm anomalies within the context of the past 20 years. *J. Geophys. Res. Ocean.* 122, 7267–7290. doi:10.1002/2017JC012952.

Pfeiffer-Herbert, A. S., Kincaid, C. R., Bergondo, D. L., and Pockalny, R. A. (2015). Dynamics of wind-driven estuarine-shelf exchange in the Narragansett Bay estuary. *Cont. Shelf Res.* 105, 42–59. doi:10.1016/j.csr.2015.06.003.

Phillips, R. C. (1984). The ecology of eelgrass meadows in the Pacific Northwest: a community profile. *US Fish Wildl. Serv.* Available at: https://linkinghub.elsevier.com/retrieve/pii/0304377083900207.

Phillips, R. C., McMillan, C., and Bridges, K. W. (1983). Phenology of eelgrass, Zostera marina L., along latitudinal gradients in North America. *Aquat. Bot.* 15, 145–156. doi:10.1016/0304-3770(83)90025-6.

Poloczanska, E. S., Brown, C. J., Sydeman, W. J., Kiessling, W., Schoeman, D. S., Moore, P. J., et al. (2013). Global imprint of climate change on marine life. *Nat. Clim. Chang.* 3, 919–925. doi:10.1038/nclimate1958.

Pritchard, C. E., Shanks, A. L., Rimler, R. N., Oates, M., and Rumrill, S. S. (2015). The olympia oyster ostrea lurida: Recent advances in natural history, ecology, and restoration. *J. Shellfish Res.* 34, 259–271. doi:10.2983/035.034.0207.

Pritchard, C., Rimler, R., Rumrill, S., Emlet, R., and Shanks, A. (2016). Variation in larval supply and recruitment of Ostrea lurida in the Coos Bay estuary, Oregon, USA. *Mar. Ecol. Prog. Ser.* 560, 159–171. doi:10.3354/meps11894.

Purkiani, K., Becherer, J., Klingbeil, K., and Burchard, H. (2016). Wind-induced variability of estuarine circulation in a tidally energetic inlet with curvature. *J. Geophys. Res. Ocean.* 121, 3261–3277. doi:10.1002/2015JC010945.

Qi, J., Chen, C., Beardsley, R. C., Perrie, W., Cowles, G. W., and Lai, Z. (2009). An unstructured-grid finite-volume surface wave model (FVCOM-SWAVE): Implementation, validations and applications. *Ocean Model.* 28, 153–166. doi:10.1016/j.ocemod.2009.01.007.

Qin, Q., and Shen, J. (2019). Physical transport processes affect the origins of harmful algal blooms in estuaries. *Harmful Algae* 84, 210–221. doi:10.1016/j.hal.2019.04.002.

Raimonet, M., and Cloern, J. E. (2017). Estuary–ocean connectivity: fast physics, slow biology. *Glob. Chang. Biol.* 23, 2345–2357. doi:10.1111/gcb.13546.

Ralston, D. K., Brosnahan, M. L., Fox, S. E., Lee, K. D., and Anderson, D. M. (2015). Temperature and Residence Time Controls on an Estuarine Harmful Algal Bloom: Modeling Hydrodynamics and Alexandrium fundyense in Nauset Estuary. *Estuaries and Coasts* 38, 2240–2258. doi:10.1007/s12237-015-9949-z.

Ralston, D. K., Geyer, W. R., and Lerczak, J. A. (2010a). Structure, variability, and salt flux in a strongly forced salt wedge estuary. *J. Geophys. Res.* 115, C06005. doi:10.1029/2009JC005806.

Ralston, D. K., Geyer, W. R., Lerczak, J. A., and Scully, M. (2010b). Turbulent mixing in a strongly forced salt wedge estuary. *J. Geophys. Res. Ocean.* 115, 1–21. doi:10.1029/2009JC006061.

Ralston, D. K., and Stacey, M. T. (2005). Longitudinal dispersion and lateral circulation in the intertidal zone. *J. Geophys. Res. C Ocean.* 110, 1–17. doi:10.1029/2005JC002888.

Ralston, D. K., and Stacey, M. T. (2007). Tidal and meteorological forcing of sediment transport in tributary mudflat channels. *Cont. Shelf Res.* 27, 1510–1527. doi:10.1016/j.csr.2007.01.010.

Rinehimer, J. P., and Thomson, J. T. (2014). Observations and modeling of heat fluxes on tidal flats. *J. Geophys. Res. Ocean.* 119, 133–146. doi:10.1002/2013JC009225.

Roegner, G. C., Armstrong, D. A., and Shanks, A. L. (2007). Wind and tidal influences on larval crab recruitment to an Oregon estuary. *Mar. Ecol. Prog. Ser.* 351, 177–188. doi:10.3354/meps07130.

Roegner, G. C., Hickey, B. M., Newton, J. a., Shanks, A. L., and Armstrong, D. a. (2002). Wind-induced plume and bloom intrusions into Willapa Bay, Washington. *Limnol. Oceanogr.* 47, 1033–1042. doi:10.4319/lo.2002.47.4.1033.

Roegner, G. C., Needoba, J. A., and Baptista, A. M. (2011). Coastal upwelling supplies oxygen-depleted water to the columbia river estuary. *PLoS One* 6. doi:10.1371/journal.pone.0018672.

Roegner, G. C., and Shanks, A. L. (2001). Import of Coastally-Derived Chlorophyll a to South Slough, Oregon. *Estuaries* 244, 244–256. doi:10.2307/1352948.

Rumrill, S. S. (2007). The Ecology of the South Slough Estuary: Site Profile of the South Slough National Estuarine Research Reserve.

Salo, T., and Pedersen, M. F. (2014). Synergistic effects of altered salinity and temperature on estuarine eelgrass (Zostera marina) seedlings and clonal shoots. *J. Exp. Mar. Bio. Ecol.* 457, 143–150. doi:10.1016/j.jembe.2014.04.008.

Sanay, R., and Valle-Levinson, A. (2005). Wind-induced circulation in semienclosed homogeneous, rotating basins. *J. Phys. Oceanogr.* 35, 2520–2531. doi:10.1175/JPO2831.1.

Sawall, Y., Ito, M., and Pansch, C. (2021). Chronically elevated sea surface temperatures revealed high susceptibility of the eelgrass <scp> *Zostera marina* </scp> to winter and spring warming. *Limnol. Oceanogr.*, 1–13. doi:10.1002/lno.11947.

Schneider, S. (1993). "Scenarios of global warming," in *Biotic interactions and Global change*, eds. P. Kareiva, J. Kingsolver, and R. Huey (Sunderland, MA: Sinauer Associates), 9–23.

Scully, M. E., Friedrichs, C., and Brubaker, J. (2005). Control of estuarine stratification and mixing by wind-induced straining of the estuarine density field. *Estuaries* 28, 321–326. doi:10.1007/BF02693915.

Seppelt, R., Dormann, C. F., Eppink, F. V., Lautenbach, S., and Schmidt, S. (2011). A quantitative review of ecosystem service studies: Approaches, shortcomings and the road ahead. *J. Appl. Ecol.* 48, 630–636. doi:10.1111/j.1365-2664.2010.01952.x.

Shanks, A. L., Rasmuson, L. K., Valley, J. R., Jarvis, M. A., Salant, C., Sutherland, D. A., et al. (2020). Marine heat waves, climate change, and failed spawning by coastal invertebrates. *Limnol. Oceanogr.* 65, 627–636. doi:10.1002/lno.11331.

Sharples, J., Middelburg, J. J., Fennel, K., and Jickells, T. D. (2017). What proportion of riverine nutrients reaches the open ocean? *Global Biogeochem. Cycles* 31, 39–58. doi:10.1002/2016GB005483.

Sherman, K., and DeBruyckere, L. A. (2018). Eelgrass Habitats on the U.S. West Coast. State of the Knowledge of Eelgrass Ecosystem Services and Eelgrass Extent. A publication prepared by the Pacific Marine and Estuarine Fish Habitat Partnership. Available at: http://www.pacificfishhabitat.org/wp-content/uploads/2017/09/EelGrass_Report_Final_ForPrint_web.pdfeation 20180109.pdf?ver=2018-01-12-102015-010.

Short, F. T., and Coles, R. G. (2001). *Global seagrass research methods*. , eds. F. T. Short and R. G. Coles Elsevier.

Short, F. T., McKenzie, L. J., Coles, R. G., Vidler, K. P., and Gaeckle, J. L. (2006). SeagrassNet Manual for Scientific Monitoring of Seagrass Habitat. 1–75.

Simpson, J. H., Vennell, R., and Souza, A. J. (2001). The Salt Fluxes in a Tidally-Energetic Estuary. *Estuar. Coast. Shelf Sci.* 52, 131–142. doi:10.1006/ecss.2000.0733.

Smith, N. P. (1983). A comparison of winter and summer temperature variations in a shallow bar-built estuary. *Estuaries* 6, 2–9. doi:10.2307/1351801.

Steele, M. O., Chang, H., Reusser, D. A., Brown, C. A., and Jung, I.-W. (2012). Potential Climate-Induced Runoff Changes and Associated Uncertainty in Four Pacific Northwest Estuaries. 52.

Stevenson, J. W., and Niiler, P. P. (1983). Upper Ocean Heat Budget During the Hawaii-to-Tahiti Shuttle Experiment. *J. Phys. Oceanogr.* 13, 1894–1907. doi:10.1175/1520-0485(1983)013<1894:UOHBDT>2.0.CO;2.

Stommel, H., and Farmer, H. G. (1952). On the nature of estuarine circulation.

Strub, P. T., Allen, J. S., Huyer, A., Smith, R. L., and Beardsley, R. C. (1987). Seasonal cycles of currents, temperatures, winds, and sea level over the northeast Pacific continental shelf: 35°N to 48°N. *J. Geophys. Res.* 92, 1507. doi:10.1029/JC092iC02p01507.

Sutherland, D. A., and O'Neill, M. A. (2016). Hydrographic and dissolved oxygen variability in a seasonal Pacific Northwest estuary. *Estuar. Coast. Shelf Sci.* 172, 47–59. doi:10.1016/j.ecss.2016.01.042.

Teodósio, M. A., Paris, C. B., Wolanski, E., and Morais, P. (2016). Biophysical processes leading to the ingress of temperate fish larvae into estuarine nursery areas: A review. *Estuar. Coast. Shelf Sci.* 183, 187–202. doi:10.1016/j.ecss.2016.10.022.

Thom, R. M., Borde, A. B., Rumrill, S., Woodruff, D. L., Williams, G. D., Southard, J. A., et al. (2003). Factors influencing spatial and annual variability in eelgrass (Zostera marina L.) meadows in Willapa Bay, Washington, and Coos Bay, Oregon, estuaries. *Estuaries* 26, 1117–1129. doi:10.1007/BF02803368.

Thomann, R. V., and Mueller, J. A. (1987). Principles of surface water quality modeling and control. *Harper Row Publ.*

U.S. Army Corps of Engineers (2015). COOS BAY FEDERAL NAVIGATION CHANNEL AND CHARLESTON SIDE CHANNEL Dredging Project. Portland, OR.

Uncles, R. J., and Stephens, J. A. (2011). The Effects of Wind, Runoff and Tides on Salinity in a Strongly Tidal Sub-estuary. *Estuaries and Coasts* 34, 758–774. doi:10.1007/s12237-010-9365-3.

Valle-Levinson, A., Schettini, C. A. F., and Truccolo, E. C. (2019). Subtidal variability of exchange flows produced by river pulses, wind stress and fortnightly tides in a subtropical stratified estuary. *Estuar. Coast. Shelf Sci.* 221, 72–82. doi:10.1016/j.ecss.2019.03.022.

Valle-Levinson, A., Wong, K.-C., and Bosley, K. T. (2001). Observations of the wind-induced exchange at the entrance to Chesapeake Bay. *J. Mar. Res.* 59, 391–416. doi:10.1357/002224001762842253.

van Sebille, E., Delandmeter, P., Schofield, J., Hardesty, B. D., Jones, J., and Donnelly, A. (2019). Basin-scale sources and pathways of microplastic that ends up in the Galápagos Archipelago. *Ocean Sci.* 15, 1341–1349. doi:10.5194/os-15-1341-2019.

Walther, G.-R., Post, E., Convey, P., Menzel, A., Parmesan, C., Beebee, T. J. C., et al. (2002). Ecological responses to recent climate change. *Nature* 416, 389–395.

Wang, C. F., Hsu, M. H., and Kuo, A. Y. (2004). Residence time of the Danshuei River estuary, Taiwan. *Estuar. Coast. Shelf Sci.* 60, 381–393. doi:10.1016/j.ecss.2004.01.013.

Wang, S.-Y., Hipps, L., Gillies, R. R., and Yoon, J.-H. (2014). Probable causes of the abnormal ridge accompanying the 2013-2014 California drought: ENSO precursor and anthropogenic warming footprint. *Geophys. Res. Lett.* 41, 3220–3226. doi:10.1002/2014GL059748.

Wasson, K., Zabin, C. J., Bible, J., Briley, S., Deck, A. K., Grosholz, T., et al. (2015). A guide to Olympia Oyster Restoration and Conservation. Monterey Bay.

Wheat, E. E., Banas, N. S., and Ruesink, J. L. (2019). Multi-day water residence time as a mechanism for physical and biological gradients across intertidal flats. *Estuar. Coast. Shelf Sci.* 227, 106303. doi:10.1016/j.ecss.2019.106303.

Wild-Allen, K., and Andrewartha, J. (2016). Connectivity between estuaries influences nutrient transport, cycling and water quality. *Mar. Chem.* 185, 12–26. doi:10.1016/j.marchem.2016.05.011.

Wyrtki, K. (1984). The slope of sea level along the equator during the 1982/1983 El Nino. *J. Geophys. Res.* 89, 10419–10424. doi:10.1029/JC089iC06p10419.

Xia, M., Xie, L., Pietrafesa, L. J., and Whitney, M. M. (2011). The ideal response of a Gulf of Mexico estuary plume to wind forcing: Its connection with salt flux and a Lagrangian view. *J. Geophys. Res.* 116, C08035. doi:10.1029/2010JC006689.

Xie, L., and Eggleston, D. B. (1999). Computer simulations of wind-induced estuarine circulation patterns and estuary-shelf exchange processes: The potential role of wind forcing on larval transport. *Estuar. Coast. Shelf Sci.* 49, 221–234. doi:10.1006/ecss.1999.0498.

Yamada, S. B., Dumbauld, B. R., Kalin, A., Hunt, C. E., Figlar-Barnes, R., and Randall, A. (2005). Growth and persistence of a recent invader Carcinus maenas in estuaries of the northeastern Pacific. *Biol. Invasions* 7, 309–321. doi:10.1007/s10530-004-0877-2.

Yamada, S. B., Randall, A., Schooler, S., Heller, R., Donaldson, L., Takacs, G., et al. (2020). Status of the European green crab, Carcinus maenas, in Oregon and Washington coastal estuaries in 2019. Portland, OR Available at: http://scholar.google.com/scholar?hl=en&btnG=Search&q=intitle:Status+of+the+European+Green+Crab+in+Oregon+and+Washington+Estuaries#3.

Yang, Z., Khangaonkar, T., and Wang, T. (2011). Use of Advanced Meteorological Model Output for Coastal Ocean Modeling in Puget Sound. *Int. J. Ocean Clim. Syst.* 2, 101–117. doi:10.1260/1759-3131.2.2.101.

Zapata, C., Puente, A., Garca, A., Garcia-Alba, J., and Espinoza, J. (2018). Assessment of ecosystem services of an urbanized tropical estuary with a focus on habitats and scenarios. *PLoS One* 13, 1–19. doi:10.1371/journal.pone.0203927.

Zimmerman, R. C., Smith, R. D., and Alberte, R. S. (1989). Thermal acclimation and whole-plant carbon balance in Zostera marina L. (eelgrass). *J. Exp. Mar. Bio. Ecol.* 130, 93–109. doi:10.1016/0022-0981(89)90197-4.

Chapter III

Alexander, M. A., Bladé, I., Newman, M., Lanzante, J. R., Lau, N.-C., and Scott, J. D. (2002). The Atmospheric Bridge: The Influence of ENSO Teleconnections on Air–Sea Interaction over the Global Oceans. *J. Clim.* 15, 2205–2231. doi:10.1175/1520-0442(2002)015<2205:TABTIO>2.0.CO;2.

Arega, F., Armstrong, S., and Badr, A. W. (2008). Modeling of residence time in the East Scott Creek Estuary, South Carolina, USA. *J. Hydro-Environment Res.* 2, 99–108. doi:10.1016/j.jher.2008.07.003.

Arneson, R. J. (1976). Seasonal Variations in Tidal Dynamics, Water Quality, and Sediments in the Coos Bay estuary.

Ascione Kenov, I., Garcia, A. C., and Neves, R. (2012). Residence time of water in the Mondego estuary (Portugal). *Estuar. Coast. Shelf Sci.* 106, 13–22. doi:10.1016/j.ecss.2012.04.008.

Baker, P. (1995). Review of ecology and fishery of the olympia oyster, Ostrea lurida with annotated bibliography. *J. Shellfish Res.* 14, 501–518.

Bakun, A., Black, B., Bograd, S. J., García-Reyes, M., Miller, a. J., Rykaczewski, R. R., et al. (2015). Anticipated Effects of Climate Change on Coastal Upwelling Ecosystems. *Curr. Clim. Chang. Reports*, 85–93. doi:10.1007/s40641-015-0008-4.

Banas, N., Hickey, B., Newton, J., and Ruesink, J. (2007). Tidal exchange, bivalve grazing, and patterns of primary production in Willapa Bay, Washington, USA. *Mar. Ecol. Prog. Ser.* 341, 123–139. doi:10.3354/meps341123.

Banas, N. S., and Hickey, B. M. (2005). Mapping exchange and residence time in a model of Willapa Bay, Washington, a branching, macrotidal estuary. *J. Geophys. Res. Ocean.* 110, 1–20. doi:10.1029/2005JC002950.

Banas, N. S., Hickey, B. M., MacCready, P., and Newton, J. A. (2004). Dynamics of Willapa Bay, Washington: A highly unsteady, partially mixed estuary. *J. Phys. Oceanogr.* 34, 2413–2427. doi:10.1175/JPO2637.1.

Banas, N. S., McDonald, P. S., and Armstrong, D. A. (2009). Green crab larval retention in Willapa Bay, Washington: An intensive Lagrangian modeling approach. *Estuaries and Coasts* 32, 893–905. doi:10.1007/s12237-009-9175-7.

Baptista, A. M. (1989). Salinity in Coos Bay, Oregon.

Barnard, P. L., Hoover, D., Hubbard, D. M., Snyder, A., Ludka, B. C., Allan, J., et al. (2017). Extreme oceanographic forcing and coastal response due to the 2015-2016 El Niño. *Nat. Commun.* 8, 6–13. doi:10.1038/ncomms14365.

Basilio, A., Searcy, S., and Thompson, A. R. (2017). Effects of the Blob on settlement of spotted sand bass, Paralabrax maculatofasciatus, to Mission Bay, San Diego, CA. *PLoS One* 12, 6–8. doi:10.1371/journal.pone.0188449.

Beca-Carretero, P., Olesen, B., Marbà, N., and Krause-Jensen, D. (2018). Response to experimental warming in northern eelgrass populations: Comparison across a range of temperature adaptations. *Mar. Ecol. Prog. Ser.* 589, 59–72. doi:10.3354/meps12439.

Bi, H., Peterson, W. T., and Strub, P. T. (2011). Transport and coastal zooplankton communities in the northern California Current system. *Geophys. Res. Lett.* 38, 1–5. doi:10.1029/2011GL047927.

Black, B. A., Sydeman, W. J., Frank, D. C., Griffin, D., Stahle, D. W., Garcia-Reyes, M., et al. (2014). Six centuries of variability and extremes in a coupled marine-terrestrial ecosystem. *Science (80-.).* 345, 1498–1502. doi:10.1126/science.1253209.

Black, B. A., van der Sleen, P., Di Lorenzo, E., Griffin, D., Sydeman, W. J., Dunham, J. B., et al. (2018). Rising synchrony controls western North American ecosystems. *Glob. Chang. Biol.* 24, 2305–2314. doi:10.1111/gcb.14128.

Blumberg, A. F., and Goodrich, D. M. (1990). Modeling of Wind-Induced Destratification in Chesapeake Bay. *Estuaries* 13, 236. doi:10.2307/1351914.

Bolaños, R., Brown, J. M., Amoudry, L. O., and Souza, A. J. (2013). Tidal, Riverine, and Wind Influences on the Circulation of a Macrotidal Estuary. *J. Phys. Oceanogr.* 43, 29–50. doi:10.1175/JPO-D-11-0156.1.

Bond, N. A., Cronin, M. F., Freeland, H., and Mantua, N. (2015). Causes and impacts of the 2014 warm anomaly in the NE Pacific. *Geophys. Res. Lett.* 42, 3414–3420. doi:10.1002/2015GL063306.

Borde, A. B., Thom, R. M., Rumrill, S., and Miller, L. M. (2003). Geospatial habitat change analysis in Pacific Northwest Coastal estuaries. *Estuaries* 26, 1104–1116. doi:10.1007/bf02803367.

Brasseale, E., Grason, E. W., McDonald, P. S., Adams, J., and MacCready, P. (2019). Larval Transport Modeling Support for Identifying Population Sources of European Green Crab in the Salish Sea. *Estuaries and Coasts* 42, 1586–1599. doi:10.1007/s12237-019-00586-2.

Brink, K. H., Beardsley, R. C., Paduan, J., Limeburner, R., Caruso, M., and Sires, J. G. (2000). A view of the 1993-1994 Califonia Current based on surface drifters, floats, and remotely sensed data. 105, 8575–8604.

Capotondi, A., Sardeshmukh, P. D., Di Lorenzo, E., Subramanian, A. C., and Miller, A. J. (2019). Predictability of US West Coast Ocean Temperatures is not solely due to ENSO. *Sci. Rep.* 9, 1–10. doi:10.1038/s41598-019-47400-4.

Chant, R. J. (2002a). Secondary circulation in a region of flow curvature : Relationship with tidal forcing and river discharge. 107, 1–11. doi:10.1029/2001JC001082.

Chant, R. J. (2002b). Secondary circulation in a region of flow curvature: Relationship with tidal forcing and river discharge. *J. Geophys. Res.* 107, 3131. doi:10.1029/2001JC001082.

Chen, C., Beardsley, R. C., Cowles, G., Qi, J., Lai, Z., Gao, G., et al. (2011a). An Unstructured-Grid, Finite-Volume Community Ocean Model. *FVCOM User Man.* 3rd editio, 1–409.

Chen, C., Liu, H., and Beardsley, R. C. (2003). An unstructured grid, finite-volume, three-dimensional, primitive equations ocean model: Application to coastal ocean and estuaries. *J. Atmos. Ocean. Technol.* 20, 159–186. doi:10.1175/1520-0426(2003)020<0159:AUGFVT>2.0.CO;2.

Chen, S.-N., Geyer, W. R., Ralston, D. K., and Lerczak, J. A. (2011b). Estuarine Exchange Flow Quantified with Isohaline Coordinates: Contrasting Long and Short Estuaries. *J. Phys. Oceanogr.* 42, 748–763. doi:10.1175/jpo-d-11-086.1.

Chen, S.-N., and Sanford, L. P. (2009). Axial Wind Effects on Stratification and Longitudinal Salt Transport in an Idealized, Partially Mixed Estuary*. *J. Phys. Oceanogr.* 39, 1905–1920. doi:10.1175/2009jpo4016.1.

Chen, T., Zhang, Q., Wu, Y., Ji, C., Yang, J., and Liu, G. (2018). Development of a wave-current model through coupling of FVCOM and SWAN. *Ocean Eng.* 164, 443–454. doi:10.1016/j.oceaneng.2018.06.062.

Chhak, K., and Di Lorenzo, E. (2007). Decadal variations in the California Current upwelling cells. *Geophys. Res. Lett.* 34, 1–6. doi:10.1029/2007GL030203.

Childers, D. L., Day, J. W., and Muller, R. A. (1990). Relating climatological forcing to coastal water levels in Louisiana estuaries and the potential importance of El Nino-Southern Oscillation events. *Clim. Res.* 1, 31–42. doi:10.3354/cr001031.

Clinton, P. J., Young, D. R., Specht, D. T., and Lee II, H. (2007). A Guide to Mapping Intertidal Eelgrass and Nonvegetated Habitats in Estuaries of the Pacific Northwest USA by Project Officer : Walter G . Nelson National Health and Environmental Effects Research Laboratory (NHEERL) Office of Research and D. Newport, OR.

Cloern, J. E., Jassby, A. D., Schraga, T. S., Nejad, E., and Martin, C. (2017). Ecosystem variability along the estuarine salinity gradient: Examples from long-term study of San Francisco Bay. *Limnol. Oceanogr.* doi:10.1002/lno.10537.

Conroy, T. B. (2018). The dynamics and exchange flow variability of the Coos estuary.

Conroy, T., Sutherland, D. A., and Ralston, D. K. (2020). Estuarine Exchange Flow Variability in a Seasonal, Segmented Estuary. *J. Phys. Oceanogr.* 50, 595–613. doi:10.1175/JPO-D-19-0108.1.

Coogan, J., and Dzwonkowski, B. (2018). Observations of wind forcing effects on estuary length and salinity flux in a river-dominated, microtidal Estuary, Mobile Bay, Alabama. *J. Phys. Oceanogr.* 48, 1787–1802. doi:10.1175/JPO-D-17-0249.1.

Coogan, J., Dzwonkowski, B., Park, K., and Webb, B. (2020). Observations of Restratification after a Wind Mixing Event in a Shallow Highly Stratified Estuary. *Estuaries and Coasts* 43, 272–285. doi:10.1007/s12237-019-00689-w.

Costanza, R., D'Arge, R., de Groot, R., Farber, S., Grasso, M., Hannon, B., et al. (1997). The value of the world's ecosystem services and natural capital. *Nature* 387, 253–260. doi:10.1038/387253a0.

Cowen, R. K., and Sponaugle, S. (2009). Larval Dispersal and Marine Population Connectivity. *Ann. Rev. Mar. Sci.* 1, 443–466. doi:10.1146/annurev.marine.010908.163757.

Csanady, G. T. (1973). Wind-Induced Barotropic Motions in Long Lakes. *J. Phys. Oceanogr.* 3, 429–438. doi:10.1175/1520-0485(1973)003<0429:WIBMIL>2.0.CO;2.

Daly, E. A., Brodeur, R. D., and Auth, T. D. (2017). Anomalous ocean conditions in 2015: Impacts on spring Chinook salmon and their prey field. *Mar. Ecol. Prog. Ser.* 566, 168–182. doi:10.3354/meps12021.

Davis, K. A., Banas, N. S., Giddings, S. N., Siedlecki, S. A., MacCready, P., Lessard, E. J., et al. (2014). Estuary-enhanced upwelling of marine nutrients fuels coastal productivity in the U.S. Pacific Northwest. *J. Geophys. Res. Ocean.*, 8778–8799. doi:10.1002/2014JC010248.Received.

de Brauwere, A., de Brye, B., Blaise, S., and Deleersnijder, E. (2011). Residence time, exposure time and connectivity in the Scheldt Estuary. *J. Mar. Syst.* 84, 85–95. doi:10.1016/j.jmarsys.2010.10.001.

Defne, Z., and Ganju, N. K. (2015). Quantifying the Residence Time and Flushing Characteristics of a Shallow, Back-Barrier Estuary: Application of Hydrodynamic and Particle Tracking Models. *Estuaries and Coasts* 38, 1719–1734. doi:10.1007/s12237-014-9885-3.

Delefosse, M., Povidisa, K., Poncet, D., Kristensen, E., and Olesen, B. (2016). Variation in size and chemical composition of seeds from the seagrass Zostera marina-Ecological implications. *Aquat. Bot.* 131, 7–14. doi:10.1016/j.aquabot.2016.02.003.

Di Lorenzo, E., Fiechter, J., Schneider, N., Braceo, A., Miller, A. J., Franks, P. J. S., et al. (2009). Nutrient and salinity decadal variations in the central and eastern North Pacific. *Geophys. Res. Lett.* 36, 2003–2008. doi:10.1029/2009GL038261.

Di Lorenzo, E., and Mantua, N. (2016). Multi-year persistence of the 2014/15 North Pacific marine heatwave. *Nat. Clim. Chang.* 6, 1042–1047. doi:10.1038/nclimate3082.

Di Lorenzo, E., Schneider, N., Cobb, K. M., Franks, P. J. S., Chhak, K., Miller, A. J., et al. (2008). North Pacific Gyre Oscillation links ocean climate and ecosystem change. *Geophys. Res. Lett.* 35, 2–7. doi:10.1029/2007GL032838.

Echavarria-Heras, H. A., Solana-Arellano, E., and Franco-Vizcaíno, E. (2006). The Role of Increased Sea Surface Temperature on Eelgrass Leaf Dynamics: Onset of El Niño as a Proxy for Global Climate Change in San Quintín Bay, Baja California. *Bull. South. Calif. Acad. Sci.* 105, 113–127. doi:https://doi.org/10.3160/0038-3872(2006)105[113:TROISS]2.0.CO;2.

Eidam, E. F., Sutherland, D. A. A., Ralston, D. K. K., Dye, B., Conroy, T., Schmitt, J., et al. (2020). Impacts of 150 Years of Shoreline and Bathymetric Change in the Coos Estuary, Oregon, USA. *Estuaries and Coasts*. doi:10.1007/s12237-020-00732-1.

Emmett, R., Llansó, R., Newton, J., Thom, R. M., Hornberger, M., Morgan, C., et al. (2000). Geographic Signatures of North American West Coast Estuaries. *Estuaries* 23, 765. doi:10.2307/1352998.

Engineers, U. S. A. C. of (2015). COOS BAY FEDERAL NAVIGATION CHANNEL AND CHARLESTON SIDE CHANNEL Dredging Project.

Epifanio, C. E., and Garvine, R. W. (2001). Larval transport on the Atlantic Continental Shelf of North America: A review. *Estuar. Coast. Shelf Sci.* 52, 51–77. doi:10.1006/ecss.2000.0727.

Evans, E. C., McGregor, G. R., and Petts, G. E. (1998). River energy budgets with special reference to river bed processes. *Hydrol. Process.* 12, 575–595. doi:10.1002/(SICI)1099-1085(19980330)12:4<575::AID-HYP595>3.0.CO;2-Y.

Ferguson, A., Eyre, B., and Gay, J. (2004). Nutrient cycling in the sub-tropical Brunswick estuary, Australia. *Estuaries* 27, 1–17. doi:10.1007/BF02803556.

Fortunato, A. B., and Oliveira, A. (2005). Influence of Intertidal Flats on Tidal Asymmetry. *J. Coast. Res.* 215, 1062–1067. doi:10.2112/03-0089.1.

Frischknecht, M., Münnich, M., and Gruber, N. (2015). Remote versus local influence of ENSO on the California Current System. *J. Geophys. Res. Ocean.* 120, 1353–1374. doi:10.1002/2014JC010531.

Gao, Y., Fang, J., Du, M., Fang, J., Jiang, W., and Jiang, Z. (2017). Response of the eelgrass (Zostera marina L.) to the combined effects of high temperatures and the herbicide, atrazine. *Aquat. Bot.* 142, 41–47. doi:10.1016/j.aquabot.2017.06.005.

Garcia, A. M. P., Geyer, W. R., and Randall, N. (2021). Exchange Flows in Tributary Creeks Enhance Dispersion by Tidal Trapping. *Estuaries and Coasts*. doi:10.1007/s12237-021-00969-4.

Garcia, A. M. P., Randall, N., Geyer, W. R., Kranenburg, W., and Ralston, D. K. (2018). Effect of Tributary Creeks on Estuarine Dispersion. *Am. Geophys. Union* 20, 1634490.

Garvine, R. W. (1991). Subtidal Frequency Estuary-Shelf Interaction: Observations Near Delaware Bay. *J. Geophys. Res.* 96, 7049–7064. doi:10.1029/91jc00079.

Gentemann, C. L., Fewings, M. R., and García-Reyes, M. (2017). Satellite sea surface temperatures along the West Coast of the United States during the 2014–2016 northeast Pacific marine heat wave. *Geophys. Res. Lett.* 44, 312–319. doi:10.1002/2016GL071039.

George, G., Vethamony, P., Sudheesh, K., and Babu, M. T. (2011). Fish larval transport in a macro-tidal regime: Gulf of Kachchh, west coast of India. *Fish. Res.* 110, 160–169. doi:10.1016/j.fishres.2011.04.002.

Geyer, W. R. (1993). Three-dimensional tidal flow around headlands. *J. Geophys. Res. Ocean.* 98, 955–966. doi:10.1029/92JC02270.

Geyer, W. R. (1997). Influence of wind on dynamics and flushing of shallow estuaries. *Estuar. Coast. Shelf Sci.* 44, 713–722. doi:10.1006/ecss.1996.0140.

Geyer, W. R., and Ralston, D. K. (2018). A mobile pool of contaminated sediment in the Penobscot Estuary, Maine, USA. *Sci. Total Environ.* 612, 694–707. doi:10.1016/j.scitotenv.2017.07.195.

Geyer, W. R., Ralston, D. K., and Chen, J. (2020). Mechanisms of exchange flow in an estuary with a narrow, deep channel and wide, shallow shoals. *J. Geophys. Res. Ocean.*, 1–25. doi:10.1029/2020jc016092.

Giddings, S. N., and MacCready, P. (2017). Reverse Estuarine Circulation Due to Local and Remote Wind Forcing, Enhanced by the Presence of Along-Coast Estuaries. *J. Geophys. Res. Ocean.* 122, 10184–10205. doi:10.1002/2016JC012479.

Goodman, A. C., Thorne, K. M., Buffington, K. J., Freeman, C. M., and Janousek, C. N. (2018). El Niño Increases High-Tide Flooding in Tidal Wetlands Along the U.S. Pacific Coast. *J. Geophys. Res. Biogeosciences* 123, 3162–3177. doi:10.1029/2018JG004677.

Grason, E., McDonald, S., Adams, J., Litle, K., Apple, J., and Pleus, A. (2018). Citizen science program detects range expansion of the globally invasive European green crab in Washington State (USA). *Manag. Biol. Invasions* 9, 39–47. doi:10.3391/mbi.2018.9.1.04.

Groner, M., Eisenlord, M., Yoshioka, R., Fiorenza, E., Dawkins, P., Graham, O., et al. (2021). Warming sea surface temperatures fuel summer epidemics of eelgrass wasting disease. *Mar. Ecol. Prog. Ser.* 679, 47–58. doi:10.3354/meps13902.

Groth, S., and Rumrill, S. (2009). History of Olympia Oysters (Ostrea lurida Carpenter 1864) in Oregon Estuaries, and a Description of Recovering Populations in Coos Bay. *J. Shellfish Res.* 28, 51–58. doi:10.2983/035.028.0111.

Guo, X., and Valle-Levinson, A. (2008). Wind effects on the lateral structure of density-driven circulation in Chesapeake Bay. *Cont. Shelf Res.* 28, 2450–2471. doi:10.1016/j.csr.2008.06.008.

Haase, A. T., Eggleston, D. B., Luettich, R. A., Weaver, R. J., and Puckett, B. J. (2012). Estuarine circulation and predicted oyster larval dispersal among a network of reserves. *Estuar. Coast. Shelf Sci.* 101, 33–43. doi:10.1016/j.ecss.2012.02.011.

Hansen, D. V., and Rattray, M. (1965). Gravitational circulation in straits and estuaries. *J. Mar. Res.* 23, 104–122. doi:10.1098/rspb.2009.2214.

Hare, J. A., Thorrold, S., Walsh, H., Reiss, C., Valle-Levinson, A., and Jones, C. (2005). Biophysical mechanisms of larval fish ingress into Chesapeake Bay. *Mar. Ecol. Prog. Ser.* 303, 295–310. doi:10.3354/meps303295.

Hessing-Lewis, M. L., Hacker, S. D., Menge, B. A., and Rumrill, S. S. (2011). Context-Dependent Eelgrass-Macroalgae Interactions Along an Estuarine Gradient in the Pacific Northwest, USA. *Estuaries and Coasts* 34, 1169–1181. doi:10.1007/s12237-011-9412-8.

Hickey, B. M., and Banas, N. S. (2003). Oceanography of the U . S . Pacific Northwest Coastal Ocean and Estuaries with Application to Coastal Ecology. *Estuaries* 26, 1010–1031.

Hickey, B. M., Zhang, X., and Banas, N. S. (2003). Coupling between the California Current System and a coastal plain estuary in low riverflow conditions. *J. Geophys. Res.* 108, 1–20. doi:10.1029/2002JC001737.

Hopkins, A. E. (1937). "Experimental observations on spawning, larval development, and setting in the Olympia oyster Ostrea lurida," in *Bulletin of the United States Bureau of fisheries*, ed. F. T. Bell, 48:66.

Hosack, G. R., Dumbauld, B. R., Ruesink, J. L., and Armstrong, D. A. (2006). Habitat associations of estuarine species: Comparisons of intertidal mudflat, seagrass (Zostera marina), and oyster (Crassostrea gigas) habitats. *Estuaries and Coasts* 29, 1150–1160. doi:10.1007/BF02781816.

Huang, H., Chen, C., Cowles, G. W., Winant, C. D., Beardsley, R. C., Hedstrom, K. S., et al. (2008). FVCOM validation experiments: Comparisons with ROMS for three idealized barotropic test problems. *J. Geophys. Res. Ocean.* 113, 1–14. doi:10.1029/2007JC004557.

Huyer, A. (1983). Coastal upwelling in the California current system. *Prog. Oceanogr.* 12, 259–284. doi:10.1016/0079-6611(83)90010-1.

Huyer, A., Smith, R. L., and Fleischbein, J. (2002). The coastal ocean off Oregon and northern California during the 1997-8 El Niño. *Prog. Oceanogr.* 54, 311–341. doi:10.1016/S0079-6611(02)00056-3.

Huyer, A., Wheeler, P. A., Strub, P. T., Smith, R. L., Letelier, R., and Kosro, P. M. (2007). Progress in Oceanography The Newport line off Oregon – Studies in the North East Pacific. 75, 126–160. doi:10.1016/j.pocean.2007.08.003.

Hyde, N. (2007). Towards national estuarine modeling and characterization / classification systems : a pilot study for Coos Bay.

Jackson, J. M., Johnson, G. C., Dosser, H. V., and Ross, T. (2018). Warming From Recent Marine Heatwave Lingers in Deep British Columbia Fjord. *Geophys. Res. Lett.* 45, 9757–9764. doi:10.1029/2018GL078971.

Jacox, M. G., Hazen, E. L., Zaba, K. D., Rudnick, D. L., Edwards, C. A., Moore, A. M., et al. (2016). Impacts of the 2015–2016 El Niño on the California Current System: Early assessment and comparison to past events. *Geophys. Res. Lett.* 43, 7072–7080. doi:10.1002/2016GL069716.

Janzen, C. D., and Wong, K.-C. (2002). Wind-forced dynamics at the estuary-shelf interface of a large coastal plain estuary. *J. Geophys. Res. Ocean.* 107, 3138. doi:10.1029/2001JC000959.

Jarvis, J. C., Moore, K. A., and Kenworthy, W. J. (2012). Characterization and ecological implication of eelgrass life history strategies near the species' southern limit in the western North Atlantic. *Mar. Ecol. Prog. Ser.* 444, 43–56. doi:10.3354/meps09428.

Johnson, M. R., Williams, S. L., Lieberman, C. H., and Solbak, A. (2003). Changes in the abundance of the seagrasses Zostera marina L. (eelgrass) and Ruppia maritima L. (widgeongrass) in San Diego, California, following an El Niño event. *Estuaries* 26, 106–115. doi:10.1007/BF02691698.

Juarez, B., Valle-levinson, A., Chant, R., and Li, M. (2019). Estuarine , Coastal and Shelf Science Observations of the lateral structure of wind-driven flow in a coastal plain estuary. *Estuar. Coast. Shelf Sci.* 217, 262–270. doi:10.1016/j.ecss.2018.11.018.

Kaldy, J. (2012). Influence of light, temperature and salinity on dissolved organic carbon exudation rates in Zostera marina L. *Aquat. Biosyst.* 8, 1–12. doi:10.1186/2046-9063-8-19.

Kaldy, J. E. (2014). Effect of temperature and nutrient manipulations on eelgrass Zostera marina L. from the Pacific Northwest, USA. *J. Exp. Mar. Bio. Ecol.* 453, 108–115. doi:10.1016/j.jembe.2013.12.020.

Kalnay, E., Kanamitsu, M., Kistler, R., Collins, W., Deaven, D., Gandin, L., et al. (1996). The NCEP/NCAR 40-Year Reanalysis Project. *Bull. Am. Meteorol. Soc.* 77, 437–471. doi:10.1175/1520-0477(1996)077<0437:TNYRP>2.0.CO;2.

Kimbro, D. L., Largier, J., and Grosholz, E. D. (2009). Coastal oceanographic processes influence the growth and size of a key estuarine species, the Olympia oyster. *Limnol. Oceanogr.* 54, 1425–1437. doi:10.4319/lo.2009.54.5.1425.

Kranenburg, W. M., Geyer, W. R., Garcia, A. M. P., and Ralston, D. K. (2019). Reversed lateral circulation in a sharp estuarine bend with weak stratification. *J. Phys. Oceanogr.* 49, 1619–1637. doi:10.1175/JPO-D-18-0175.1.

Lacy, J. R., and Monismith, S. G. (2001). Secondary currents in a curved, stratified, estuarine channel. *J. Geophys. Res. Ocean.* 106, 31283–31302. doi:10.1029/2000JC000606.

Lai, W., Pan, J., and Devlin, A. T. (2018). Impact of tides and winds on estuarine circulation in the Pearl River Estuary. *Cont. Shelf Res.* 168, 68–82. doi:10.1016/j.csr.2018.09.004.

Largier, J. L. (2003). Consideration in estimating larval dispersal distances. *Ecol. Appl.* 13, 71–89.

Largier, J. L. (2020). Upwelling Bays: How Coastal Upwelling Controls Circulation, Habitat, and Productivity in Bays. *Ann. Rev. Mar. Sci.* 12, 415–447. doi:10.1146/annurev-marine-010419-011020.

Lee II, H., and Brown, C. A. (2009). Classification of Regional Patterns of Environmental Drivers And Benthic Habitats in Pacific Northwest Estuaries.

Lee, K. S., Park, S. R., and Kim, Y. K. (2007). Effects of irradiance, temperature, and nutrients on growth dynamics of seagrasses: A review. *J. Exp. Mar. Bio. Ecol.* 350, 144–175. doi:10.1016/j.jembe.2007.06.016.

Lemagie, E. P., and Lerczak, J. A. (2015). A Comparison of Bulk Estuarine Turnover Timescales to Particle Tracking Timescales Using a Model of the Yaquina Bay Estuary. *Estuaries and Coasts* 38, 1797–1814. doi:10.1007/s12237-014-9915-1.

Lerczak, J. A., and Geyer, W. R. (2004). Modeling the Lateral Circulation in Straight, Stratified Estuaries*. *J. Phys. Oceanogr.* 34, 1410–1428. doi:10.1175/1520-0485(2004)034<1410:MTLCIS>2.0.CO;2.

Lerczak, J. A., Geyer, W. R., and Chant, R. J. (2006). Mechanisms Driving the Time-Dependent Salt Flux in a Partially Stratified Estuary*. *J. Phys. Oceanogr.* 36, 2296–2311. doi:10.1175/jpo2959.1.

Li, Y., and Li, M. (2011). Effects of winds on stratification and circulation in a partially mixed estuary. *J. Geophys. Res. Ocean.* 116. doi:10.1029/2010JC006893.

Liu, W. C., Chen, W. B., and Hsu, M. H. (2011). Using a three-dimensional particle-tracking model to estimate the residence time and age of water in a tidal estuary. *Comput. Geosci.* 37, 1148–1161. doi:10.1016/j.cageo.2010.07.007.

Logerwell, E. A., Mantua, N., Lawson, P. W., Francis, R. C., and Agostini, V. N. (2003). Tracking environmental processes in the coastal zone for understanding and predicting Oregon coho (Oncorhynchus kisutch) marine survival. *Fish. Oceanogr.* 12, 554–568. doi:10.1046/j.1365-2419.2003.00238.x.

Lucas, L. V., Thompson, J. K., and Brown, L. R. (2009). Why are diverse relationships observed between phytoplankton biomass and transport time? *Limnol. Oceanogr.* 54, 381–390. doi:10.4319/lo.2009.54.1.0381.

MacCready, P. (2011). Calculating Estuarine Exchange Flow Using Isohaline Coordinates [*]. *J. Phys. Oceanogr.* 41, 1116–1124. doi:10.1175/2011JPO4517.1.

MacCready, P., and Geyer, W. R. (2010). Advances in Estuarine Physics. *Ann. Rev. Mar. Sci.* 2, 35–58. doi:10.1146/annurev-marine-120308-081015.

MacVean, L. J., and Stacey, M. T. (2011). Estuarine Dispersion from Tidal Trapping: A New Analytical Framework. *Estuaries and Coasts* 34, 45–59. doi:10.1007/s12237-010-9298-x.

McIntyre, B. A., McPhee-Shaw, E. E., Hatch, M. B. A., and Arellano, S. M. (2020). Location Matters: Passive and Active Factors Affect the Vertical Distribution of Olympia Oyster (Ostrea lurida) Larvae. *Estuaries and Coasts*. doi:10.1007/s12237-020-00771-8.

McKay, P., and Iorio, D. Di (2008). Heat budget for a shallow, sinuous salt marsh estuary. *Cont. Shelf Res.* 28, 1740–1753. doi:10.1016/j.csr.2008.04.008.

Menniti, C. M., Whitney, M. M., and Deignan-Schmidt, S. R. (2020). The Importance of Offshore Exchange for Water Temperatures in Norwalk Harbor. *Estuaries and Coasts*, 787–800. doi:10.1007/s12237-020-00710-7.

Meyers, S. D., and Luther, M. E. (2008). A Numerical Simulation of Residual Circulation in Tampa Bay. Part II: Lagrangian Residence Time. *Estuaries and Coasts* 31, 815–827. doi:10.1007/s12237-008-9085-0.

Milcu, A. I., Hanspach, J., Abson, D., and Fischer, J. (2013). Cultural ecosystem services: A literature review and prospects for future research. *Ecol. Soc.* 18. doi:10.5751/ES-05790-180344.

Miller, J. A., and Shanks, A. L. (2004). Ocean-estuary coupling in the Oregon upwelling region: Abundance and transport of juvenile fish and of crab megalopae. *Mar. Ecol. Prog. Ser.* 271, 267–279. doi:10.3354/meps271267.

Minello, T. J., Rozas, L. P., and Baker, R. (2012). Geographic Variability in Salt Marsh Flooding Patterns may Affect Nursery Value for Fishery Species. *Estuaries and Coasts* 35, 501–514. doi:10.1007/s12237-011-9463-x.

Monismith, S. (1986). An experimental study of the upwelling response of stratified reservoirs to surface shear stress. *J. Fluid Mech.* 171, 407. doi:10.1017/S0022112086001507.

Monsen, N. E., Cloern, J. E., Lucas, L. V., and Monismith, S. G. (2002). A comment on the use of flushing time, residence time, and age as transport time scales. *Limnol. Oceanogr.* 47, 1545–1553. doi:10.4319/lo.2002.47.5.1545.

Nejrup, L. B., and Pedersen, M. F. (2008). Effects of salinity and water temperature on the ecological performance of Zostera marina. *Aquat. Bot.* 88, 239–246. doi:10.1016/j.aquabot.2007.10.006.

Nidzieko, N. J., and Monismith, S. G. (2013). Contrasting Seasonal and Fortnightly Variations in the Circulation of a Seasonally Inverse Estuary, Elkhorn Slough, California. *Estuaries and Coasts* 36, 1–17. doi:10.1007/s12237-012-9548-1.

NOAA National Estuarine Research Reserve System (NERRS) (2020). System-wide Monitoring Program. *NOAA NERRS Cent. Data Manag. Off. website http//www.nerrsdata.org*. Available at: http://www.nerrsdata.org/ [Accessed June 11, 2020].

O'Higgins, T., and Rumrill, S. S. (2007). Tidal and Watershed Forcing of Nutrients and Dissolved Oxygen Stress within Four Pacific Coast Estuaries: Analysis of Time-Series Data collected by the National Estuarine Research Reserve System-Wide Monitoring Program (2000-2006) within Padilla Bay (WA),. *NOAA/UNH Coop. Inst. Coast. Estuar. Environ. Technol.*, 1689–1699. doi:10.1017/CBO9781107415324.004.

Oates, M. S. (2013). Obervations of Gonad Structure and Gametogenic Timing in a recovering population of Ostrea Lurida (Carpenter, 1864).

Officer, C. B., Biggs, R. B., Taft, J. L., Cronin, L. E., Tyler, M. A., and Boynton, W. R. (1984). Chesapeake Bay Anoxia: Origin, Development, and Significance. *Science (80-.).* 223, 22–27. doi:10.1126/science.223.4631.22.

Okubo, A. (1973). Effect of shoreline irregularities on streamwise dispersion in estuaries and other embayments. *Netherlands J. Sea Res.* 6, 213–224. doi:10.1016/0077-7579(73)90014-8.

OSU (1971). Oceanography of the nearshore coastal waters of the Pacific Northwest relating to possible pollution - Volume 1. Corvallis, Oregon 97331.

Parmesan, C., and Yohe, G. (2003). A globally coherent fingerprint of climate change. *Nature* 421, 37–42.

Pawlowicz, R., Beardsley, R. C., and Lentz, S. J. (2002). Classical tidal harmonic analysis including error estimates in MATLAB using T TIDE $. 28, 929–937.

Pawlowicz, R., Hannah, C., and Rosenberger, A. (2019). Lagrangian observations of estuarine residence times, dispersion, and trapping in the Salish Sea. *Estuar. Coast. Shelf Sci.* 225, 106246. doi:10.1016/j.ecss.2019.106246.

Pecly, J. O. G., and Roldão, J. S. F. (2013). Dye tracers as a tool for outfall studies: Dilution measurement approach. *Water Sci. Technol.* 67, 1564–1573. doi:10.2166/wst.2013.027.

Peteiro, L. G., and Shanks, A. L. (2015). Up and down or how to stay in the bay: Retentive strategies of Olympia oyster larvae in a shallow estuary. *Mar. Ecol. Prog. Ser.* 530, 103–117. doi:10.3354/meps11283.

Peterson, M. S. (2003). A Conceptual View of Environment-Habitat-Production Linkages in Tidal River Estuaries. *Rev. Fish. Sci.* 11, 291–313. doi:10.1080/10641260390255844.

Peterson, W. T., Fisher, J. L., Strub, P. T., Du, X., Risien, C., Peterson, J., et al. (2017). The pelagic ecosystem in the Northern California Current off Oregon during the 2014-2016 warm anomalies within the context of the past 20 years. *J. Geophys. Res. Ocean.* 122, 7267–7290. doi:10.1002/2017JC012952.

Pfeiffer-Herbert, A. S., Kincaid, C. R., Bergondo, D. L., and Pockalny, R. A. (2015). Dynamics of wind-driven estuarine-shelf exchange in the Narragansett Bay estuary. *Cont. Shelf Res.* 105, 42–59. doi:10.1016/j.csr.2015.06.003.

Phillips, R. C. (1984). The ecology of eelgrass meadows in the Pacific Northwest: a community profile. *US Fish Wildl. Serv.* Available at: https://linkinghub.elsevier.com/retrieve/pii/0304377083900207.

Phillips, R. C., McMillan, C., and Bridges, K. W. (1983). Phenology of eelgrass, Zostera marina L., along latitudinal gradients in North America. *Aquat. Bot.* 15, 145–156. doi:10.1016/0304-3770(83)90025-6.

Poloczanska, E. S., Brown, C. J., Sydeman, W. J., Kiessling, W., Schoeman, D. S., Moore, P. J., et al. (2013). Global imprint of climate change on marine life. *Nat. Clim. Chang.* 3, 919–925. doi:10.1038/nclimate1958.

Pritchard, C. E., Shanks, A. L., Rimler, R. N., Oates, M., and Rumrill, S. S. (2015). The olympia oyster ostrea lurida: Recent advances in natural history, ecology, and restoration. *J. Shellfish Res.* 34, 259–271. doi:10.2983/035.034.0207.

Pritchard, C., Rimler, R., Rumrill, S., Emlet, R., and Shanks, A. (2016). Variation in larval supply and recruitment of Ostrea lurida in the Coos Bay estuary, Oregon, USA. *Mar. Ecol. Prog. Ser.* 560, 159–171. doi:10.3354/meps11894.

Purkiani, K., Becherer, J., Klingbeil, K., and Burchard, H. (2016). Wind-induced variability of estuarine circulation in a tidally energetic inlet with curvature. *J. Geophys. Res. Ocean.* 121, 3261–3277. doi:10.1002/2015JC010945.

Qi, J., Chen, C., Beardsley, R. C., Perrie, W., Cowles, G. W., and Lai, Z. (2009). An unstructured-grid finite-volume surface wave model (FVCOM-SWAVE): Implementation, validations and applications. *Ocean Model.* 28, 153–166. doi:10.1016/j.ocemod.2009.01.007.

Qin, Q., and Shen, J. (2019). Physical transport processes affect the origins of harmful algal blooms in estuaries. *Harmful Algae* 84, 210–221. doi:10.1016/j.hal.2019.04.002.

Raimonet, M., and Cloern, J. E. (2017). Estuary–ocean connectivity: fast physics, slow biology. *Glob. Chang. Biol.* 23, 2345–2357. doi:10.1111/gcb.13546.

Ralston, D. K., Brosnahan, M. L., Fox, S. E., Lee, K. D., and Anderson, D. M. (2015). Temperature and Residence Time Controls on an Estuarine Harmful Algal Bloom: Modeling Hydrodynamics and Alexandrium fundyense in Nauset Estuary. *Estuaries and Coasts* 38, 2240–2258. doi:10.1007/s12237-015-9949-z.

Ralston, D. K., Geyer, W. R., and Lerczak, J. A. (2010a). Structure, variability, and salt flux in a strongly forced salt wedge estuary. *J. Geophys. Res.* 115, C06005. doi:10.1029/2009JC005806.

Ralston, D. K., Geyer, W. R., Lerczak, J. A., and Scully, M. (2010b). Turbulent mixing in a strongly forced salt wedge estuary. *J. Geophys. Res. Ocean.* 115, 1–21. doi:10.1029/2009JC006061.

Ralston, D. K., and Stacey, M. T. (2005). Longitudinal dispersion and lateral circulation in the intertidal zone. *J. Geophys. Res. C Ocean.* 110, 1–17. doi:10.1029/2005JC002888.

Ralston, D. K., and Stacey, M. T. (2007). Tidal and meteorological forcing of sediment transport in tributary mudflat channels. *Cont. Shelf Res.* 27, 1510–1527. doi:10.1016/j.csr.2007.01.010.

Rinehimer, J. P., and Thomson, J. T. (2014). Observations and modeling of heat fluxes on tidal flats. *J. Geophys. Res. Ocean.* 119, 133–146. doi:10.1002/2013JC009225.

Roegner, G. C., Armstrong, D. A., and Shanks, A. L. (2007). Wind and tidal influences on larval crab recruitment to an Oregon estuary. *Mar. Ecol. Prog. Ser.* 351, 177–188. doi:10.3354/meps07130.

Roegner, G. C., Hickey, B. M., Newton, J. a., Shanks, A. L., and Armstrong, D. a. (2002). Wind-induced plume and bloom intrusions into Willapa Bay, Washington. *Limnol. Oceanogr.* 47, 1033–1042. doi:10.4319/lo.2002.47.4.1033.

Roegner, G. C., Needoba, J. A., and Baptista, A. M. (2011). Coastal upwelling supplies oxygen-depleted water to the columbia river estuary. *PLoS One* 6. doi:10.1371/journal.pone.0018672.

Roegner, G. C., and Shanks, A. L. (2001). Import of Coastally-Derived Chlorophyll a to South Slough, Oregon. *Estuaries* 244, 244–256. doi:10.2307/1352948.

Rumrill, S. S. (2007). The Ecology of the South Slough Estuary: Site Profile of the South Slough National Estuarine Research Reserve.

Salo, T., and Pedersen, M. F. (2014). Synergistic effects of altered salinity and temperature on estuarine eelgrass (Zostera marina) seedlings and clonal shoots. *J. Exp. Mar. Bio. Ecol.* 457, 143–150. doi:10.1016/j.jembe.2014.04.008.

Sanay, R., and Valle-Levinson, A. (2005). Wind-induced circulation in semienclosed homogeneous, rotating basins. *J. Phys. Oceanogr.* 35, 2520–2531. doi:10.1175/JPO2831.1.

Sawall, Y., Ito, M., and Pansch, C. (2021). Chronically elevated sea surface temperatures revealed high susceptibility of the eelgrass <scp> *Zostera marina* </scp> to winter and spring warming. *Limnol. Oceanogr.*, 1–13. doi:10.1002/lno.11947.

Schneider, S. (1993). "Scenarios of global warming," in *Biotic interactions and Global change*, eds. P. Kareiva, J. Kingsolver, and R. Huey (Sunderland, MA: Sinauer Associates), 9–23.

Scully, M. E., Friedrichs, C., and Brubaker, J. (2005). Control of estuarine stratification and mixing by wind-induced straining of the estuarine density field. *Estuaries* 28, 321–326. doi:10.1007/BF02693915.

Seppelt, R., Dormann, C. F., Eppink, F. V., Lautenbach, S., and Schmidt, S. (2011). A quantitative review of ecosystem service studies: Approaches, shortcomings and the road ahead. *J. Appl. Ecol.* 48, 630–636. doi:10.1111/j.1365-2664.2010.01952.x.

Shanks, A. L., Rasmuson, L. K., Valley, J. R., Jarvis, M. A., Salant, C., Sutherland, D. A., et al. (2020). Marine heat waves, climate change, and failed spawning by coastal invertebrates. *Limnol. Oceanogr.* 65, 627–636. doi:10.1002/lno.11331.

Sharples, J., Middelburg, J. J., Fennel, K., and Jickells, T. D. (2017). What proportion of riverine nutrients reaches the open ocean? *Global Biogeochem. Cycles* 31, 39–58. doi:10.1002/2016GB005483.

Sherman, K., and DeBruyckere, L. A. (2018). Eelgrass Habitats on the U.S. West Coast. State of the Knowledge of Eelgrass Ecosystem Services and Eelgrass Extent. A publication prepared by the Pacific Marine and Estuarine Fish Habitat Partnership. Available at: http://www.pacificfishhabitat.org/wp-content/uploads/2017/09/EelGrass_Report_Final_ForPrint_web.pdfeation 20180109.pdf?ver=2018-01-12-102015-010.

Short, F. T., and Coles, R. G. (2001). *Global seagrass research methods*. , eds. F. T. Short and R. G. Coles Elsevier.

Short, F. T., McKenzie, L. J., Coles, R. G., Vidler, K. P., and Gaeckle, J. L. (2006). SeagrassNet Manual for Scientific Monitoring of Seagrass Habitat. 1–75.

Simpson, J. H., Vennell, R., and Souza, A. J. (2001). The Salt Fluxes in a Tidally-Energetic Estuary. *Estuar. Coast. Shelf Sci.* 52, 131–142. doi:10.1006/ecss.2000.0733.

Smith, N. P. (1983). A comparison of winter and summer temperature variations in a shallow bar-built estuary. *Estuaries* 6, 2–9. doi:10.2307/1351801.

Steele, M. O., Chang, H., Reusser, D. A., Brown, C. A., and Jung, I.-W. (2012). Potential Climate-Induced Runoff Changes and Associated Uncertainty in Four Pacific Northwest Estuaries. 52.

Stevenson, J. W., and Niiler, P. P. (1983). Upper Ocean Heat Budget During the Hawaii-to-Tahiti Shuttle Experiment. *J. Phys. Oceanogr.* 13, 1894–1907. doi:10.1175/1520-0485(1983)013<1894:UOHBDT>2.0.CO;2.

Stommel, H., and Farmer, H. G. (1952). On the nature of estuarine circulation.

Strub, P. T., Allen, J. S., Huyer, A., Smith, R. L., and Beardsley, R. C. (1987). Seasonal cycles of currents, temperatures, winds, and sea level over the northeast Pacific continental shelf: 35°N to 48°N. *J. Geophys. Res.* 92, 1507. doi:10.1029/JC092iC02p01507.

Sutherland, D. A., and O'Neill, M. A. (2016). Hydrographic and dissolved oxygen variability in a seasonal Pacific Northwest estuary. *Estuar. Coast. Shelf Sci.* 172, 47–59. doi:10.1016/j.ecss.2016.01.042.

Teodósio, M. A., Paris, C. B., Wolanski, E., and Morais, P. (2016). Biophysical processes leading to the ingress of temperate fish larvae into estuarine nursery areas: A review. *Estuar. Coast. Shelf Sci.* 183, 187–202. doi:10.1016/j.ecss.2016.10.022.

Thom, R. M., Borde, A. B., Rumrill, S., Woodruff, D. L., Williams, G. D., Southard, J. A., et al. (2003). Factors influencing spatial and annual variability in eelgrass (Zostera marina L.) meadows in Willapa Bay, Washington, and Coos Bay, Oregon, estuaries. *Estuaries* 26, 1117–1129. doi:10.1007/BF02803368.

Thomann, R. V., and Mueller, J. A. (1987). Principles of surface water quality modeling and control. *Harper Row Publ.*

U.S. Army Corps of Engineers (2015). COOS BAY FEDERAL NAVIGATION CHANNEL AND CHARLESTON SIDE CHANNEL Dredging Project. Portland, OR.

Uncles, R. J., and Stephens, J. A. (2011). The Effects of Wind, Runoff and Tides on Salinity in a Strongly Tidal Sub-estuary. *Estuaries and Coasts* 34, 758–774. doi:10.1007/s12237-010-9365-3.

Valle-Levinson, A., Schettini, C. A. F., and Truccolo, E. C. (2019). Subtidal variability of exchange flows produced by river pulses, wind stress and fortnightly tides in a subtropical stratified estuary. *Estuar. Coast. Shelf Sci.* 221, 72–82. doi:10.1016/j.ecss.2019.03.022.

Valle-Levinson, A., Wong, K.-C., and Bosley, K. T. (2001). Observations of the wind-induced exchange at the entrance to Chesapeake Bay. *J. Mar. Res.* 59, 391–416. doi:10.1357/002224001762842253.

van Sebille, E., Delandmeter, P., Schofield, J., Hardesty, B. D., Jones, J., and Donnelly, A. (2019). Basin-scale sources and pathways of microplastic that ends up in the Galápagos Archipelago. *Ocean Sci.* 15, 1341–1349. doi:10.5194/os-15-1341-2019.

Walther, G.-R., Post, E., Convey, P., Menzel, A., Parmesan, C., Beebee, T. J. C., et al. (2002). Ecological responses to recent climate change. *Nature* 416, 389–395.

Wang, C. F., Hsu, M. H., and Kuo, A. Y. (2004). Residence time of the Danshuei River estuary, Taiwan. *Estuar. Coast. Shelf Sci.* 60, 381–393. doi:10.1016/j.ecss.2004.01.013.

Wang, S.-Y., Hipps, L., Gillies, R. R., and Yoon, J.-H. (2014). Probable causes of the abnormal ridge accompanying the 2013-2014 California drought: ENSO precursor and anthropogenic warming footprint. *Geophys. Res. Lett.* 41, 3220–3226. doi:10.1002/2014GL059748.

Wasson, K., Zabin, C. J., Bible, J., Briley, S., Deck, A. K., Grosholz, T., et al. (2015). A guide to Olympia Oyster Restoration and Conservation. Monterey Bay.

Wheat, E. E., Banas, N. S., and Ruesink, J. L. (2019). Multi-day water residence time as a mechanism for physical and biological gradients across intertidal flats. *Estuar. Coast. Shelf Sci.* 227, 106303. doi:10.1016/j.ecss.2019.106303.

Wild-Allen, K., and Andrewartha, J. (2016). Connectivity between estuaries influences nutrient transport, cycling and water quality. *Mar. Chem.* 185, 12–26. doi:10.1016/j.marchem.2016.05.011.

Wyrtki, K. (1984). The slope of sea level along the equator during the 1982/1983 El Nino. *J. Geophys. Res.* 89, 10419–10424. doi:10.1029/JC089iC06p10419.

Xia, M., Xie, L., Pietrafesa, L. J., and Whitney, M. M. (2011). The ideal response of a Gulf of Mexico estuary plume to wind forcing: Its connection with salt flux and a Lagrangian view. *J. Geophys. Res.* 116, C08035. doi:10.1029/2010JC006689.

Xie, L., and Eggleston, D. B. (1999). Computer simulations of wind-induced estuarine circulation patterns and estuary-shelf exchange processes: The potential role of wind forcing on larval transport. *Estuar. Coast. Shelf Sci.* 49, 221–234. doi:10.1006/ecss.1999.0498.

Yamada, S. B., Dumbauld, B. R., Kalin, A., Hunt, C. E., Figlar-Barnes, R., and Randall, A. (2005). Growth and persistence of a recent invader Carcinus maenas in estuaries of the northeastern Pacific. *Biol. Invasions* 7, 309–321. doi:10.1007/s10530-004-0877-2.

Yamada, S. B., Randall, A., Schooler, S., Heller, R., Donaldson, L., Takacs, G., et al. (2020). Status of the European green crab, Carcinus maenas, in Oregon and Washington coastal estuaries in 2019. Portland, OR Available at: http://scholar.google.com/scholar?hl=en&btnG=Search&q=intitle:Status+of+the+European+Green+Crab+in+Oregon+and+Washington+Estuaries#3.

Yang, Z., Khangaonkar, T., and Wang, T. (2011). Use of Advanced Meteorological Model Output for Coastal Ocean Modeling in Puget Sound. *Int. J. Ocean Clim. Syst.* 2, 101–117. doi:10.1260/1759-3131.2.2.101.

Zapata, C., Puente, A., Garca, A., Garcia-Alba, J., and Espinoza, J. (2018). Assessment of ecosystem services of an urbanized tropical estuary with a focus on habitats and scenarios. *PLoS One* 13, 1–19. doi:10.1371/journal.pone.0203927.

Zimmerman, R. C., Smith, R. D., and Alberte, R. S. (1989). Thermal acclimation and whole-plant carbon balance in Zostera marina L. (eelgrass). *J. Exp. Mar. Bio. Ecol.* 130, 93–109. doi:10.1016/0022-0981(89)90197-4.

Chapter IV

Alexander, M. A., Bladé, I., Newman, M., Lanzante, J. R., Lau, N.-C., and Scott, J. D. (2002). The Atmospheric Bridge: The Influence of ENSO Teleconnections on Air–Sea Interaction over the Global Oceans. *J. Clim.* 15, 2205–2231. doi:10.1175/1520-0442(2002)015<2205:TABTIO>2.0.CO;2.

Arega, F., Armstrong, S., and Badr, A. W. (2008). Modeling of residence time in the East Scott Creek Estuary, South Carolina, USA. *J. Hydro-Environment Res.* 2, 99–108. doi:10.1016/j.jher.2008.07.003.

Arneson, R. J. (1976). Seasonal Variations in Tidal Dynamics, Water Quality, and Sediments in the Coos Bay estuary.

Ascione Kenov, I., Garcia, A. C., and Neves, R. (2012). Residence time of water in the Mondego estuary (Portugal). *Estuar. Coast. Shelf Sci.* 106, 13–22. doi:10.1016/j.ecss.2012.04.008.

Baker, P. (1995). Review of ecology and fishery of the olympia oyster, Ostrea lurida with annotated bibliography. *J. Shellfish Res.* 14, 501–518.

Bakun, A., Black, B., Bograd, S. J., García-Reyes, M., Miller, a. J., Rykaczewski, R. R., et al. (2015). Anticipated Effects of Climate Change on Coastal Upwelling Ecosystems. *Curr. Clim. Chang. Reports*, 85–93. doi:10.1007/s40641-015-0008-4.

Banas, N., Hickey, B., Newton, J., and Ruesink, J. (2007). Tidal exchange, bivalve grazing, and patterns of primary production in Willapa Bay, Washington, USA. *Mar. Ecol. Prog. Ser.* 341, 123–139. doi:10.3354/meps341123.

Banas, N. S., and Hickey, B. M. (2005). Mapping exchange and residence time in a model of Willapa Bay, Washington, a branching, macrotidal estuary. *J. Geophys. Res. Ocean.* 110, 1–20. doi:10.1029/2005JC002950.

Banas, N. S., Hickey, B. M., MacCready, P., and Newton, J. A. (2004). Dynamics of Willapa Bay, Washington: A highly unsteady, partially mixed estuary. *J. Phys. Oceanogr.* 34, 2413–2427. doi:10.1175/JPO2637.1.

Banas, N. S., McDonald, P. S., and Armstrong, D. A. (2009). Green crab larval retention in Willapa Bay, Washington: An intensive Lagrangian modeling approach. *Estuaries and Coasts* 32, 893–905. doi:10.1007/s12237-009-9175-7.

Baptista, A. M. (1989). Salinity in Coos Bay, Oregon.

Barnard, P. L., Hoover, D., Hubbard, D. M., Snyder, A., Ludka, B. C., Allan, J., et al. (2017). Extreme oceanographic forcing and coastal response due to the 2015-2016 El Niño. *Nat. Commun.* 8, 6–13. doi:10.1038/ncomms14365.

Basilio, A., Searcy, S., and Thompson, A. R. (2017). Effects of the Blob on settlement of spotted sand bass, Paralabrax maculatofasciatus, to Mission Bay, San Diego, CA. *PLoS One* 12, 6–8. doi:10.1371/journal.pone.0188449.

Beca-Carretero, P., Olesen, B., Marbà, N., and Krause-Jensen, D. (2018). Response to experimental warming in northern eelgrass populations: Comparison across a range of temperature adaptations. *Mar. Ecol. Prog. Ser.* 589, 59–72. doi:10.3354/meps12439.

Bi, H., Peterson, W. T., and Strub, P. T. (2011). Transport and coastal zooplankton communities in the northern California Current system. *Geophys. Res. Lett.* 38, 1–5. doi:10.1029/2011GL047927.

Black, B. A., Sydeman, W. J., Frank, D. C., Griffin, D., Stahle, D. W., Garcia-Reyes, M., et al. (2014). Six centuries of variability and extremes in a coupled marine-terrestrial ecosystem. *Science (80-.).* 345, 1498–1502. doi:10.1126/science.1253209.

Black, B. A., van der Sleen, P., Di Lorenzo, E., Griffin, D., Sydeman, W. J., Dunham, J. B., et al. (2018). Rising synchrony controls western North American ecosystems. *Glob. Chang. Biol.* 24, 2305–2314. doi:10.1111/gcb.14128.

Blumberg, A. F., and Goodrich, D. M. (1990). Modeling of Wind-Induced Destratification in Chesapeake Bay. *Estuaries* 13, 236. doi:10.2307/1351914.

Bolaños, R., Brown, J. M., Amoudry, L. O., and Souza, A. J. (2013). Tidal, Riverine, and Wind Influences on the Circulation of a Macrotidal Estuary. *J. Phys. Oceanogr.* 43, 29–50. doi:10.1175/JPO-D-11-0156.1.

Bond, N. A., Cronin, M. F., Freeland, H., and Mantua, N. (2015). Causes and impacts of the 2014 warm anomaly in the NE Pacific. *Geophys. Res. Lett.* 42, 3414–3420. doi:10.1002/2015GL063306.

Borde, A. B., Thom, R. M., Rumrill, S., and Miller, L. M. (2003). Geospatial habitat change analysis in Pacific Northwest Coastal estuaries. *Estuaries* 26, 1104–1116. doi:10.1007/bf02803367.

Brasseale, E., Grason, E. W., McDonald, P. S., Adams, J., and MacCready, P. (2019). Larval Transport Modeling Support for Identifying Population Sources of European Green Crab in the Salish Sea. *Estuaries and Coasts* 42, 1586–1599. doi:10.1007/s12237-019-00586-2.

Brink, K. H., Beardsley, R. C., Paduan, J., Limeburner, R., Caruso, M., and Sires, J. G. (2000). A view of the 1993-1994 Califonia Current based on surface drifters, floats, and remotely sensed data. 105, 8575–8604.

Capotondi, A., Sardeshmukh, P. D., Di Lorenzo, E., Subramanian, A. C., and Miller, A. J. (2019). Predictability of US West Coast Ocean Temperatures is not solely due to ENSO. *Sci. Rep.* 9, 1–10. doi:10.1038/s41598-019-47400-4.

Chant, R. J. (2002a). Secondary circulation in a region of flow curvature : Relationship with tidal forcing and river discharge. 107, 1–11. doi:10.1029/2001JC001082.

Chant, R. J. (2002b). Secondary circulation in a region of flow curvature: Relationship with tidal forcing and river discharge. *J. Geophys. Res.* 107, 3131. doi:10.1029/2001JC001082.

Chen, C., Beardsley, R. C., Cowles, G., Qi, J., Lai, Z., Gao, G., et al. (2011a). An Unstructured-Grid, Finite-Volume Community Ocean Model. *FVCOM User Man.* 3rd editio, 1–409.

Chen, C., Liu, H., and Beardsley, R. C. (2003). An unstructured grid, finite-volume, three-dimensional, primitive equations ocean model: Application to coastal ocean and estuaries. *J. Atmos. Ocean. Technol.* 20, 159–186. doi:10.1175/1520-0426(2003)020<0159:AUGFVT>2.0.CO;2.

Chen, S.-N., Geyer, W. R., Ralston, D. K., and Lerczak, J. A. (2011b). Estuarine Exchange Flow Quantified with Isohaline Coordinates: Contrasting Long and Short Estuaries. *J. Phys. Oceanogr.* 42, 748–763. doi:10.1175/jpo-d-11-086.1.

Chen, S.-N., and Sanford, L. P. (2009). Axial Wind Effects on Stratification and Longitudinal Salt Transport in an Idealized, Partially Mixed Estuary*. *J. Phys. Oceanogr.* 39, 1905–1920. doi:10.1175/2009jpo4016.1.

Chen, T., Zhang, Q., Wu, Y., Ji, C., Yang, J., and Liu, G. (2018). Development of a wave-current model through coupling of FVCOM and SWAN. *Ocean Eng.* 164, 443–454. doi:10.1016/j.oceaneng.2018.06.062.

Chhak, K., and Di Lorenzo, E. (2007). Decadal variations in the California Current upwelling cells. *Geophys. Res. Lett.* 34, 1–6. doi:10.1029/2007GL030203.

Childers, D. L., Day, J. W., and Muller, R. A. (1990). Relating climatological forcing to coastal water levels in Louisiana estuaries and the potential importance of El Nino-Southern Oscillation events. *Clim. Res.* 1, 31–42. doi:10.3354/cr001031.

Clinton, P. J., Young, D. R., Specht, D. T., and Lee II, H. (2007). A Guide to Mapping Intertidal Eelgrass and Nonvegetated Habitats in Estuaries of the Pacific Northwest USA by Project Officer : Walter G . Nelson National Health and Environmental Effects Research Laboratory (NHEERL) Office of Research and D. Newport, OR.

Cloern, J. E., Jassby, A. D., Schraga, T. S., Nejad, E., and Martin, C. (2017). Ecosystem variability along the estuarine salinity gradient: Examples from long-term study of San Francisco Bay. *Limnol. Oceanogr.* doi:10.1002/lno.10537.

Conroy, T. B. (2018). The dynamics and exchange flow variability of the Coos estuary.

Conroy, T., Sutherland, D. A., and Ralston, D. K. (2020). Estuarine Exchange Flow Variability in a Seasonal, Segmented Estuary. *J. Phys. Oceanogr.* 50, 595–613. doi:10.1175/JPO-D-19-0108.1.

Coogan, J., and Dzwonkowski, B. (2018). Observations of wind forcing effects on estuary length and salinity flux in a river-dominated, microtidal Estuary, Mobile Bay, Alabama. *J. Phys. Oceanogr.* 48, 1787–1802. doi:10.1175/JPO-D-17-0249.1.

Coogan, J., Dzwonkowski, B., Park, K., and Webb, B. (2020). Observations of Restratification after a Wind Mixing Event in a Shallow Highly Stratified Estuary. *Estuaries and Coasts* 43, 272–285. doi:10.1007/s12237-019-00689-w.

Costanza, R., D'Arge, R., de Groot, R., Farber, S., Grasso, M., Hannon, B., et al. (1997). The value of the world's ecosystem services and natural capital. *Nature* 387, 253–260. doi:10.1038/387253a0.

Cowen, R. K., and Sponaugle, S. (2009). Larval Dispersal and Marine Population Connectivity. *Ann. Rev. Mar. Sci.* 1, 443–466. doi:10.1146/annurev.marine.010908.163757.

Csanady, G. T. (1973). Wind-Induced Barotropic Motions in Long Lakes. *J. Phys. Oceanogr.* 3, 429–438. doi:10.1175/1520-0485(1973)003<0429:WIBMIL>2.0.CO;2.

Daly, E. A., Brodeur, R. D., and Auth, T. D. (2017). Anomalous ocean conditions in 2015: Impacts on spring Chinook salmon and their prey field. *Mar. Ecol. Prog. Ser.* 566, 168–182. doi:10.3354/meps12021.

Davis, K. A., Banas, N. S., Giddings, S. N., Siedlecki, S. A., MacCready, P., Lessard, E. J., et al. (2014). Estuary-enhanced upwelling of marine nutrients fuels coastal productivity in the U.S. Pacific Northwest. *J. Geophys. Res. Ocean.*, 8778–8799. doi:10.1002/2014JC010248.Received.

de Brauwere, A., de Brye, B., Blaise, S., and Deleersnijder, E. (2011). Residence time, exposure time and connectivity in the Scheldt Estuary. *J. Mar. Syst.* 84, 85–95. doi:10.1016/j.jmarsys.2010.10.001.

Defne, Z., and Ganju, N. K. (2015). Quantifying the Residence Time and Flushing Characteristics of a Shallow, Back-Barrier Estuary: Application of Hydrodynamic and Particle Tracking Models. *Estuaries and Coasts* 38, 1719–1734. doi:10.1007/s12237-014-9885-3.

Delefosse, M., Povidisa, K., Poncet, D., Kristensen, E., and Olesen, B. (2016). Variation in size and chemical composition of seeds from the seagrass Zostera marina-Ecological implications. *Aquat. Bot.* 131, 7–14. doi:10.1016/j.aquabot.2016.02.003.

Di Lorenzo, E., Fiechter, J., Schneider, N., Braceo, A., Miller, A. J., Franks, P. J. S., et al. (2009). Nutrient and salinity decadal variations in the central and eastern North Pacific. *Geophys. Res. Lett.* 36, 2003–2008. doi:10.1029/2009GL038261.

Di Lorenzo, E., and Mantua, N. (2016). Multi-year persistence of the 2014/15 North Pacific marine heatwave. *Nat. Clim. Chang.* 6, 1042–1047. doi:10.1038/nclimate3082.

Di Lorenzo, E., Schneider, N., Cobb, K. M., Franks, P. J. S., Chhak, K., Miller, A. J., et al. (2008). North Pacific Gyre Oscillation links ocean climate and ecosystem change. *Geophys. Res. Lett.* 35, 2–7. doi:10.1029/2007GL032838.

Echavarria-Heras, H. A., Solana-Arellano, E., and Franco-Vizcaíno, E. (2006). The Role of Increased Sea Surface Temperature on Eelgrass Leaf Dynamics: Onset of El Niño as a Proxy for Global Climate Change in San Quintín Bay, Baja California. *Bull. South. Calif. Acad. Sci.* 105, 113–127. doi:https://doi.org/10.3160/0038-3872(2006)105[113:TROISS]2.0.CO;2.

Eidam, E. F., Sutherland, D. A. A., Ralston, D. K. K., Dye, B., Conroy, T., Schmitt, J., et al. (2020). Impacts of 150 Years of Shoreline and Bathymetric Change in the Coos Estuary, Oregon, USA. *Estuaries and Coasts*. doi:10.1007/s12237-020-00732-1.

Emmett, R., Llansó, R., Newton, J., Thom, R. M., Hornberger, M., Morgan, C., et al. (2000). Geographic Signatures of North American West Coast Estuaries. *Estuaries* 23, 765. doi:10.2307/1352998.

Engineers, U. S. A. C. of (2015). COOS BAY FEDERAL NAVIGATION CHANNEL AND CHARLESTON SIDE CHANNEL Dredging Project.

Epifanio, C. E., and Garvine, R. W. (2001). Larval transport on the Atlantic Continental Shelf of North America: A review. *Estuar. Coast. Shelf Sci.* 52, 51–77. doi:10.1006/ecss.2000.0727.

Evans, E. C., McGregor, G. R., and Petts, G. E. (1998). River energy budgets with special reference to river bed processes. *Hydrol. Process.* 12, 575–595. doi:10.1002/(SICI)1099-1085(19980330)12:4<575::AID-HYP595>3.0.CO;2-Y.

Ferguson, A., Eyre, B., and Gay, J. (2004). Nutrient cycling in the sub-tropical Brunswick estuary, Australia. *Estuaries* 27, 1–17. doi:10.1007/BF02803556.

Fortunato, A. B., and Oliveira, A. (2005). Influence of Intertidal Flats on Tidal Asymmetry. *J. Coast. Res.* 215, 1062–1067. doi:10.2112/03-0089.1.

Frischknecht, M., Münnich, M., and Gruber, N. (2015). Remote versus local influence of ENSO on the California Current System. *J. Geophys. Res. Ocean.* 120, 1353–1374. doi:10.1002/2014JC010531.

Gao, Y., Fang, J., Du, M., Fang, J., Jiang, W., and Jiang, Z. (2017). Response of the eelgrass (Zostera marina L.) to the combined effects of high temperatures and the herbicide, atrazine. *Aquat. Bot.* 142, 41–47. doi:10.1016/j.aquabot.2017.06.005.

Garcia, A. M. P., Geyer, W. R., and Randall, N. (2021). Exchange Flows in Tributary Creeks Enhance Dispersion by Tidal Trapping. *Estuaries and Coasts*. doi:10.1007/s12237-021-00969-4.

Garcia, A. M. P., Randall, N., Geyer, W. R., Kranenburg, W., and Ralston, D. K. (2018). Effect of Tributary Creeks on Estuarine Dispersion. *Am. Geophys. Union* 20, 1634490.

Garvine, R. W. (1991). Subtidal Frequency Estuary-Shelf Interaction: Observations Near Delaware Bay. *J. Geophys. Res.* 96, 7049–7064. doi:10.1029/91jc00079.

Gentemann, C. L., Fewings, M. R., and García-Reyes, M. (2017). Satellite sea surface temperatures along the West Coast of the United States during the 2014–2016 northeast Pacific marine heat wave. *Geophys. Res. Lett.* 44, 312–319. doi:10.1002/2016GL071039.

George, G., Vethamony, P., Sudheesh, K., and Babu, M. T. (2011). Fish larval transport in a macro-tidal regime: Gulf of Kachchh, west coast of India. *Fish. Res.* 110, 160–169. doi:10.1016/j.fishres.2011.04.002.

Geyer, W. R. (1993). Three-dimensional tidal flow around headlands. *J. Geophys. Res. Ocean.* 98, 955–966. doi:10.1029/92JC02270.

Geyer, W. R. (1997). Influence of wind on dynamics and flushing of shallow estuaries. *Estuar. Coast. Shelf Sci.* 44, 713–722. doi:10.1006/ecss.1996.0140.

Geyer, W. R., and Ralston, D. K. (2018). A mobile pool of contaminated sediment in the Penobscot Estuary, Maine, USA. *Sci. Total Environ.* 612, 694–707. doi:10.1016/j.scitotenv.2017.07.195.

Geyer, W. R., Ralston, D. K., and Chen, J. (2020). Mechanisms of exchange flow in an estuary with a narrow, deep channel and wide, shallow shoals. *J. Geophys. Res. Ocean.*, 1–25. doi:10.1029/2020jc016092.

Giddings, S. N., and MacCready, P. (2017). Reverse Estuarine Circulation Due to Local and Remote Wind Forcing, Enhanced by the Presence of Along-Coast Estuaries. *J. Geophys. Res. Ocean.* 122, 10184–10205. doi:10.1002/2016JC012479.

Goodman, A. C., Thorne, K. M., Buffington, K. J., Freeman, C. M., and Janousek, C. N. (2018). El Niño Increases High-Tide Flooding in Tidal Wetlands Along the U.S. Pacific Coast. *J. Geophys. Res. Biogeosciences* 123, 3162–3177. doi:10.1029/2018JG004677.

Grason, E., McDonald, S., Adams, J., Litle, K., Apple, J., and Pleus, A. (2018). Citizen science program detects range expansion of the globally invasive European green crab in Washington State (USA). *Manag. Biol. Invasions* 9, 39–47. doi:10.3391/mbi.2018.9.1.04.

Groner, M., Eisenlord, M., Yoshioka, R., Fiorenza, E., Dawkins, P., Graham, O., et al. (2021). Warming sea surface temperatures fuel summer epidemics of eelgrass wasting disease. *Mar. Ecol. Prog. Ser.* 679, 47–58. doi:10.3354/meps13902.

Groth, S., and Rumrill, S. (2009). History of Olympia Oysters (Ostrea lurida Carpenter 1864) in Oregon Estuaries, and a Description of Recovering Populations in Coos Bay. *J. Shellfish Res.* 28, 51–58. doi:10.2983/035.028.0111.

Guo, X., and Valle-Levinson, A. (2008). Wind effects on the lateral structure of density-driven circulation in Chesapeake Bay. *Cont. Shelf Res.* 28, 2450–2471. doi:10.1016/j.csr.2008.06.008.

Haase, A. T., Eggleston, D. B., Luettich, R. A., Weaver, R. J., and Puckett, B. J. (2012). Estuarine circulation and predicted oyster larval dispersal among a network of reserves. *Estuar. Coast. Shelf Sci.* 101, 33–43. doi:10.1016/j.ecss.2012.02.011.

Hansen, D. V., and Rattray, M. (1965). Gravitational circulation in straits and estuaries. *J. Mar. Res.* 23, 104–122. doi:10.1098/rspb.2009.2214.

Hare, J. A., Thorrold, S., Walsh, H., Reiss, C., Valle-Levinson, A., and Jones, C. (2005). Biophysical mechanisms of larval fish ingress into Chesapeake Bay. *Mar. Ecol. Prog. Ser.* 303, 295–310. doi:10.3354/meps303295.

Hessing-Lewis, M. L., Hacker, S. D., Menge, B. A., and Rumrill, S. S. (2011). Context-Dependent Eelgrass-Macroalgae Interactions Along an Estuarine Gradient in the Pacific Northwest, USA. *Estuaries and Coasts* 34, 1169–1181. doi:10.1007/s12237-011-9412-8.

Hickey, B. M., and Banas, N. S. (2003). Oceanography of the U . S . Pacific Northwest Coastal Ocean and Estuaries with Application to Coastal Ecology. *Estuaries* 26, 1010–1031.

Hickey, B. M., Zhang, X., and Banas, N. S. (2003). Coupling between the California Current System and a coastal plain estuary in low riverflow conditions. *J. Geophys. Res.* 108, 1–20. doi:10.1029/2002JC001737.

Hopkins, A. E. (1937). "Experimental observations on spawning, larval development, and setting in the Olympia oyster Ostrea lurida," in *Bulletin of the United States Bureau of fisheries*, ed. F. T. Bell, 48:66.

Hosack, G. R., Dumbauld, B. R., Ruesink, J. L., and Armstrong, D. A. (2006). Habitat associations of estuarine species: Comparisons of intertidal mudflat, seagrass (Zostera marina), and oyster (Crassostrea gigas) habitats. *Estuaries and Coasts* 29, 1150–1160. doi:10.1007/BF02781816.

Huang, H., Chen, C., Cowles, G. W., Winant, C. D., Beardsley, R. C., Hedstrom, K. S., et al. (2008). FVCOM validation experiments: Comparisons with ROMS for three idealized barotropic test problems. *J. Geophys. Res. Ocean.* 113, 1–14. doi:10.1029/2007JC004557.

Huyer, A. (1983). Coastal upwelling in the California current system. *Prog. Oceanogr.* 12, 259–284. doi:10.1016/0079-6611(83)90010-1.

Huyer, A., Smith, R. L., and Fleischbein, J. (2002). The coastal ocean off Oregon and northern California during the 1997-8 El Niño. *Prog. Oceanogr.* 54, 311–341. doi:10.1016/S0079-6611(02)00056-3.

Huyer, A., Wheeler, P. A., Strub, P. T., Smith, R. L., Letelier, R., and Kosro, P. M. (2007). Progress in Oceanography The Newport line off Oregon – Studies in the North East Pacific. 75, 126–160. doi:10.1016/j.pocean.2007.08.003.

Hyde, N. (2007). Towards national estuarine modeling and characterization / classification systems : a pilot study for Coos Bay.

Jackson, J. M., Johnson, G. C., Dosser, H. V., and Ross, T. (2018). Warming From Recent Marine Heatwave Lingers in Deep British Columbia Fjord. *Geophys. Res. Lett.* 45, 9757–9764. doi:10.1029/2018GL078971.

Jacox, M. G., Hazen, E. L., Zaba, K. D., Rudnick, D. L., Edwards, C. A., Moore, A. M., et al. (2016). Impacts of the 2015–2016 El Niño on the California Current System: Early assessment and comparison to past events. *Geophys. Res. Lett.* 43, 7072–7080. doi:10.1002/2016GL069716.

Janzen, C. D., and Wong, K.-C. (2002). Wind-forced dynamics at the estuary-shelf interface of a large coastal plain estuary. *J. Geophys. Res. Ocean.* 107, 3138. doi:10.1029/2001JC000959.

Jarvis, J. C., Moore, K. A., and Kenworthy, W. J. (2012). Characterization and ecological implication of eelgrass life history strategies near the species' southern limit in the western North Atlantic. *Mar. Ecol. Prog. Ser.* 444, 43–56. doi:10.3354/meps09428.

Johnson, M. R., Williams, S. L., Lieberman, C. H., and Solbak, A. (2003). Changes in the abundance of the seagrasses Zostera marina L. (eelgrass) and Ruppia maritima L. (widgeongrass) in San Diego, California, following an El Niño event. *Estuaries* 26, 106–115. doi:10.1007/BF02691698.

Juarez, B., Valle-levinson, A., Chant, R., and Li, M. (2019). Estuarine , Coastal and Shelf Science Observations of the lateral structure of wind-driven flow in a coastal plain estuary. *Estuar. Coast. Shelf Sci.* 217, 262–270. doi:10.1016/j.ecss.2018.11.018.

Kaldy, J. (2012). Influence of light, temperature and salinity on dissolved organic carbon exudation rates in Zostera marina L. *Aquat. Biosyst.* 8, 1–12. doi:10.1186/2046-9063-8-19.

Kaldy, J. E. (2014). Effect of temperature and nutrient manipulations on eelgrass Zostera marina L. from the Pacific Northwest, USA. *J. Exp. Mar. Bio. Ecol.* 453, 108–115. doi:10.1016/j.jembe.2013.12.020.

Kalnay, E., Kanamitsu, M., Kistler, R., Collins, W., Deaven, D., Gandin, L., et al. (1996). The NCEP/NCAR 40-Year Reanalysis Project. *Bull. Am. Meteorol. Soc.* 77, 437–471. doi:10.1175/1520-0477(1996)077<0437:TNYRP>2.0.CO;2.

Kimbro, D. L., Largier, J., and Grosholz, E. D. (2009). Coastal oceanographic processes influence the growth and size of a key estuarine species, the Olympia oyster. *Limnol. Oceanogr.* 54, 1425–1437. doi:10.4319/lo.2009.54.5.1425.

Kranenburg, W. M., Geyer, W. R., Garcia, A. M. P., and Ralston, D. K. (2019). Reversed lateral circulation in a sharp estuarine bend with weak stratification. *J. Phys. Oceanogr.* 49, 1619–1637. doi:10.1175/JPO-D-18-0175.1.

Lacy, J. R., and Monismith, S. G. (2001). Secondary currents in a curved, stratified, estuarine channel. *J. Geophys. Res. Ocean.* 106, 31283–31302. doi:10.1029/2000JC000606.

Lai, W., Pan, J., and Devlin, A. T. (2018). Impact of tides and winds on estuarine circulation in the Pearl River Estuary. *Cont. Shelf Res.* 168, 68–82. doi:10.1016/j.csr.2018.09.004.

Largier, J. L. (2003). Consideration in estimating larval dispersal distances. *Ecol. Appl.* 13, 71–89.

Largier, J. L. (2020). Upwelling Bays: How Coastal Upwelling Controls Circulation, Habitat, and Productivity in Bays. *Ann. Rev. Mar. Sci.* 12, 415–447. doi:10.1146/annurev-marine-010419-011020.

Lee II, H., and Brown, C. A. (2009). Classification of Regional Patterns of Environmental Drivers And Benthic Habitats in Pacific Northwest Estuaries.

Lee, K. S., Park, S. R., and Kim, Y. K. (2007). Effects of irradiance, temperature, and nutrients on growth dynamics of seagrasses: A review. *J. Exp. Mar. Bio. Ecol.* 350, 144–175. doi:10.1016/j.jembe.2007.06.016.

Lemagie, E. P., and Lerczak, J. A. (2015). A Comparison of Bulk Estuarine Turnover Timescales to Particle Tracking Timescales Using a Model of the Yaquina Bay Estuary. *Estuaries and Coasts* 38, 1797–1814. doi:10.1007/s12237-014-9915-1.

Lerczak, J. A., and Geyer, W. R. (2004). Modeling the Lateral Circulation in Straight, Stratified Estuaries*. *J. Phys. Oceanogr.* 34, 1410–1428. doi:10.1175/1520-0485(2004)034<1410:MTLCIS>2.0.CO;2.

Lerczak, J. A., Geyer, W. R., and Chant, R. J. (2006). Mechanisms Driving the Time-Dependent Salt Flux in a Partially Stratified Estuary*. *J. Phys. Oceanogr.* 36, 2296–2311. doi:10.1175/jpo2959.1.

Li, Y., and Li, M. (2011). Effects of winds on stratification and circulation in a partially mixed estuary. *J. Geophys. Res. Ocean.* 116. doi:10.1029/2010JC006893.

Liu, W. C., Chen, W. B., and Hsu, M. H. (2011). Using a three-dimensional particle-tracking model to estimate the residence time and age of water in a tidal estuary. *Comput. Geosci.* 37, 1148–1161. doi:10.1016/j.cageo.2010.07.007.

Logerwell, E. A., Mantua, N., Lawson, P. W., Francis, R. C., and Agostini, V. N. (2003). Tracking environmental processes in the coastal zone for understanding and predicting Oregon coho (Oncorhynchus kisutch) marine survival. *Fish. Oceanogr.* 12, 554–568. doi:10.1046/j.1365-2419.2003.00238.x.

Lucas, L. V., Thompson, J. K., and Brown, L. R. (2009). Why are diverse relationships observed between phytoplankton biomass and transport time? *Limnol. Oceanogr.* 54, 381–390. doi:10.4319/lo.2009.54.1.0381.

MacCready, P. (2011). Calculating Estuarine Exchange Flow Using Isohaline Coordinates [*]. *J. Phys. Oceanogr.* 41, 1116–1124. doi:10.1175/2011JPO4517.1.

MacCready, P., and Geyer, W. R. (2010). Advances in Estuarine Physics. *Ann. Rev. Mar. Sci.* 2, 35–58. doi:10.1146/annurev-marine-120308-081015.

MacVean, L. J., and Stacey, M. T. (2011). Estuarine Dispersion from Tidal Trapping: A New Analytical Framework. *Estuaries and Coasts* 34, 45–59. doi:10.1007/s12237-010-9298-x.

McIntyre, B. A., McPhee-Shaw, E. E., Hatch, M. B. A., and Arellano, S. M. (2020). Location Matters: Passive and Active Factors Affect the Vertical Distribution of Olympia Oyster (Ostrea lurida) Larvae. *Estuaries and Coasts*. doi:10.1007/s12237-020-00771-8.

McKay, P., and Iorio, D. Di (2008). Heat budget for a shallow, sinuous salt marsh estuary. *Cont. Shelf Res.* 28, 1740–1753. doi:10.1016/j.csr.2008.04.008.

Menniti, C. M., Whitney, M. M., and Deignan-Schmidt, S. R. (2020). The Importance of Offshore Exchange for Water Temperatures in Norwalk Harbor. *Estuaries and Coasts*, 787–800. doi:10.1007/s12237-020-00710-7.

Meyers, S. D., and Luther, M. E. (2008). A Numerical Simulation of Residual Circulation in Tampa Bay. Part II: Lagrangian Residence Time. *Estuaries and Coasts* 31, 815–827. doi:10.1007/s12237-008-9085-0.

Milcu, A. I., Hanspach, J., Abson, D., and Fischer, J. (2013). Cultural ecosystem services: A literature review and prospects for future research. *Ecol. Soc.* 18. doi:10.5751/ES-05790-180344.

Miller, J. A., and Shanks, A. L. (2004). Ocean-estuary coupling in the Oregon upwelling region: Abundance and transport of juvenile fish and of crab megalopae. *Mar. Ecol. Prog. Ser.* 271, 267–279. doi:10.3354/meps271267.

Minello, T. J., Rozas, L. P., and Baker, R. (2012). Geographic Variability in Salt Marsh Flooding Patterns may Affect Nursery Value for Fishery Species. *Estuaries and Coasts* 35, 501–514. doi:10.1007/s12237-011-9463-x.

Monismith, S. (1986). An experimental study of the upwelling response of stratified reservoirs to surface shear stress. *J. Fluid Mech.* 171, 407. doi:10.1017/S0022112086001507.

Monsen, N. E., Cloern, J. E., Lucas, L. V., and Monismith, S. G. (2002). A comment on the use of flushing time, residence time, and age as transport time scales. *Limnol. Oceanogr.* 47, 1545–1553. doi:10.4319/lo.2002.47.5.1545.

Nejrup, L. B., and Pedersen, M. F. (2008). Effects of salinity and water temperature on the ecological performance of Zostera marina. *Aquat. Bot.* 88, 239–246. doi:10.1016/j.aquabot.2007.10.006.

Nidzieko, N. J., and Monismith, S. G. (2013). Contrasting Seasonal and Fortnightly Variations in the Circulation of a Seasonally Inverse Estuary, Elkhorn Slough, California. *Estuaries and Coasts* 36, 1–17. doi:10.1007/s12237-012-9548-1.

NOAA National Estuarine Research Reserve System (NERRS) (2020). System-wide Monitoring Program. *NOAA NERRS Cent. Data Manag. Off. website http//www.nerrsdata.org*. Available at: http://www.nerrsdata.org/ [Accessed June 11, 2020].

O'Higgins, T., and Rumrill, S. S. (2007). Tidal and Watershed Forcing of Nutrients and Dissolved Oxygen Stress within Four Pacific Coast Estuaries: Analysis of Time-Series Data collected by the National Estuarine Research Reserve System-Wide Monitoring Program (2000-2006) within Padilla Bay (WA),. *NOAA/UNH Coop. Inst. Coast. Estuar. Environ. Technol.*, 1689–1699. doi:10.1017/CBO9781107415324.004.

Oates, M. S. (2013). Obervations of Gonad Structure and Gametogenic Timing in a recovering population of Ostrea Lurida (Carpenter, 1864).

Officer, C. B., Biggs, R. B., Taft, J. L., Cronin, L. E., Tyler, M. A., and Boynton, W. R. (1984). Chesapeake Bay Anoxia: Origin, Development, and Significance. *Science (80-.).* 223, 22–27. doi:10.1126/science.223.4631.22.

Okubo, A. (1973). Effect of shoreline irregularities on streamwise dispersion in estuaries and other embayments. *Netherlands J. Sea Res.* 6, 213–224. doi:10.1016/0077-7579(73)90014-8.

OSU (1971). Oceanography of the nearshore coastal waters of the Pacific Northwest relating to possible pollution - Volume 1. Corvallis, Oregon 97331.

Parmesan, C., and Yohe, G. (2003). A globally coherent fingerprint of climate change. *Nature* 421, 37–42.

Pawlowicz, R., Beardsley, R. C., and Lentz, S. J. (2002). Classical tidal harmonic analysis including error estimates in MATLAB using T TIDE $. 28, 929–937.

Pawlowicz, R., Hannah, C., and Rosenberger, A. (2019). Lagrangian observations of estuarine residence times, dispersion, and trapping in the Salish Sea. *Estuar. Coast. Shelf Sci.* 225, 106246. doi:10.1016/j.ecss.2019.106246.

Pecly, J. O. G., and Roldão, J. S. F. (2013). Dye tracers as a tool for outfall studies: Dilution measurement approach. *Water Sci. Technol.* 67, 1564–1573. doi:10.2166/wst.2013.027.

Peteiro, L. G., and Shanks, A. L. (2015). Up and down or how to stay in the bay: Retentive strategies of Olympia oyster larvae in a shallow estuary. *Mar. Ecol. Prog. Ser.* 530, 103–117. doi:10.3354/meps11283.

Peterson, M. S. (2003). A Conceptual View of Environment-Habitat-Production Linkages in Tidal River Estuaries. *Rev. Fish. Sci.* 11, 291–313. doi:10.1080/10641260390255844.

Peterson, W. T., Fisher, J. L., Strub, P. T., Du, X., Risien, C., Peterson, J., et al. (2017). The pelagic ecosystem in the Northern California Current off Oregon during the 2014-2016 warm anomalies within the context of the past 20 years. *J. Geophys. Res. Ocean.* 122, 7267–7290. doi:10.1002/2017JC012952.

Pfeiffer-Herbert, A. S., Kincaid, C. R., Bergondo, D. L., and Pockalny, R. A. (2015). Dynamics of wind-driven estuarine-shelf exchange in the Narragansett Bay estuary. *Cont. Shelf Res.* 105, 42–59. doi:10.1016/j.csr.2015.06.003.

Phillips, R. C. (1984). The ecology of eelgrass meadows in the Pacific Northwest: a community profile. *US Fish Wildl. Serv.* Available at: https://linkinghub.elsevier.com/retrieve/pii/0304377083900207.

Phillips, R. C., McMillan, C., and Bridges, K. W. (1983). Phenology of eelgrass, Zostera marina L., along latitudinal gradients in North America. *Aquat. Bot.* 15, 145–156. doi:10.1016/0304-3770(83)90025-6.

Poloczanska, E. S., Brown, C. J., Sydeman, W. J., Kiessling, W., Schoeman, D. S., Moore, P. J., et al. (2013). Global imprint of climate change on marine life. *Nat. Clim. Chang.* 3, 919–925. doi:10.1038/nclimate1958.

Pritchard, C. E., Shanks, A. L., Rimler, R. N., Oates, M., and Rumrill, S. S. (2015). The olympia oyster ostrea lurida: Recent advances in natural history, ecology, and restoration. *J. Shellfish Res.* 34, 259–271. doi:10.2983/035.034.0207.

Pritchard, C., Rimler, R., Rumrill, S., Emlet, R., and Shanks, A. (2016). Variation in larval supply and recruitment of Ostrea lurida in the Coos Bay estuary, Oregon, USA. *Mar. Ecol. Prog. Ser.* 560, 159–171. doi:10.3354/meps11894.

Purkiani, K., Becherer, J., Klingbeil, K., and Burchard, H. (2016). Wind-induced variability of estuarine circulation in a tidally energetic inlet with curvature. *J. Geophys. Res. Ocean.* 121, 3261–3277. doi:10.1002/2015JC010945.

Qi, J., Chen, C., Beardsley, R. C., Perrie, W., Cowles, G. W., and Lai, Z. (2009). An unstructured-grid finite-volume surface wave model (FVCOM-SWAVE): Implementation, validations and applications. *Ocean Model.* 28, 153–166. doi:10.1016/j.ocemod.2009.01.007.

Qin, Q., and Shen, J. (2019). Physical transport processes affect the origins of harmful algal blooms in estuaries. *Harmful Algae* 84, 210–221. doi:10.1016/j.hal.2019.04.002.

Raimonet, M., and Cloern, J. E. (2017). Estuary–ocean connectivity: fast physics, slow biology. *Glob. Chang. Biol.* 23, 2345–2357. doi:10.1111/gcb.13546.

Ralston, D. K., Brosnahan, M. L., Fox, S. E., Lee, K. D., and Anderson, D. M. (2015). Temperature and Residence Time Controls on an Estuarine Harmful Algal Bloom: Modeling Hydrodynamics and Alexandrium fundyense in Nauset Estuary. *Estuaries and Coasts* 38, 2240–2258. doi:10.1007/s12237-015-9949-z.

Ralston, D. K., Geyer, W. R., and Lerczak, J. A. (2010a). Structure, variability, and salt flux in a strongly forced salt wedge estuary. *J. Geophys. Res.* 115, C06005. doi:10.1029/2009JC005806.

Ralston, D. K., Geyer, W. R., Lerczak, J. A., and Scully, M. (2010b). Turbulent mixing in a strongly forced salt wedge estuary. *J. Geophys. Res. Ocean.* 115, 1–21. doi:10.1029/2009JC006061.

Ralston, D. K., and Stacey, M. T. (2005). Longitudinal dispersion and lateral circulation in the intertidal zone. *J. Geophys. Res. C Ocean.* 110, 1–17. doi:10.1029/2005JC002888.

Ralston, D. K., and Stacey, M. T. (2007). Tidal and meteorological forcing of sediment transport in tributary mudflat channels. *Cont. Shelf Res.* 27, 1510–1527. doi:10.1016/j.csr.2007.01.010.

Rinehimer, J. P., and Thomson, J. T. (2014). Observations and modeling of heat fluxes on tidal flats. *J. Geophys. Res. Ocean.* 119, 133–146. doi:10.1002/2013JC009225.

Roegner, G. C., Armstrong, D. A., and Shanks, A. L. (2007). Wind and tidal influences on larval crab recruitment to an Oregon estuary. *Mar. Ecol. Prog. Ser.* 351, 177–188. doi:10.3354/meps07130.

Roegner, G. C., Hickey, B. M., Newton, J. a., Shanks, A. L., and Armstrong, D. a. (2002). Wind-induced plume and bloom intrusions into Willapa Bay, Washington. *Limnol. Oceanogr.* 47, 1033–1042. doi:10.4319/lo.2002.47.4.1033.

Roegner, G. C., Needoba, J. A., and Baptista, A. M. (2011). Coastal upwelling supplies oxygen-depleted water to the columbia river estuary. *PLoS One* 6. doi:10.1371/journal.pone.0018672.

Roegner, G. C., and Shanks, A. L. (2001). Import of Coastally-Derived Chlorophyll a to South Slough, Oregon. *Estuaries* 244, 244–256. doi:10.2307/1352948.

Rumrill, S. S. (2007). The Ecology of the South Slough Estuary: Site Profile of the South Slough National Estuarine Research Reserve.

Salo, T., and Pedersen, M. F. (2014). Synergistic effects of altered salinity and temperature on estuarine eelgrass (Zostera marina) seedlings and clonal shoots. *J. Exp. Mar. Bio. Ecol.* 457, 143–150. doi:10.1016/j.jembe.2014.04.008.

Sanay, R., and Valle-Levinson, A. (2005). Wind-induced circulation in semienclosed homogeneous, rotating basins. *J. Phys. Oceanogr.* 35, 2520–2531. doi:10.1175/JPO2831.1.

Sawall, Y., Ito, M., and Pansch, C. (2021). Chronically elevated sea surface temperatures revealed high susceptibility of the eelgrass <scp> *Zostera marina* </scp> to winter and spring warming. *Limnol. Oceanogr.*, 1–13. doi:10.1002/lno.11947.

Schneider, S. (1993). "Scenarios of global warming," in *Biotic interactions and Global change*, eds. P. Kareiva, J. Kingsolver, and R. Huey (Sunderland, MA: Sinauer Associates), 9–23.

Scully, M. E., Friedrichs, C., and Brubaker, J. (2005). Control of estuarine stratification and mixing by wind-induced straining of the estuarine density field. *Estuaries* 28, 321–326. doi:10.1007/BF02693915.

Seppelt, R., Dormann, C. F., Eppink, F. V., Lautenbach, S., and Schmidt, S. (2011). A quantitative review of ecosystem service studies: Approaches, shortcomings and the road ahead. *J. Appl. Ecol.* 48, 630–636. doi:10.1111/j.1365-2664.2010.01952.x.

Shanks, A. L., Rasmuson, L. K., Valley, J. R., Jarvis, M. A., Salant, C., Sutherland, D. A., et al. (2020). Marine heat waves, climate change, and failed spawning by coastal invertebrates. *Limnol. Oceanogr.* 65, 627–636. doi:10.1002/lno.11331.

Sharples, J., Middelburg, J. J., Fennel, K., and Jickells, T. D. (2017). What proportion of riverine nutrients reaches the open ocean? *Global Biogeochem. Cycles* 31, 39–58. doi:10.1002/2016GB005483.

Sherman, K., and DeBruyckere, L. A. (2018). Eelgrass Habitats on the U.S. West Coast. State of the Knowledge of Eelgrass Ecosystem Services and Eelgrass Extent. A publication prepared by the Pacific Marine and Estuarine Fish Habitat Partnership. Available at: http://www.pacificfishhabitat.org/wp-content/uploads/2017/09/EelGrass_Report_Final_ForPrint_web.pdfeation 20180109.pdf?ver=2018-01-12-102015-010.

Short, F. T., and Coles, R. G. (2001). *Global seagrass research methods*. , eds. F. T. Short and R. G. Coles Elsevier.

Short, F. T., McKenzie, L. J., Coles, R. G., Vidler, K. P., and Gaeckle, J. L. (2006). SeagrassNet Manual for Scientific Monitoring of Seagrass Habitat. 1–75.

Simpson, J. H., Vennell, R., and Souza, A. J. (2001). The Salt Fluxes in a Tidally-Energetic Estuary. *Estuar. Coast. Shelf Sci.* 52, 131–142. doi:10.1006/ecss.2000.0733.

Smith, N. P. (1983). A comparison of winter and summer temperature variations in a shallow bar-built estuary. *Estuaries* 6, 2–9. doi:10.2307/1351801.

Steele, M. O., Chang, H., Reusser, D. A., Brown, C. A., and Jung, I.-W. (2012). Potential Climate-Induced Runoff Changes and Associated Uncertainty in Four Pacific Northwest Estuaries. 52.

Stevenson, J. W., and Niiler, P. P. (1983). Upper Ocean Heat Budget During the Hawaii-to-Tahiti Shuttle Experiment. *J. Phys. Oceanogr.* 13, 1894–1907. doi:10.1175/1520-0485(1983)013<1894:UOHBDT>2.0.CO;2.

Stommel, H., and Farmer, H. G. (1952). On the nature of estuarine circulation.

Strub, P. T., Allen, J. S., Huyer, A., Smith, R. L., and Beardsley, R. C. (1987). Seasonal cycles of currents, temperatures, winds, and sea level over the northeast Pacific continental shelf: 35°N to 48°N. *J. Geophys. Res.* 92, 1507. doi:10.1029/JC092iC02p01507.

Sutherland, D. A., and O'Neill, M. A. (2016). Hydrographic and dissolved oxygen variability in a seasonal Pacific Northwest estuary. *Estuar. Coast. Shelf Sci.* 172, 47–59. doi:10.1016/j.ecss.2016.01.042.

Teodósio, M. A., Paris, C. B., Wolanski, E., and Morais, P. (2016). Biophysical processes leading to the ingress of temperate fish larvae into estuarine nursery areas: A review. *Estuar. Coast. Shelf Sci.* 183, 187–202. doi:10.1016/j.ecss.2016.10.022.

Thom, R. M., Borde, A. B., Rumrill, S., Woodruff, D. L., Williams, G. D., Southard, J. A., et al. (2003). Factors influencing spatial and annual variability in eelgrass (Zostera marina L.) meadows in Willapa Bay, Washington, and Coos Bay, Oregon, estuaries. *Estuaries* 26, 1117–1129. doi:10.1007/BF02803368.

Thomann, R. V., and Mueller, J. A. (1987). Principles of surface water quality modeling and control. *Harper Row Publ.*

U.S. Army Corps of Engineers (2015). COOS BAY FEDERAL NAVIGATION CHANNEL AND CHARLESTON SIDE CHANNEL Dredging Project. Portland, OR.

Uncles, R. J., and Stephens, J. A. (2011). The Effects of Wind, Runoff and Tides on Salinity in a Strongly Tidal Sub-estuary. *Estuaries and Coasts* 34, 758–774. doi:10.1007/s12237-010-9365-3.

Valle-Levinson, A., Schettini, C. A. F., and Truccolo, E. C. (2019). Subtidal variability of exchange flows produced by river pulses, wind stress and fortnightly tides in a subtropical stratified estuary. *Estuar. Coast. Shelf Sci.* 221, 72–82. doi:10.1016/j.ecss.2019.03.022.

Valle-Levinson, A., Wong, K.-C., and Bosley, K. T. (2001). Observations of the wind-induced exchange at the entrance to Chesapeake Bay. *J. Mar. Res.* 59, 391–416. doi:10.1357/002224001762842253.

van Sebille, E., Delandmeter, P., Schofield, J., Hardesty, B. D., Jones, J., and Donnelly, A. (2019). Basin-scale sources and pathways of microplastic that ends up in the Galápagos Archipelago. *Ocean Sci.* 15, 1341–1349. doi:10.5194/os-15-1341-2019.

Walther, G.-R., Post, E., Convey, P., Menzel, A., Parmesan, C., Beebee, T. J. C., et al. (2002). Ecological responses to recent climate change. *Nature* 416, 389–395.

Wang, C. F., Hsu, M. H., and Kuo, A. Y. (2004). Residence time of the Danshuei River estuary, Taiwan. *Estuar. Coast. Shelf Sci.* 60, 381–393. doi:10.1016/j.ecss.2004.01.013.

Wang, S.-Y., Hipps, L., Gillies, R. R., and Yoon, J.-H. (2014). Probable causes of the abnormal ridge accompanying the 2013-2014 California drought: ENSO precursor and anthropogenic warming footprint. *Geophys. Res. Lett.* 41, 3220–3226. doi:10.1002/2014GL059748.

Wasson, K., Zabin, C. J., Bible, J., Briley, S., Deck, A. K., Grosholz, T., et al. (2015). A guide to Olympia Oyster Restoration and Conservation. Monterey Bay.

Wheat, E. E., Banas, N. S., and Ruesink, J. L. (2019). Multi-day water residence time as a mechanism for physical and biological gradients across intertidal flats. *Estuar. Coast. Shelf Sci.* 227, 106303. doi:10.1016/j.ecss.2019.106303.

Wild-Allen, K., and Andrewartha, J. (2016). Connectivity between estuaries influences nutrient transport, cycling and water quality. *Mar. Chem.* 185, 12–26. doi:10.1016/j.marchem.2016.05.011.

Wyrtki, K. (1984). The slope of sea level along the equator during the 1982/1983 El Nino. *J. Geophys. Res.* 89, 10419–10424. doi:10.1029/JC089iC06p10419.

Xia, M., Xie, L., Pietrafesa, L. J., and Whitney, M. M. (2011). The ideal response of a Gulf of Mexico estuary plume to wind forcing: Its connection with salt flux and a Lagrangian view. *J. Geophys. Res.* 116, C08035. doi:10.1029/2010JC006689.

Xie, L., and Eggleston, D. B. (1999). Computer simulations of wind-induced estuarine circulation patterns and estuary-shelf exchange processes: The potential role of wind forcing on larval transport. *Estuar. Coast. Shelf Sci.* 49, 221–234. doi:10.1006/ecss.1999.0498.

Yamada, S. B., Dumbauld, B. R., Kalin, A., Hunt, C. E., Figlar-Barnes, R., and Randall, A. (2005). Growth and persistence of a recent invader Carcinus maenas in estuaries of the northeastern Pacific. *Biol. Invasions* 7, 309–321. doi:10.1007/s10530-004-0877-2.

Yamada, S. B., Randall, A., Schooler, S., Heller, R., Donaldson, L., Takacs, G., et al. (2020). Status of the European green crab, Carcinus maenas, in Oregon and Washington coastal estuaries in 2019. Portland, OR Available at: http://scholar.google.com/scholar?hl=en&btnG=Search&q=intitle:Status+of+the+European+Green+Crab+in+Oregon+and+Washington+Estuaries#3.

Yang, Z., Khangaonkar, T., and Wang, T. (2011). Use of Advanced Meteorological Model Output for Coastal Ocean Modeling in Puget Sound. *Int. J. Ocean Clim. Syst.* 2, 101–117. doi:10.1260/1759-3131.2.2.101.

Zapata, C., Puente, A., Garca, A., Garcia-Alba, J., and Espinoza, J. (2018). Assessment of ecosystem services of an urbanized tropical estuary with a focus on habitats and scenarios. *PLoS One* 13, 1–19. doi:10.1371/journal.pone.0203927.

Zimmerman, R. C., Smith, R. D., and Alberte, R. S. (1989). Thermal acclimation and whole-plant carbon balance in Zostera marina L. (eelgrass). *J. Exp. Mar. Bio. Ecol.* 130, 93–109. doi:10.1016/0022-0981(89)90197-4.